Studies of *N*-Heterocyclic Olefins as Donors in Triarylboranes and Electron-Poor Phenylpyridyl-Fused Boroles

Dissertation zur Erlangung des naturwissenschaftlichen Doktorgrades
der Julius-Maximilians-Universität Würzburg

vorgelegt von

Jiang He
Aus Fuzhou City, Jiangxi Province, P. R. China

Würzburg, 2020

CC BY

Eingereicht bei der Fakultät für Chemie und Pharmazie am

_____

Gutachter der schriftlichen Arbeit

1. Gutachter: Prof. Dr. Dr. h.c. Todd B. Marder

2. Gutachter: Prof. Dr. Maik Finze

Prüfer des öffentlichen Promotionskolloquiums

1. Prüfer: Prof. Dr. Dr. h.c. Todd B. Marder

2. Prüfer: Prof. Dr. Maik Finze

3. Prüfer: Dr. Florian Beuerle

Datum des öffentlichen Promotionskolloquiums

_____

Doktorurkunde ausgehändigt am

_____

For my family

“If a man keeps cherishing his old knowledge,

so as continually to be acquiring new,

he may be a teacher of others.”

Confucius (孔子)

Die Experimente zur vorliegenden Arbeit wurden in der Zeit von Oktober 2016 bis September 2020 am Institut für Anorganische Chemie der Julius-Maximilians-Universität Würzburg unter der Aufsicht von Prof. Dr. Dr. h.c. Todd B. Marder und Prof. Dr. Maik Finze durchgeführ.

Acknowledgements

First of all, I would like to thank **Prof. Dr. Maik Finze** and **Prof. Dr. Dr. h.c. Todd B. Marder** to offer me the opportunity to do my Ph.D. in your groups. I enjoyed my life in Germany a lot. I am very thankful for the scientific freedom that I had since I joined our big family. Thank you, **Todd**, for always teaching me the meaning of real science (NOT only impact factor). It was always a lot of fun when we talked about China and also, America. I'm so happy to be part of the Marder family. Thank you for the house parties with **Anne** during Christmas. Thank you also for funding me to attend the EUROBORON8 conference in Montpellier and the meetings in Germany. Thank you **Maik** for involving me in your group and discussing the topics with me. I had a good time in Lab 304 in the old inorganic chemistry building.

I would also like to thank **Prof. Dr. Holger Braunschweig,** for the generous offering of numerous cyclic voltammetry measurements. I am also very grateful for **Dr. Ivo Krummenacher** for always finding time to perform the measurements and discuss the results with me.

Thank you, **Dr. Florian Rauch**. Thank you for training me how to do chemistry here. Thank you for teaching me how to perform photophysical measurements. Thank you for the DFT/TD-calculations you performed for me. Thank you for helpful discussions about my papers and also, thank you for building a bicycle for me. Most importantly, thank you for having beers with me and be such a good friend to me!

Thank you, **Raphael Wirthensohn**. Thank you for training me in Lab 304. Thank you for your help, not only in chemistry but also in life. Thank you for introducing me to other members in **Maik**'s group. Thank you for ordering chemicals for me. I will remember the Grignard accident my whole life. All in all, thank you for being such a good friend to me!

I want to thank **Dr. Alexandra Friedrich**, for solving X-Ray crystal structures for me and for writing the X-ray part in my papers. I want to thank **Dr. Rüdiger Bertermann**,

thank you for all special NMR measurements, analysis of the NMR spectra and helpful discussions. I want to thank **Dr. Daniel Sieh** for measuring and solving crystal structures for me. I want to thank **Dr. Stefan Wagner** for the maintenance of the GC-MS and giving safety instructions. Thank you, **Dr. Jörn Nitsch**, for the helpful discussions, proof reading and the Hausseminar.

One special thank goes to **materials subgroup**! You guys are always ready to help. Thank you, **Dr. Stefanie Griesbeck** and **Sarina Berger,** for organizing the trip, I had a great time in Marseille and Avignon. I will remember it my whole life. Also thank **Sarina** for organizing so much in our group. Thank you, **Dr. Julia Merz,** for inviting me to Vodka Evening. Thank you for organizing activities in our group. Thank you for your hearty laugh. Thank you, **Dr. Ji Lei**, for the helpful discussions about chemistry. **Matthias Ferger**, thank you so much for being such a good friend and comforting me when I was depressed. **Johannes Krebs**, thank you for measuring the crystals for me. Thank you for discussing chemistry while drinking beer. Thank you, **Zhu Wu** for the discussions about photophysics. Thank you also **Dr. Jiefeng Hu**, **Dr. Xiaolei Zhang**, **Dr. Jian Zhao**, **Dr. Xiangqing Jia** and **Dr. Hua Wang**.

Another special thank goes to the Lab 304 in old inorganic chemistry building. Thank you, **Dr. Christoph Kerpen**, you are always so nice and ready to help me. Thank you to be such a good friend to me. Thank you, **Dr. Matthias Häring**. My first impression of you is a cool guy. But after we work together, I figure it out you are so nice and work so hard. Thank you for welcoming me to join Lab 304, although I threw away your gloves on the first day when I joined the lab. Also thank you for helping me to put off the fire caused by *n*-BuLi. Thank you, **Dr. Tatjana Ribbeck**, you always have a heart smile on your face. I still remember the morning I fell asleep after your presentation during group meeting, which was a result of the Vodka evening.

Thank you, **Dr. Yaming Tian**, we arrived here and started our Ph.D. almost the same time. Thank you for discussing, supporting and having fun with me. Thank you, **Dr. Xiaoning Guo**, for acting as an elder brother to me. Thank you, **Dr. Florian Kerner**, for

your accompany during the weekends. Thank you for organizing the glovebox and making fun with each other. Thank you, **Robert Ricker**, for organizing the lab. Thank you for helping me to install the network in my flat. It is always a lot of fun to have a morning coffee with you. Thank you, **Jan Maier**, for taking pictures, for taking care of beer, for organizing wine tasting evening and so on. Thank you, **Dr. Martin Eck**, for the good time in the office. Thank you, **Dr. Wenbo Ming** and **Dr. Xiaocui Liu**, for introducing me into the lab and the Chinese community in Würzburg. Also thank you for your kind help in my life here. Thank you, **Dr. Lujia Mao** and **Dr. Qing Ye**, for your help in both life and chemistry. I want to thank **Zhiqiang Liu**, **Mingming Huang**, for organizing the solvents.

Thank you, **Dr. Benjamin Hupp**, for organizing the material glovebox and so on. I still remember the time we celebrated our birthdays together. You are so nice and always ready to help. Thank you, **Markus Gernert**, for teaching me to do photophysical measurements. Thank you for offering your solvents and CAAC.

I also want to thank the family of **Finze**. Thank you, **Dr. Jan A. P. Sprenger**, for your generous offer of stuff, e.g., Teflon rings, J. Young NMR tubes and so on, to me. Thank you, **Dr. Phillipp T. Hennig**, for helping me to find chemicals. Thank you for cyclic voltammetry measurements. Thank you, **Leon Schneider**, for inviting me to your party at your home. You are always so nice to me and always ready to help and thank you so much. Thank you, **Jarno Riefer**, you are such a warm-hearted guy. I like you so much and thank you for being my friend. Thank you, **Dr. Fabian Keppner,** for the helpful discussion about chemistry. I want to thank **Tobias Bischof** for the helpful synthetic strategies of boroles. I want to thank **Dr. Laura Wolz** for the DOSY NMR measurements. I want to thank **Nils Schopper** and **Ludwig Zapf** for having fun together.

Furthermore, I want to thank **Sabine Lorenzen**. Thank you for synthesizing the starting materials for me. Thank you for organizing the lab. Whenever we got technical problems, you are always the first person whom we are going to ask. Thank you so much. I also want to thank **Christioph Mahler**, for HRMS measurements that your performed for

me. Thank you for organizing the lab. Thank you also to **Hildegard Holzinger**, for all the chemicals and consumables that you ordered for us.

I also want to thank **Bianca Putz**, **Stefanie Ziegler** and especially **Maria Eckhardt**. Thank you, **Maria,** for reimbursement of travel expenses, and other things you did for the group. Thank you, **Cornelia Walter**, for organizing pencils, printing papers and so on for us. Thank you, **Gertrud Wunderling**, for cleaning the kitchen, then lab coats and so on.

I also want to thank **Marie-Luise Schäfer**, for all the NMR measurements for me. Thank you, **Sabine Timmroth** and **Liselotte Michels**, for the elemental analysis measurements. Thank you, **Alfred Schertzer**, for the gas supply and dry ice! Thank you, **Bernhard Werner** and **Berthold Fertig**, for the repairing my broken glassware, and building special glassware devices for me.

I am so grateful to all the members in **Inorganic Institute**, for your hard work to ensure that the lab works well. I had a good time in our institute and thank you all so much.

Last, I want to thank my **family**. Thank you, **Mom** and **Dad**, for your unselfish dedication, for your concern and for everything. Thank you, my **sisters** and my **brother**, for your countless help and encouragement. Thank you, **Rui Liu**, for your support, for your waiting and your encouragement. The luckiest thing for me of last year is finding you. I also want to thank my **nephews** and **nieces**, for the happiness they brought to me.

All in all, I thank all of you and I love you guys three thousand.

List of Publications

The publications listed below are partly reproduced in this dissertation with permission from the Wiley-VCH. Reference [1] is published under a creative common license (CC BY-NC 4.0) and do not require a further permission statement from the publisher.

Publications	**Position**
J. He, F. Rauch, A. Friedrich, D. Sieh, T. Ribbeck, I. Krummenacher, H. Braunschweig, M. Finze, T. B. Marder, *Chem. Eur. J.* **2019**, *25*, 13777–13784.	Chapter 1
J. He, F. Rauch, M. Finze, T. B. Marder, *Chem. Sci.* Submitted.	Chapter 2
J. He, F. Rauch, A. Friedrich, J. Krebs, I. Krummenacher, R. Bertermann, J. Nitsch, H. Braunschweig, M. Finze, T. B. Marder, *Angew. Chem. Int. Ed.* Submitted.	Chapter 3
J. He, F. Rauch, I. Krummenacher, H. Braunschweig, M. Finze, T. B. Marder, *Dalton Trans.* Submitted.	Chapter 4

And in the following (under supervision of Jiang He):

Carbon-bound Pyridyl or Bipyridyl Boranes, J. Hartmann, Bachelor Thesis, Julius-Maximilians-Universität Würzburg, **2019**.

Further publication:

X. Chen, G. Y. Meng, F. Rauch, J. He, A. Friedrich, T. B. Marder, N. Wang, P. K. Chen, S. Wang, X. D. Yin, *Chem. Eur. J.* **2020**, submitted.

List of Abbreviations

A	acceptor
Å	Ångström (1 Å = 10^{-10} m)
Abs	absorption
AIE	aggregation-induced emission
APCI	atmospheric pressure chemical ionization
ASAP	atmospheric solids analysis probe
br	broad
CAAC	cyclic (alkyl)(amino) carbene
CT	charge transfer
D	donor
D	diffusion constant
d	doublet
DOSY	diffusion-ordered spectroscopy
DFT	density functional theory
Dip	2,6-di*iso*propylphenyl
Em	emission
eq	equivalents
^{F}Mes	2,4,6-tri(trifluoromethyl)phenyl
FLP	frustrated Lewis pair
^{F}Xyl	2,6-di(trifluoromethyl)phenyl
FTIR	fourier-transform infrared spectroscopy
HOMO	highest occupied molecular orbital
HPLC	high-pressure liquid chromatography
ICT	intramolecular charge transfer
IRF	instrument response function
k_r	radiative decay

k_{nr}	non-radiative decay rate
LE	locally excited
LIFDI	liquid injection field desorption ionization
LUMO	lowest unoccupied molecular orbital
m	multiplet
MAS	magic-angle spinning
MeCN	acetonitrile
Mes	2,4,6-trimethylphenyl
HRMS	high resolution mass spectrometry
NHCs	*N*-heterocyclic carbenes
NHOs	*N*-heterocyclic olefins
NIR	near-infrared
NMR	nuclear magnetic resonance
NOESY	nuclear overhauser enhancement spectroscopy
NLO	nonlinear optical
η	dynamic viscosity
OFET	organic field-effect transistor
OLED	organic light emitting diode
OPV	organic photovoltaic cell
PAH	polycyclic aromatic hydrocarbons
q	quartet
r.t.	room temperature
S	singlet state
s	singlet
T	triplet state
t	triplet
t	tert
TADF	thermally activated delayed fluorescence

TBAB	tetrabutylammonium bromide
TCSPC	time-correlated single photon counting
TD-DFT	time-dependent density functional theory
THF	tetrahydrofuran
TICT	twisted intramolecular charge transfer
TLC	thin-layer chromatography
Tip	2,4,6-tri*iso*propylphenyl
TTA	triplet-triplet annihilation
UV	ultraviolet
Vis	visible
WCA	weakly coordinating anion

Table of Contents

1 *N*-Heterocyclic Olefins as Electron Donors in Combination with Triarylborane Acceptors: Synthesis, Optical and Electronic Properties of D-π-A Compounds 1

1.1 Introduction 1

1.2 Results and discussion 4

1.2.1 Synthesis 4

1.2.2 Crystal structures 6

1.2.3 Electrochemical properties 9

1.2.4 Photophysical properties 11

1.2.5 Theoretical studies 13

1.3 Conclusions 16

2 (Hetero)Arene-Fused Boroles: A Broad Spectrum of Applications 17

2.1 Introduction 17

2.2 Results and discussion 20

2.2.1 Synthetic methodology 20

2.2.2 Stability of 9-boroafluorenes 24

2.2.3 9-Borafluorenes with a fluorinated backbone 28

2.2.4 Donor-acceptor 9-borafluorenes 33

2.2.5 Heteroarene-fused boroles 39

2.2.6 Intramolecular dative bond in 9-borafluorenes 43

2.2.7 9-Borafluorene-based main chain polymers 47

2.2.8 Electrochemistry 49

2.2.9 Chemical reduction of fused boroles 51

2.2.10 Three-coordinate borafluorenium cations 56

2.3 Conclusions and outlook 59

3 Phenylpyridyl-fused Boroles: A Unique Coordination Mode and Weak B–N Coordination Induced Dual Fluorescence 60

3.1 Introduction 60

3.2 Results and discussion 62

3.2.1 Synthesis and crystal structures 62
3.2.2 Electrochemical properties 66
3.2.3 Photophysical properties 68
3.2.4 Theoretical studies 73
3.3 Conclusions 76
4 Two Derivatives of Phenylpyridyl-fused Boroles with Contrasting Electronic Directions: Decreasing and Enhancing the Electron Accepting Ability 77
4.1 Introduction 77
4.2 Results and discussion 79
4.2.1 Synthesis 79
4.2.2 Electrochemical properties 82
4.2.3 Photophysical properties 84
4.2.4 Theoretical studies 86
4.3 Conclusion 88
5 Synthesis and Structural Characterization of a Bis(2-pyridyl)methoxyborate Li^+ Complex 89
5.1 Introduction 89
5.2 Results and discussion 91
5.3 Conclusions 95
6 Summary/Zusammenfassung 96
6.1 Summary 96
6.1.1 Chapter 1 96
6.1.2 Chapter 2 98
6.1.3 Chapter 3 100
6.1.4 Chapter 4 102
6.1.5 Chapter 5 104
6.2 Zusammenfassung 106
6.2.1 Kapitel 1 106
6.2.2 Kapitel 2 108
6.2.3 Kapitel 3 109

6.2.4 Kapitel 4 112

6.2.5 Kapitel 5 114

7 Experimental 116

7.1 Synthesis 116

7.2 Single-crystal X-ray diffraction 128

7.3 Photophysical measurements 139

7.4 Electrochemical measurements 147

7.5 Theoretical studies 151

8 References 190

9 Appendix 208

9.1 NMR spectra 208

9.2 Cartesian coordinates 247

1 *N*-Heterocyclic Olefins as Electron Donors in Combination with Triarylborane Acceptors: Synthesis, Optical and Electronic Properties of D-π-A Compounds

The following section is slightly modified and reproduced from ref.[1] *with permission from Wiley-VCH.*

1.1 Introduction

Three-coordinate boron is sp^2 hybridized[2] and adopts a trigonal planar geometry, which leaves an unoccupied p-orbital. This vacant orbital can act as an excellent π-acceptor (A) in the excited state, leading to intramolecular charge transfer (ICT) after photo excitation. As such, applications of three-coordinate boranes as selective anion sensors,[3-6] nonlinear optical (NLO) materials,[7-15] for two photon absorption and two photon excited fluorescence,[16-20] and live cell imaging,[21-23] etc.[4, 6, 24-33] have been intensively studied.

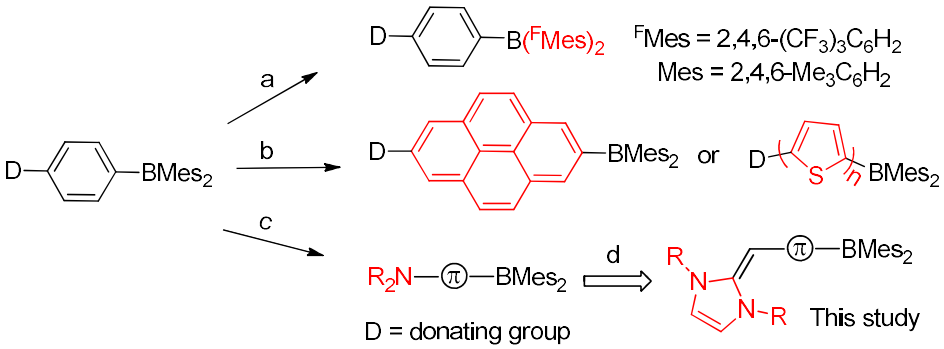

Scheme 1.1. Reported strategies to narrow the energy gap of boron containing D–π–A systems (a, b, c) and new systems reported in this study (d).

We are interested in designing small molecules (donor (D)-π-A type three-coordinate boranes) with narrow energy gaps. One approach is to stabilize the lowest unoccupied molecular orbital (LUMO) by enhancement of the electron acceptor strength of the boron center. Instead of using mesityls as steric protecting groups to avoid water or other nucleophiles binding to the empty orbital of boron,[34] Marder[35-39] and others[40-45]

applied 2,4,6-$(CF_3)_3C_6H_2$ (^{F}Mes) as a new steric protecting group in three-coordinate boranes (Scheme 1.1, a). A second approach is modification of the π-linker in D-π-A systems, for example, using pyrene[46-53] or thiophenes[13, 39] (Scheme 1.1, b), potentially influencing both the highest occupied molecular orbital (HOMO) and LUMO. The third method is to use a very electron rich donor group which reduces the energy gap by destabilizing the HOMO (Scheme 1.1, c). As an example, Marder, Braunschweig *et al.* have recently reported the use of a diborene (B=B) system as the π-donor resulting in NIR absorbing and emitting quadrupolar systems,[54] but these compounds are rather unstable in air.

Amines are among the most efficient and well-studied π-electron donors in organic materials,[55] and triarylamines connected to triarylboranes were found to be suitable materials for OLEDs.[56-63] However, using two nitrogen atoms linked 1,1 to a C=C double bond, known as an *N*-heterocyclic olefin (NHO), as a donor (Scheme 1.1, d), to the best of our knowledge, has never been combined with a three-coordinate borane acceptor.[64-66] NHOs are widely used as catalysts in transesterification, to turn CO_2 into valuable chemicals,[67] promote polymerization, etc.[68] Due to the donating effect of two nitrogen atoms, as well as the 6π-electrons of the imidazole ring, the exocyclic C=C bond becomes highly polarized and electron rich,[69] thus making NHOs potential strong donors.

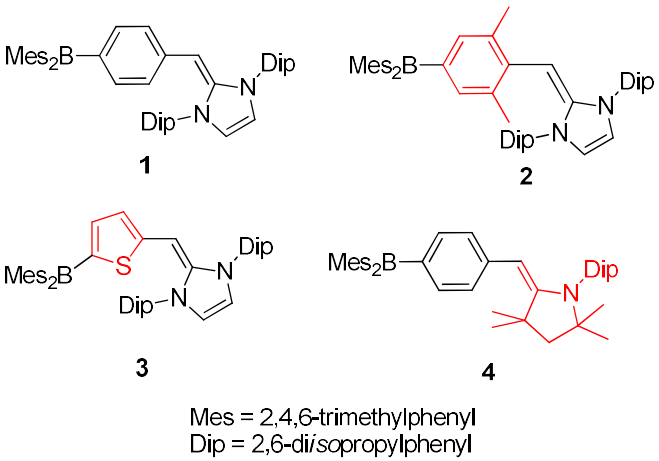

Scheme 1.2. Three-coordinate boranes **1**-**4** developed in this study.

With this in mind, we designed and synthesized four different boranes, **1**-**4** (Scheme 1.2), with **1**-**3** having an NHO as the donating group, while in **4,** an enamine is the donating group. The two extra methyl groups in **2** vs. **1** should improve the stability by protecting the exocyclic C=C bond. For a more efficient and π-electron rich linker, borane **3** was designed. Herein, we report about the synthesis and properties of these new donor-π-acceptor three-coordinate boranes.

1.2 Results and discussion

1.2.1 Synthesis

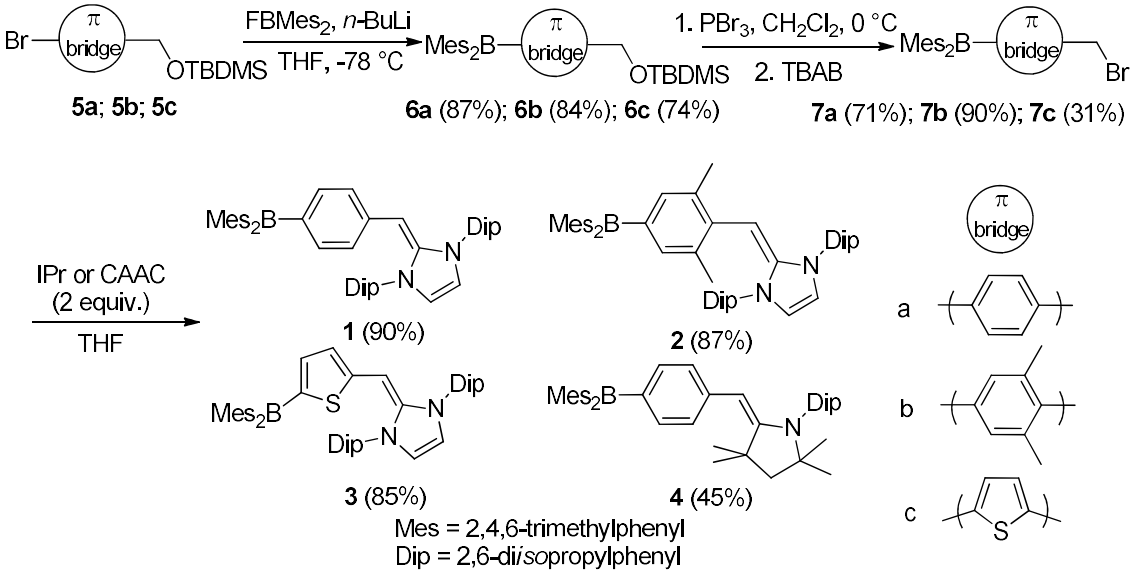

Scheme 1.3. Synthesis of three-coordinate boranes **1**-**4**.

The synthesis of the four boranes is shown in Scheme 1.3. Our strategy was to employ bromomethyl triarylboranes **7a**, **7b**, **7c** as precursors for the final step of the synthesis, namely the introduction of the NHO or enamine moiety. Thus, the corresponding silyl-protected brominated alcohols were treated with *n*-BuLi at –78 °C, followed by the addition of $FBMes_2$, giving the intermediate boranes **6a**, **6b**, **6c** in high yields. Subsequent consecutive treatment with PBr_3 and tetrabutylammonium bromide (TBAB) in CH_2Cl_2 at 0 °C, deprotection and bromination in one step, gave precursors in good (**7a** and **7b**) to acceptable (**7c**) yields. TBAB is necessary in these reactions, otherwise the products are formed in much lower yields.[70] All compounds were fully characterized by NMR, high resolution mass spectrometry (HRMS), as well as elemental analysis. Single crystals of **7a** and **7b** suitable for X-ray diffraction analysis were grown from CH_2Cl_2/hexane at –30 °C and of **7c** by evaporation of a hexane solution at room temperature. These precursors were then treated with 2 equiv. of 1,3-bis-(2,6-di*iso*propylphenyl)imidazole-2-ylidene (IPr) (for **7a**, **7b** and **7c**) or 1-(2,6-di*iso*propylphenyl)-3,3,5,5-tetramethylpyrrolidine-2-

ylidene (cyclic (alkyl)(amino) carbene (CAAC)), for **7a**), respectively, at room temperature. The solutions turned reddish-orange (for reactions with IPr) or yellow (for reaction with CAAC), immediately. After work-up and crystallization, **1**-**4** were isolated in 90%, 87%, 85% and 45% yields, respectively.

The identity and purity of **1**-**4** was confirmed by NMR spectroscopy, HRMS and elemental analysis. The chemical shifts in the $^{11}B\{^1H\}$ NMR spectra are in the typical range of three-coordinate boranes (δ (^{11}B) = 69.6, 71.9, 57.5 and 73.3 ppm for **1**, **2**, **3** and **4**, respectively). Compound **3** has the highest field ^{11}B chemical shift which is attributed to the more efficient conjugation and donor ability of the thienyl group. In the ^1H NMR spectra, the signals of the protons of the exocyclic double bond appear at 4.00 (**1**), 3.69 (**2**), 4.38 (**3**) and 4.50 (**4**) ppm. Another interesting observation is that the ^1H NMR spectra of **1** and **2** show broad signals in C_6D_6, but in CD_2Cl_2, all signals are sharp with well-resolved H-H couplings. In contrast, the ^1H NMR signals of **3** and **4** are well-resolved in both solvents, C_6D_6 and CD_2Cl_2.

Stability tests indicate that **1**-**3** decompose slowly in solution in air, so they have to be handled under an inert atmosphere. In stark contrast, compound **4** is a bench-stable yellow solid and shows no decomposition even in common solvents for several months, as evident from NMR spectroscopy.

1.2.2 Crystal structures

Reddish-orange single crystals suitable for X-ray diffraction analysis of **1** and **3** were grown by evaporation of a hexane solution at room temperature. Single crystals of **2** were obtained from a saturated acetonitrile solution and of **4** by crystallization from a CH_2Cl_2/acetonitrile solution at –30 °C. The molecular structures in the solid state are shown in Figure 1.1 and selected bond lengths (Å) and interplanar angles (°) are listed in Table 1.1. The three aryl groups attached to boron adopt propeller-like configurations in all four compounds. The BC_3 moieties are planar with the sum of the C–B–C bond angles equal to 360°. The interplanar angles between the BC_3 plane and the aryl groups bonded to boron depend on the steric demand of the aryl moieties. The terminal mesityl rings P3 and P4 are strongly twisted with respect to the BC_3 plane (50-66°, Table 1.1), a behavior that is generally observed in triarylboranes.[12, 14, 15, 20, 37, 39, 71] The bridging aryl rings P1, which are sterically less demanding, are only slightly twisted with respect to the BC_3 plane (12-29°, Table 1.1). The B–C bond lengths lie in the expected range. They are longer to the mesityl groups (1.572(3)-1.588(3) Å), while they are significantly shorter to the bridging rings, i.e. 1.547(2)-1.564(3) Å for the phenyl and xylyl rings (**1**, **2**, and **4**) and shortest at 1.512(3) Å for the thiophene group in **3** (Table 1.1). In **1**-**3** the exocyclic C=C double bond (h) length is significantly longer (1.361(3)-1.382(3) Å, Table 1.1) than a normal C=C double bond[72] or the exocyclic C=C bond of 1,3-bis(2,6-di*iso*propylphenyl)-2-methylene-2,3-dihydro-1H-imidazole (IPr=CH_2, 1.332(4) Å).[69] This suggests some degree of charge transfer in the ground-state and a polarized ground-state in **1**-**3**. This is not the case for **4**, in which h = 1.334(3) Å, close to the expected C=C double bond length. A pronounced bond-length alternation (0.036(3) Å, Table 7.2-6) is observed for the phenyl and xylyl units of **1** and **2** consistent with a partially quinoidal structure. This indicates strong conjugation between the boron centers and the bridging units, which also suggests ground-state ICT. The bond length alternation is less pronounced in **4** (0.018(3) Å). The interplanar angle between the bridging ring P1 and the *N*-heterocyclic carbene ring P2, which are connected via the exocyclic C=C double (h) and a C–C single bond (g), varies strongly among the compounds. While these are smallest for **1** (38°) and

3 (25°), the angle is larger for **2** (58°), which has a sterically more demanding bridging ring, and largest for **4** (80° and 84°). Borane **4** has the largest dihedral angle between rings P1 and P2, probably due to less effective conjugation between the boron center and the bridging unit, which also is reflected by less bond length alternation of the bridge-phenyl group.

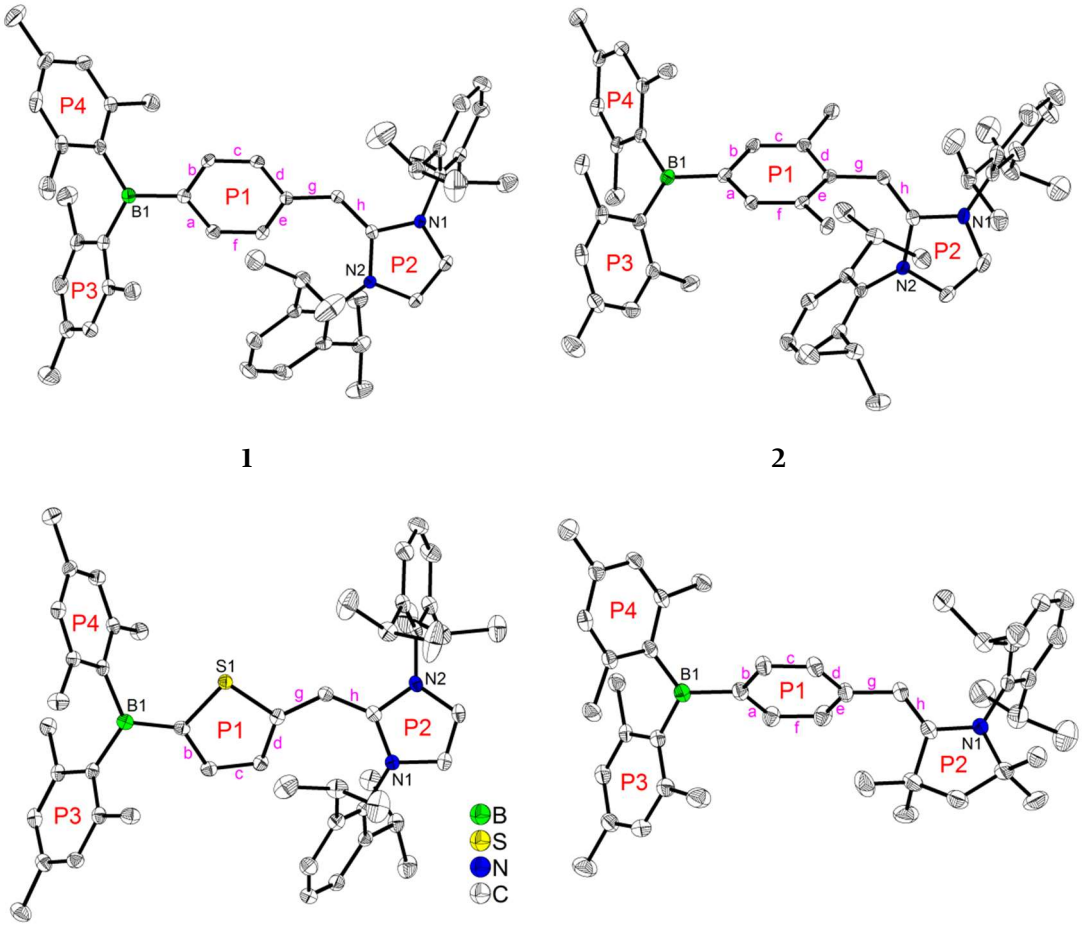

1 **2**

3 **4**

Figure 1.1. Molecular structures of **1**-**4** from single-crystal X-ray diffraction data at 100 K. Atomic displacement ellipsoids are drawn at the 50% probability level, and hydrogen atoms are omitted for clarity. For **4**, only one of two symmetrically independent molecules is shown. With regard to the aryl rings bonded to boron atoms, the central ring is labelled P1 and the terminal rings are labelled P3 and P4. The five-membered nitrogen containing ring is labelled P2. The pyrrolidine moiety of one of the two molecules of **4** is disordered, and only the part with 87% occupancy is shown.

Table 1.1. Selected bond lengths (Å) and angles (°) of **1**-**4**.

Compound	**1**	**2**	**3**	**4** (mole. 1) [a]	**4** (mole. 2)[a]
B1–C (P1)	1.547(2)	1.552(3)	1.512(3)	1.564(3)	1.558(3)
B1–C (P3)	1.581(2)	1.588(3)	1.586(3)	1.572(3)	1.572(3)
B1–C (P4)	1.583(2)	1.585(3)	1.583(3)	1.581(3)	1.584(3)
∠BIC_3-P1	17.69(7)	17.86(11)	11.72(10)	27.13(10)	29.13(10)
∠BIC_3-P3	56.72(6)	56.45(5)	58.10(8)	58.76(9)	58.07(9)
∠BIC_3-P4	60.31(6)	66.42(6)	61.13(8)	50.36(7)	50.56(7)
Sum ∠CBIC	359.9(1)	360.0(2)	360.0(2)	360.0(2)	360.0(2)
h (C=C)	1.379(2)	1.361(3)	1.382(3)	1.337(3)	1.334(3)
C–N1	1.388(2)	1.395(2)	1.376(2)	1.389(3)	-
C–N2	1.387(2)	1.407(2)	1.381(2)	-	1.392(3)
∠P1-P2	37.76(7)	57.74(7)	24.65(7)	83.89(9)	79.89(8)

[a]In borane **4**, the boron and nitrogen atoms are labeled B1 and N1 in molecule 1 and B2 and N2 in molecule 2.

1.2.3 Electrochemical properties

To investigate their electrochemical properties, **1**-**4** were also studied by cyclic voltammetry (Table 1.2). Boranes **1**-**3** show both a reversible reduction wave and a reversible oxidation wave, while **4** reveals only a reversible reduction wave and a partially reversible oxidation wave (Figure 1.2). The reversible reduction waves are attributed to the $BMes_2$ moieties and the oxidation processes are related to the NHOs or the enamine moiety. The half-wave reduction potentials of **1** and **3** at –2.86 V are the most negative potentials among the four compounds. As expected, **4** ($E_{1/2}^{red}$ = –2.66 V) has the most positive half-wave reduction potential. The half-wave reduction potential of **2** ($E_{1/2}^{red}$ = –2.82 V) is 40 mV more positive than that for **1**, which may be due to the larger dihedral angle between rings P1 and P2, as discussed above and the more rigid structure of **2**. The reversible reduction potentials of the NHO donor compounds are about 0.2 V more negative than that of the enamine donor compound. These reduction potentials are all comparable to those of other structurally related D-π-A boranes.[73, 74] Obviously, the donor ability of the NHO or enamine unit does not have a large influence on the electron accepting ability of the three-coordinate boron center in our compounds.

Table 1.2. Cyclic voltammetry data for boranes **1**-**4**.[a]

Compound	$E_{1/2}^{ox}$/ V	$E_{1/2}^{red}$/ V	HOMO/ eV[c]	LUMO/ eV[c]
1	–0.36	–2.86	–4.37	–2.00
2	–0.36	–2.82	–4.38	–2.05
3	–0.40	–2.86	–4.33	–2.00
4	0.27[b]	–2.66	–5.00	–2.20

[a]Measured in THF in the presence of 0.1 M $TBAPF_6$, scan rates of 250 mV s^{-1}, half-wave potentials given vs. the Fc/Fc^+ couple. [b]Partially reversible half-wave oxidation potential. [c]Calculated from the onset potentials of the first oxidation and reduction waves, respectively, assuming that the HOMO of Fc lies 4.8 eV below the vacuum level.

In sharp contrast to their very similar reduction potentials, large differences were found for their oxidation potentials depending on the donor moiety. Compounds **1** and **2** have

the same half-wave oxidation potential (–0.36 V) and $E_{1/2}^{ox}$ of **3** (–0.40 V) is shifted to a more negative value by 40 mV, only. This small difference is caused by the more electron rich thienyl-bridge. Compounds **1-3** are easily oxidized and show far more negative oxidation potentials than **4** ($E_{1/2}^{ox}$ = 0.27 V). This larger difference indicates that the NHO is far more electron rich than the enamine, and also suggests a much smaller HOMO-LUMO gap in NHO-containing **1-3** compared to enamine-containing **4**. The comparably low reversible oxidation potentials of **1-3** are possibly the reason for their air-sensitivity (*vide supra*).

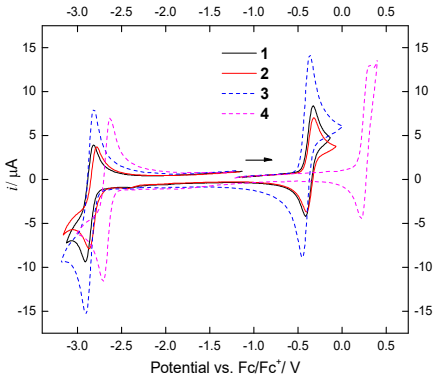

Figure 1.2. Cyclic voltammograms of **1** (black, solid), **2** (red, solid), **3**(blue, dash), and **4** (pink, dash).

1.2.4 Photophysical properties

UV-visible absorption spectra of **1**-**4** were measured in different solvents and the data are listed in Table 1.3. Compounds **1**-**4** have a strong, structureless lowest-energy absorption band in toluene with maxima at 495, 494, 516 and 421 nm, respectively (Figure 1.3), which can be attributed to ICT. The lowest-energy absorption of **4** in solution is similar to that of related D-π-$BMes_2$ compounds.[15, 19] A comparison of the lowest-energy absorption bands shows a large red shift (e.g., in toluene, ca. 3500 cm^{-1} for **1** and **2**, 4300 cm^{-1} for **3**) between NHO-containing **1**-**3** and enamine-containing **4**, indicating the stronger π-electron donating ability of the NHO than the enamine. The red shift of ca. 20 nm (860 cm^{-1}) observed for **3** compared to **1** confirms the more efficient conjugation of a thienyl compared to a phenyl group, which was discussed for the electrochemical data (*vide supra*). Another interesting finding is that **1** has a very large molar extinction coefficient (8.5×10^4 cm^{-1} M^{-1} in toluene and 7.4×10^4 cm^{-1} M^{-1} in THF) for the lowest-energy absorption. With increasing solvent polarity, positive absorption solvatochromism (ca. 15 nm from hexane to THF) was observed in all four boranes, which suggests polarized ground-states and moderate ground-state dipole moments,[15, 75] caused by ground-state ICT.

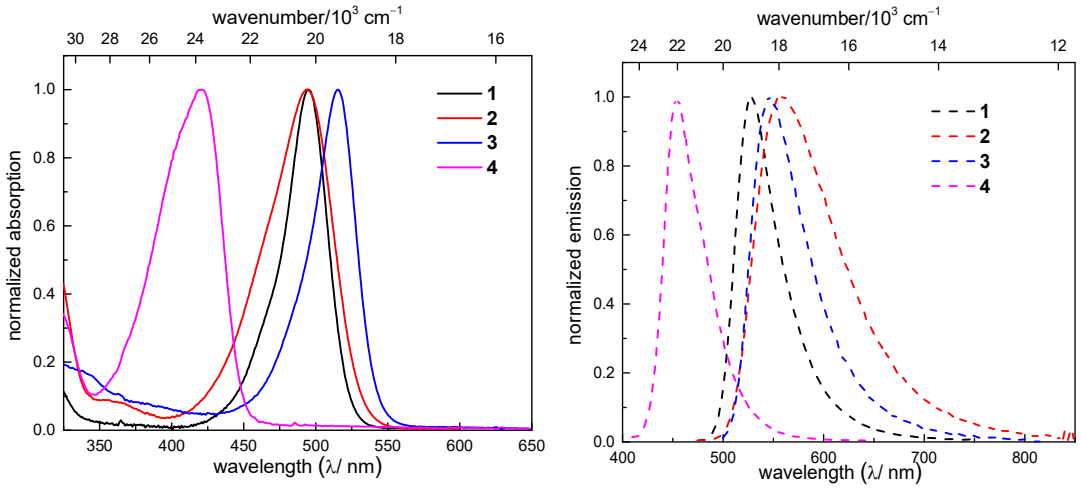

Figure 1.3. UV-visible absorption (left) and emission spectra (right) of boranes **1**-**4** in toluene.

All of the boranes show weak to moderate emission in solution and in the solid state.

Solvent-dependent emission studies indicate that all of the boranes show a moderate red shift with increasing solvent polarity. This is a typical phenomenon observed in D-π-A compounds due to ICT, resulting in a more polarized excited state, which is stabilized by a higher polarity solvent relative to the ground-state. The Stokes shift of the boranes also increase with increasing solvent polarity. In THF, **2** has the largest Stokes shift (4552 cm^{-1}) among all four boranes in different solvents. In the solid state, **1** exhibits the highest quantum yield (0.11) and **3** has the lowest energy emission (591 nm) but with a much lower quantum yield (0.037). It was not possible to determine the molar extinction coefficient, quantum yield and lifetime of **3** in solution accurately due to slow decomposition in highly dilute solution.

Table 1.3. Photophysical data for **1**-**4** at room temperature.

Compound	Solvent	λ_{abs}[a]/ nm ($\varepsilon/10^4$ cm^{-1} M^{-1})	λ_{em}/ nm	Φ_F[b]	τ_F/ ns	Stokes shift/ cm^{-1}
1	hexane	485 (5.8)	499	[c]	[c]	578
	toluene	495 (8.5)	528	0.15	2.1	1263
	THF	504 (7.4)	572	0.15	< 1.0	2359
	solid	-	576	0.11	1.9	-
2	hexane	484 (3.0)	510	0.012	< 1.0	1053
	toluene	494 (3.4)	555	0.29	7.3	2225
	THF	501 (3.2)	649	0.033	1.6	4552
	solid	-	569	0.074	[d]	-
3	hexane	508[e]	525	(N.D.)[e]	[e]	638
	toluene	516[e]	547	(N.D.)[e]	[e]	1098
	THF	522[e]	575	(N.D.)[e]	[e]	1766
	solid	-	591	0.037	[d]	-
4	hexane	411 (2.2)	432	[c]	< 1.0	1183
	toluene	421 (3.1)	454	0.005	< 1.0	1727
	THF	421 (2.9)	475	0.012	< 1.0	2700
	acetonitrile	426 (3.6)	501	0.031	< 1.0	3514
	solid	-	467	0.003	< 1.0	-

[a]Lowest-energy absorption maximum. [b]Absolute fluorescence quantum yields measured using an integrating sphere. [c]Not determined due to very weak emission. [d]Borane **2**: τ_1 < 1.0 (87.6%), τ_2 = 1.1 (11.7%), τ_3 = 3.8 (0.7%) (ns); Borane **3**: τ_1 < 1.0 (87.7%), τ_2 = 1.9 (12.2%), τ_3 = 11.2(0.1%) (ns). [e]Not determined due to slow decomposition in highly dilute solution.

1.2.5 Theoretical studies

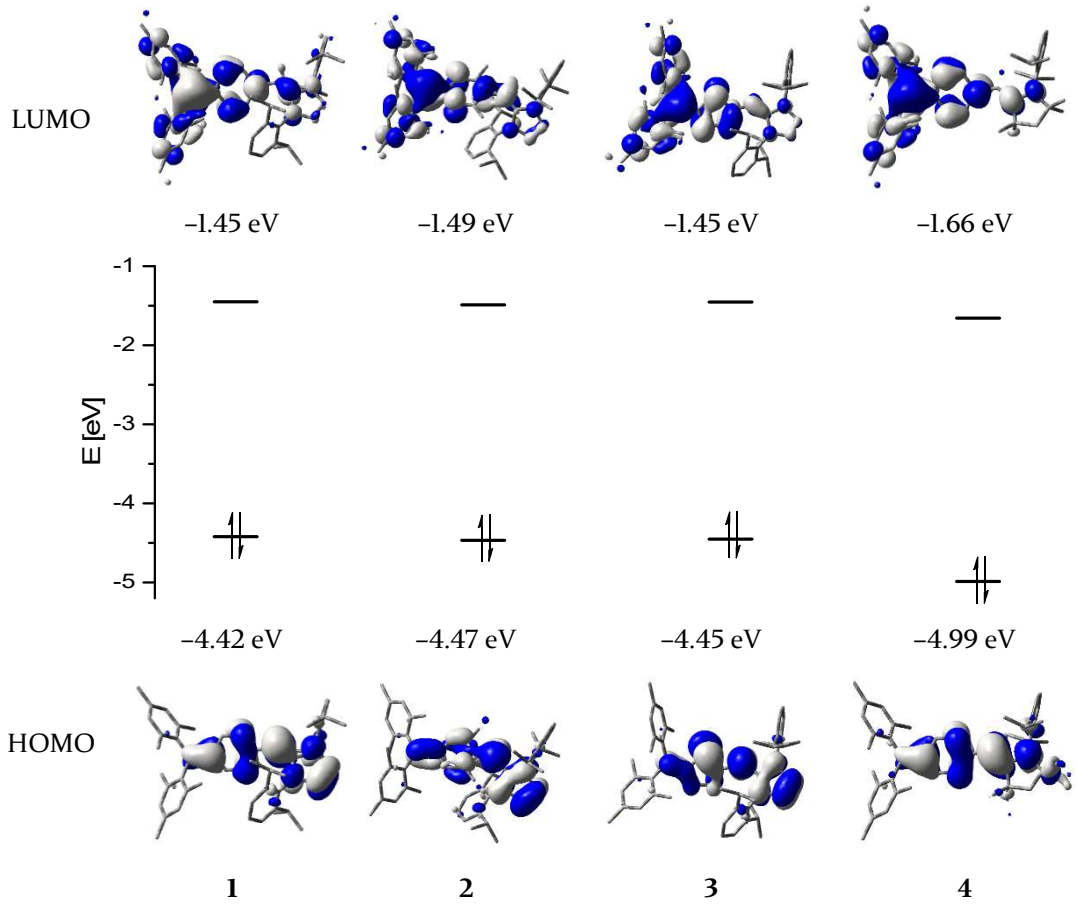

Figure 1.4. HOMO and LUMO of **1**-**4**, calculated at the B3LYP/6-31+G(d) level of theory and corresponding energies.

DFT calculations were carried out to gain deeper insight into the electronic and photophysical properties of **1**-**4**. Optimized ground-state structures were obtained at the B3LYP/6-31+G(d) level of theory using the crystal structures as the starting geometries. The solid-state structures were nicely reproduced. Similar to the crystal structures, the mesityl C–B bonds are about 0.04 Å (**1**), 0.03 Å (**2**), 0.06 Å (**3**) and 0.03 Å (**4**) longer than the π-bridge B–C bonds. In comparison to experimental values, the angles between the BC_3 plane and the π-bridge are slightly larger for **1**-**3** (Δ = 3.90°, 0.71° and 2.32° respectively) and smaller for **4** (Δ = 4.12° and 6.13°). The optimized structures also exhibit a quinoidal distortion of the π-bridge. The mean quinoidal distortions of the phenylene-

bridged compounds **1** and **4** are 0.03 and 0.026 Å, respectively. In the xylene-bridged derivative **2**, it is not sensible to use the mean distortion as the methyl groups on the donor side also influence the aromatic bond lengths. In this case, a/b are 0.02 Å longer than c/f, while e/d are 0.03 Å longer (Figure 1.1). In the thiophene-bridged **3**, all bond lengths are similar to those in the crystal structure.

The optimized structures also reproduce the shortened C–C single bond (g) and the elongated exocyclic C=C double bond (h) that connects the donor to the bridge for **1**-**3**. In **4**, this convergence is more pronounced than in the crystal structure. This might be due to a significantly smaller angle between the P1 and P2 rings (33.55° vs 80/84°) in **1**-**3**. This would lead to an increased interaction between the donor and acceptor which is most likely responsible for the changes in these bond lengths.

Table 1.4. Lowest energy transitions calculated at the B3LYP/6-31+G(d) level of theory. (H = HOMO; L = LUMO).

Compound	Transition	E/ eV	λ/ nm	f	Major contributions	Λ	Dipole moment
1	$S_1 \leftarrow S_0$	2.63	471	0.59	H→L (98%)	0.54	6.27
2	$S_1 \leftarrow S_0$	2.56	484	0.36	H→L (99%)	0.46	5.53
3	$S_1 \leftarrow S_0$	2.65	467	0.62	H→L (98%)	0.64	7.03
4	$S_1 \leftarrow S_0$	2.99	415	0.75	H→L (98%)	0.56	6.26

For **1**-**3**, the HOMO is mainly delocalized over the π-bridge, the exocyclic C=C double bond and the imidazole ring (Figure 1.4). For **4**, the HOMO is mainly delocalized over the π-bridge, the exocyclic C=C double bond and the nitrogen of the pyrrolidine ring. Interestingly, the boron also contributes to the HOMO in all compounds confirming the ground-state ICT. In all compounds, the LUMO is mainly localized on boron and the π-bridge, with the two mesityl groups and the exocyclic C=C double bond also contributing to some extent, along with a small contribution from the imidazole or pyrrolidine ring. The HOMOs of **1**-**3** are very similar in energy (ΔE < 0.05 eV), as are the LUMOs, which indicates only a small influence of the different bridges on the frontier orbitals. Borane **4**, however, exhibits a lower HOMO as well as LUMO energy (ΔE = 0.5

and 0.2 eV, respectively, in comparison to **1**), which nicely fits with the electrochemical study. This is due to the significantly lower donor strength of the enamine than the NHO.

Subsequently, TD-DFT calculations were carried out at the B3LYP/6-31+G(d) level of theory. In the gas phase, the $S_1 \leftarrow S_0$ transitions of all four derivatives are almost exclusively HOMO to LUMO transitions (Table 1.4). For ICT-based transitions it is recommended to use the Coulomb attenuated functional CAM-B3LYP.[76] We have carried out these calculations as well. However, the calculations performed using B3LYP more accurately reproduced the energies found experimentally. As this was unexpected, we further determined the overlap coefficients (Λ) (Table 1.4).[77] Compounds **1**-**4** exhibit Λ coefficients around 0.5 for their lowest energy transitions, which indicates only moderate ICT character in the excited state. For this reason, the B3LYP functional was used for the TD-DFT calculations as well.

This moderate ICT character of the lowest energy absorptions could be due to an already partially polarized ground-state, which would decrease the change in dipole moment and necessity for solvent rearrangement upon excitation. All calculated structures exhibit moderate dipole moments in the ground-state (Table 1.4), which also supports that assumption. The moderate positive absorption solvatochromism of all compounds with increasing solvent polarity also confirms the moderate ground-state dipole moments.

1.3 Conclusions

In summary, four different D-π-A boranes were synthesized in three steps each, providing an efficient synthetic strategy for introducing *N*-heterocyclic olefins (NHOs) into boron-containing D-π-A systems. Photophysical studies show that NHO is a much stronger electron donor than an enamine (or amine). The electrochemical investigations reveal extremely low reversible oxidation potentials for the three NHO-containing boranes **1**-**3** compared to those of enamine- (**4**) or amine-containing boranes. DFT calculations indicate a much higher HOMO for **1**-**3** in agreement with the strong electron donating ability of the NHO moiety. Our studies confirmed the electron rich property of NHOs, suggesting their potential for using as donors in other push-pull systems. The reversible oxidation potentials of **1**-**3** suggest that radical cations may be isolable, which is currently under investigation.

2 (Hetero)Arene-Fused Boroles: A Broad Spectrum of Applications

2.1 Introduction

Three-coordinate boranes have been studied intensely for applications such as anion sensors,[3, 78, 79] nonlinear optical materials (NLOs),[7-9, 11-15, 19, 20, 80] live cell imaging,[21-23, 81] sensing of DNA, RNA and proteins,[82, 83] etc.[4, 6, 24-32, 84] Among them, boroles are distinct, being 5-membered unsaturated 4π-electron heterocycles containing a 3-coordinate boron center. Interest in boroles originates from their being isoelectronic with the cyclopentadiene cation (Cp^+) which, in terms of Hückel's rule,[85-88] is antiaromatic and thus highly reactive. The isolation of "free" Cp^+ has not been achieved. Cp^+ has a triplet electronic ground state, which was confirmed by ESR spectroscopic measurements of the pentaphenylcyclopentadienyl cation at low temperature.[89] The C_{2v} symmetry of a borole is lower than that of Cp^+ (D_{5h}, Figure 2.1), which results in a splitting of the previously degenerate half-filled molecular orbitals. The orbital with a nodal plane passing through the boron atom ("as" in Figure 2.1) is lowered in energy and occupied, which leads to a singlet ground state and diamagnetic character of boroles, in contrast to the biradical character of Cp^+. The small HOMO-LUMO gap in boroles leads to their intense color.

Similar to Cp^+, the "free" HBC_4H_4 is inaccessible due to its high reactivity caused by its antiaromaticity[90-92] and low lying LUMO. Via kinetic protection, monomeric pentaphenylborole ($PhBC_4Ph_4$, **PhB**) was first synthesized in 1969 by Eisch and co-workers,[93] but its crystal structure was only determined in 2008 by Braunschweig and co-workers.[94] Kinetic protection of boroles was not only achieved with phenyl group but also with other even bulkier protecting groups, e.g., ^{F}Ph (pentafluorophenyl),[95] Mes (2,4,6-trimethylphenyl)[96] and ^{F}Mes (2,4,6-tritrifluoromethylphenyl).[38] However, these non-fused "free" boroles are still highly reactive compounds. The chemistry of non-fused "free" boroles was previously reviewed by Eisch,[97] Marder and co-workers,[98] Braunschweig and co-workers,[99-101] Wakamiya,[102] Martin and co-workers[103] and Kinjo

and co-workers.[104, 105]

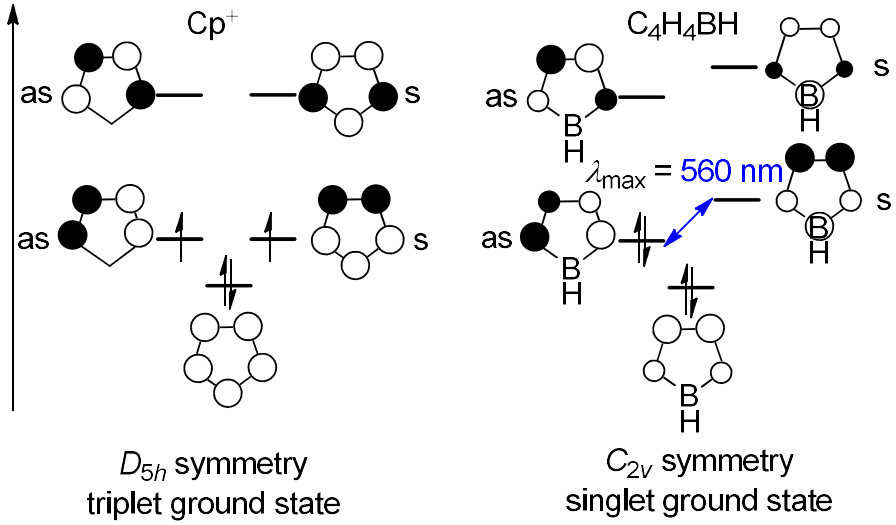

Figure 2.1. Molecule orbitals of the cyclopentadiene cation (Cp^+) and borole; "as" and "s" denote the antisymmetric and symmetric orbitals, respectively, with respect to the mirror plane perpendicular to the molecule.

The stability of boroles is largely enhanced by annulation, and fused boroles are readily accessible and functionalizable (Scheme 2.1). In comparison to related triarylboranes, the electron accepting ability and Lewis acidity of the boron atom is largely enhanced in boroles, as a result of the antiaromaticity and strain of the 5-membered borole ring. Such fused boroles can be considered to be boron-doped polycyclic antiaromatic hydrocarbons.

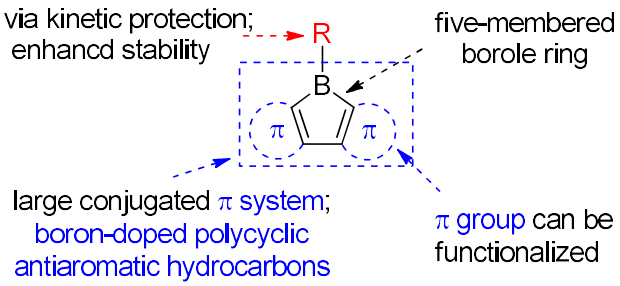

Scheme 2.1. (Hetero)Arene-fused boroles.

The first dibenzo-fused borole, namely the parent 9-borafluorene (**Bf**), was reported in the early 1960s by Köster and Benedikt,[106] but only at the start of this century, has the chemistry of **Bf**s started to attract increasing interest. (Hetero)Arene-fused boroles have been reviewed very briefly either as part of reviews on "free" boroles[98, 100, 102, 105] or on boron-doped polycyclic aromatic hydrocarbons (PAHs).[107, 108] In this perspective, we address the synthesis, properties and applications of (hetero)arene-fused boroles in detail, including new developments in the use of aryl groups as *exo*-substituents on boron.

2.2 Results and discussion

2.2.1 Synthetic methodology

There are three main approaches for the synthesis of 9-aryl-9-borafluorenes: (1) the use of easy-to-functionalize 9-X-9-borafluorenes (**XBf**s, X = Cl or Br or I) as key intermediate; (2) assembling 9-aryl-9-borafluorenes in one step; and (3) stepwise substitution reactions at boron.

The first approach relies on readily available 9-X-9-borafluorenes (**XBf**s, X = Cl or Br or I). Four synthetic approaches to **XBf** derivatives have been developed. In 1985, Nöth and co-workers applied a boron-mercury exchange reaction (Scheme 2.2, path **a**).[109] Analogous to the preparation of **PhB**,[110] a boron-tin exchange reaction can also be utilized for the synthesis of **XBf**s (Scheme 2.2, path **b**).[111, 112] To avoid using these highly toxic metals, a boron-silicon exchange reaction was developed (Scheme 2.2, path **c**).[113] **ClBf** can be obtained directly from reaction of 2,2'-dilithiobiphenyl with BCl_3 in aliphatic solvent (Scheme 2.2, path **d**).[114] The advantage of this approach is that once the intermediate of **XBf** is obtained, it is useful for subsequent derivatization.

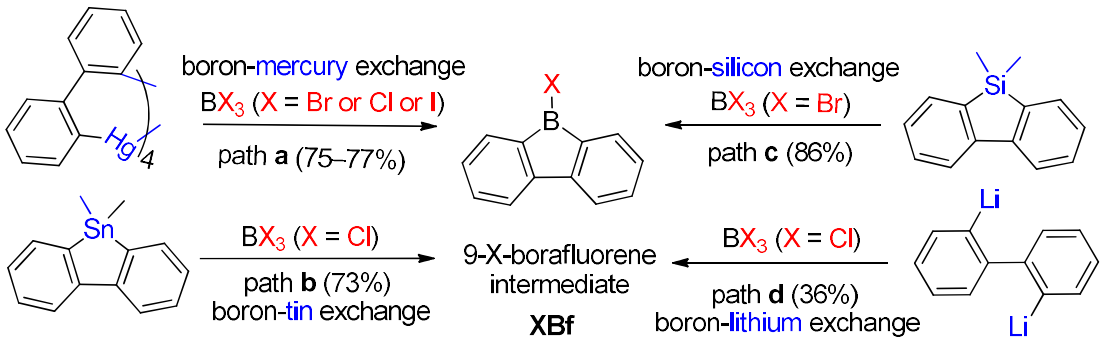

Scheme 2.2. Synthesis of 9-X-9-borafluorenes.

For the one-step assembly of 9-aryl-9-borafluorenes, a boron-tin exchange reaction was utilized.[110] Instead of using BX_3 (X = Cl or Br or I), $PhBCl_2$ was used directly (Scheme 2.3, path **e**).[115] The drawback of this methodology is that only sterically relatively

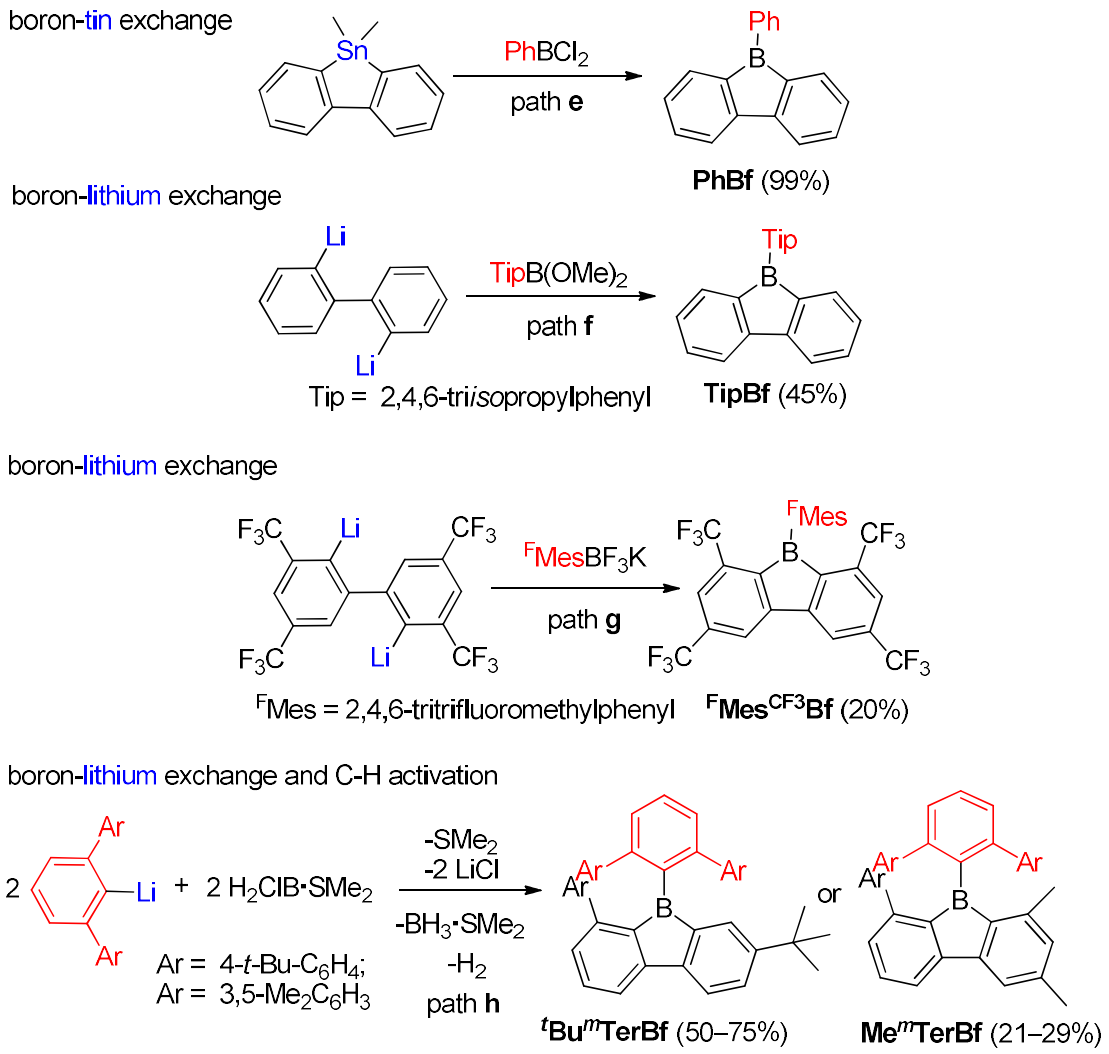

Scheme 2.3. One-step synthesis of 9-aryl-9-borafluorenes.

unencumbered groups (e.g., phenyl and pentafluorophenyl) can be used;[111] e.g., $MesBCl_2$ (Mes = mesityl group) is unsuitable for this methodology. By changing the boron source from $PhBCl_2$ to dimethoxy aryl borates, and subsequent reaction with dilithiobiphenyl, 9-aryl-9-borafluorenes can be synthesized (Scheme 2.3, path **f**).[116, 117] There are two advantages to this approach: (1) dimethoxy aryl borates can tolerate coordinating solvents and are much more stable than their corresponding aryldihaloboranes, which makes the work up much easier; and (2) bulkier aryl groups (e.g. 2,4,6-tri*iso*propylphenyl (Tip)) can be used. The third approach which can assemble 9-aryl-9-borafluorenes in one step was reported by Marder and co-workers, in

which more stable aryltrifluoroborate salts were used as the boron source (Scheme 2.3, path **g**).[38, 118] The downside of this approach is the comparably low yields. Besides these widely applied three approaches, which can assemble 9-aryl-9-borafluorenes in one step, the Wehmschulte group synthesized two unsymmetric 9-borafluorenes in one step by using $H_2ClB{\bullet}SMe_2$ as the boron source (Scheme 2.3, path **h**). The formation of the borole ring takes place via a facile intramolecular C–H activation process, but the requirement of bulky terphenyl precursors limits its further application.[119, 120]

The third approach is a stepwise substitution reaction at boron, which was first reported in 1963 by Köster and Benedikt (Scheme 2.4). Thus, 9-alky-9-borafluorenes can be synthesized from *B*,*B*-dialkyl-2-biphenylborane intermediates by thermal dissociation of one alkyl-group at 180-200 °C. The compound 9-phenyl-9-borafluorene (**PhBf**) can also be synthesized from *B*,*B*-dipheny-2-biphenylborane in the same way, but the temperature needs to be increased to 280-300 °C.[106] The harsh conditions in this approach limit its further application. In 2011, the Yamaguchi group applied boronic esters as the boron source for the synthesis of heteroarene-fused boroles.[121] Using the dithiophene-fused borole (**TipD^{TMS}ThB**) as an example, the boronic ester was introduced at the bithiophene via boron-lithium exchange in the first step, then the protecting group at the boron was introduced with a Grignard reagent. Finally, an intramolecular cyclization reaction completed the synthesis of **TipD^{TMS}ThB**. More recently, Urban and co-workers applied a similar strategy, but used an intramolecular cyclization in the second step, obtaining 9-methoxy-9-borafluorene (**MeOBf**),[122] a potential intermediate for synthesizing other 9-substituted-9-borafluorenes. In 2012, the Piers group used a reductive route with a haloborane (**Precursor1**, obtained by three stepwise boron-metal exchange reactions) while attempting to synthesize the diborole **TipDBf** (Scheme 2.4, bottom). Instead, they initially obtained an isomer of **TipDBf** (**Isomer-TipDBf**) which, under irradiation with UV light (254 nm), isomerized to the desired diborole **TipDBf**.[123] Subsequently, the same group reported another, more efficient, thermal route to the diborole **TipDBf** from **Isomer-TipDBf**.[124]

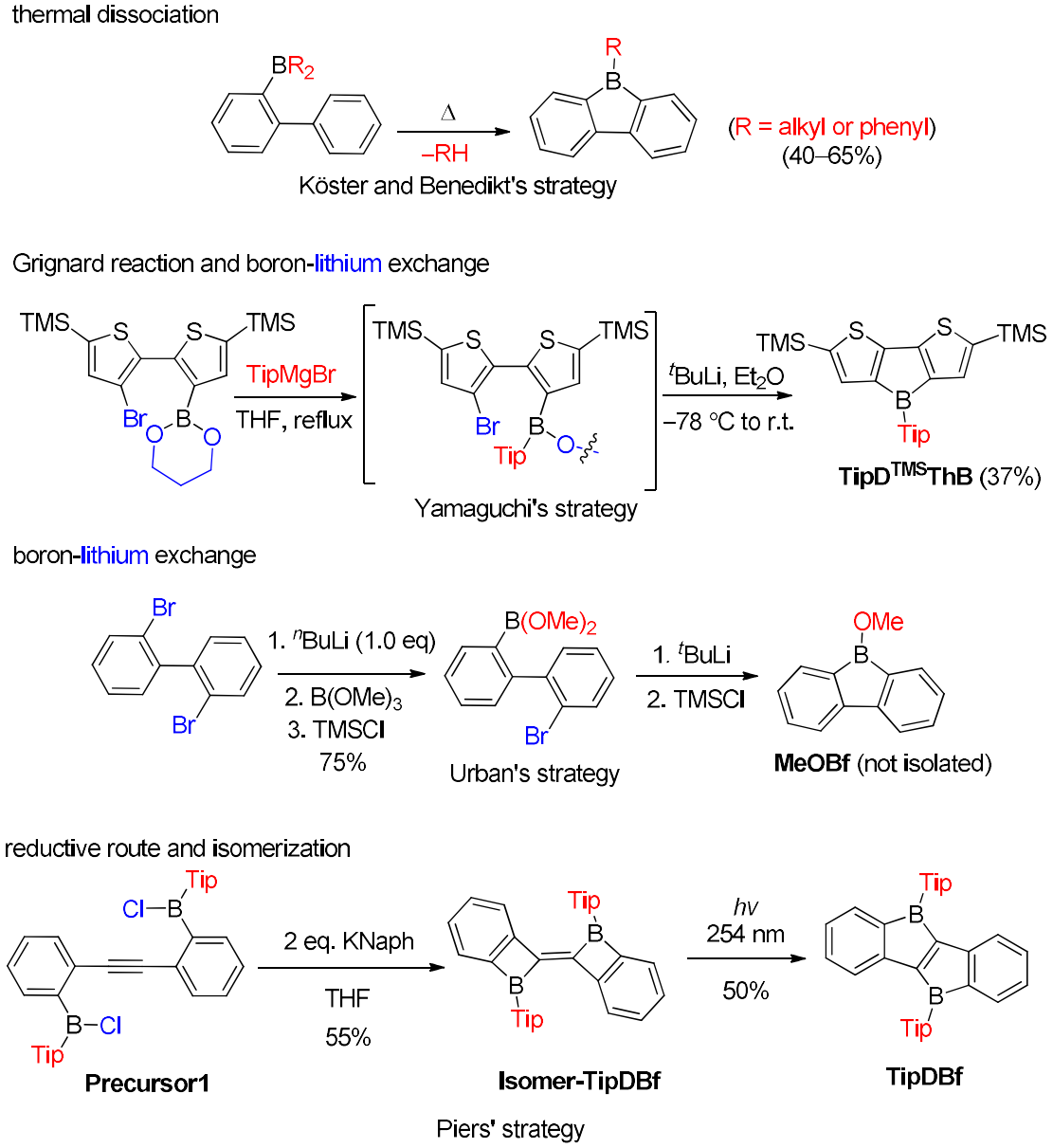

Scheme 2.4. Stepwise substitution reactions to synthesize fused boroles.

2.2.2 Stability of 9-boroafluorenes

The advantage of incorporating a boron atom into a 5-membered diene-ring is the enhancement of electron accepting ability and Lewis acidity, but at the same time, stability is sacrificed. By fusing two phenyl rings onto a borole, the stability is greatly enhanced. The stability of the resulting 9-borafluorenes depends largely on the *exo*-substituent at boron. In this section, we compare the stability of different 9-broafluorenes.

When the *exo*-substituent is not a bulky aryl group, 9-borafluorenes remain highly reactive (Scheme 2.5). In fact, **HBf** is a C_1-symmetric dimer in solution and, after some time, it forms oligomers via a ring-opening mechanism even in dry and deoxygenated C_6D_6.[106, 125-128] **ClBf**[65, 129, 130] and **^{i}Pr$_2$NBf** both show more than 50% decomposition within 1 hour in solution when exposed to the atmosphere.[45] **^{t}BuOBf** is much more stable and exhibits less than 10% decomposition after 1 hour in $CDCl_3$ in air. This can be attributed to the steric demand of the *tert*-butyl group as the less bulky derivative **MeOBf**[109] is as sensitive to air/atmosphere as **^{i}Pr$_2$NBf** and **ClBf**.[45]

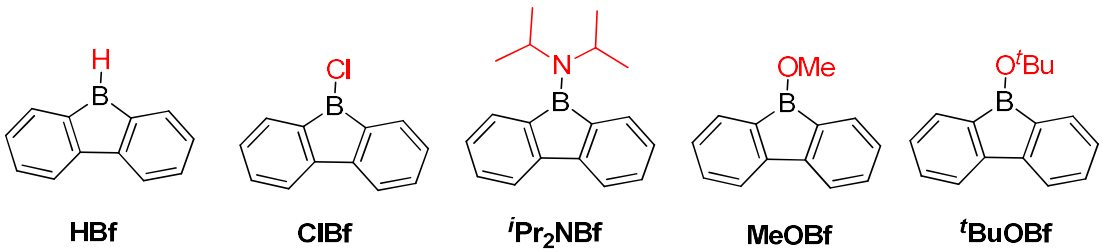

HBf ClBf ^{i}Pr$_2$NBf MeOBf ^{t}BuOBf

Scheme 2.5. Non-aryl group substituted 9-borafluorenes.

An aryl group as the *exo*-substituent at 9-borafluorene increases the stability drastically (Scheme 2.6). **PhBf** and **MesBf** decompose only slowly in the air.[105] **PhBf** nonetheless retains high reactivity, e.g., azides can insert into one of the B–C bonds of **PhBf** to generate 9,10-*B*,*N*-phenanthrenes.[112, 131] The reaction of **PhBf** with 1,2-dipolar substrates

leads to the formation of the corresponding ring expansion adducts.[132, 133] By employing Tip or ^{F}Mes as the protecting group at the boron atom of 9-borafluorenes, their stability is greatly enhanced, and both derivatives can be purified by column chromatography, even in air.[45, 116] Stability tests indicate that **TipBf** shows ca. 15% decomposition in solution in air after 24 hours and **^{F}MesBf** shows only ca. 5% decomposition under the same conditions. Considering that the trifluoromethyl group is less bulky than the *iso*propyl group,[134] this observation initially seems counterintuitive. In fact, the higher stability of **^{F}MesBf** is due to the stabilizing interaction of the vacant p_z-orbital of boron by lone pairs of the fluorine atoms of the two *ortho*-CF_3 groups of the *exo*-^{F}Mes. This σ-donation was confirmed by the short B···F distances (2.682(6) and 2.577(5) Å) observed in the solid state (Figure 2.2), which are much shorter than the sum of the van der Waals radii for boron and fluorine (3.39 Å).[135] The σ-donation from the fluorine atom(s) of *ortho*-CF_3 group(s) to the vacant p_z-orbital of boron was also observed in other boranes[35, 36, 42, 136-141] and boroles.[38, 118] The 2,4,6-tri-*tert*-butylphenyl (Mes*) group is the bulkiest substituent among these protecting groups and, thus, provides the most stable 9-borafluorenes. Compared to **TipBf**, which still exhibits reactivity towards the small F^- anion and can be applied as a F^- sensor, **Mes*Bf** is inert to F^-. This demonstrates the superior stability of **Mes*Bf**.[142]

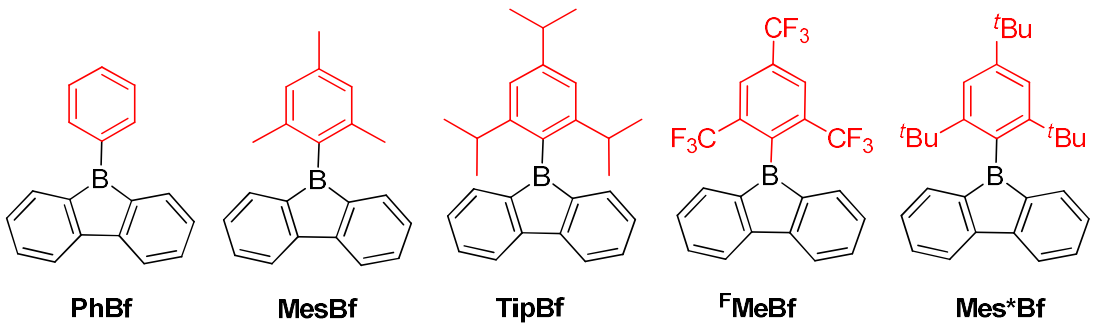

Scheme 2.6. 9-Aryl-9-borafluroenes.

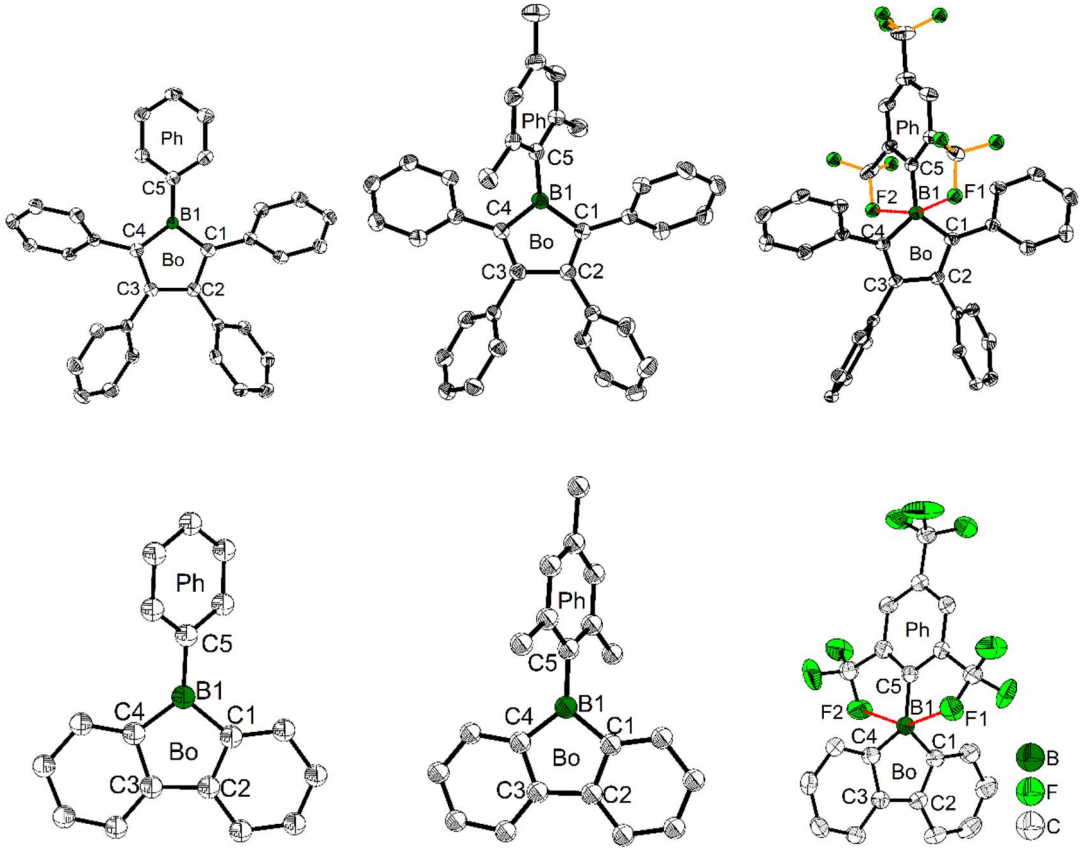

Figure 2.2. Molecular structures of **PhB** (top, left), **MesB** (top, middle), **^{F}MesB** (top, right), **PhBf** (bottom, left), **MesBf** (bottom, middle) and **^{F}MesBf** (bottom, right). For **PhBf** and **^{F}MesBf**, only one of the two symmetry independent molecules is shown. Hydrogen atoms and the minor component of disordered CF_3 groups of **^{F}MesB** are omitted for clarity. Red dashed lines in **^{F}MesB** and **^{F}MesBf** indicate short B–F contacts. 'Bo' and 'Ph' denote the planes of the borole and the *exo*-aryl groups, respectively.

To gain a deeper understanding of the relation between the structure and the stability, selected bond parameters of **PhBf**,[143] **MesBf**,[144] and **^{F}MesBf**[45] derived from single-crystal X-ray studies are listed in Table 2.1 and the molecular structures are depicted in Figure 2.2. The free non-fused boroles, **PhB**, 1-mesityl-2,3,4,5-tetraphenylborole (**MesB**)[96] and 1-(2,4,6-tritrifluoromethylphenyl)-2,3,4,5-tetraphenylborole (**^{F}MesB**),[38] are included for comparison.

Table 2.1. Selected bond lengths (Å) and angles (°) of **PhB**, **MesB**, **^{F}MesB**, **PhBf**, **MesBf** and **^{F}MesBf**. For **PhBf** and **^{F}MesBf**, only one of the two symmetry independent molecules is listed.

	PhB	**MesB**	**^{F}MesB**	**PhBf**	**MesBf**	**^{F}MesBf**
B1–C1	1.526(2)	1.586(2)	1.571(3)	1.573(9)	1.566(2)	1.550(6)
B1–C4	1.539(2)	1.575(2)	1.576(3)	1.59(1)	1.567(2)	1.556(5)
B1-C5	1.516(2)	1.560(2)	1.580(3)	1.58(1)	1.565(2)	1.584(5)
C1–C2	1.428(2)	1.356(2)	1.359(3)	1.431(9)	1.416(2)	1.421(5)
C3–C4	1.426(2)	1.351(2)	1.358(3)	1.421(9)	1.415(2)	1.411(5)
C2–C3	1.470(2)	1.537(2)	1.526(3)	1.51(1)	1.485(2)	1.485(5)
B1–F1			2.385(3)			2.682(6)
B1–F2			2.556(5)			2.576(5)
∠C1–B1–C4	105.4(1)	105.2(1)	106.19(17)	104.2(5)	103.7(1)	105.1(3)
∠Bo–Ph	32.71(5)	68.7(1)	82.4(3)	39.2	84.1	82.2(2)

Compared to **PhB**, the C–B bond lengths of the other five compounds are significantly longer. The short C–B bond lengths of **PhB** are a result of the strong p_{π}(B) – π^* conjugation. The C1–C2 and C3–C4 bonds in **MesB** (1.356(2) and 1.351(2) Å) and **^{F}MesB** (1.359(3) and 1.358(3) Å) are obviously double bonds, but in the other four compounds, these bonds are significantly longer. In contrast, the remaining inner-borole C2–C3 bond is quite long in **MesB** (1.537(2)) and **^{F}MesB** (1.526(3)) compared to those in **PhB** and the three fused boroles. So, similar to **PhB**, the C_{ring}–C_{ring} distances in fused boroles are indicative of some electron delocalization, which is in stark contrast to typical non-fused boroles such as **MesB**, resulting in significant differences in the properties of fused vs. typical non-fused boroles. The ∠C1–B1–C4 angles of the six compounds shown in Figure 2.2 are quite similar. The torsion angles between the *exo*-aryl ring bonded to boron and the borole core are 32.71(5)° (**PhB**), 68.7(1)° (**MesB**), 82.4(3)° (**^{F}MesB**), 32.8° and 39.2° (**PhBf**), 84.1° (**MesBf**), 80.9(12)° and 82.2 (2)° (**^{F}MesBf**) (the unit cell of **PhBf** and **^{F}MesBf** exhibit two distinct molecules), respectively. Apparently, the bulkier the *exo*-aryl group is, the larger the torsion angle becomes, resulting in more efficient kinetic protection.

2.2.3 9-Borafluorenes with a fluorinated backbone

Inspired by the wide application of $B(C_6F_5)_3$,[145-147] and the fact that 9-borafluorenes are more Lewis acidic than their corresponding boranes, Piers and co-workers synthesized a series of 9-borafluorenes with fluorinated backbones (Scheme 2.7). **Me^{F}Bf** and **^{F}Ph^{F}Bf** are pale yellow or orange solids which exhibit lowest energy absorption maxima at 398 nm and 440 nm in hexane, respectively.[111] To explore the effect of two fluorinated 9-borafluorene centers in a molecular framework on the Lewis acidity, **^{F}PhD^{F}Bf** was synthesized.[148] In **^{F}PhD^{F}Bf**, two fluorinated 9-borafluorenes are situated *ortho* to one another, forming a chelating bidentate Lewis acid. **^{F}PhD^{F}Bf** is a deep orange solid with a lowest energy absorption maximum at 425 nm (ε = 590 M^{-1} cm^{-1}) in hexane, comparable to that of **^{F}Ph^{F}Bf**, indicating that the two chromophores of the fluorinated 9-borafluorenes are not coupled. To the best of our knowledge, **^{F}PhM^{F}PhB** is the only example of mono-aryl fused borole.[149] **^{F}PhM^{F}PhB** is a red solid with its lowest energy absorption maximum at 465 nm (ε = 900 M^{-1} cm^{-1} in toluene), and is readily soluble in most solvents.[150]

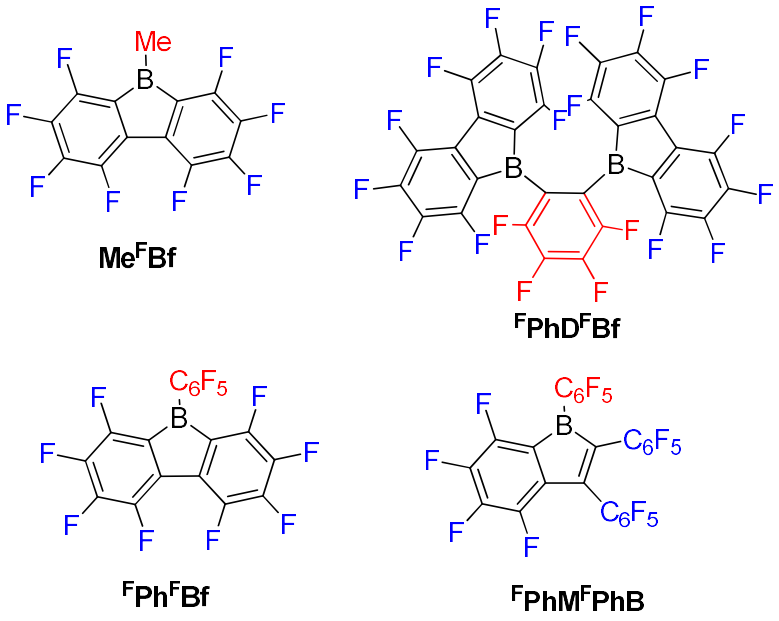

Scheme 2.7. 9-Borafluorenes with a fluorinated backbone.

Compared with corresponding fluorinated perfluoroboranes ($MeB(C_6F_5)_2$, $B(C_6F_5)_3$ and C_6F_4-1,2-$[B(C_6F_5)_2]_2$),[148, 151-153] the fluorinated 9-borafluorenes show stronger Lewis acidities, as demonstrated by Lewis base competition reactions, the Childs method,[154] and semiempirical MNDO calculations.[155] Apparently, compared to the corresponding fluorinated triarylboranes, the loss of two fluorine atoms is compensated by the antiaromaticity and strain of the 5-membered borole ring. Weak Lewis bases (LBs), e.g., THF and CH_3CN, both bind to these four fluorinated 9-borafluorenes. After introduction of a Lewis base, the orange solutions of **Me^{F}Bf** and **^{F}PhD^{F}Bf**, or lime green solution of **^{F}Ph^{F}Bf**, become colorless,[156] and the red solution of **^{F}PhM^{F}PhB** turns pale yellow.[150] This color change is due to the interruption of $p_\pi(B) - \pi^*$ conjugation upon coordination of the Lewis base to the boron center, which results in a higher LUMO energy.[116]

In a CH_3CN competition reaction between **^{F}Ph^{F}Bf** and $B(C_6F_5)_3$•CH_3CN at 25 °C, an equilibrium constant of ca. 1.3 was found indicating a preference for formation of **^{F}Ph^{F}Bf**•CH_3CN vs. $B(C_6F_5)_3$•CH_3CN.[156] In another competition experiment, with the bulkier THF as the base (in a ratio of 1:1:1 for **^{F}Ph^{F}Bf**, $B(C_6F_5)_3$ and THF in d_8-toluene), only the **^{F}Ph^{F}Bf**•THF adduct was observed by NMR spectroscopy. Applying the Childs method, **Me^{F}Bf** and **^{F}Ph^{F}Bf** have a relative Lewis acidity value of 0.58 ± 0.02 and 0.70 ± 0.02, respectively, which is only slightly higher than that of the corresponding $MeB(C_6F_5)_2$ (0.56 ± 0.02) and $B(C_6F_5)_3$ (0.68 ± 0.02 obtained by Piers).[111] For the smaller Lewis base CH_3CN, **^{F}Ph^{F}Bf** and $B(C_6F_5)_3$ show comparable Lewis acidities, but for the larger Lewis base THF, **^{F}Ph^{F}Bf** shows a much stronger Lewis acidity than $B(C_6F_5)_3$. Based on these results, the authors concluded that the relative Lewis acidities of **^{F}Ph^{F}Bf** and $B(C_6F_5)_3$ are determined by steric factors, rather than the antiaromaticity of **^{F}Ph^{F}Bf**.

Addition of $Cp_2Zr(CH_3)_2$ to **Me^{F}Bf** or **^{F}Ph^{F}Bf**, leads to Me^- abstraction, and the corresponding ion pairs are formed rapidly.[111] Both of them are remarkably more stable than their corresponding borane ion pairs in toluene (the ion pairs formed from $MeB(C_6F_5)_2$ and $Cp_2Zr(CH_3)_2$ can exchange a C_6F_5 group from $MeB(C_6F_5)_2$ with a methyl group from $Cp_2Zr(CH_3)_2$, resulting in $Me_2B(C_6F_5)$ and $Cp_2Zr(CH_3)(C_6F_5)$ under similar conditions).[157] **Me^{F}Bf**/$Cp_2Zr(CH_3)_2$ and **^{F}Ph^{F}Bf**/$Cp_2Zr(CH_3)_2$ are more active and stable

than the corresponding borane/$Cp_2Zr(CH_3)_2$ ion pairs as activators for olefin polymerization. To investigate further the coordination chemistry of **Me^{F}Bf** and **^{F}Ph^{F}Bf**, $[Cp^*Al]_4$ was used.[115] Surprisingly, only the thermally robust η^1 Lewis acid-base adduct was observed. Thus, the fragment of Cp*Al behaves only as a Lewis base rather than as a two-electron reducing agent. The reaction of Cp*Al with the less Lewis acidic **PhBf** also provides the η^1 Lewis acid-base adduct. Alternative routes to η^5 9-borafluorene aluminum complexes via reaction of **PhBf**Li_2•$(THF)_n$ with $Cp^*AlCl_2(THF)$ were also unsuccessful. The reaction of **^{F}Ph^{F}Bf** with $L^{tBu}ScR_2$ (L^{tBu} = ((Ar)NC(^{t}Bu)CHC(R)N(^{t}Bu), Ar = 2,6-^{i}Pr-C_6H_3) produced the corresponding contact ion pairs, the structures of which were thoroughly investigated both in solution and the solid state.[158]

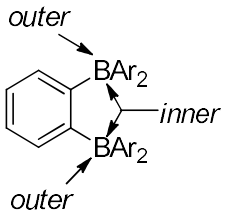

Scheme 2.8. A description of facial coordination modes of *ortho*-phenylene-bridged diboranes.

Ortho-phenylene-bridged diboranes are interesting compounds and can be applied as co-initiators for olefin polymerizations.[159] Depending on the binding position of the Lewis base, *ortho*-phenylene-bridged diboranes (and diborole **^{F}PhD^{F}Bf**) can adopt inner or outer facial coordination modes (Scheme 2.8).[151-153, 160] By adding a neutral Lewis base, e.g., CH_3CN or THF, exclusive coordination to the less sterically encumbered outer face of **^{F}PhD^{F}Bf** was observed.[148] This is in contrast to CH_3CN which coordinates to the inner face of the corresponding diborane C_6F_4-1,2-$[B(C_6F_5)_2]_2$. The reaction of **^{F}PhD^{F}Bf** with $PhCMe_2X$ (X = Cl, OMe or N_3) gives thermally stable and isolable ion pairs which feature a weakly coordinating anion (WCA). The application of these ion pairs as initiators for *iso*butene polymerization were studied and the results show that the combination of C_6F_4-1,2-$[B(C_6F_5)_2]_2$ with $PhCMe_2X$ is more suitable than **^{F}PhD^{F}Bf** with

$PhCMe_2X$.[161]

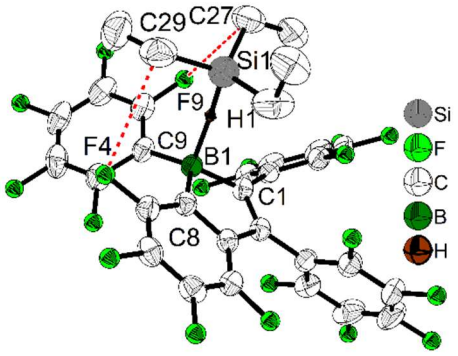

Figure 2.3. Structure of the adduct between ^{F}**PhM**^{F}**PhB** and Et_3SiH. Only hydrogen H1 is shown, whereas other hydrogen atoms are omitted for clarity. Red dashed lines indicate the close non-bonded contacts. Selected bond lengths (Å) and angles (°): B1–C1 1.616(3), B1–C8 1.608(3), B1–C9 1.605(3), B1–H1 1.46(2), Si1–H1 1.51(2), C27–F9 3.138(3), C29–F4 3.262(2), ∠B1–H1–Si1 157, sum of ∠C–B–C 344.3(2).

While perfluoropentaphenylborole (**P**^{F}**PhB**) reacts rapidly and irreversibly with dihydrogen (H_2),[162, 163] ^{F}**PhD**^{F}**Bf** is inert to H_2 under various conditions. Therefore, ^{F}**PhM**^{F}**PhB**, which is a structural hybrid of ^{F}**PhD**^{F}**Bf** and **P**^{F}**PhB** was designed and synthesized.[149] The reaction between ^{F}**PhM**^{F}**PhB** and H_2 was investigated experimentally and by theoretical calculations. ^{F}**PhM**^{F}**PhB** reacts reversibly with H_2, but side reactions occur resulting in only limited turnover numbers of this metal-free H_2 activation reaction. ^{F}**PhM**^{F}**PhB** has a comparable Lewis acidity to that of **P**^{F}**PhB** but exhibits a much better solubility than **P**^{F}**PhB** in non-coordinating solvents. Due to the better solubility of ^{F}**PhM**^{F}**PhB**, a low temperature experiment between ^{F}**PhM**^{F}**PhB** and Et_3SiH was possible.[150] The borole-silane complex formation in d_8-toluene was studied by variable-temperature NMR spectroscopy. The trends of the Si–H coupling constant and the infrared stretching frequency of the Si–H bond as a function of temperature, and the molecular structure of the complex determined by X-ray diffraction (Figure 2.3), clearly prove that an interaction exists between the boron atom and the silicon atom

through the Si–H bond. These direct observations thus confirmed the previously proposed mechanism, i.e., that perfluoroarylboranes catalyze the hydrosilyation of C=C, C=N and C=O bonds via borane activation of the Si–H bond, not via a classical Lewis acid/base adduct process.[164]

2.2.4 Donor-acceptor 9-borafluorenes

The 9-borafluorenes exhibit a weakly allowed lowest energy absorption which extends into the visible region. This absorption was attributed to the low-lying LUMO which originates from the $p_\pi - \pi^*$ conjugation through the vacant p_z orbital of boron.[165] By incorporating electron donating group(s) or electron withdrawing group(s) at different positions, the photophysical properties can be modified (Scheme 2.9). In this section, the 9-borafluorenes are classified according to their functional groups at different positions.

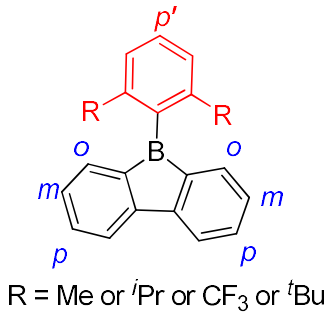

Scheme 2.9. A depiction of the different positions on a 9-borafluorene to which functional groups are attached.

Pioneered by Yamaguchi and co-workers in 2002, three functionalized **TipBf**s (**TipBf^m(PhNPh$_2$)$_2^p$(OMe)$_2$**, **TipBf^{m}Th$_2^p$(OMe)$_2$** and **TipBf^m(BTh)$_2^p$(OMe)$_2$**) with donors (methoxy and amine groups or methoxy and thiophene groups) at the *m*- and *p*-positions were reported (Scheme 2.10).[116] Compared with the non-functionalized **TipBf**, both the absorption and emission of these functionalized **TipBf**s are red shifted and the quantum yields decrease (Table 2.2). Addition of F^- (or coordinating solvents) leads to a blue shift of both the absorption and emission of these functionalized **TipBf**s and, the quantum yields dramatically increase to ca. 0.5-0.9. Thus, these functionalized **TipBf**s can be applied as F^- sensor. In contrast to tri(9-anthryl)borane, which loses its fluorescence properties after coordination with F^- and was labeled as a "turn off"

sensor,[78] due to the increase of the emission intensity after adding F^-, these functionalized 9-borafluorenes were termed fluorescence "turn on" sensors.

Table 2.2. Photophysical data for (hetero)arene-fused boroles.

compound	solvent	λ_{abs}/ nm (log (ε))	λ_{em}/ nm	Φ_F
Me^{F}Bf[111]	hexane	398 (-)	*a*	*a*
^{F}Ph^{F}Bf[111]	hexane	440 (-)	*a*	*a*
^{F}PhD^{F}Bf[148]	hexane	425 (2.77)	*a*	*a*
^{F}PhM^{F}PhB[150]	hexane	465 (2.95)	*a*	*a*
TipBf[116]	THF	410 (2.39)	514	0.09
TipBf^p(OMe)$_2$[45]	CH_2Cl_2	398 (2.80)	499	0.10
TipBf^m(PhNPh$_2$)$_2$^{p}(OMe)$_2$[116]	THF	480 (3.08)	561	0.03
TipBf^{m}Th$_2$^{p}(OMe)$_2$[116]	THF	488 (2.95)	550	0.041
TipBf^m(BTh)$_2$^{p}(OMe)$_2$[116]	THF	504 (3.51)	576	0.022
Mes*Bf[142]	THF	397 (2.42)	501	0.35
Mes*Bf^m(PhNPh$_2$)$_2$[142]	THF	470 (4.06)	608	0.24
Mes*Bf^m(BTh)$_2$[142]	THF	457 (3.80)	600	0.48
TipBf^{p}In-Me[166]	cyclohexane	430 (3.28)	529	0.21
TipBf^{p}In-Ph[166]	cyclohexane	430 (3.27)	527	0.36
TipBf^{o}In-Me[166]	cyclohexane	451 (4.03)	567	0.13
TipBf^{p}BTh[167]	cyclohexane	380 (3.75)	519	0.55
TipBf^{o}BTh[167]	cyclohexane	411 (3.81)	513	0.42
^{F}Xyl^{CF3}Bf[118]	hexane	400 (2.48)	521	0.37
^{F}Mes^{CF3}Bf[118]	hexane	386 (2.60)	510	0.30
$^{p'}$NMe$_2$^{F}Xyl^{CF3}Bf[118]	hexane	396 (2.48)	627	0.03
TipD^{TMS}ThB[121]	CH_2Cl_2	552 (3.05)	*b*	*b*
TipBThBB[121]	CH_2Cl_2	469 (2.93)	*b*	*b*
TipDBThB[121]	CH_2Cl_2	600 (3.04)	*b*	*b*
MesInBB[144]	CH_2Cl_2	479 (3.09)	*a*	*a*
MesBFuBB[144]	CH_2Cl_2	468 (3.06)	*a*	*a*
MesBThBB[144]	CH_2Cl_2	474 (3.05)	*a*	*a*
[TipPBB$_1$]$_4$[168]	THF	322 (4.70)	495	0.12
TipPBB2[168]	THF	375 (2.95)	520	0.27

[a]Not reported. [b]Non-emissive.

Six years later, the same group synthesized another two 9-Mes*-borafluorenes (**Mes*Bf^m(PhNPh$_2$)$_2$** and **Mes*Bf^m(BTh)$_2$**) with donors (amine or thiophene groups) at

the *m*-positions (Scheme 2.10). Compared with the non-functionalized **Mes*Bf**, the molar extinction coefficients are much higher and a red shift was observed in both absorption and emission. Compared to the corresponding 9-Tip-9-borafluorenes, the fluorescence quantum yields of 9-Mes*-9-borafluorenes are increased, which is most likely due to the restricted rotation of the bulky Mes* group. The bulky Mes* group also leads to enhanced stability of these 9-Mes*-9-borafluorenes, which paves the way for their application as accepting units in organic (opto)electronics.[142]

In 2016, Rupar and co-workers synthesized **TipBf^{p}(OMe)$_2$** with two methoxy donors at the *p*-positions (Scheme 2.10). The lowest energy absorption and emission peak of **TipBf^{p}(OMe)$_2$** appear in the same range as that of **TipBf**, and the quantum yields are also the same. The similar photophysical properties of these two compounds may be due to the weak donating ability of the methoxy groups.[45]

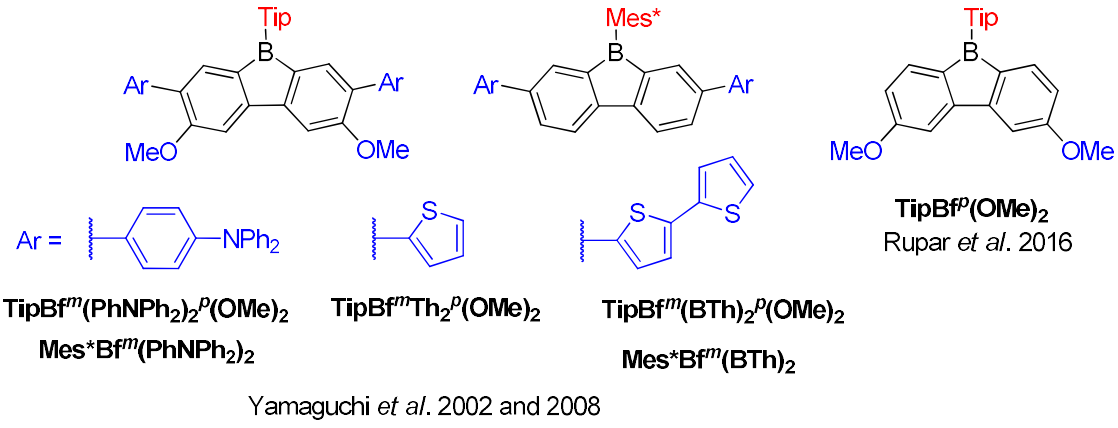

Scheme 2.10. 9-Borafluorenes with donors incorporated at the biphenyl core.

Encouraged by the wide application of carbazole as a donating group and 9-borafluorene as an accepting group, the Zhao group synthesized three ladder-type *B*,*N*-bridged *p*-terphenyls, with indole fused at the *p*-, *m*-positions (**TipBf^{p}In-Me** and **TipBf^{p}In-Ph**) or *o*-, *m*-positions (**TipBf^{o}In-Me**) on one side of the borafluorene (Scheme 2.11).[166] Later, the same group replaced the indole with benzothiophene and reported another two

ladder-type *B*,*S*-bridged *p*-terphenyls (**TipBf^{p}BTh** and **TipBf^{o}BTh**).[167] In these ladder-type boroles, the products of fusing at the *p*-, *m*-positions (**TipBf^{p}In-Me**, **TipBf^{p}In-Ph** and **TipBf^{p}BTh**), are tolerant to air and moisture, but fusing at the *o*-, *m*-positions (**TipBf^{o}In-Me** and **TipBf^{o}BTh**) leads to products that show slow decomposition in dilute solution in air (no specific solvent is mentioned), which is probably caused by steric congestion.

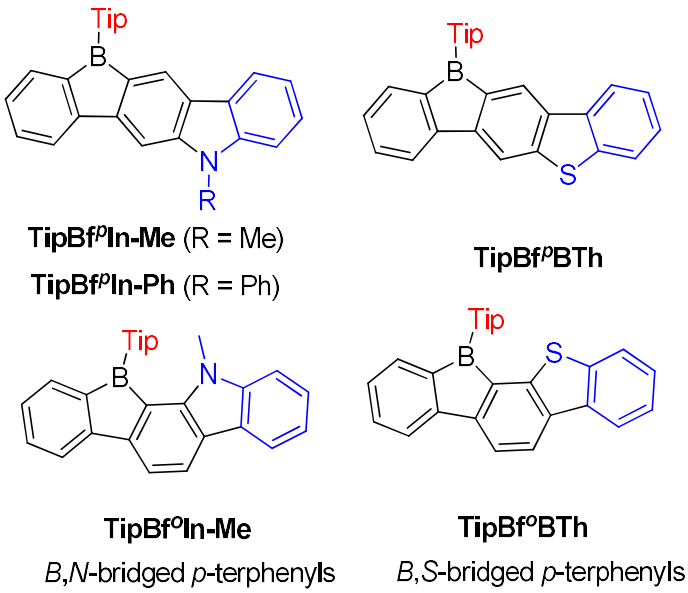

Scheme 2.11. Ladder-type *B*,*N*-bridged and *B*,*S*-bridged *p*-terphenyls.

Both absorption and emission show negligible solvatochromism for these ladder-type boroles which indicates only a small polarity change between the ground state and the excited state. No difference of absorption and emission was observed between *N*-methyl **TipBf^{p}In-Me** and *N*-phenyl **TipBf^{p}In-Ph**, which may be due to the large torsion angle between the phenyl group and pyrrole. Compared to **TipBf^{p}In-Me**, **TipBf^{o}In-Me** shows a red shift in both absorption and emission which was attributed to the lower LUMO energy as evidenced by computational studies. Compared with carbazole-fused 9-borafluorenes, the benzothiophene-fused 9-borafluorenes show only slight hypochromism of both absorption and emission, but double the quantum yields. In

addition to the broad use of 9-borafluorenes as F^- sensors, the **TipBf*p*BTh** was applied as a Hg^{2+} sensor due to its high affinity for Hg^{2+} due to the S atom. Additionally, all these ladder-type boroles exhibit considerable potential for application as bipolar electron-transporting materials.

In contrast to the incorporation of donating groups at the 9-borafluorene core, more recently, Marder and co-workers reported a **^{F}Xyl^{CF3}Bf** with four inductively withdrawing CF_3 groups attached to the *o*- and *p*-positions at the biphenyl core (Scheme 2.12).[118] To investigate the effect of substitution at the *p'*-position in **^{F}Xyl^{CF3}Bf**, **^{F}Mes^{CF3}Bf** with a CF_3 acceptor at the *p'*-position and ***p'*NMe$_2$^{F}Xyl^{CF3}Bf** with an NMe_2 donor at the *p'*-position were also synthesized. Although examples appear in patents,[169] ***p'*NMe$_2$^{F}Xyl^{CF3}Bf** is the only example of a 3-coordinate 9-borafluorene which incorporated a donor at the *exo*-aryl to have been reported in a paper.[118]

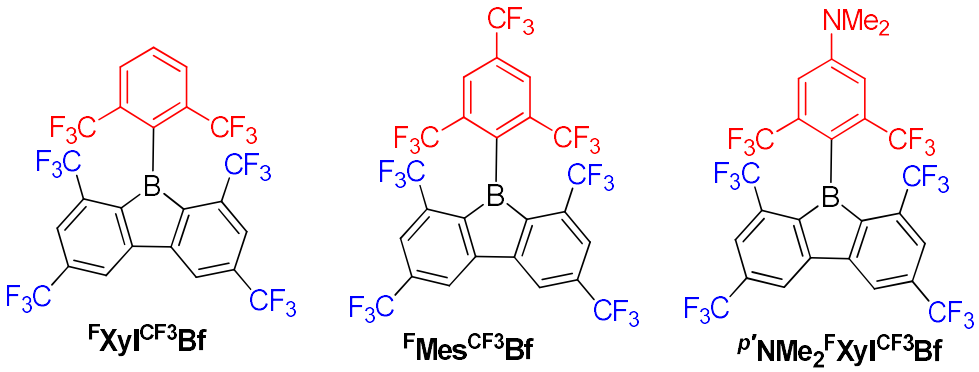

Scheme 2.12. 9-Borafluorenes with four CF_3 groups at the biphenyl main core.

Due to the strong electron withdrawing ability of the four CF_3 groups at the 9-borafluorene core, the electron accepting ability of boron was greatly enhanced, as evidenced by cyclic voltammetry (see below in the electrochemistry section). With the extra protection of two CF_3 groups at the *o*-positions, **^{F}Xyl^{CF3}Bf** and **^{F}Mes^{CF3}Bf** are more stable than **^{F}MesBf**. Surprisingly, although ***p'*NMe$_2$^{F}Xyl^{CF3}Bf** has a strong donor at the *p'*-position, its absorption appears in the same region as those of **^{F}Xyl^{CF3}Bf** and **^{F}Mes^{CF3}Bf**

(this could be also caused by the weak absorption of $^{p'}$**NMe$_2$^{F}Xyl^{CF3}Bf** in the lower energy region), but the emission shows a large red shift (^{F}**Xyl^{CF3}Bf**: λ_{em} = 510 nm; ^{F}**Mes^{CF3}Bf**: λ_{em} = 521 nm; $^{p'}$**NMe$_2$^{F}Xyl^{CF3}Bf**: λ_{em} = 627 nm in hexane). Both ^{F}**Xyl^{CF3}Bf** (τ_F = 151 ns) and ^{F}**Mes^{CF3}Bf** (τ_F = 224 ns) exhibit very long fluorescence lifetimes in hexane but behave differently; $^{p'}$**NMe$_2$^{F}Xyl^{CF3}Bf** exhibits two radiative processes (τ_p = 9.2 ns and τ_d = 1.6 µs), the latter resulting from thermally activated delayed fluorescence (TADF). $^{p'}$**NMe$_2$^{F}Xyl^{CF3}Bf** is the first example of a borafluorene to exhibit TADF, but the rather low quantum yield (Φ_F = 0.03 in hexane) limits its further application. In contrast to the low quantum yield of $^{p'}$**NMe$_2$^{F}Xyl^{CF3}Bf** in hexane, ^{F}**Xyl^{CF3}Bf** (Φ_F = 0.30) and ^{F}**Mes^{CF3}Bf** (Φ_F = 0.37) exhibit relatively high quantum yields. Theoretical studies indicate that the LUMO of $^{p'}$**NMe$_2$^{F}Xyl^{CF3}Bf** is located on the biphenyl core with a large contribution from the boron atom, whereas the HOMO is located on the *exo*-aryl moiety. Thus, the HOMO to LUMO transition is an intramolecular charge transfer (ICT) process with a small overlap coefficient (Λ) which also fits the requirement for TADF.

2.2.5 Heteroarene-fused boroles

In 2011, the Yamaguchi group fused electron-rich thiophene(s) onto boroles by stepwise substitution reactions and synthesized **TipD^{TMS}ThB**, **TipBThBB**, and **TipDBThB** (Scheme 2.13).[121] Surprisingly, these three Tip-protected thiophene-fused boroles are air- and moisture-sensitive. Considering that **TipBf** is stable enough to be purified in air, this instability is opposite an expectation that applying electron-rich thiophene would decrease the Lewis acidity of boron to form more stable compounds. The antiaromaticity of the borole rings was evaluated by DFT calculations of the nucleus-independent chemical shifts (NICS) values (Table 2.3).

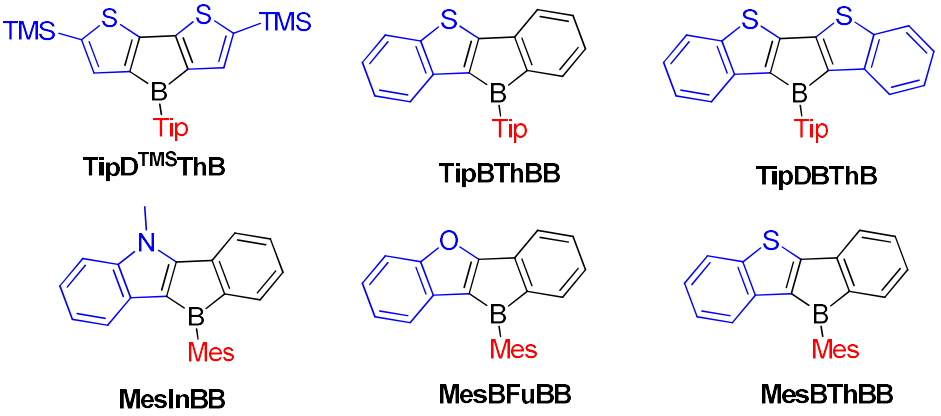

Scheme 2.13. Electron-rich heteroarene(s)-fused boroles.

The NICS(1)$_{ZZ}$ (ppm) values increase in the order **TipBf** < **TipB** < **TipBThBB** < **TipD^{TMS}ThB** < **TipDBThB**. Thus, the biphenyl-fused borole, **TipBf** exhibits a less antiaromatic character whereas the antiaromaticity of the electron-rich thiophene-fused boroles is enhanced, and is even higher than that of the non-fused "free" borole (1-Tip-1-borole, **TipB**), as suggested by the NICS(1)$_{ZZ}$ values. This result is also opposite to the conventional understanding that fusing electron-rich aromatic arenes decreases the antiaromaticity of the 5-membered borole ring.[170, 171]

Table 2.3. NICS(1)$_{zz}$ (ppm) values for the 5-membered borole rings of (hetero)arene-fused boroles.

	NICS(1)$_{zz}$		NICS(1)$_{zz}$		NICS(1)$_{zz}$
$^{p'}$**NMe$_2$^{F}Xyl^{CF3}Bf**[118]	+20.0	^{F}**Xyl^{CF3}Bf**[118]	+20.2	^{F}**Mes^{CF3}Bf**[118]	+20.7
TipDBf[123]	+21.8	**MesBf**[144]	+23.0	**TipBf^{o}In-Me**[166]	+24.2
TipBf[121]	+24.5	**TipBf^{p}In-Me**[166]	+24.8	**TipBf^{p}In-Ph**[166]	+25.4
MesBFuBB[144]	+27.6	**MesB**[144]	+28.3	**TipB**[121]	+29.4
TipBThBB[121]	+30.1	**MesBThBB**[144]	+30.4	**MesInBB**[144]	+31.7
TipD^{TMS}ThB[121]	+40.3	**TipDBThB**[121]	+45.3		

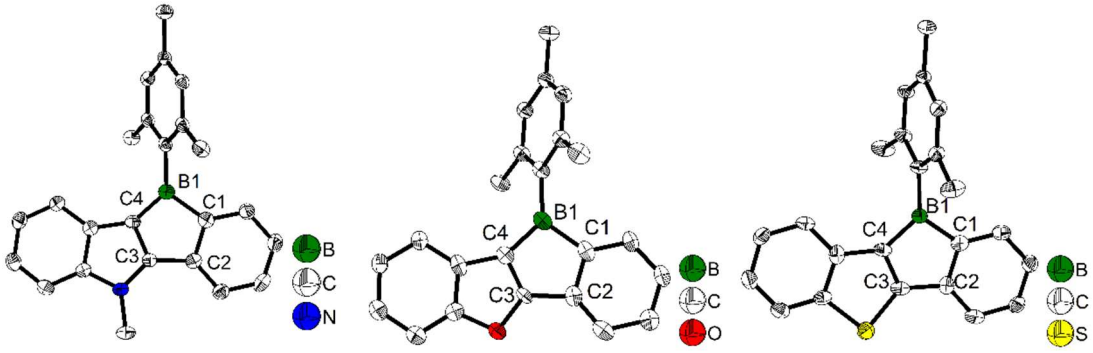

Figure 2.4. Molecular structures of **MesInBB** (left), **MesBFuBB** (middle), and **MesBThBB** (right). Selected bond lengths (Å): **MesInBB**: B1–C1 1.613(3), C1–C2 1.419(3), C2–C3 1.471(3), C3–C4 1.394(3), C4–B1 1.528(3). **MesBFuBB**: B1–C1 1.612(4), C1–C2 1.408(4), C2–C3 1.490(3), C3–C4 1.347(3), C4–B1 1.549(4). **MesBThBB**: B1–C1 1.595(5), C1–C2 1.400(5), C2–C3 1.495(5), C3–C4 1.375(5), C4–B1 1.554(5).

To study what governs the antiaromaticity and Lewis acidity of heteroarene-fused boroles, another three heteroarene-fused boroles, **MesInBB**, **MesBFuBB** and **MesBThBB** were synthesized (Scheme 2.13). NICS calculations were conducted with the geometries derived from the crystal structures of these heteroarene-fused boroles (Figure 2.4). The conclusion reached was that the lesser extent of bond alternation in the 5-membered borole ring in heteroarene-fused boroles is responsible for the high degree of antiaromaticity. Theoretical and experimental studies suggest that the LUMO energy of these heteroarene-fused boroles are relevant to the antiaromaticity, which also

linearly correlates with their Lewis acidities.[144]

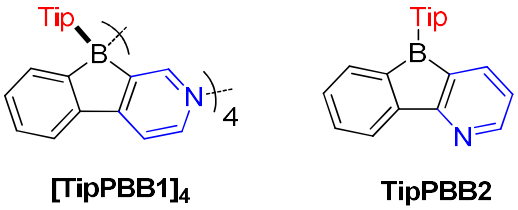

Scheme 2.14. Electron-poor pyridyl-fused boroles.

In contrast to the Yamaguchi group's fused boroles with electron-rich heteroarene(s), more recently, Marder and co-workers switched to the electron-poor pyridine to synthesize phenylpyridyl-fused boroles (Scheme 2.14).[168] Using 4-phenylpyridine to prepare a fused borole, **[TipPBB1]**$_4$ was obtained as a white solid and adopts a unique coordination mode, forming a tetramer with a central cavity in both the solid state (X-ray diffraction, Figure 2.5) and solution (^{1}H diffusion-ordered spectroscopy (^{1}H DOSY)). The coordination mode of **[TipPBB1]**$_4$ is similar to that of dimethyl(3-pyridyl)borane and diethyl(3-pyridyl)borane.[172-174] The B–N bond lengths of **[TipPBB1]**$_4$ (1.644(2)–1.655(2) Å) are comparable to those of pentaphenylborole•2,6-lutidine (1.6567(3) Å)[175] and sterically hindered dibenzoborole•pyridine (1.638(3) Å);[119] however, in contrast to both pentaphenylborole•2,6-lutidine and the sterically hindered dibenzoborole•pyridine which dissociate in solution at room temperature, the **[TipPBB1]**$_4$ persists as a tetramer in C_6D_6 even at 50 °C (^{1}H DOSY). By switching 4-phenylpyridine to 2-phenylpyridine, **TipPBB2** was prepared and isolated as a light yellow solid. The boron center of **TipPBB2** is 3-coordinate in solution but 4-coordinate in the solid state, as evident from solid-state ^{11}B{H} RSHE/MAS NMR measurements. The difference is ascribed to the steric protection of the pyridine nitrogen by the attached phenyl group at the 2-position.

Due to the inherent electron withdrawing properties of pyridine, the electron accepting

ability of **TipPBB2** is enhanced (see electrochemical section below). The lowest energy absorption maximum of **[TipPBBI]**$_4$ appears at 322 nm in hexane, which is blue shifted compared to those of **TipPBB2** (375 nm) and other 3-coordinate 9-borafluorenes. Compared with other Tip-protected 9-borafluorenes, **TipPBB2** exhibits a relatively high quantum yield (0.34 in hexane) in solution and shows an interesting dual fluorescence property. Two lifetimes are observed at the same emission wavelength of 520 nm. The authors suggested that the dual fluorescence in solution is caused by an equilibrium between the free 3-coordinate **TipPBB2** and a weak intermolecular coordination adduct of **TipPBB2**. This hypothesis was further supported by lifetime measurements at different concentrations, low temperature excitation spectra, low temperature ^{1}H NMR spectra and lifetime measurements upon addition of DMAP to a solution of **TipPBB2** to simulate the 4-coordiante **TipPBB2** species. Thus, this dual fluorescence is different from dual fluorescence induced by B–N dissociation in the excited state.[176] Interestingly, the ratios of the relative percentage of the two lifetimes shows a linear relationship with temperature, thus **TipPBB2** could serve as a fluorescent thermometer.

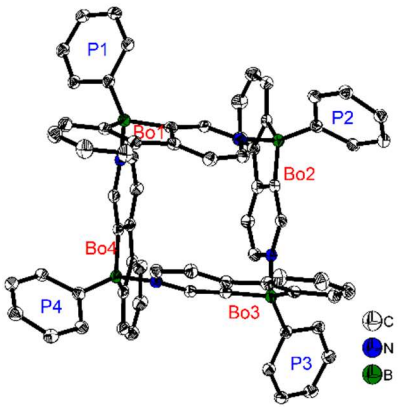

Figure 2.5. Molecular structure of **[TipPBBI]**$_4$. H atoms, *iso*propyl groups, and C_6D_6 solvent molecules are omitted for clarity. 'Bo' and 'P' denote the planes of the phenylpyridyl-fused borole and the Tip phenyl groups, respectively. Selected bond lengths (Å) and angles (°): B_{Bo1}–N_{Bo4} 1.655(2), B_{Bo2}–N_{Bo1} 1.652(2), B_{Bo3}–N_{Bo2} 1.644(2), B_{Bo4}–N_{Bo3} 1.644(2), B_{Bo1}–B_{Bo2} 5.420(2), B_{Bo2}–B_{Bo3} 5.365(2), B_{Bo3}–B_{Bo4} 5.407(2), B_{Bo4}–B_{Bo1} 5.402(2), ∠Bo1–Bo2 89.70(2), ∠Bo2–Bo3 81.78(2), ∠Bo3–Bo4 89.22(2), ∠Bo4–Bo1 78.44(2), ∠Bo1–Bo3 33.29(3), ∠Bo2–Bo4 33.21(2).

2.2.6 Intramolecular dative bond in 9-borafluorenes

Instead of using bulky Tip or Mes* as the protecting group at boron, Chujo and co-workers used the Mamx ligand (Mamx = 2,4-di-*tert*-butyl-6-[(dimethylamino)methyl]phenyl) as the steric protecting group at boron in 9-borafluorenes (Scheme 2.15).[177] The X-ray crystal structure of **MamxBf** indicates that the nitrogen atom coordinates to the boron atom with a B–N bond length of 1.712 Å. The ^{11}B NMR spectrum shows a peak at 5.96 ppm, which is in the typical range for 4-coordinate boron. With the double protection of steric hindrance and nitrogen atom coordination to boron, **MamxBf** is stable to moisture and can be purified in air. The lowest energy absorption of **MamxBf** is at ca. 280 nm and it exhibits a weak emission at ca. 360 nm. Interestingly, by addition of $B(C_6F_5)_3$ to a benzene solution of **MamxBf**, phosphorescence (τ_p = 8.95 μs (69%)) with a peak at 597 nm was observed at room temperature, which the authors suggest is caused by triplet exciplexes. Theoretical analysis for the excited state of **MamxBf** suggests that this robust B–N coordination in the ground state is cleaved in the S_1 state. This B–N bond cleavage in the excited state is also suggested to be responsible for the weak emission of **MamxBf**.

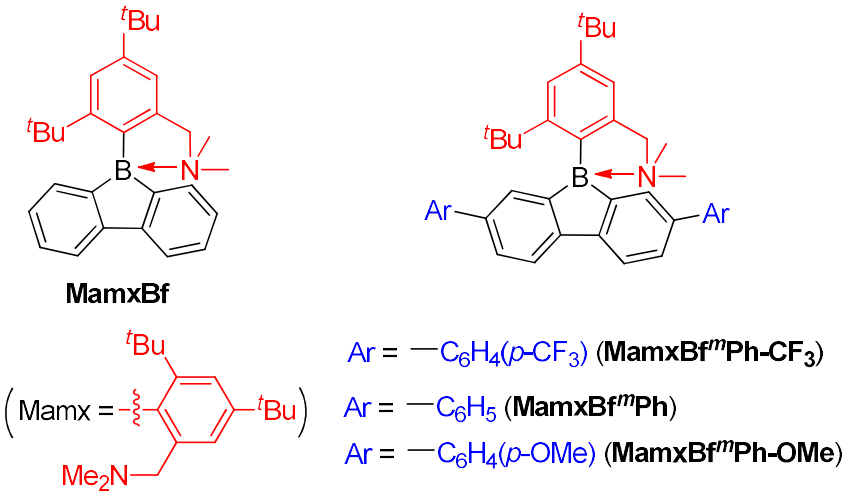

Scheme 2.15. 9-Borafluorenes with Mamx as the *exo*-aryl group.

By incorporating electron withdrawing or electron donating groups at the biphenyl core, the energy levels of 9-Mamx-9-borafluorenes are modulated and emission from bond-cleavage-induced intramolecular charge transfer (BICT) was realized. **MamxBf^{m}Ph-CF$_3$** has two electron withdrawing trifluoromethylphenyl groups at the biphenyl core and it shows a single emission with a peak at 373 nm, which is similar to that of **MamxBf**. Changing the electron withdrawing trifluoromethylphenyl groups to electron-neutral phenyl groups or electron donating methoxyphenyl groups in **MamxBf^{m}Ph** and **MamxBf^{m}Ph-OMe**, respectively, result in similar shaped dual emissions (ca. 330 nm and ca. 520 nm, respectively), which is in contrast to the single emission of **MamxBf^{m}Ph-CF$_3$** and **MamxBf** (Scheme 2.15). The authors concluded that by incorporation of electron donating groups at the biphenyl core, the boron atom exhibits a more negative charge, and a BICT process thus occurs which results in dual emission. Theorical calculations further support the BICT transition. The short wavelength emission was assigned to a locally-excited (LE) emission from a π – π* transition and the long wavelength emission was assigned to the BICT transition. The BICT emission is highly sensitive to the solvent viscosity, and thus **MamxBf^{m}Ph-OMe** can be applied as a ratiometric sensor.[178]

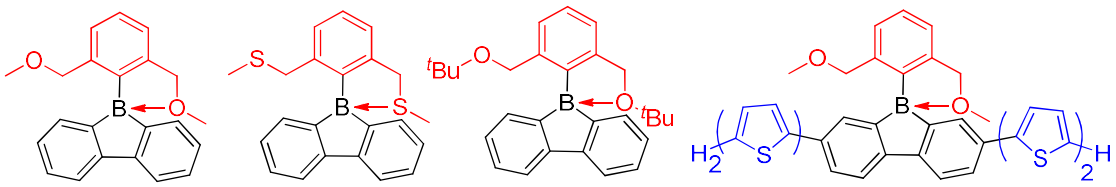

Scheme 2.16. Intramolecular O→B or S→B dative bond of 9-borafluorenes.

By exchanging the strongly donating dimethylamino group with the weakly donating methoxy group, Rupar and co-workers synthesized **MOMPhBf** (Scheme 2.16).[179] **MOMPhBf** is a colorless powder which is air-stable in the solid state and solution. The absorption maximum appears at 284 nm and the emission maximum appears at 536 nm

with a long lifetime (τ_F = 122 ns) in CH_2Cl_2. This is an extraordinary large Stokes shift (16500 cm^{-1}) for a small molecule, in fact, it is the largest Stoke shifts ever reported.[180] This large Stokes shift is caused by the photodissociation of the B–O dative bond in the excited state, which is further supported by theoretical studies. By changing the methoxy groups to methylthio groups or *tert*-butoxy groups, **MSMPhBf** and **^{t}BuOMPhBf** were synthesized, respectively. **MSMPhBf** and **^{t}BuOMPhBf** show nearly identical structural and optical properties to that of **MOMPhBf**. By incorporation of two bithiophene groups as donors at the biphenyl core of **MOMPhBf**, the photophysical properties change significantly. The lowest energy absorption of **MOMPhBf^m(BT)$_2$** red shifts to 408 nm and the compound exhibits dual emission with peaks at 446 (τ_F = 0.5 ns) and 639 nm (τ_F = 4.38 ns). DFT calculations indicate that two stable structures are present in the excited state: in one, the B–O bond remains intact (4-coordinate excited state) and in the other one, the B–O bond dissociates (3-coordinate excited state). The shorter wavelength emission exhibits the shorter lifetime and is assigned to the emission from the 4-coordinate S_1 state. The long wavelength emission exhibits the longer lifetime and is assigned to the 3-coordinate S_1 state.

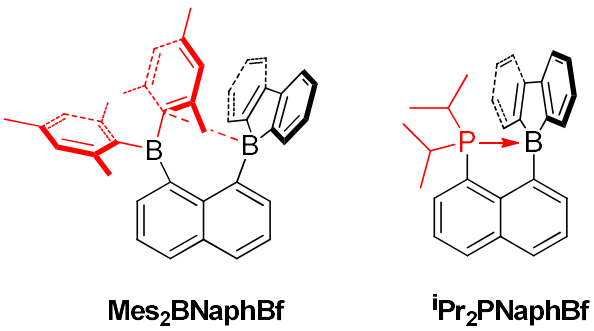

Scheme 2.17. Intramolecular C→B or P→B dative bonds in 9-borafluorenes.

The Gabbaï group synthesized a diborane (**Mes$_2$BNaphBf**) with a $BMes_2$ group and a 9-borafluorene group at the 1 and 8 position of a naphthalene, respectively (Scheme 2.17).[181] Interestingly, an interaction occurs between the boron atom of the 9-

borafluorene and one of the Mes groups. This interaction was confirmed by a short B–C distance (2.730(3) Å) between the boron atom of 9-borafluorene and the carbon atom of the Mes group which is connected to boron. Due to this interaction, the boron atom of the 9-borafluorene is slightly pyramidalized. By changing the $BMes_2$ group to a di*iso*propylphosphino group, Bourissou and co-workers synthesized the naphthyl-protected 9-borafluorene (**^{i}Pr$_2$PNaphBf**).[182] **^{i}Pr$_2$PNaphBf** is only stable under an inert atmosphere, but is much more stable than 9-(2-di*iso*propylphosphinophenyl)-9-borafluorene.[183, 184] The ^{11}B NMR signal appears at –8.5 ppm, confirming the presence of a P–B dative bond. The short P–B distance (2.011(2) Å) and the significant pyramidalization ($\Sigma_{C\text{-}B\text{-}C}$ = 338.45(5)°) of the boron confirmed the strong P→B interaction. This strong P→B interaction, even with fairly bulky substituents on the phosphine, indicates the flexibility of the system.

2.2.7 9-Borafluorene-based main chain polymers

By incorporating 3-coordinate boron atoms into the main chain of conjugated polymer systems, the π-systems are extended compared to the corresponding monomers, leading to different optical properties.[25] It could be envisaged that incorporation of more electron-deficient 9-borafluorenes into polymers will lead to interesting properties.[185] In 2008, Scherf and co-workers reported a co-polymer incorporating polyfluorenes and 9-borafluorenes in the main chain, and applied it as an anion sensor (Scheme 2.18).[186] Interestingly, the *para*-cyanophenyl group surprisingly stabilize the 9-borafluorene, supposedly providing good environmental stability. In contrast to the bulky Tip or ^{F}Mes groups, *para*-cyanophenyl is an "unprotected" phenyl group. Unfortunately, changing the *para*-cyanophenyl group to other "unprotected" phenyl groups provided unstable 9-borafluorenes. Recently, Rupar and co-workers tried to reinvestigate this compound, but although different techniques were applied, they could not reproduce the reported results.[45]

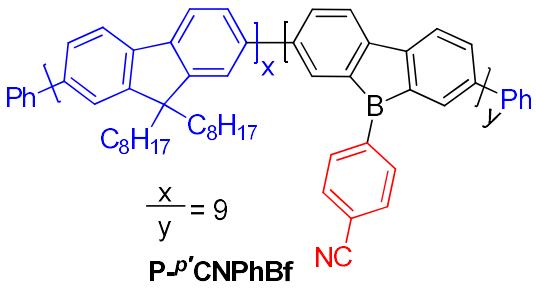

Scheme 2.18. Polymer of polyfluorenes with in-chain 9-borafluorenes.

The Rupar group adopted Yamamoto or Stille coupling reactions to synthesize two 9-Tip-9-borafluorenes based polymers (Scheme 2.19).[187] Compared with their monomeric precursor, a red shift of the absorption and emission was observed which can be ascribed to the extended conjugation in the polymers. Quantum yields of 0.50 (**P-TipBf**) and 0.28 (**P-TipBf^{m}V**) in solution were obtained. **P-TipBf** and **P-TipBf^{m}V** have a much smaller optical bandgap (calculated from the onset of the lowest energy absorption)

than polyfluorenes or polycarbazoles, which is mainly attributed to the lower LUMO energies of borafluorenes, and their lower LUMO energies were confirmed by measurements of their electrochemical reduction potentials and further supported by calculations. In solution, **P-TipBf** and **P-TipBf^{m}V** are suitable F^- sensors. In a film, **P-TipBf** can also be applied as a sensor for gaseous NH_3.

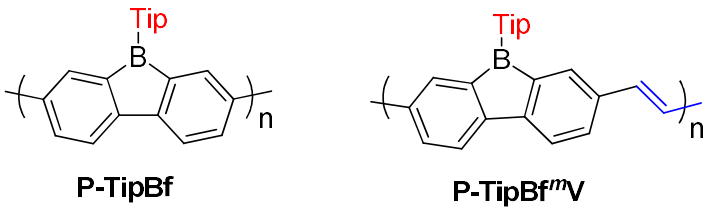

Scheme 2.19. 9-Tip-9-borafluorene-based polymers.

Chujo and co-workers prepared three 9-Mamx-9-borafluorene-based conjugated polymers by Suzuki-Miyaura cross-coupling reactions (Scheme 2.20).[188] These polymers are atmospherically stable, and contain 4-coordinate boron. Compared with the corresponding gallafluorene polymers, the borafluorene polymers show stronger electron accepting abilities and lower LUMO energy.

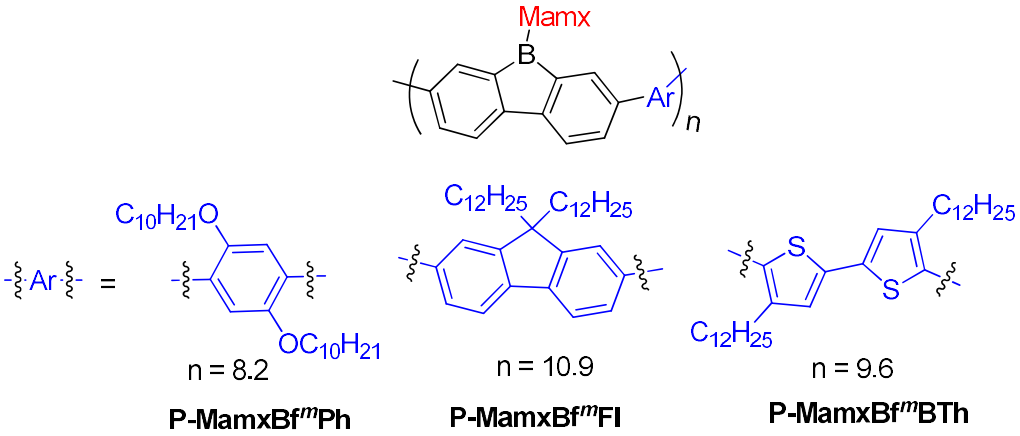

Scheme 2.20. 9-Mamx-9-borafluorene-based polymers.

2.2.8 Electrochemistry

In this section, selected fused boroles are chosen for comparison of their electron accepting abilities as determined by electrochemical measurements. Although many fused boroles can be reduced twice, here only the first reduction potentials are compared. The reduction potentials for all known aryl group protected fused boroles range from –1.1 to –2.5 V (Table 2.4). **PhBf**[156] exhibits a first reversible reduction potential at –2.16 V, which is in the same range as **TipBf** (–2.11 V[121] and –2.31 V[45] were obtained by two different groups) and **Mes*Bf** (–2.28 V).[142] After incorporation of donating groups (methoxy, amino, or thiophene) on the core of 9-borafluorene, the first reduction potentials of **TipBf^{p}(OMe)$_2$**,[45] **Mes*Bf^{m}(Ph$_2$NPh)$_2$**[142] and **Mes*Bf^{m}(BTh)$_2$**[142] do not change strongly, indicating that the donating groups have only a small effect on the electron accepting ability of boron in 9-borafluorenes.

By employing the electron withdrawing ^{F}Mes group as the *exo*-aryl group on a **Bf**, the electron accepting ability of **^{F}MesBf** was enhanced and the reduction potential shifts to –1.93 V.[45] The first reduction potential of **TipPBB2** ($E_{1/2}^{red}$ = –1.94 V)[168] is comparable to that of **^{F}MesBf**, which suggests that the effect of fusing pyridyl group onto boroles on their reducibility is comparable to that of the *exo*-^{F}Mes group in 9-borafluorenes. **TipDBThB**[121] exhibits a first reversible reduction potential of –1.72 V, which is less negative than the electron withdrawing group-functionalized **^{F}MesBf** and **TipPBB2**. The strong electron accepting property of **TipDBThB** is attributed to its enhanced antiaromaticity. **TipDBf**[124] and the biphenyl-linked diborole **BPhDBf** (Scheme 2.21)[129, 189] exhibit much less negative half reduction potentials of –1.51 and –1.49 V, respectively. The strong electron accepting ability of **TipDBf** and **BPhDBf** is due to the two boron centers being linked to a π-conjugated unit. This enhancement is also observed in triarylboranes with two or more boron centers.[139, 190-192] By incorporation of four additional CF_3 groups at the biphenyl core, the first half reduction potentials of **^{F}Xyl^{CF3}Bf** and **^{F}Mes^{CF3}Bf** shift to –1.21 and –1.13 V, respectively.[118] Surprisingly, although **^{F}Xyl^{CF3}Bf** and **^{F}Mes^{CF3}Bf** exhibit extraordinarily low reduction potentials, both are stable in air.

Table 2.4. First and second reduction potentials of (hetero)arene-fused boroles.

compound	$E_{1/2}$/ V (1)	E_{pc}/ V (2)	conditions
PhBf[156]	–2.16	-	0.1 M [^{n}Bu$_4$N][B(C$_6$F$_5$)$_4$] in THF
TipBf[121]	–2.11	–3.05	0.1 M[^{n}Bu$_4$N][PF$_6$] in THF
TipBf[45]	–2.31	-	0.1 M[^{n}Bu$_4$N][PF$_6$] in THF
Mes*Bf[142]	–2.28	-	0.1 M [^{n}Bu$_4$N][ClO$_4$] in THF
TipBf^p(OMe)$_2$[45]	–2.36	-	0.1 M[^{n}Bu$_4$N][PF$_6$] in THF
Mes*Bf^m(PhNPh$_2$)$_2$[142]	–2.04	–2.70 (r)	0.1 M [^{n}Bu$_4$N][ClO$_4$] in THF
Mes*Bf^m(BTh)$_2$[142]	–2.19	–3.00	0.1 M [^{n}Bu$_4$N][ClO$_4$] in THF
^{F}MesBf[45]	–1.93	-	0.1 M[^{n}Bu$_4$N][PF$_6$] in THF
TipPBB2[168]	–1.94	–2.90	0.1 M[^{n}Bu$_4$N][PF$_6$] in THF
TipD^{TMS}ThB[45]	–1.98	–2.79	0.1 M[^{n}Bu$_4$N][PF$_6$] in THF
TipBThBB[45]	–1.96	–2.89	0.1 M[^{n}Bu$_4$N][PF$_6$] in THF
TipDBThB[121]	–1.72	–2.61	0.1 M[^{n}Bu$_4$N][PF$_6$] in THF
MesInBB[144]	–2.25	–3.04	0.1 M [^{n}Bu$_4$N][PF$_6$] in CH$_2$Cl$_2$
MesBFuBB[144]	–1.97	–2.85	0.1 M [^{n}Bu$_4$N][PF$_6$] in CH$_2$Cl$_2$
MesBThBB[144]	–1.89	–2.78	0.1 M [^{n}Bu$_4$N][PF$_6$] in CH$_2$Cl$_2$
TipDBf[124]	–1.51	–2.42	0.1 M[^{n}Bu$_4$N][PF$_6$] in THF
BPhDBf[189]	–1.49	–1.75	0.1 M[^{n}Bu$_4$N][PF$_6$] in THF
^{F}Xyl^{CF3}Bf[118]	–1.21	–2.12	0.1 M [^{n}Bu$_4$N][PF$_6$] in CH$_2$Cl$_2$
^{F}Mes^{CF3}Bf[118]	–1.13	–2.04	0.1 M [^{n}Bu$_4$N][PF$_6$] in CH$_2$Cl$_2$
$^{p'}$NMe$_2$FXyl^{CF3}Bf[118]	–1.28	–2.15	0.1 M [^{n}Bu$_4$N][PF$_6$] in CH$_2$Cl$_2$
^{F}Ph^{F}Bf•THF[156]	–2.42 (ir)	-	0.1 M [^{n}Bu$_4$N][B(C$_6$F$_5$)$_4$] in THF
^{i}Pr$_2$NBf[45]	–2.95	-	0.1 M[^{n}Bu$_4$N][PF$_6$] in THF

Attempts to use noncoordinating solvents (CH_2Cl_2 and *α,α,α*-trifluorotoluene) for the cyclic voltammetry study of **^{F}Ph^{F}Bf** were unsuccessful, so THF was employed.[156] An irreversible process with a reduction potential at –2.42 V vs. Fc/Fc$^+$ was observed. Such a negative reduction potential, which is even more negative than that of **PhBf**, was not expected. The authors suggested that the reduction process actually takes place at the fluorinated aromatic framework, not at the boron center due to the formation of **^{F}Ph^{F}Bf**•THF in THF.[156] **^{i}Pr$_2$NBf** has the most negative reversible half reduction potential of –2.95 V.[45] The weak electron accepting ability of **^{i}Pr$_2$NBf** is caused by the electron-rich nitrogen atom π-backbonding to the vacant p_z-orbital of boron.

2.2.9 Chemical reduction of fused boroles

Boroles readily accept one electron to form a radical anion or two successive electrons to give a dianion. The chemical reduction of non-fused "free" boroles and some 9-boraflurenes was reviewed by the Braunschweig group in 2011[99] and 2016.[100] Here we focus only on fused boroles.

One electron reduction of 9-boraflurene leads to a radical anion. In 2008, the Yamaguchi group reduced **Mes*Bf** with potassium in THF and the EPR signal of the reduced **Mes*Bf** exhibits an eleven-line signal (g = 2.002). According to the simulation of the spectrum, the spin density on boron is estimated to be 0.21, indicating delocalization over the biphenylene unit of the 9-borafluorene. A similar reaction was also carried out with **Mes*Bf^m(BTh)$_2$** and a spin density of 0.18 on boron was estimated by simulation. The lower spin density on boron in **Mes*Bf^m(BTh)$_2$** suggested that it is delocalized over the bithiophene skeleton.[142] The Piers group synthesized the ladder-type diborole **TipDBf** which exhibits a first reversible reduction at –1.51 V. Such a small negative reduction potential makes it possible to perform a one electron reduction with bis(pentamethylcyclopentadienyl)cobalt(II) ($E^{0'}$(Cp*$_2$Co) = –1.9 V).[193] Isolated **[TipDBf]**[CoCp*$_2$] is a deep blue solid (Scheme 2.21).[124] The C1–C1' distance in **[TipDBf]**[CoCp*$_2$] of 1.410(3) Å is significantly longer than that of its neutral form for which d(C1–C1') = 1.367(5) Å while d(B1-C1) of **[TipDBf]**[CoCp*$_2$] with 1.524(3) Å is significantly shorter compared to 1.571(4) Å for **TipDBf**. A detailed inspection of the structure combined with a theoretical analysis shows that there is still a high degree of delocalization of the unpaired electron throughout the whole π-system.

In 2014, Wagner and co-workers linked two 9-borafluorenes by a biphenyl (**BPhDBf**) and carried out the one electron reduction with lithium naphthalenide in toluene (Scheme 2.21),[189] obtaining **BPhDBf**Li•(THF)$_4$ × 0.5$C_{10}H_8$ as black crystals. Single crystal X-ray diffraction shows that the distance between the two boron centers of **BPhDBf**Li•(THF)$_4$ × 0.5$C_{10}H_8$ is 2.265(4) Å, which is 0.655 Å shorter than that in its precursor **BPhDBf** (2.920(6) Å) (Figure 2.6),[128] and lies between those of **BPhDBf** (no

B–B bond) and $[\mathbf{HBf\text{-}HBf}]^{2-}$ (1.83(2) Å) (B–B two electron σ-bond).[194] In **BPhDBf**Li•$(THF)_4 \times 0.5C_{10}H_8$, only a moderate pyramidalization of the two boron centers was observed ($\Sigma_{C\text{-}B\text{-}C}$ = 351.6° and 353.0°). The EPR spectrum of **BPhDBf**Li•$(THF)_4 \times 0.5C_{10}H_8$ in THF exhibits a seven-line signal. The spectrum was successfully simulated, assuming the two boron nuclei to be magnetically equivalent ($a(^{11}B)$ = 4.8 ± 0.1 G and $a(^{10}B)$ = 1.6 ± 0.1 G), and the small $a(^{11}B)$ value strongly supports the contribution of the unpaired electron to a $2p_z\sigma$(B•B) bond. The computed SOMO and the localization of the spin-density mainly between the two boron centers further confirm the existence of a B•B one electron σ-bond. **BPhDBf**Li•$(THF)_4 \times 0.5C_{10}H_8$ is the first crystallographic characterized compound to have a B•B one electron σ-bond.

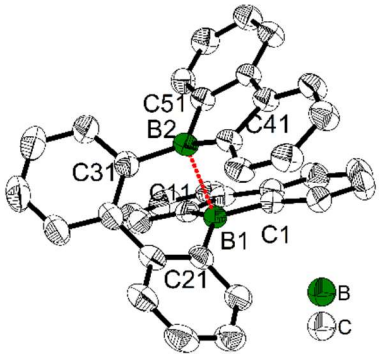

Figure 2.6. Molecular structure of $[\mathbf{BPhDBf}]^{\bullet-}$. Hydrogen atoms, THF, $C_{10}H_8$ and the lithium cation are omitted for clarity. The dashed red line indicates the one-electron σ-bond. Selected bond lengths (Å) and angles (°): B1–B2 2.265(4), B1–C1 1.579(3), B1–C11 1.582(3), B1–C21 1.583(3), B2–C41 1.582(3), B2–C51 1.578(3), B2–C31 1.576(3), sum of ∠C–B1–C 351.6, sum of ∠C–B2–C 353.0.

The borafluorene $^{F}\mathbf{Mes}^{CF3}\mathbf{Bf}$ synthesized by Marder and co-workers exhibits a first half-reduction potential at –1.13 V, and thus can be reduced by Cp_2Co ($E^{0'}(Cp_2Co)$ = –1.3 V).[193] $[^{F}\mathbf{Mes}^{CF3}\mathbf{Bf}][Cp_2Co]$ was obtained as a dark purple solid with a complex EPR signal centered at g_{iso} = 2.004 in THF, consisting of hyperfine splitting to boron ($a(^{11}B)$ = 3.3 G), the fluorine atoms ($a(^{19}F)$ = 11.3 and 6.0 G) from the CF_3 groups at the 9-borafluorene core, and the hydrogen atoms ($a(^{1}H)$ = 6.1 and 2.9 G) at the 9-borafluorene core. The

relatively large proton and fluorine hyperfine couplings, in contrast to the relatively small boron hyperfine coupling, indicates that the spin density is delocalized significantly over the biphenyl core of the 9-borafluorene. Compared to the crystal structure of neutral ^{F}**Mes**^{CF3}**Bf**, changes in bond lengths of [^{F}**Mes**^{CF3}**Bf**][Cp_2Co] were mainly observed on the 9-borafluorene core, indicating delocalization of the unpaired electron on the 9-borafluorene core, with no contribution from the *exo*-aryl ^{F}Mes group.[118]

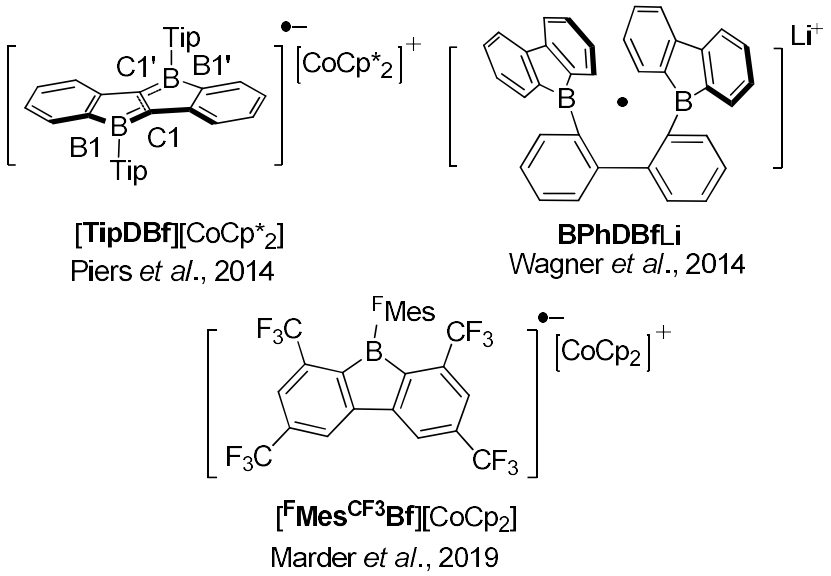

Scheme 2.21. One electron reduced arene-fused boroles.

The discovery and study of 9-borafluorenyl dianions were reported earlier than that of the radical anions of 9-borafluorenes. In 1996, during an investigation of the reduction of sterically encumbered arylboron dihalides, the Power group isolated a bislithium-9-borafluorenyl complex **MeBf**Li_2•$(Et_2O)_2$ (Scheme 2.22),[194] obtained directly by treatment of 2,6-$Mes_2C_6H_3BX_2$ (X = Br or Cl) with an excess of lithium in Et_2O. **MeBf**Li_2•$(Et_2O)_2$ is a red solid with a ^{11}B NMR (C_6D_6) chemical shift of 14.3 ppm (s, $W_{1/2}$ ≈ 380 Hz). **MeBf**Li_2•$(Et_2O)_2$ was the first structurally characterized 9-borafluorenyl dianion, the core of which is still planar. The lithium ions are solvated by diethyl ether

and adopt an η^5-coordination to the 5-membered borole ring. Reduction of 2,6-$Mes_2C_6H_3BBr_2$ with lithium in benzene over 5 days and extraction with ether/hexane gave a dimer that has a structure analogous to that of **MeBf**Li_2•$(Et_2O)_2$. **^{t}Bu^{m}TerBf**Li_2•$(Et_2O)_2$[119] and **PhBf**Li_2•$(THF)_n$[115] were isolated by treatment of the corresponding 9-borafluorenes with lithium in diethyl ether or THF. **^{t}Bu^{m}TerBf**Li_2•$(Et_2O)_2$ is a deep red, almost black solid with a ^{11}B NMR (C_6D_6) chemical shift of 13.6 ppm (s, $W_{1/2} \approx 430$ Hz). The two lithium ions are also solvated by diethyl ether and are situated almost symmetrically above and below of the 5-membered borole core. The ^{11}B NMR (d_8-THF) chemical shift of **PhBf**Li_2•$(THF)_n$ shows a sharp peak at 6.3 ppm. By treatment of diborole **TipDBf** with potassium naphthalenide (2 eq.) in THF, **TipDBf**K_2•$(THF)_n$ was isolated as a red solid with a ^{11}B NMR (C_6D_6) chemical shift of 32.1 ppm. Its X-ray crystal structure indicates that the two potassium atoms are situated above and below the center of the dibenzo-fused-diborole core in a centrosymmetric arrangement.[124]

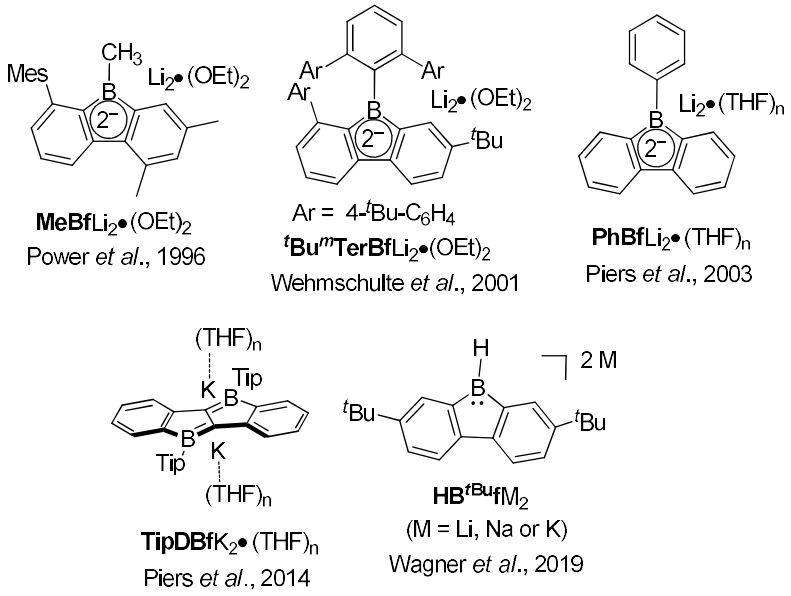

Scheme 2.22. Two electrons reduced arene-fused boroles.

The Wagner group investigated the redox chemistry of **HB$^{t\text{Bu}}$f** (Scheme 2.22).[195, 196]

Upon reduction, adducts arising from extensive structural rearrangement were formed and the corresponding mechanism was studied. Besides rearrangement adducts, recently, the dianion **[HB$^{t\mathrm{Bu}}$f]$^{2-}$** was isolated upon reduction of monomeric **HB$^{t\mathrm{Bu}}$f**•THF.[197] Treatment of **HB$^{t\mathrm{Bu}}$f** with lithium, sodium or potassium in THF led to the isolation of the respective dianions. **HB$^{t\mathrm{Bu}}$f**Li_2•$(THF)_3$ and **HB$^{t\mathrm{Bu}}$f**[Na•$(THF)_3$][Na•THF] were obtained as greenish-brown solids and **HB$^{t\mathrm{Bu}}$f**K_2•(THF) as a brown solid. The ^{11}B NMR (d_8-THF) chemical shifts are 3.7 ppm (s, $W_{1/2}$ ≈ 290 Hz, **HB$^{t\mathrm{Bu}}$f**Li_2•$(THF)_3$), 3.9 ppm (s, $W_{1/2}$ ≈ 290 Hz, **HB$^{t\mathrm{Bu}}$f**[Na•$(THF)_3$][Na•THF]) and 8.0 ppm (s, $W_{1/2}$ ≈ 360 Hz, **HB$^{t\mathrm{Bu}}$f**K_2•(THF)). From a comparison of the bond lengths of the computed structure of neutral **HB$^{t\mathrm{Bu}}$f** and of the reduced form **HB$^{t\mathrm{Bu}}$f**[Na•$(THF)_3$][Na•THF], the authors drew the conclusion that the two added electrons are delocalized over the 9-borafluorene core, rather than being localized at the p_z-orbital of boron. **[HB$^{t\mathrm{Bu}}$f]$^{2-}$** is the first example of a hydride ligand-stabilized **[Bflu]**$^-$ anion. Due to the easy abstraction of the hydride, **[HB$^{t\mathrm{Bu}}$f]$^{2-}$** is a surrogate of a nucleophilic **[Bflu]**$^-$ anion. The reaction of **[HB$^{t\mathrm{Bu}}$f]$^{2-}$** with MeI and Et_3SiCl further proves that **[HB$^{t\mathrm{Bu}}$f]$^{2-}$** can be applied as a **[Bflu]**$^-$ anion. At the same time, radical reactivity of **[HB$^{t\mathrm{Bu}}$f]$^{2-}$** was found, e.g., by the reaction of **[HB$^{t\mathrm{Bu}}$f]$^{2-}$** with Me_3SnCl or (bromomethyl)cyclopropane.

2.2.10 Three-coordinate borafluorenium cations

Instead of adding electrons to **Bf**s in a reduction process, another interesting topic is extracting an anion from 3-coordinate **Bf** to generate a 3-coordinate borafluorenium cation. In 1985, Nöth and co-workers applied $GaCl_3$ and $AlCl_3$ as a Cl^- acceptor for the pyridine adduct of **ClBf** and the acridine adduct of **ClBf** (Scheme 2.23).[198] Both [**PyBf**][$GaCl_4$] and [**AcrBf**][$GaCl_4$] are red solids. Due to the insolubility of [**PyBf**][$GaCl_4$] in most solvents, the only direct proof of the formation of [**PyBf**][$GaCl_4$] is its IR spectrum which exhibits a strong band at 373 cm^{-1}. This band is in the typical range for ν_{abs} ($GaCl_4$).[199] The structure of [**AcrBf**][$GaCl_4$] was confirmed by single crystal X-ray diffraction, but without further characterization or study.

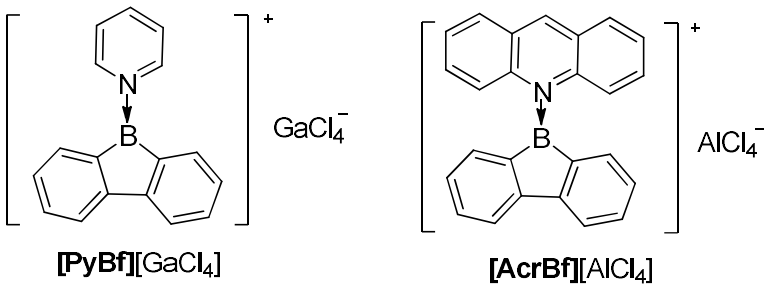

Scheme 2.23. Pyridine or acridine coordinated borafluorenium cations.

Interested in the properties of borafluorenium cations,[65] more recently, Gilliard Jr. and co-workers extracted a bromide ion from carbene-stabilized **BrBf**s with $AgSbF_6$ and synthesized [**IPrBf**][SbF_6] and [^{Et2}**CAACBf**][SbF_6] (Scheme 2.24).[200] The ^{11}B NMR spectra of [**IPrBf**][SbF_6] and [^{Et2}**CAACBf**][SbF_6] show signals at 63.6 and 65.5 ppm, respectively, confirming that these two borafluorenium cations are 3-coordinate. Inspired by the decolorization upon addition of THF, they designed [**IPrB^{MeO}f**][SbF_6] to tune the color.

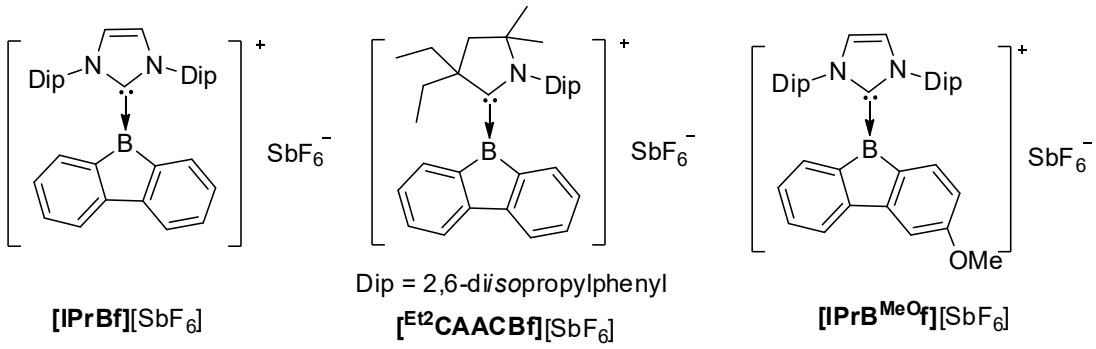

Scheme 2.24. Carbene stabilized borafluorenium cations.

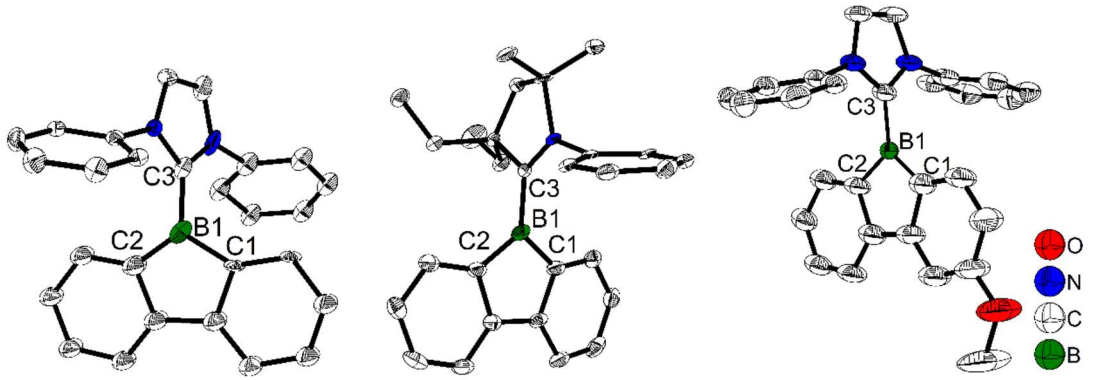

Figure 2.7. Molecular structures of **[IPrBf]**[SbF_6] (left), [^{Et2}**CAACBf**][SbF_6] (middle) and [**IPrB^{MeO}f**][SbF_6] (right). H atoms, *iso*propyl groups and SbF_6^- are omitted for clarity. Selected bond lengths (Å) and angles (°): **[IPrBf]**[SbF_6]: B1–C1 1.57(2), B1–C2 1.528(3), B1–C3 1.618(2), ∠C1–B1–C2 111.9(10). [^{Et2}**CAACBf**][SbF_6]: B1–C1 1.553(10), B1–C2 1.567(10), B1–C3 1.581(10), ∠C1–B1–C2 104.7(6). [**IPrB^{MeO}f**][SbF_6]: B1–C1 1.509(7), B1–C2 1.602(7), B1–C3 1.586(6), C_{sp^2}–O 1.354(8), ∠C1–B1–C2 106.4(4).

The single-crystal X-ray diffraction analyses indicate that the two C–B bond lengths in the borole ring are the same for **[IPrBf]**[SbF_6] (C1–B1 1.615(11) and C2–B1 1.57 (2) Å, Figure 2.7) and [^{Et2}**CAACBf**][SbF_6] (C1–B1 1.553(10) and C2–B1 1.567 (10) Å). However, in [**IPrB^{MeO}f**][SbF_6], the C1–B1 bond (1.509(7) Å) is much shorter than the C2–B1 bond

(1.602(7) Å). The authors suggested this is caused by the conjugation of the lone pair on oxygen with the cationic boron center. Interestingly, compared to **[IPrBf]**[SbF_6] and [^{Et2}**CAACBf**][SbF_6] which exhibit a very weak absorbance in the 400–600 nm range in CH_2Cl_2, a strong absorbance at 430–600 nm in CH_2Cl_2 was found for **[IPrB^{MeO}f]**[SbF_6]. Another interesting finding is that **[IPrB^{MeO}f]**[SbF_6] shows thermochromic behavior; the red color of **[IPrB^{MeO}f]**[SbF_6] faded to colorless in non-coordinating solvent upon cooling. The authors suggested that this phenomenon is caused by an intermolecular O···B interaction of **[IPrB^{MeO}f]**[SbF_6] which is favored at low temperature. Attempts to grow colorless crystals of **[IPrB^{MeO}f]**[SbF_6] which feature an O···B interaction at low temperature was unsuccessful. Furthermore, to support their hypothesis, THF was added to simulate the intermolecular coordination. After addition of 50 equivalents of THF to a red CH_2Cl_2 solution of **[IPrB^{MeO}f]**[SbF_6], the solution became colorless. When this solution was heated to 40 °C, the red color was recovered. After cooling, this solution became colorless again. These phenomena further support the hypothesis of an intermolecular O···B interaction at low temperature.

2.3 Conclusions and outlook

This perspective begins with fundamental synthetic strategies for preparing (hetero)arene-fused boroles and the stability of different 9-substiutent-9-borafluorenes, and then discusses functionalized (hetero)arene-fused boroles which can be applied as Lewis acids, activators of H_2, fluorescent materials, electron accepting units, etc. For functionalized (hetero)arene-fused boroles, the chemistry of reported 9-borafluorenes is classified, and a guide for the design of novel (hetero)arene-fused boroles to achieve different properties is provided.

Compared to the corresponding triarylboranes, (hetero)arene-fused boroles exhibit a stronger electron accepting ability, which is attributed to the antiaromaticity and the strain of 5-member borole ring. Triarylboranes have found wide application, e.g., as acceptors in TADF materials. The *exo*-aryl group of 9-aryl-9-borafluorene adopts a twisted arrangement with respect to the 9-borafluorene core and thus, by functionalization, may also generate good candidates for TADF materials. Surprisingly, thus far, only one such example was reported outside of patents. More studies on the functionalization of the *exo*-aryl moiety will be of particular interest.

Compared to non-fused "free" boroles, arene-fused boroles exhibit higher stability and potential for functionalization. Depending on the fused aryl groups, enhanced electron accepting ability and enhanced antiaromaticity, even greater than that of non-fused "free" boroles, unique coordination mode, and dual fluorescence, can be realized. Heteroarene-fused boroles are interesting compounds which require further study, (e.g., other electron-rich or -poor heteroarene-fused boroles), as they have many potential applications.

3 Phenylpyridyl-fused Boroles: A Unique Coordination Mode and Weak B–N Coordination Induced Dual Fluorescence

3.1 Introduction

Triarylboranes are of current interest due to their potential applications in various fields, such as non-linear optics,[7-9, 11-15, 19, 20, 80] live cell imaging,[21-23, 81] DNA/ RNA/ protein binding,[82, 83] anion sensors,[3, 78, 79] frustrated Lewis pairs (FLPs),[201-204] etc.,[4, 6, 24-32] with their properties resulting from the vacant p_z orbital on the 3-coordinate boron atom. This vacant p_z orbital can be attacked by nucleophiles, thus 3-coordinate boranes have been widely used as Lewis acids. It can also act as an excellent π-acceptor (A) which is of particular interest with respect to our studies. To enhance boron's electron accepting ability, Marder[35-37, 39, 139-141, 205] and others[40-44] introduced electron withdrawing fluoromesityl (2,4,6-$(CF_3)_3C_6H_2$, ^{F}Mes) and related group(s) at boron. The ^{F}Mes group is able to protect the boron center, and thus generate air- and moisture-stable compounds. Another way to enhance the electron accepting ability of boron is by embedding it into a 5-membered diene-ring, in compounds known as boroles.[97-105]

In terms of Hückel's rule, boroles are antiaromatic. While the first borole derivative, 1,2,3,4,5-pentaphenylborole, was reported by Eisch and co-workers 50 years ago,[93] its single-crystal structure was determined only recently.[94, 206] Due to the antiaromaticity and strain of the 5-membered borole ring, the electron accepting ability of boron is enhanced, and thus, boroles are highly reactive. By benzannulation, the antiaromaticity can be decreased and the stability of boroles improved, which can result in air- and moisture-stable dibenzoboroles.[107, 116, 142] One exception is the family of electron-rich heteroarene (e.g., thiophene)-fused boroles, which were reported by Yamaguchi[121, 144] and others.[207] Instead of decreasing antiaromaticity, it was increased, and thus these compounds are air- and moisture-sensitive. The drawback of decreasing the antiaromaticity by benzannulation is that the electron accepting ability is also decreased.

Fusing electron withdrawing aromatic systems onto boroles is another efficient way to increase their electron accepting ability. Marder and others enhanced the electron accepting ability of boroles by introducing CF_3 groups at either their *exo*-aryl[38, 45] moiety or at both the biphenyl core and the *exo*-aryl moiety of a dibenzoborole.[118]

Compared to benzene, pyridine is electron withdrawing, which is due to the higher electronegativity of nitrogen compared to that of carbon. Using pyridine as one of the substituents in triarylboranes enhances the acceptor strength of boron, as demonstrated by the reduction potentials of pyridine-containing triarylboranes,[208-211] 9-borylated acridine[212, 213] and boron-doped polycyclic aromatic hydrocarbons (PAHs) with pyridine bound to boron.[214] Additionally, the coordination ability of pyridine can be used for further functionalization. For example, triarylborane-functionalized N,C-chelate or N,N-chelate Pt[192, 215-223] and N,C-chelate Ir complexes[224-227] were systematically studied and applied in optoelectronic devices. Besides their use as ligands in transition metal complexes, Wang and co-workers found that triarylborane-functionalized N,C-chelated tetrahedral boron centers display interesting reversible photo-thermochromic properties.[228-230] Liu and co-workers reported an interesting example of a pyridine-substituted monobenzofused 1,4-azaborine, which forms a dimer.[231] In the present study, we synthesized two isomers of phenylpyridyl-fused boroles, **[TipPBB1]$_4$** and **TipPBB2** (Scheme 3.1) and investigated their structural, photophysical and electrochemical properties.

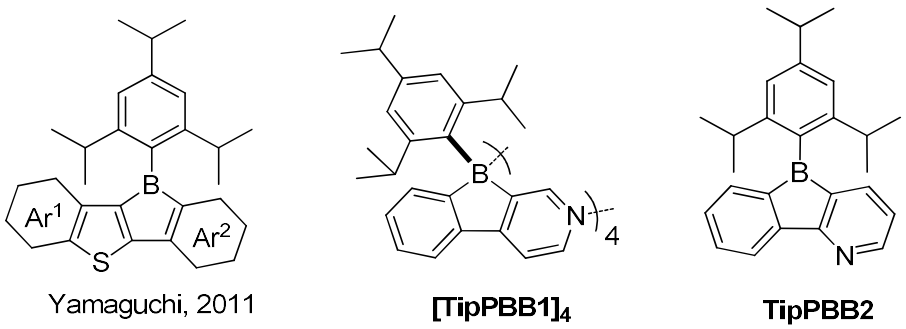

Scheme 3.1. Electron rich thiophene-fused boroles[121, 144] and electron-poor pyridyl-fused boroles, **[TipPBB1]$_4$** and **TipPBB2** of this study.

3.2 Results and discussion

3.2.1 Synthesis and crystal structures

[TipPBBl]$_4$ and **TipPBB2** were synthesized from the corresponding precursors **8** or **9** in a single step via a lithiation-borylation sequence (Scheme 3.2).[232] Both derivatives are moderately air-stable, decomposing slowly when exposed to air. Compound **[TipPBBl]**$_4$ is a white solid with a $^{11}B\{^1H\}$ NMR chemical shift of 2.9 ppm in $CDCl_3$, which indicates that the boron is 4-coordinate in solution.

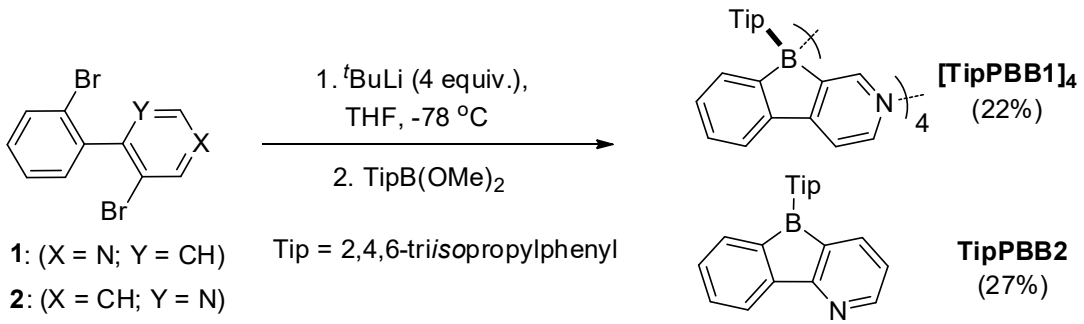

Scheme 3.2. Synthesis of **[TipPBBl]**$_4$ and **TipPBB2**.

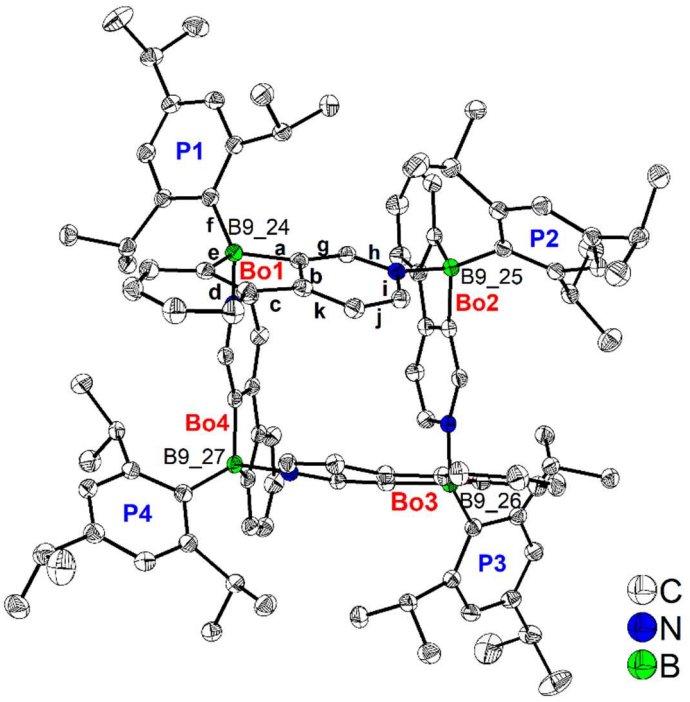

Figure 3.1. Molecular structure of **[TipPBBl]**$_4$ in the solid state at 100 K. Atomic displacement

ellipsoids are drawn at the 50% probability level, and H atoms as well as C_6D_6 solvent molecules are omitted for clarity. 'Bo' and 'P' denote the planes of the phenylpyridyl-fused borole and the Tip phenyl groups, respectively. Selected B–C and C–C bond distances are labelled with letters.

Table 3.1. Selected bond lengths (Å) and angles (°) of **[TipPBBI]$_4$**. 'Bo' and 'P' denote the planes of phenylpyridyl-fused borole and the Tip phenyl groups, respectively (according to Figure 3.1).

	Bo1	Bo2	Bo3	Bo4
a: B–C10$_{Bo}$	1.656(2)	1.643(2)	1.662(2)	1.655(2)
e: B–C13$_{Bo}$	1.630(2)	1.621(2)	1.633(2)	1.628(2)
f: B–Cl$_{Tip}$	1.639(2)	1.628(2)	1.645(2)	1.639(2)
b: C10–C11 (Bo)	1.409(2)	1.412(2)	1.413(2)	1.408(2)
c: C11–C12 (Bo)	1.467(2)	1.474(2)	1.467(2)	1.472(2)
d: C12–C13 (Bo)	1.410(2)	1.413(2)	1.412(2)	1.412(2)
B–N	B_{Bo1}–N_{Bo4}	B_{Bo2}–N_{Bo1}	B_{Bo3}–N_{Bo2}	B_{Bo4}–N_{Bo3}
	1.655(2)	1.652(2)	1.644(2)	1.644(2)
B–B	B_{Bo1}–B_{Bo2}	B_{Bo2}–B_{Bo3}	B_{Bo3}–B_{Bo4}	B_{Bo4}–B_{Bo1}
	5.420(2)	5.365(2)	5.407(2)	5.402(2)
∠Bo–P	65.64(3)	57.80(4)	67.53(4)	60.14(3)
∠Bo–Bo ⊥	Bo1–Bo2	Bo2–Bo3	Bo3–Bo4	Bo4–Bo1
	89.70(2)	81.78(2)	89.33(2)	78.44(2)
∠Bo–Bo ||	Bo1–Bo3	Bo2–Bo4		
	33.29(3)	33.21(2)		
∠Bo–B_4 plane	72.08(3)	71.94(2)	74.73(3)	74.87(2)

Colorless crystals suitable for X-ray diffraction analysis of **[TipPBBI]$_4$** were grown by evaporation of a C_6D_6 solution at room temperature (Figure 3.1). The pyridine moiety from one molecule coordinates to the boron atom of the neighboring molecule in such a way that four monomers become a tetramer with a central empty cavity. The square-like (B–C–C–N–)$_4$ coordination mode is similar to that in dimethyl(3-pyridyl)borane and diethyl(3-pyridyl)borane.[172-174] The four 2,4,6-tri*iso*propylphenyl (Tip) groups of the tetramer are oriented towards the outside of the cavity. The phenylpyridyl-fused borole core is nearly planar. The torsion angles between the planes of these core moieties and the Tip phenyl groups attached to boron range from 57.80(4)–67.53(4)° (Table 3.1). Adjacent borole planes are oriented approximately perpendicular to one another with torsion angles of 78.44(2)–89.70(2)° between the planes. The opposing borole planes

have angles of 33.29(3)° and 33.21(2)° between the respective pairs of planes. This configuration is similar to the two-fold rotational symmetry of the opposing planes in diethyl(3-pyridyl)borane, while the opposing planes in dimethyl(3-pyridyl)borane exhibit an inverted orientation. The torsion angles between the phenylpyridyl-fused borole and the plane of the tetramer spanned by the four boron atoms are in the range of 71.94(2)–74.87(2)°, hence, exhibiting a similar configuration to that of the pyridine rings in diethyl(3-pyridyl)borane. In contrast, in dimethyl(3-pyridyl)borane, only two opposing pyridine rings show a similar orientation, i.e., close to perpendicular to the tetramer plane, while the other pair of planes lies in the plane of the tetramer. In the 5-membered borole rings of the tetramer, the B–C bond distances to the pyridyl rings (1.643(2)–1.662(2) Å) are significantly longer than those to the phenyl rings (1.621(2)–1.633(2) Å, Table 3.1), as observed for other heteroarene-fused boroles.[144] The shorter B–C bond distances are in the same range as those in dimethyl(3-pyridyl)borane (1.612(4)–1.638(3) Å) and diethyl(3-pyridyl)borane (1.608(6)–1.642(5) Å).[172-174] The B–N bond distances (1.644(2)–1.655(2) Å) are in the same range as those in pentaphenylborole•2,6-lutidine (1.6567(3) Å)[175] and sterically hindered dibenzoborole•pyridine (1.638(3) Å).[119] Interestingly, in contrast to both pentaphenylborole•2,6-lutidine and the sterically hindered dibenzoborole•pyridine, which dissociate in solution at room temperature, the tetramer of **TipPBB1** persists in C_6D_6 even at +50 °C (see below). The C–C bonds of the borole moiety (bonds b and d in Figure 3.1) which are shared with the pyridine and the phenyl ring have lengths typical for aromatic bonds, while the connecting C–C bond (c) is significantly longer, comparable to a Csp^2–Csp^2 single bond. The distances between two adjacent boron atoms are 5.365(2)–5.420(2) Å and hence, slightly longer than the corresponding distances in dimethyl(3-pyridyl)borane (5.267(4) and 5.286(4) Å) and diethyl(3-pyridyl)borane (5.124(6) and 5.313(5) Å).[172-174]

To investigate the coordination mode in solution, we performed a diffusion-ordered spectroscopy (^{1}H DOSY) study in C_6D_6. All signals appeared on the same horizontal axis with log(*D* (diffusion constant)) = –9.35 (log(m^2/s)) at +25 °C. Even at +50 °C, the signals

are still on the same horizontal axis with log(*D*) = –9.18 (log(m²/s)) (see Figures 9.1-37 and 9.1-38), which indicates that only one species is present in solution. Using the diffusion constants, the van der Waals radius, r ≈ 7.63 at +25 °C and 7.78 Å at +50 °C, of **[TipPBBI]**$_4$ was calculated using the Stokes–Einstein equation $r = \frac{k_B T}{6\pi\eta D}$ (k_B is the Boltzmann constant, T is temperature (K), η is the dynamic viscosity (ca. 0.64 and 0.46 mPa·s of C_6D_6 at +25 and +50 °C, respectively) and r is the van der Waals radius).[233, 234] The molecular volume of **[TipPBBI]**$_4$ as a tetramer was calculated to be 1351.79(15) Å^3 in the solid state using the Olex2 program package (the following element radii were used: C = 1.7 Å; H = 1.09 Å; B = 2 Å; N = 1.55 Å).[235] The van der Waals radius was estimated approximately 6.86 Å by using equation $V = \frac{4}{3}\pi r^3$, which nicely matches the volume derived from the DOSY study, and thus proves that the tetramer persists in solution.

As it seemed clear that the position of the nitrogen atom in the annulated pyridine ring is crucial for the unique coordination mode of **[TipPBBI]**$_4$, we switched the position of nitrogen, to hinder intermolecular coordination, and thus obtained **TipPBB2**. In $CDCl_3$, the $^{11}B\{^1H\}$ NMR signal of **TipPBB2** was observed at 72.8 ppm, which is in the typical range of 3-coordinate boron. All attempts to obtain crystals of **TipPBB2** using different solvents were unsuccessful. The solid-state $^{11}B\{^1H\}$ RSHE/MAS NMR study (128 MHz) results in a signal with an isotropic chemical shift of 4.4 ppm, which shows that the boron center of **TipPBB2** is 4-coordinate in the solid state, most likely a result of oligomerization or polymerization via B–N bonds. It is unlikely that a different donor is attached to boron.

3.2.2 Electrochemical properties

The cyclic voltammetry studies were performed with a scan rate of 250 mV s^{-1} in THF. **[TipPBB1]**$_4$ has two reduction potentials (Figure 3.2). The first reduction (E_{pc} = –2.31 V) is irreversible and is comparable to that of the reported phenylpyridyl core chelate 4-coordinate organoboron compounds, and the reduction is attributed to the phenylpyridyl core.[236] The second reduction is partially reversible with a half-wave reduction potential of $E_{1/2}$ = –2.54 V. The ratio of the integrals of the first and the second reductions is ca. 1 to 3. After reduction, the integration ratio between the corresponding first and second oxidations is ca. 2 to 2 (the second oxidation peak may constitute two or more overlapping peaks). We suggest that the two reduction processes arise from different phenylpyridyl cores.

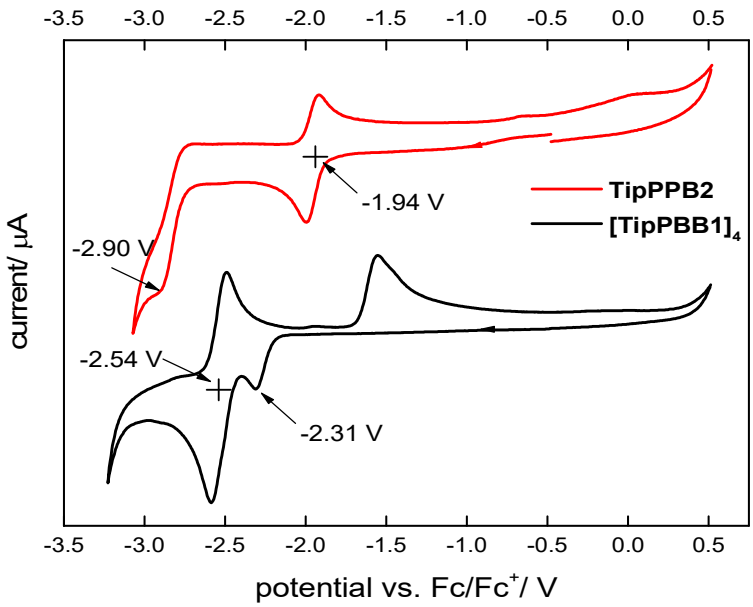

Figure 3.2. Cyclic voltammetry diagrams of **[TipPBB1]**$_4$ (black line) and **TipPBB2** (red line). Measured in THF in the presence of 0.1 M $TBAPF_6$, scan rates of 250 mV s^{-1} with potentials given vs. the Fc/Fc^+ couple.

TipPBB2 also exhibits two reduction potentials. The first reduction is reversible with a half-wave reduction potential of $E_{1/2}^{red}$ = –1.94 V which can be attributed to the borole

unit. The first reduction potential of **TipPBB2** is comparable to that of 9-^{F}Mes-borafluorene (^{F}**MesBf**, $E_{1/2}^{red}$ = –1.93 V), and is ca. 0.4 V more positive than that of 9-Tip-borafluorene (**TipBf**, $E_{1/2}^{red}$ = –2.36 V).[45, 116] The second reduction is irreversible, with the peak at E_{pc} = –2.90 V.[142, 144] The two reduction processes indicate the generation of a stable radical anion and the irreversible generation of a dianion. From the first reduction potential, we conclude that the effect of the pyridyl group in boroles on their reducibility is comparable to that of the *exo*-^{F}Mes group, as both of them can greatly enhance the electron accepting ability of boron.

3.2.3 Photophysical properties

One of the interesting photophysical properties of fused-boroles is their weakly allowed lowest energy absorption,[237] which extends into the visible region of the spectrum. This absorption is attributed to the $p_\pi - \pi^*$ conjugation through the vacant p-orbital of boron. The intermolecular coordination mode of **[TipPBB1]**$_4$ interrupts this conjugation, thus **[TipPBB1]**$_4$ does not exhibit this weakly allowed transition (Figure 3.3, left and Table 3.2). This is in line with previously reported 4-coordinate dibenzoboroles.[45, 116, 118] The lowest energy absorption of **[TipPBB1]**$_4$ appears at 322 nm with ε = 49600 cm^{-1} M^{-1} in THF, and the emission peak occurs at 495 nm, which is slightly red shifted compared to that in a hexane solution (λ_{em} = 446 nm). The quantum yield of **[TipPBB1]**$_4$ is ca. Φ_F = 0.1 and the lifetime is ca. 6 ns in both THF and hexane. It was previously reported by Marder and co-workers[118] and Rupar and co-workers[179] that dissociation of a 4-coordinate borole to a 3-coordinate borole in the excited state leads to a very similar long lifetime as for the 3-coordinate borole. Thus, the short lifetime of **[TipPBB1]**$_4$ suggests that the coordination persists in solution even in the excited state.

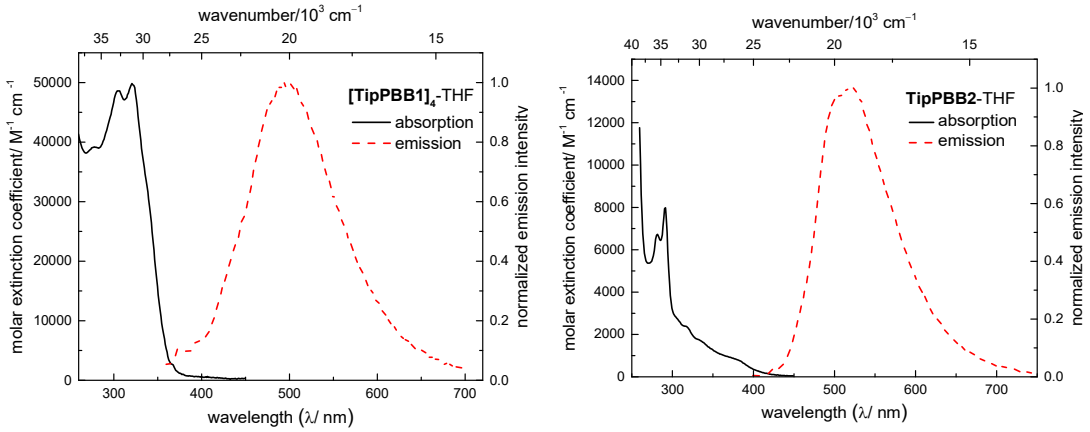

Figure 3.3. UV-vis absorption (black solid line) and emission (red dash line) spectra of **[TipPBB1]**$_4$ (left) and **TipPBB2** (right) in THF.

TipPBB2 shows a small extinction coefficient (ca. ε = 900 cm^{-1} M^{-1}) for the lowest energy absorption at ca. 375 nm and tails to ca. 425 nm in THF, which is similar to those of

previously reported dibenzoboroles.[45, 121] The emission of **TipPBB2** has a maximum at 520 nm with a quantum yield of ca. Φ_F = 0.27 in THF, which is much higher than those of **TipBf** and most reported dibenzoboroles.[45, 121] In CH_3CN, the lowest energy absorption and the emission maximum of **TipPBB2** are comparable to the ones in THF, which suggests that CH_3CN does not coordinate to **TipPBB2**.[116, 118] In CH_3CN, the quantum yield of **TipPBB2** still reaches a value of Φ_F = 0.21. In the solid state, **TipPBB2** has a low quantum yield of 0.05. Interestingly, **TipPBB2** shows two fluorescent lifetimes at 520 nm in solution at room temperature, e.g., in CH_2Cl_2, one long (145 ns, 93.4%), which is in agreement with the weakly allowed lowest energy transition (Strickler-Berg relation)[238] and one short (7.3 ns (6.6%)).

Table 3.2. Photophysical data for **[TipPBB1]**$_4$ and **TipPBB2** at room temperature.

	Solvent	λ_{abs}[a]/ nm ($\varepsilon/10^3$ cm^{-1} M^{-1})	λ_{em}/ nm	Φ_F[b]	τ_F/ ns (rel.%)	Stokes shift/ cm^{-1}
[TipPBB1]$_4$	hexane	304 323	446	0.11	5.7	8540
	THF	306 (46.7); 322 (49.6)	495	0.12	6.3	10850
TipPBB2	hexane	317; 375	514	0.34	5.7 (2.5%); 165 (97.5%)	6180
	CH_2Cl_2	319; 375	516	0.26	7.3 (6.6%); 145 (93.4%)	7290
	THF	320 (2.3); 375 (0.9)	520	0.27	5.6 (5.0%); 151 (95.0%)	7440
	CH_3CN	318; 375	528	0.21	5.8 (3.9%); 146 (96.1%)	7730
	solid state	385[c]	520	0.05	6.1 (61.6%); 87.7 (38.4%)	6740

[a]Lowest-energy absorption maximum. [b]Absolute fluorescence quantum yields measured using an integrating sphere. [c]Lowest-energy excitation maximum.

The two lifetimes and dual fluorescence of **TipPBB2** indicate two radiative decay processes. The purity of **TipPBB2** was confirmed by NMR spectroscopy and elemental analysis and, in addition, several independently synthesized samples showed the same

phenomenon, thus ruling out the presence of impurities as being responsible for the dual fluorescence. Due to the bulky Tip group and the fact that almost no red shift of the emission maximum was observed with increasing polarity of the solvent (from hexane to CH_3CN, Table 3.2), the two decay processes are unlikely to be caused by dual emission from twisted intramolecular charge transfer or planar intramolecular charge transfer.[239-241] Due to the low concentration (ca. 2 x 10^{-5} M) at which the measurement was performed, we can rule out the formation of nanoparticle-induced emission (also termed aggregation-induced emission (AIE)).[242-244]

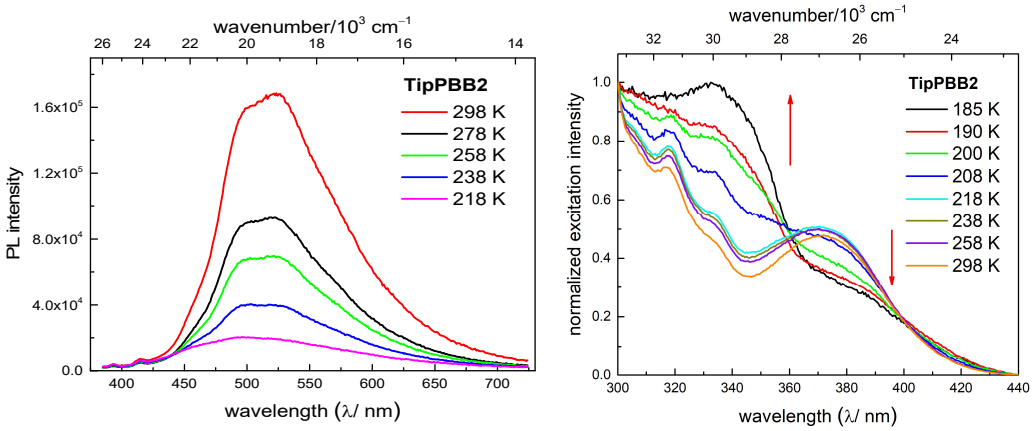

Figure 3.4. Temperature dependence of the emission spectra in 2-methyl-THF (left) and temperature dependence of excitation spectra (right) with emission at 520 nm in CH_2Cl_2.

To gain further insight into those processes, we measured the temperature dependence of the emission spectra and lifetime in 2-methyl-THF (Figure 3.4, left). The intensity of the emission decreases when the temperature is lower and, at the same time, the relative percentage of the short lifetime emission increases until the long lifetime emission disappears completely at ca. 168 K. We suggest that the two lifetimes are caused by the dual fluorescence originating from 3-coordinate **TipPBB2** and a weak intermolecular adduct of **TipPBB2**. The emission spectrum of **TipPBB2** at room temperature in solution is actually an overlay of the two independent emission bands. The weak intermolecular adduct is generated by weak intermolecular coordination via a B–N bond,

which is favored at lower temperature. When the temperature is decreased, the equilibrium shifts towards the weak intermolecular adduct of **TipPBB2** and, thus, the emission becomes weaker. To support our hypothesis, fluorescence lifetime measurements on **TipPBB2** were performed at different concentrations (2 x 10^{-5}, 1 x 10^{-4} and 5 x 10^{-4} M in CH_2Cl_2) (Figure 7.3-23). At 298 K, the relative percentages of the short and long lifetimes show only negligible change at different concentrations (Table 7.3-1) but, at 213 K, the more concentrated samples show a higher relative percentage of the short lifetime component, which support our suggestion of the presence of an equilibrium. Furthermore, the temperature dependence of the excitation spectra in CH_2Cl_2 were recorded (Figure 3.4, right). The excitation spectra do not show a large difference until the temperature is decreased to 218 K. When the temperature is decreased further, the intensity of the band at ca. 380 nm decreases and, at the same time, the intensity of the band at ca. 340 nm increases. The isosbestic point at ca. 360 nm indicates that the observed phenomena are a result of a change in the ground state, which fits our hypothesis nicely. It is important to note that this is different from previously reported examples of dual fluorescence arising from photodissociation of the B–N bond in the excited state.[176, 178] Furthermore, we recorded the low temperature ^{1}H and $^{11}B\{^{1}H\}$ NMR spectra from +25 °C to –90 °C in CD_2Cl_2. In the ^{1}H NMR spectra, new signals started to appear when the temperature is decreased to –50 °C, but 3-coordinate **TipPBB2** remains the major species even when the temperature is decreased to –90 °C (Figure 9.1-42). Among these new signals, three new characteristic peaks (δ (ppm) 0.72 (d, J = 7 Hz), 0.36 (d, J = 7 Hz) and 0.11 (d, J = 7 Hz), Figure 9.1-42, red box), which can be assigned to the methyl groups of the *ortho-iso*propyl moieties, shift upfield. This is likely a result of intermolecular coordination leading to a shielding effect by ring-current effects of the 4-coordinate borole core.[121] The same effect was also observed for **[TipPBB1]**$_4$, as three methyl groups of the *ortho-iso*propyl moieties resonate in the same range (δ (ppm), 0.95 (d, J = 6 Hz), 0.77 (d, J = 6 Hz), 0.30 (d, J = 6 Hz)). In the $^{11}B\{^{1}H\}$ spectra, the signal from the 3-coordinate boron becomes very broad at ca. –50 °C, but no 4-coordinate boron was observed, even when the temperature was decreased to –90

°C (Figure 9.1-43). Most likely, oligomerization starts at lower temperature. Even at –90 °C, there seems to be an equilibrium between the "free" **TipPBB2** and the oligomer(s) of **TipPBB2**, as a distinct sharp signal for one or more 4-coordinate boron species was not observed. Additionally, 4-dimethylaminopyridine (DMAP) was added to **TipPBB2** to simulate the 4-coordinate species (formation of adduct was confirmed by *in situ* ^{1}H and ^{11}B{^{1}H} NMR spectra in $CDCl_3$, Figures 9.1-45 and 9.1-46). After addition of excess of DMAP to a solution of **TipPBB2** in THF, the emission maximum blue shifts to 490 nm (Figure 7.3-22) with only a single lifetime of τ_F = 6.8 ns. No long lifetime component is observed, indicating that DMAP coordinates to boron and a 4-coordinate adduct is formed (*vide supra*). The lifetime of the DMAP-**TipPBB2** adduct is comparable to the short lifetime component of **TipPBB2** in THF.

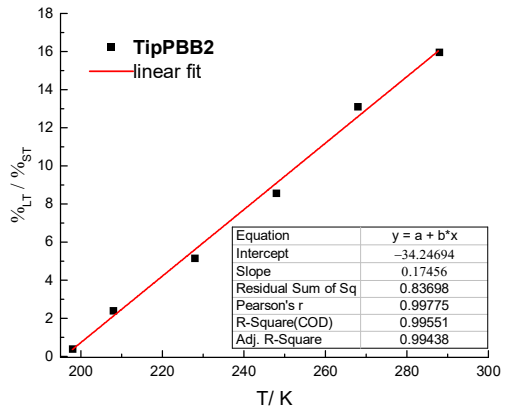

Figure 3.5. Plot of $\%_{LT}/\%_{ST}$ ($\%_{LT}$ and $\%_{ST}$ are the relative percentages of the long lifetime and the short the lifetime components, respectively) vs. T (K) of **TipPBB2** in 2-methyl-THF.

Interestingly, the ratio of the long lifetime ($\%_{LT}$) to the short lifetime ($\%_{ST}$) (Figure 3.5 and Table 7.3-2) of **TipPBB2** in 2-methyl-THF changes linearly with decreasing temperature, which suggests that **TipPBB2** may be applied as a fluorescent thermometer between 198 K and 288 K.[245, 246]

3.2.4 Theoretical studies

To gain deeper insight into the electronic properties, TD-DFT and DFT calculations were carried out on **TipPBB2**. In order to reduce the calculation costs, two models, (**(BMe$_3$)TipPBB1(NMe$_3$)** and **(BMe$_3$)TipPBB2(NMe$_3$)**), which utilize a BMe$_3$ group as the Lewis acid coordinated to pyridine and a NMe$_3$ group as the Lewis base coordinated to the boron center of the borole, were used to simulate the **[TipPBB1]$_4$** and intermolecular 4-coordinate **TipPBB2**, respectively (Figure 3.6). The ground-state geometries of all compounds were optimized at the B3LYP level of theory (see experimental part for details).[247, 248] In addition, the influence of *exo*-aryl groups was evaluated using Dip (2,6-di*iso*propylphenyl) and ^{F}Xyl (2,6-di(trifluoromethyl)phenyl) as models. Furthermore, the isomers of **TipPBB2** were also examined (see experimental part).

The orbitals of **(BMe$_3$)TipPBB1(NMe$_3$)** and **(BMe$_3$)TipPBB2(NMe$_3$)** are quite similar. In both compounds, the NMe$_3$ group coordinates to the boron atom and interrupts the p_π(B) – π* conjugation, and thus the LUMOs of **(BMe$_3$)TipPBB1(NMe$_3$)** (–2.07 eV) and **(BMe$_3$)TipPBB2(NMe$_3$)** (–1.91 eV) are delocalized over the phenylpyridyl core. The HOMOs of **(BMe$_3$)TipPBB1(NMe$_3$)** (–6.05 eV) and **(BMe$_3$)TipPBB2(NMe$_3$)** (–6.02 eV) are mainly located at the Tip group with a small contribution from the phenyl group of the phenylpyridyl core. The HOMO-1 is located at the Tip group for both models. The HOMO-2 of **(BMe$_3$)TipPBB1(NMe$_3$)** (–6.35 eV) delocalizes over the phenylpyridyl core with a large contribution from the BMe$_3$ group. However, HOMO-2 of **(BMe$_3$)TipPBB2(NMe$_3$)** (–6.39 eV) is delocalized over the phenylpyridyl core with some contribution from the Tip and the BMe$_3$ group. In the gas phase, the HOMO and HOMO-1 to LUMO transitions of **(BMe$_3$)TipPBB1(NMe$_3$)** correspond to the $S_1 \leftarrow S_0$ and $S_2 \leftarrow S_0$ transitions, which are weakly allowed with small oscillator strengths (Table 3.3, f = 0.0195 and 0.0108, respectively). The HOMO-2 to LUMO transition ($S_3 \leftarrow S_0$) is allowed (f = 0.1167) with an energy gap of 3.77 eV (λ = 329 nm), which fits the UV-vis absorption spectrum of **[TipPBB1]$_4$** well. For **(BMe$_3$)TipPBB2(NMe$_3$)**, the HOMO to LUMO transition corresponds to $S_1 \leftarrow S_0$ which is weakly allowed (f = 0.016) and is

associated with an energy of 3.47 eV (λ = 357 nm).

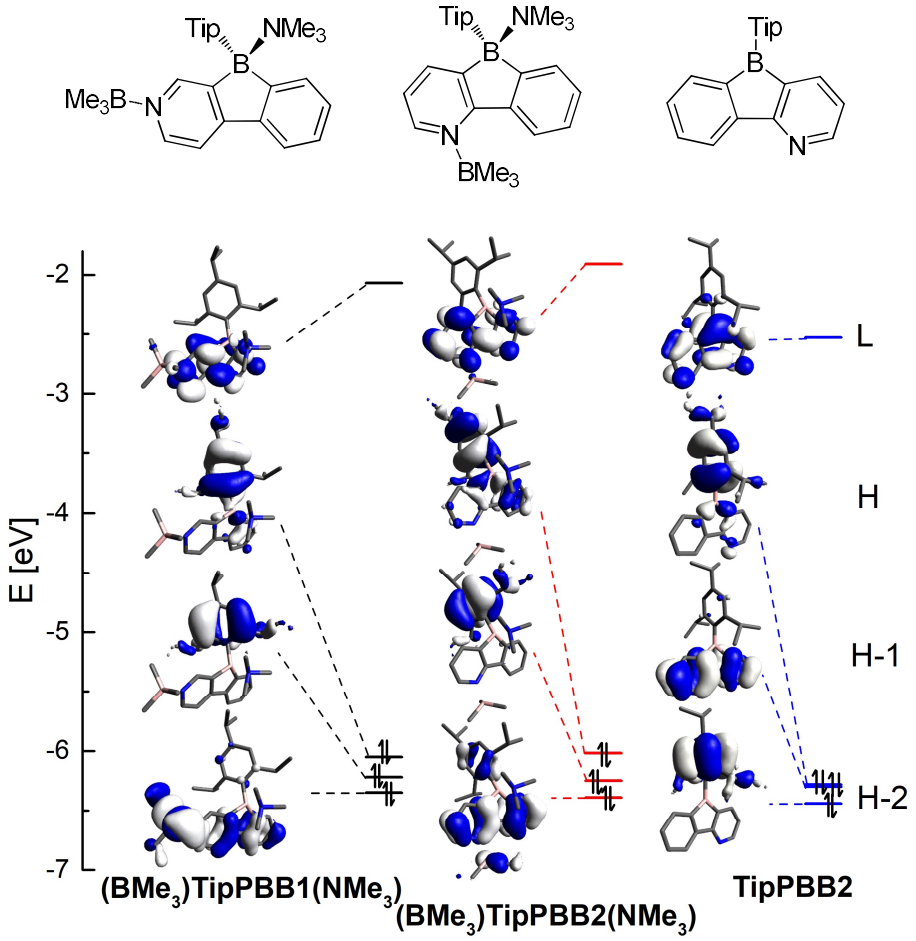

Figure 3.6. Depiction of the LUMO (L), HOMO (H), HOMO-1 (H-1) and HOMO-2 (H-2) of **(BMe3)TipPBB1(NMe3)**, **(BMe3)TipPBB2(NMe3)** and **TipPBB2**, calculated at the B3LYP/6-31+G(d) level of theory, and corresponding energies.

The LUMO (–2.53 eV) of **TipPBB2** delocalizes over the phenylpyridyl core with a large contribution from boron, which leads to it being 0.62 eV lower in energy than the LUMO of **(BMe3)TipPBB2(NMe3)**. The LUMO of **TipPBB2** is similar to the LUMO of **TipBf** which delocalizes over the biphenyl core with a large contribution from the boron.[45, 116] The HOMO (–6.28 eV) and HOMO-1 (–6.30 eV) have almost the same energy, but the orbitals distribution are quite different. The HOMO of **TipPBB2** is mainly localized on the Tip group and is different from previously reported **TipBf**,[45, 116]

but similar to **^{p}'NMe$_2$^{F}Xyl^{CF3}Bf**, which possesses a strong amine donating group at the *para*-position of the *exo*-aryl moiety.[118] HOMO-1 of **TipPBB2** is similar to the HOMO of **TipBf** which is distributed over the phenylpyridyl-fused borole core. Thus, by changing the biphenyl core to the phenylpyridyl core, the Tip group becomes a donating group, not just a protecting group at boron. The HOMO-2 (–6.44 eV) of **TipPBB2** is also located on the Tip group. In the gas phase, for **TipPBB2**, the $S_1 \leftarrow S_0$ transition is attributed to a HOMO to LUMO transition which is forbidden. The $S_2 \leftarrow S_0$ and $S_3 \leftarrow S_0$ transitions of **TipPBB2** are weakly allowed with very small oscillator strengths (f = 0.0002 and 0.0004, respectively), which is in line with the small extinction coefficient observed in the UV-vis spectrum in the corresponding range (above 375 nm).

Table 3.3. Lowest energy transitions of **(BMe$_3$)TipPBBI(NMe$_3$)**, **(BMe$_3$)TipPBB2(NMe$_3$)** and **TipPBB2**.

Compound	Transition	E/ eV	λ/ nm	f	Major contributions	Λ
(BMe$_3$)TipPBBI(NMe$_3$)	$S_1 \leftarrow S_0$	3.36	358	0.0195	H→L (99%)	0.31
	$S_2 \leftarrow S_0$	3.62	343	0.0108	H-1→L (99%)	0.20
	$S_3 \leftarrow S_0$	3.77	329	0.2167	H-2→L (96%)	0.63
(BMe$_3$)TipPBB2(NMe$_3$)	$S_1 \leftarrow S_0$	3.47	357	0.016	H→L (98%)	0.36
	$S_2 \leftarrow S_0$	3.81	326	0.008	H-1→L (99%)	0.20
	$S_3 \leftarrow S_0$	3.80	318	0.0039	H-3→L (97%)	0.18
TipPBB2	$S_1 \leftarrow S_0$	2.92	424	0.0	H→L (98%)	0.27
	$S_2 \leftarrow S_0$	2.95	420	0.0002	H-1→L (98%)	0.65
	$S_3 \leftarrow S_0$	3.25	382	0.0004	H-2→L (99%)	0.21

3.3 Conclusions

Two boroles with a phenylpyridyl core were synthesized. **[TipPBBl]**$_4$ was obtained as a tetramer with a central cavity both in the solid state and in solution. The cavity formed by the coordination may potentially be enlarged by expanding the fused system. **TipPBB2** was obtained as 4-coordinate species in the solid state but dissociates to a 3-coordinate species in solution. To the best of our knowledge, **TipPBB2** is the only example of an electron-poor 3-coordinate heteroarene-fused borole. Due to the electron withdrawing property of the pyridyl group, the electron accepting ability of **TipPBB2** ($E_{1/2}^{red}$ = –1.94 V) was largely enhanced, as demonstrated by cyclic voltammetry. Interestingly, **TipPBB2** shows dual fluorescence in solution. We suggest that the dual fluorescence is caused by an equilibrium between 3-coordinate **TipPBB2** and a weak intermolecular oligomeric adduct of **TipPBB2** via B–N coordination. This equilibrium was investigated in detail by photophysical and low temperature NMR studies. Further derivatives of **TipPBB2**, e.g., Ir, Pt complexes are under investigation. Theoretical studies indicate that the HOMO of **TipPBB2** is located on the Tip group which is different from that of **TipBf** for which the HOMO is located at the biphenyl main core.

4 Two Derivatives of Phenylpyridyl-fused Boroles with Contrasting Electronic Directions: Decreasing and Enhancing the Electron Accepting Ability

4.1 Introduction

Boroles, 5-membered diene rings with a 3-coordinate boron center, have attracted increasing interest in the past 20 years.[97-105] According to Hückel's rule, boroles are antiaromatic.[90-92] Due to the vacant p_z-orbital, antiaromaticity and strain of the 5-membered ring, the boron atom in boroles becomes highly electron-deficient; thus, boroles exhibit a high reactivity and are typically unstable (e.g., to H_2O). Via kinetic protection (e.g., phenyl,[93, 94] 2,4,6-trimethylphenyl (Mes)[96] and 2,4,6-tritrifluoromethylphenyl (^{F}Mes)),[38] the stability of boroles can be greatly enhanced, but boroles still exhibit high reactivities. Another way to enhance the stability of boroles drastically is via benzannulation, resulting in 9-borafluorenes (**Bf**s).[107, 108] However, via annulation, the electron-deficient property of the boron atom is sacrificed to some extent.[78, 142, 156]

Besides annulation with phenyl groups which leads to **Bf**s, Yamaguchi and co-workers annulated boroles with electron-rich heteroarenes (e.g., thiophene(s), benzofuran and indole) and interestingly, the borole rings of some of these annulated boroles exhibit even greater antiaromaticity than the non-annulated "free" boroles.[121, 144] Due to the high degree of antiaromaticity, the electron accepting ability was enhanced, which was confirmed by electrochemical and theoretical studies. Another strategy which can enhance the electron accepting ability of **Bf**s is the introduction of an electron-deficient moiety as the *exo*-aryl group (e.g., perfluorophenyl[95] and ^{F}Mes).[45] Recently, Marder and co-workers[118] introduced four CF_3 groups at the biphenyl core of an ^{F}Mes-protected borafluorene. The reduction potential of this compound, $E_{1/2}^{red}$ = –1.13 V, is significantly anodically shifted even compared to non-annulated "free" boroles (e.g., ^{F}MesBC$_4$Ph$_4$, $E_{1/2}^{red}$ = –1.52 V).[38, 96, 100, 249] Inspired by the annulation with heteroarenes or electron-

deficient groups leading to interesting properties, more recently, Marder and co-workers annulated electron-poor pyridyl groups with boroles and prepared two phenylpyridyl-fused boroles ([**TipPBB1**]$_4$ and **TipPBB2**, Scheme 4.1).[168] Interestingly, [**TipPBB1**]$_4$ forms a tetramer in both the solid state and solution. **TipPBB2** exhibits dual fluorescence in solution which is caused by weak B–N coordination leading to an equilibrium between 3- and 4-coordinate boron centers.

In this study, further functionalization of the pyridyl groups of phenylpyridyl-fused boroles with contrasting electronic directions was achieved. For compound **10**, the electron-poor pyridyl group was transformed into an electron-rich dihydropyridine moiety;[214, 250-252] thus, compound **10** becomes a donor-π-acceptor (D-π-A) system. Compound **11** was obtained from **TipPBB2**, with the electron-poor pyridyl group being transformed into an even more electron-deficient *N*-methylpyridinium cation.[212, 213, 253] In the latter systems, the cationic property of *N*-methylpyridinium is analogous to alkyl ammonium systems, which were previously applied in triarylborane materials. The cationic NMe_3^+ substituents leads to good water solubility and thus these compounds can be applied as cyanide sensors in water,[254] in live-cell imaging[21-23, 81] and sensing of DNA/ RNA and proteins.[82, 83] Herein, the synthesis of compounds **10** and **11**, and their electrochemical, photophysical properties and theoretical studies are reported.

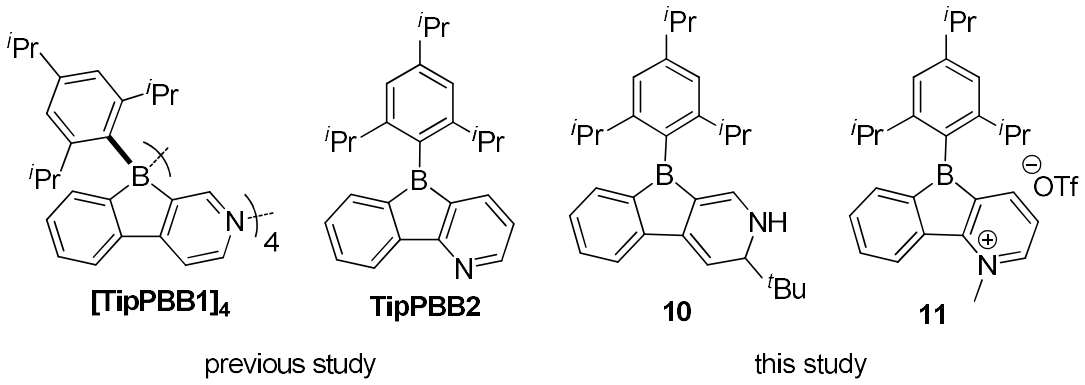

Scheme 4.1. Previously reported phenylpyridyl-fused boroles ([**TipPBB1**]$_4$ and **TipPBB2**)[168] and their derivatives (**10** and **11**) in this study.

4.2 Results and discussion

4.2.1 Synthesis

Besides our reported synthetic methodology[168] for preparing **[TipPBBl]**$_4$, a stepwise substitution reaction developed by Yamaguchi and co-workers was also investigated (Scheme 4.2, top).[121, 144] In the first step, 3-bromo-4-(2-bromophenyl)pyridine[232] was reacted with *n*-BuLi (1.0 eq) and the $B(OMe)_2$ group was selectively introduced at the pyridine ring (the selectivity was confirmed by NOESY NMR spectra of its derivative (compound **14**), Figures 9.1-69 and 9.1-70). Then the *exo*-aryl group, 2,4,6-tri*iso*propylphenyl (Tip) was introduced by reaction with the Grignard reagent, TipMgBr.[255] Finally, for an intramolecular cyclization, different bases were investigated. Interestingly, following the reported strategy,[121, 144] using *t*-BuLi (2.0 eq) as the base, instead of the formation of **[TipPBBl]**$_4$ (later, we found that *n*-BuLi leads to **[TipPBBl]**$_4$), compound **10** was obtained as a light yellow solid in 10% yield over three steps. By using *t*-BuLi as the base, the borole ring forms as expected, but at the same time, the electron-poor pyridyl group is transformed into an electron-rich dihydropyridine moiety via nucleophilic attack of *t*-Bu^- at the *meta*-position of the pyridyl group.[256-258] The proton attached to the nitrogen atom likely comes from the CH_2Cl_2, which was used as a solvent during the workup procedure (see experimental part for details). Compound **10** was fully characterized by NMR spectroscopy, high-resolution mass spectrometry (HRMS), and elemental analysis. To investigate whether the formation of compound **10** occurs via nucleophilic addition of *t*-Bu^- to **[TipPBBl]**$_4$, the reaction between **[TipPBBl]**$_4$ and *t*-BuLi was investigated. However, compound **10** was not observed, which suggests that the nucleophilic addition of *t*-Bu^- to pyridine occurs before or at the same time as the formation of the borole ring.

Compound **11** was synthesized from **TipPBB2** via methylation with MeOTf in CH_2Cl_2 and it was obtained as a yellow solid in 39% yield (Scheme 4.2, bottom). Compound **11** decomposes slowly in solution (e.g., dry and degassed CH_2Cl_2 and C_6H_6) at r.t., even under an inert atmosphere. The formation of 2-D-1,3,5-tri*iso*propylbenzene in C_6D6

solvent, evidenced by HRMS measurements, suggest that decomposition occurs via a radical process. However, as a solid, it can be stored under –30 °C under an inert atmosphere.

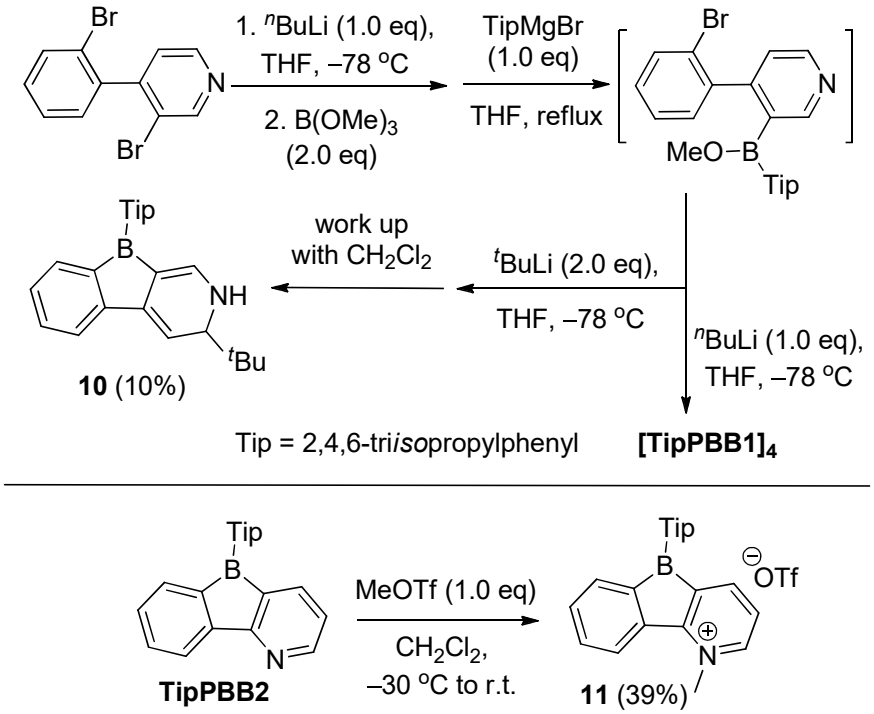

Scheme 4.2. Synthesis of compounds **10** (top) and **11** (bottom).

In solution, compound **10** is greenish-yellow and light sensitive. It slowly decomposed under UV light, evidenced by *in situ* NMR spectroscopy after irradiation with 365 nm light in $CDCl_3$ for 3 hours. The boron signal disappeared and, at the same time, 1,3,5-tri*iso*propylbenze and a pyridine moiety formed (see Figures 9.1-52 and 9.1-53). The $^{11}B\{^1H\}$NMR signal of compound **10** was observed at 58.8 ppm in $CDCl_3$, which is shifted upfield compared to those of **TipPBB2** or other 3-coordinate **Bf**s[45, 118] suggesting strong conjugation between the boron atom and the dihydropyridine moiety. Compound **11** is bright greenish-yellow in CH_2Cl_2 but, interestingly, when **11** was dissolved in THF, the color of the solution became light yellow. We hypothesized that this phenomenon is caused by THF coordinating to compound **11** which interrupts the $p_\pi - \pi^*$ conjugation through the vacant p-orbital of boron.[116] To confirm our hypothesis, the ^1H and $^{11}B\{^1H\}$

NMR spectra of compound **1l** in CD_2Cl_2 and d_8-THF, respectively, were measured. In CD_2Cl_2, a ^{11}B NMR signal was observed at 72.3 ppm, which is almost the same as that of **TipPBB2** (72.8 ppm in $CDCl_3$), and is in the typical range of 3-coordinate boron atoms. In d_8-THF, however, the ^{11}B NMR signal was observed at ca. 1.3 ppm, which is in the typical range of 4-coordinate boron atoms, and no signal corresponding to a 3-coordinate boron atom was observed, thus confirming our hypothesis. After removing the d_8-THF and then re-dissolving the compound in CD_2Cl_2, the ^1H NMR spectrum was the same (except for the 1,3,5-tri*iso*propylbenzene formed from decomposition, see Figure 9.1-60) as that of compound **1l** directly dissolved in CD_2Cl_2. The ^{11}B NMR signal was also observed in the same range as that of compound **1l** directly dissolved in CD_2Cl_2, suggesting that the coordination of THF to compound **1l** is reversible. It is worth mentioning that Tip-protected 9-borafluorenes have been reported which coordinate CH_3CN and DMF, but none of them coordinate THF, which is bulkier and less basic.[116] The coordination of THF to compound **1l** thus suggests an extremely electron-deficient boron center.

4.2.2 Electrochemical properties

As compounds **10** and **11** have fundamentally different electronic structures (electron-rich dihydropyridine moiety vs. electron-deficient *N*-methylpyridinium cation), their electrochemical properties are of interest. In CH_2Cl_2, compound **10** exhibits an irreversible oxidation with a peak at E_{pa} = +0.37 V, which confirms the electron-rich property of the dihydropyridine moiety (Figure 4.1, left). To our surprise, no reduction process for compound **10** was observed in CH_2Cl_2, which indicates that the reduction potential of compound **10** is more negative than –2.5 V. We suggest that such a negative reduction potential is the result of the strong conjugation between the dihydropyridine moiety and the boron atom. This strong conjugation was also confirmed by the upfield chemical shift of the ^{11}B NMR signal in solution (*vide supra*).

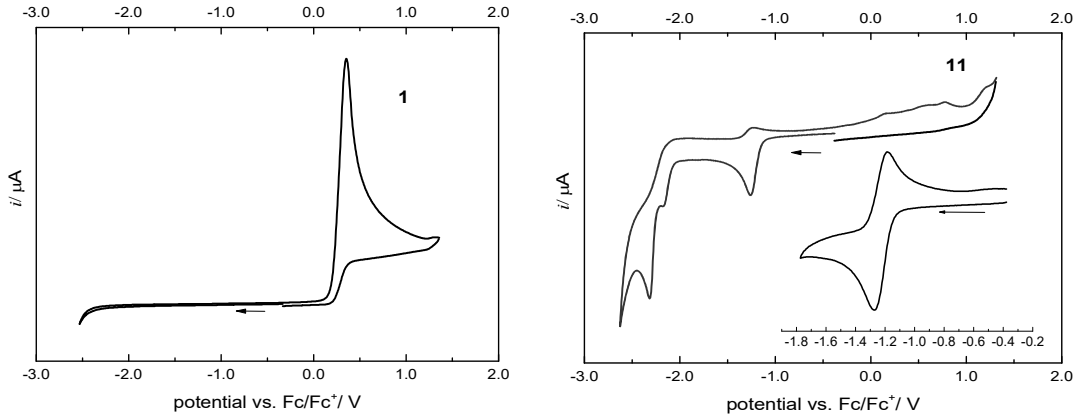

Figure 4.1. Cyclic voltammograms of compounds **10** (left) and **11** (right). Measured in CH_2Cl_2 in the presence of 0.1 M $TBAPF_6$, scan rates of 250 mV s^{-1} and potentials given vs. the Fc/Fc^+ couple.

Compound **11** exhibits three reduction processes. The first reduction process is reversible with a half-wave reduction potential of $E_{1/2}^{red}$ = –1.23 V. The second and third reduction processes are irreversible with peaks at E_{pc} = –2.17 and –2.31 V, respectively. Compared to its precursor, **TipPBB2**, which exhibits only one reversible reduction ($E_{1/2}^{red}$ = –1.94 V) under the same conditions (see experimental part), the first reduction potential of compound **11** shifts anodically by 0.71 V. For comparison, 1-methyl-2-phenylpyridin-1-

ium triflate (**12**),[259] the framework of compound **11** without the boron atom, was also investigated under the same conditions. Compound **12** exhibits an irreversible reduction process with a peak at E_{pc} = –1.68 V under the same conditions (see experimental part). Thus, the reduction potential of compound **12** is cathodically shifted by 0.41 V compared to that of compound **11** (E_{pc} = –1.27 V). This indicates that the combination of an electron-deficient 3-coordinate boron atom with an electron-deficient *N*-methylpyridinium cation is an efficient means by which to enhance the electron accepting ability. The same effect was also observed in the methylated 9-borylated acridine compound reported by Gabbaï and co-workers.[212]

4.2.3 Photophysical properties

There-coordinate **Bf**s exhibit a weakly allowed lowest energy absorption which is attributed to the $p_\pi - \pi^*$ conjugation through the vacant p-orbital of boron. For compound **10**, the strong conjugation between boron and the dihydropyridine moiety leads to a decreased electron accepting ability; thus, this weakly allowed absorption was not observed, as evidenced by the high molar extinction coefficient in different solvents (Figure 4.2, left). In toluene, compound **10** exhibits a lowest energy absorption maximum at 386 nm (ca. ε = 14500 cm^{-1} M^{-1}) with a shoulder at ca. 400 nm (ca. ε = 11800 cm^{-1} M^{-1}). The emission maximum of compound **10** occurs at ca. 441 nm in toluene. Both the absorption and emission of compound **10** are independent of the solvent polarity (toluene, CH_2Cl_2 and THF, Table 4.1), which suggests that the lowest energy absorption of compound **10** is more likely a locally-excited (LE) transition. In the solid state, compound **10** exhibits an emission maximum at 440 nm, which is almost the same as that in solution. In the solid state, the average lifetime of compound **10** is ca. 1.1 ns and the quantum yield is ca. 0.05.

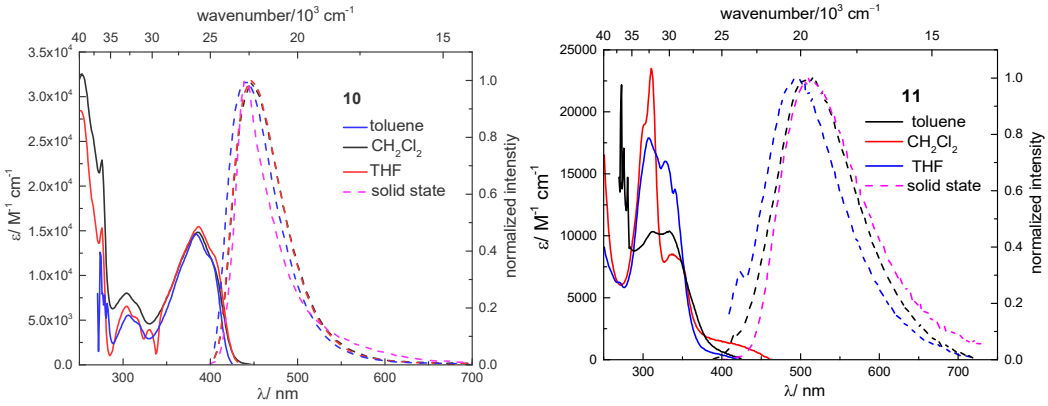

Figure 4.2. UV-vis absorption (solid line) and emission (dashed line) spectra of compounds **10** (left) and **11** (right) in toluene, CH_2Cl_2, THF and in the solid state.

The lowest energy absorption maximum of compound **11** was observed at ca. 390 nm in toluene, which red shifts to ca. 400 nm in CH_2Cl_2, but blue shifted to ca. 370 nm in THF.

With increasing polarity of the solvents (from toluene to CH_2Cl_2), the red shifted absorption suggests a polarized ground state of the chromophore,[1, 260, 261] as is expected due to the cationic nature of compound **11**. The blue shifted absorption of compound **11** in THF can be explained by THF coordination to the boron atom (*vide supra*). The lowest energy absorption maximum of compound **11** in CH_2Cl_2 is red shifted by ca. 25 nm (ca. 1667 cm^{-1}) compared to that of its precursor **TipPBB2** (λ_{abs} = 375 nm). The red shifted absorption of compound **11** can be attributed to its enhanced electron accepting ability, leading to a lower LUMO energy, which results in a small energy gap for the lowest energy transition. The molar extinction coefficient of the lowest energy absorption of compound **11** is in the same range as for **TipPBB2**, which suggests that it is a weakly allowed transition. The emission maximum of compound **11** in toluene was observed at 516 nm, which blue shifts to 494 nm in THF. The blue shifted emission of compound **11** in THF is the result of THF coordination to the boron atom, which also suggests that this coordination persists in the excited sate, as photo-induced dissociation in the excited state leads to similar or red shifted emission as that in the uncoordinated ground state.[45, 176] In the solid state, the emission maximum of compound **11** is at 511 nm, which is almost the same as that in toluene. The quantum yield is ca. 0.11 and two lifetimes (3.3 (71%) and 11.7 (29%) ns) were observed in the solid state.

Table 4.1. Absorption and emission of compounds **10** and **11** in different solvents and in the solid state.[a]

	toluene		CH_2Cl_2		THF		solid state
	λ_{abs}/ nm	λ_{em}/ nm	λ_{abs}/ nm	λ_{em}/ nm	λ_{abs}/ nm	λ_{em}/ nm	λ_{em}/ nm
10	386; 399	441	385; 399	447	387; 402	448	440
11	339; 390	516	344; 400	-	342; 370	494	511

[a]Due to the instability of both compounds in dilute solutions, their lifetimes and quantum yields, and the emission spectrum of compound **11** in CH_2Cl_2 were not measured. For compound **11**, due to the weak absorption, the wavelength for the lowest energy absorption may be not accurate.

4.2.4 Theoretical studies

To gain deeper insight into the electronic properties of these two compounds, TD-DFT and DFT calculations were carried out. The ground state geometries were optimized using the B3LYP functional[262] in combination with the 6-31+G(d, p) basis set (**10**) or CAM-B3LYP in combination with the 6-31++G(d, p) basis set (**11**).[247, 248] The LUMO of compound **10** shows a large contribution from the boron atom with a minor contribution from the annulated phenyl group and the allylamine moiety (Figure 4.3). The HOMO of compound **10** is distributed over the dihydropyridine moiety, with some contribution from the boron atom, which indicates a strong conjugation between the boron atom and dihydropyridine moiety in the ground state. This result is in agreement with the upfield-shifted ^{11}B NMR signal and the cathodically shifted reduction potential. The calculated HOMO energy of compound **10** is –5.33 eV, which fits nicely with the electrochemical studies (–5.22 eV, E_{exp} = –5.16 – E_{oxd}, E_{oxd} = +0.06 is the onset of oxidation potential).[263, 264]

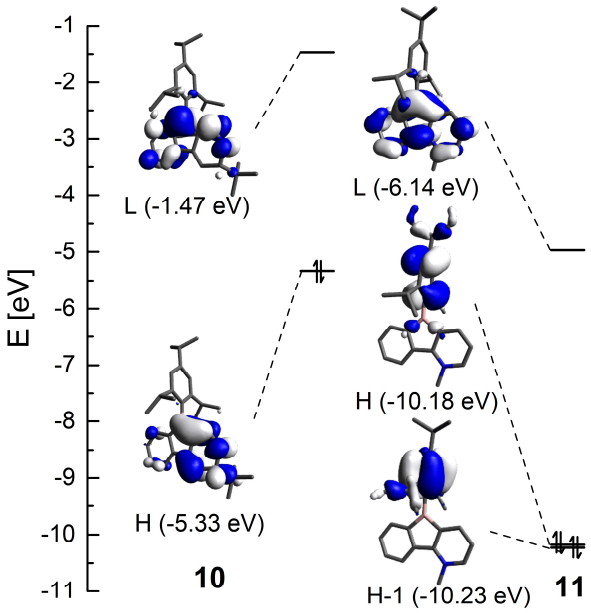

Figure 4.3. Depiction of the LUMO (L), HOMO (H) and HOMO-1 (H-1) for compounds **10** and **11**.

The LUMO of compound **11** is distributed over the phenylpyridyl core with a large contribution from the boron atom. The LUMO of compound **11** is similar to that of its precursor **TipPBB2**, but the energy is ca. 2.4 eV lower (–4.97 eV for compound **11** vs. –2.53 eV for **TipPBB2**). The HOMO and HOMO-1 of compound **11** are located at the Tip group with almost the same energies (–10.18 eV vs. –10.23 eV). The HOMO and HOMO-1 of compound **11** are similar to the HOMO and HOMO-2 of **TipPBB2**. The HOMO-2 of compound **11** is distributed over the phenylpyridyl core without any contribution from the boron atom, which is similar to the HOMO-1 of **TipPBB2** (see experimental part).

Table 4.2. Lowest energy transitions of compounds **10** and **11**.

Compound	Transition	*E*/ eV	λ/ nm	*f*	Major contributions
10	$S_1 \leftarrow S_0$	3.41	363	0.1505	H→L (91%)
	$S_2 \leftarrow S_0$	3.50	354	0.0358	H→L+1 (95%)
	$S_3 \leftarrow S_0$	3.72	333	0.0001	H-1→L (98%)
11	$S_1 \leftarrow S_0$	2.78	445	0	H→L (73%), H→L+1 (14%)
	$S_2 \leftarrow S_0$	3.19	389	0.0009	H-1→L (78%), H-1→L+1 (13%)
	$S_3 \leftarrow S_0$	3.55	350	0.0376	H-2→L (84%)

In the gas phase, the $S_0 \rightarrow S_1$ transition of compound **10** can be attributed to a HOMO to LUMO transition (Table 4.2). This transition is allowed with an oscillator strength of *f* = 0.1505. The $S_0 \rightarrow S_1$ transition (λ = 363 nm) is responsible for the lowest energy absorption and fits the UV-vis spectrum (i.e., λ = 386 nm in CH_2Cl_2) well. For compound **11**, the $S_0 \rightarrow S_1$ transition is mainly attributed to a HOMO to LUMO transition, which is forbidden. The $S_0 \rightarrow S_2$ transition is mainly attributed to a HOMO-1 to LUMO transition, which is an intermolecular charge transfer (ICT) process. The $S_0 \rightarrow S_2$ transition is weakly allowed (*f* = 0.0009) with an energy of 3.19 eV (λ = 389 nm), which fits nicely with the weak lowest energy absorption (i.e., λ = ca. 400 nm in CH_2Cl_2) observed in the UV-vis spectrum.

4.3 Conclusion

Two derivatives of phenylpyridyl-fused boroles were prepared and studied. Compound **10** transformed the electron-poor pyridyl group into an electron-rich dihydropyridine moiety, thus it becomes a donor-π-acceptor-type compound. The electron-rich property of the dihydropyridine moiety was confirmed by its oxidation potential (E_{pc} = +0.37 V). The cathodically shifted reduction potential and upfield chemical shift of the ^{11}B NMR signal suggest strong conjugation between the dihydropyridine moiety and the boron atom, which was confirmed by the theoretical studies. Compound **11** transformed the electron-poor pyridyl group into an even more electron-deficient *N*-methylpyridinium cation. Compound **11** is extremely electron-deficient which was confirmed by the anodically shifted first reduction potential ($E_{1/2}^{red}$ = –1.23 V). The extreme electron-deficiency of compound **11** leads to reversible coordination to THF, which was confirmed by ^{1}H and ^{11}B NMR studies. The electron-deficient property of compound **11** was further confirmed by the extremely low calculated LUMO energy. Photophysical properties for both compounds were investigated which suggest a LE transition for compound **10** and a polarized ground state for compound **11**.

5 Synthesis and Structural Characterization of a Bis(2-pyridyl)methoxyborate Li^+ Complex

5.1 Introduction

Three-coordinate boron has a vacant p_z-orbital which can serve as a strong π-electron acceptor leading to a wide range of applications, for example, as anion sensors (e.g., F^-),[3, 78, 79] nonlinear optical materials (NLOs),[7-9, 11-14] in live cell imaging,[21-23] etc.[4, 6, 24-32] However, the vacant p_z-orbital can be attacked by nucleophiles (e.g., H_2O), and thus triarylboranes are moisture-sensitive. Generally, two Mes groups (Mes = 2,4,6-trimethylphenyl)[34] or one Tip group (Tip = 2,4,6-tri*iso*propylpehnyl)[116, 265-272] at the boron center are sterically demanding enough to provide moisture-stable triarylboranes. In order to enhance the electron accepting ability, instead of using Mes group(s), Marder[35-37, 39, 118, 139-141] and others[40-44] have employed electron withdrawing 2,4,6-$(CF_3)_3C_6H_2$ (^{F}Mes) group(s) at the boron, which also enhanced stability, the latter is attributed to the combined effect of the steric bulk of the ^{F}Mes group and B···F intramolecular interactions involving F atoms from CF_3 group(s) at the *ortho*-positions.[35, 36, 38, 42, 135-137]

Due to the higher electronegativity of nitrogen compared to carbon, pyridine is relatively electron deficient. Thus, introduction of pyridine groups at the boron center, enhance its electron accepting ability,[208-211] as confirmed by the reduction potentials of mono-pyridine containing triarylboranes. In addition, pyridine-containing triarylboranes are potentially useful for further functionalization, e.g., methylation,[212, 213] chelation to metals[192, 215-227] and chelation to main group elements.[228-230] Thus far, only limited examples of triarylboranes which contain one pyridyl group attached to boron by B–C bonds have been reported, and we are not aware of any reports of three-coordinate bis(C-bound pyridyl)boranes. Considering the enhancement of the electron accepting ability of triaryboranes with increasing numbers of electron withdrawing groups[254] and potential for the further functionalization of pyridine, we initiated an investigation of the properties of bis(pyridyl)arylboranes. In our attempt to synthesize a

bis(pyridyl)arylborane, we obtained a bis(2-pyridyl)methoxyborate Li^+ complex which is a dimer both in solution and the solid state (Scheme 5.1).

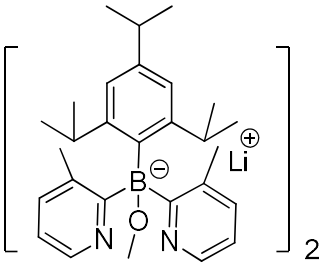

Scheme 5.1. Bis(2-pyridyl)methoxyborate Li^+ complex of dimer **[16]**$_2$.

5.2 Results and discussion

To provide enough steric hindrance around the boron center to avoid intermolecular coordination, 2-bromo-3-methylpyridine (**15**) was chosen as the substrate and Tip was selected as the aryl group at boron. Compound **15** was reacted with *n*-BuLi in Et_2O at –78 °C for 90 minutes, and then $TipB(OMe)_2$ in Et_2O was added. After purification, compound **[16]**$_2$ was obtained as a white solid in 37% yield (Scheme 5.2). In solution, compound **[16]**$_2$ decomposes slowly in the air (evidenced by NMR spectroscopy). In the ^1H NMR spectrum (500 MHz, CD_2Cl_2), the three *iso*propyl groups at the Tip group show three distinct peaks indicating different chemical environments for all three *iso*propyl groups on the NMR time scale (Figure 9.1-71). The six aromatic protons at the two pyridyl groups show three peaks but, interestingly, the peaks for *ortho*- and *para*-protons are broad. The $^{11}B\{^1H\}$ NMR chemical shift of **[16]**$_2$ is 3.5 ppm in CD_2Cl_2, which is in the typical range of a 4-coordinate boron. The $^7Li\{^1H\}$ NMR shows a sharp peak at 2.9 ppm in CD_2Cl_2 which confirms the presence of lithium cations.

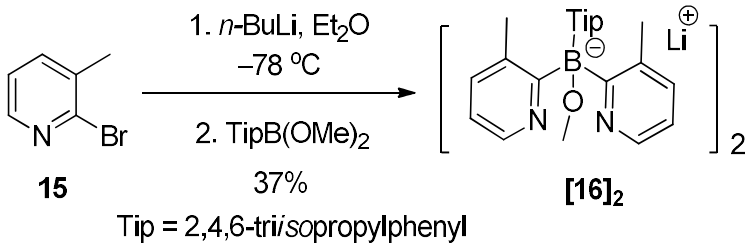

Scheme 5.2. Synthesis of bis(2-pyridyl)methoxyborate Li^+ complex **[16]**$_2$.

Colorless single crystals suitable for X-ray diffraction analysis of **[16]**$_2$ were grown from a saturated CH_2Cl_2 solution at –30 °C. The molecular structure is shown in Figure 5.1 and selected bond lengths (Å) and angles (°) are listed in Table 5.1. In the solid state, compound **[16]**$_2$ is a dimer containing two bis(2-pyridyl)methoxyborate anions which are linked by two lithium cations. Each lithium cation coordinates to one methoxy group and two pyridyl nitrogen atoms, one from each of the two bis(2-pyridyl)methoxyborate anions. The two lithium atoms and two oxygen atoms are almost in the same plane with

a dihedral angle of 5.56(12)° between the O1Li1Li2 and the O2Li1Li2 planes. The two bis(2-pyridyl)methoxyborates of **[16]**$_2$ are situated above and below the O1Li1Li2O2 plane, respectively.

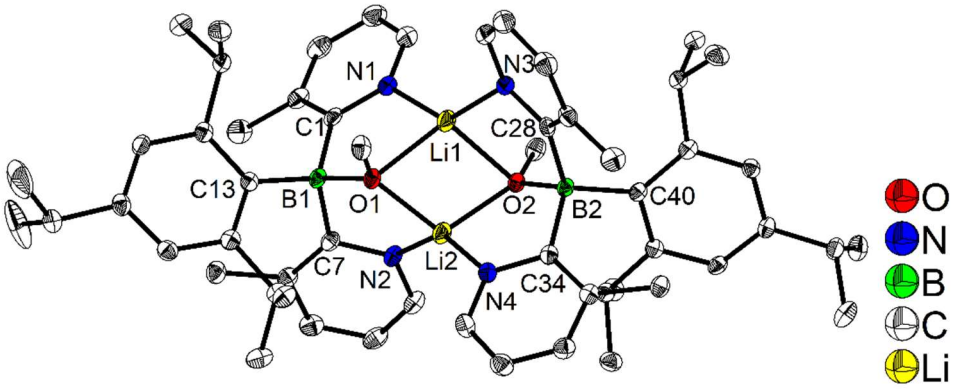

Figure 5.1. Molecular structure of **[16]**$_2$ from single-crystal X-ray diffraction data in the sold state at 100 K. Atomic displacement ellipsoids are drawn at the 50% probability level, and hydrogen atoms as well as dichloromethane solvent molecules are omitted for clarity.

Table 5.1. Selected bond lengths (Å) and angles (°) of **[16]**$_2$.			
B1–C1	1.680(3)	B2–C28	1.679(3)
B1–C7	1.674(3)	B2–C34	1.668(3)
B1–C13	1.652(3)	B2–C40	1.664(3)
B1–O1	1.544(2)	B2–O2	1.545(2)
Li1–N1	1.974(4)	Li1–N3	1.981(4)
Li1–O1	2.036(4)	Li1–O2	1.997(4)
Li2–N2	1.988(4)	Li2–N4	1.965(4)
Li2–O1	1.924(4)	Li2–O2	1.931(4)
Li1–Li2	2.379(4)		
O1–O2	3.140(2)		
∠C1–B1–C13	119.76(16)	∠C28–B2–C40	119.23(15)
∠C7–B1–C13	112.24(15)	∠C34–B2–C40	108.73(15)
∠C1–B1–O1	105.29(15)	∠C28–B2–O2	103.78(14)
∠C7–B1–O1	105.02(14)	∠C34–B2–O2	105.20(14)
$\angle plane_{O1Li1Li2}–plane_{O2Li1Li2}$	5.56(12)		

To study the behavior of **[16]**$_2$ in solution (dimer vs. monomer), diffusion-ordered

spectroscopy (^{1}H DOSY) was performed in CD_2Cl_2 at +25 °C. All proton signals of **[16]**$_2$ appear on the same horizonal axis with log(D (diffusion constant)) = –9.07 (log(m^2/s)) (Figure 9.1-75). Applying the Stokes–Einstein equation $r = \frac{k_B T}{6\pi\eta D}$ (k_B is the Boltzmann constant, T is temperature (K), η is dynamic viscosity (ca. 0.417 mPa·s of CD_2Cl_2 at +25 °C),[273] the van der Waals radius was estimated approximately 6.15 Å.[233] The molecular volume of **[16]**$_2$ in the solid state was calculated to be 819.41 Å^3 using the Olex2 program package (the following element radii were used: C = 1.7 Å; H = 1.09 Å; B = 2 Å; N = 1.55 Å; Li = 1.82 Å; O = 1.52 Å)[235] The van der Waals radius of **[16]**$_2$ was calculated to be 5.8 Å using the equation $V = \frac{4}{3}\pi r^3$. The van der Waals radius obtained by DOSY nicely matches the result from the solid state, thus indicating that and the dimer of **16** is persists in solution.

Bis(2-pyridyl)borate has been widely applied as a ligand for Pt(II),[274-280] Ru(II),[281-283] Ni(II),[284] Cu(I),[285, 286] Ir(I),[287] and Rh(I).[287] Via oxidation-induced methyl transfer in methanol or hydrolysis of corresponding bis(2-pyridyl)dimethylborate complexes, bis(2-pyridyl)methoxyborate stabilized Pt(IV) complex[275, 278, 280] and bis(2-pyridyl)hydroxylborate-stabilized Ru(II)[281-283] were obtained as monomers. The B–C bond lengths of the boron atoms and the carbon atoms of the pyridyl rings of **[16]**$_2$ (1.668(3)–1.680(3) Å, Table 5.1) are significantly longer than the corresponding bond lengths of hydrogen dimethylbis(2-pyridyl)borate (1.631(3) and 1.632(3) Å)[288] and phenylbis(2-pyridyl)*iso*propoxyborate-stabilized Pt(IV) complex (1.637(4)-1.645(4) Å, two distinct molecules in the unit cell).[276] The B–C bond lengths of the boron atoms and the carbon atoms of the Tip groups of **[16]**$_2$ (1.652(3) and 1.664(3) Å, Table 5.1) are also longer than the B–C bond lengths from the boron atom to the carbon atoms of the phenyl groups of phenylbis(2-pyridyl)*iso*propoxyborate-stabilized Pt(IV) complex (1.615(4) and 1.618(4) Å). The B–O bond lengths are the same for **[16]**$_2$ (1.544(2) Å and 1.545(2) Å, Table 5.1) and phenylbis(2-pyridyl)*iso*propoxyborate-stabilized Pt(IV) complex (1.544(4) and 1.546(4) Å) within standard uncertainties. The elongated B–C bond lengths of **[16]**$_2$ are attributed to the larger steric demands of the Tip group and

the methyl substituents on the pyridyl rings. The Li–N bond lengths (1.965(4)-1.988(4) Å) are significantly shorter than those of tetrakis(pyridine)lithium (2.042(4) and 2.048(4) Å)[289] which suggests strong coordination of pyridine to Li^+ in **[16]**$_2$. The reaction of a tris(2-pyridyl)aluminate with alcohols leads to similar coordination dimers.[290-293] Compared to the dimer of EtAl(OMe)(2-pyridyl)$_2$Li, the distance between two lithium cations in dimer of EtAl(OMe)(2-pyridyl)$_2$Li (2.657(4) Å) is significantly longer than in **[16]**$_2$ (2.379(4) Å), the distance between two oxygen atoms in dimer of EtAl(OMe)(2-pyridyl)$_2$Li (2.973(2) Å) is significantly shorter than in **[16]**$_2$ (3.140(4) Å).[290]

After we obtained the **[16]**$_2$, different Lewis acids (e.g., TMSCl, BF_3•Et_2O, $AlCl_3$, HCl) were used to attempt to detach the methoxy group and synthesize the three-coordinate bis(pyridyl)borane. However, we observed either decomposition or selective cleavage of the Tip group, or no reaction at all, rather than the cleavage of the methoxy group from boron.

5.3 Conclusions

In conclusion, we synthesized and structural characterized an interesting bis(2-pyridyl)borate Li^+ complex which is a dimer in the solid state and in solution. Due to the large steric demand of the groups attached to the boron center, all the bond lengths between the boron atom and the attached carbon atoms are elongated. The short Li–N bond lengths suggest strong coordination between the boron atom and pyridyl groups, which become problematic when we tried to detach the methoxy group of $[\mathbf{16}]_2$.

6 Summary/Zusammenfassung

6.1 Summary

6.1.1 Chapter 1

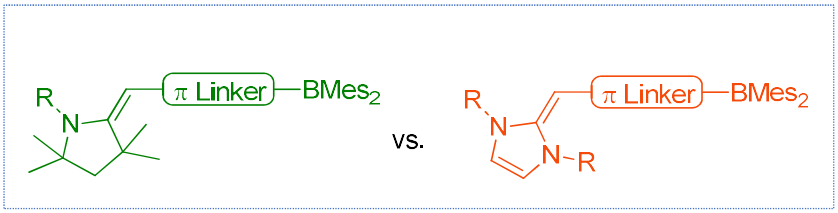

N-Heterocyclic olefins (NHOs), relatives of *N*-heterocyclic carbenes (NHCs), exhibit high nucleophilicity and soft Lewis basic character. To investigate their π-electron donating ability, NHOs were attached to triarylborane π-acceptors (A) giving donor(D)-π-A compounds **1**-**3**. In addition, an enamine π-donor analogue (**4**) was synthesized for comparison (Scheme 6.1).

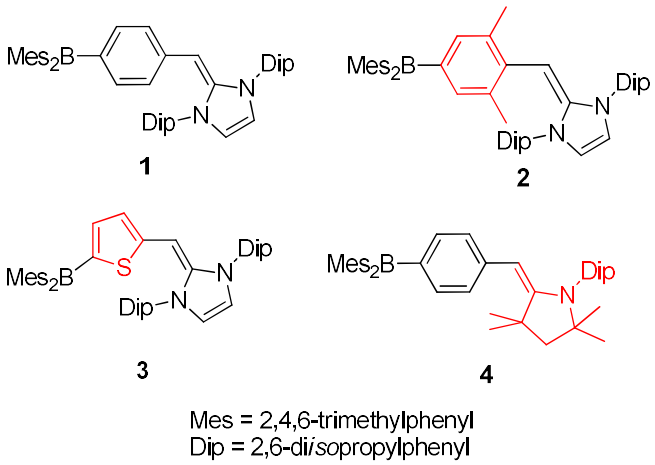

Scheme 6.1. Three-coordinate boranes **1**-**4** developed in this study.

UV-visible absorption studies show a larger red shift for the NHO-containing boranes than for the enamine analogue, a relative of a CAAC. The red shifted absorption of NHO-containing boranes indicate smaller energy gaps of NHO-containing boranes than CAAC-containing boranes. Solvent-dependent emission studies indicate that **1**-**4** have moderate intramolecular charge transfer (ICT) behavior (Figure 6.1).

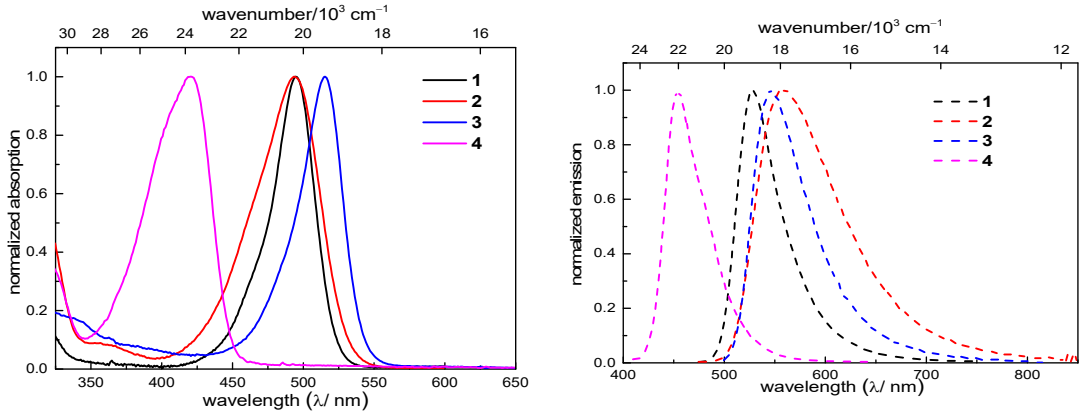

Figure 6.1. UV-visible absorption (left) and emission spectra (right) of boranes **1**-**4** in toluene.

Electrochemical investigations reveal that the NHO-containing boranes have extremely low reversible oxidation potentials (e.g., for **3**, $E_{1/2}^{ox}$ = –0.40 V vs. Fc/Fc^+ in THF) which indicate the electron rich property of NHOs (Figure 6.2).

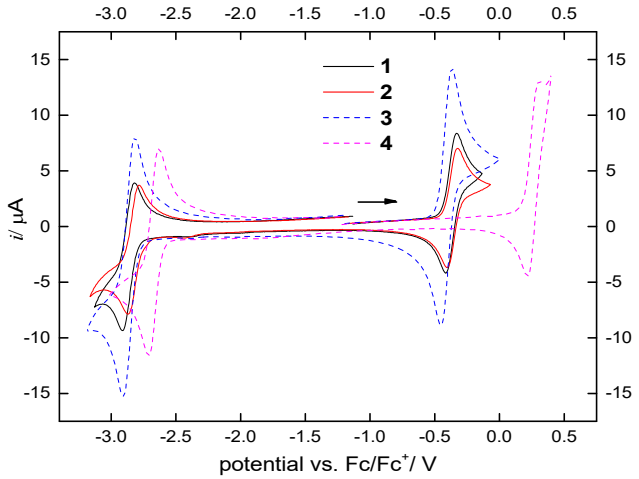

Figure 6.2. Cyclic voltammograms of **1** (black, solid), **2** (red, solid), **3** (blue, dash), and **4** (pink, dash).

Furthermore, TD-DFT calculations were carried out on these four D-π-A boranes. The results show that the LUMOs of **1**-**4** only show a small difference, but the HOMOs of **1**-**3** are much more destabilized than that of the enamine-containing **4**, which is in agreement with the electrochemical investigations and confirms the stronger donating ability of NHOs.

6.1.2 Chapter 2

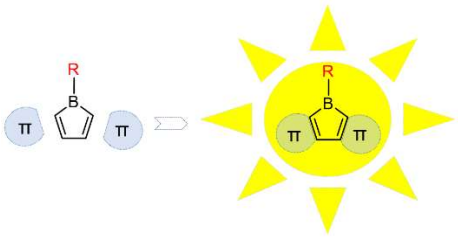

Since the beginning of this century, the chemistry of (hetero)arene-fused boroles has attracted increasing interest. (Hetero)arene-fused boroles exhibit strong Lewis acidity, distinct fluorescence properties, strong electron accepting abilities, etc. However, their chemistry been only very briefly reviewed either as part of reviews on "free" boroles or on boron-doped polycyclic aromatic hydrocarbons (PAHs). In this chapter, we addressed the chemistry of (hetero)arene-fused boroles from fundamentals to their widely varying applications. It includes:

1) Synthetic methodology ⇒ Both historical and recently developed strategies for the synthesis of fused boroles.
2) Stabilities ⇒ A comparison of different kinetic protection strategies.
3) 9-Borafluorenes with a fluorinated backbone ⇒ Application as Lewis acids, forming ion pairs with $Cp_2Zr(CH_3)_2$ and applied as activators for polymerization, activators of H_2, and other related applications.
4) Donor-acceptor 9-borafluorenes ⇒ Applications as F^- "turn on" sensors, potential applications as electron accepting units for organic (opto)electronics, bipolar transporting materials, TADF materials, and different functionalization strategies.
5) Heteroarene-fused boroles ⇒ Enhanced antiaromaticity, unique coordination mode and their interesting properties.
6) Intramolecular dative bonding in 9-borafluorenes ⇒ Bond-cleavage-induced intramolecular charge transfer (BICT), BICT-induced large Stoke shifts and dual emissions, application as a ratiometric sensor.
7) 9-Borafluorene-based main chain polymers ⇒ Application in polymer chemistry and their distinct properties, e.g., as a sensor for gaseous NH_3.

8) Electrochemistry ⇒ A comparison of electron-accepting ability of different functionalized fused boroles through electrochemical studies.
9) Chemical reduction of fused boroles ⇒ Stable radical anions and dianions of fused boroles and their properties.
10) Three-coordinate borafluorenium cations ⇒ Cationic 9-borafluorenes and their interesting properties, e.g., in THF, reversible thermal colour switching properties.

Finally, a conclusion and outlook regarding the chemistry, properties and applications, and suggestions for areas which require further study was provided.

6.1.3 Chapter 3

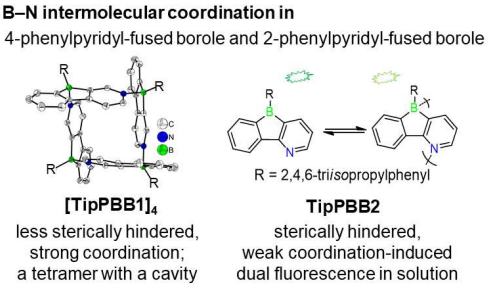

Interested in fusing electron-poor arene onto boroles, two electron-poor phenylpyridyl-fused boroles, **[TipPBB1]**$_4$ and **TipPBB2** were prepared. **[TipPBB1]**$_4$ is a white solid adopting a unique coordination mode, which forming a tetramer with a cavity in both the solid state (Figure 6.3) and solution (^{1}H DOSY). The boron center of **TipPBB2** is 4-coordinate in the solid state, evidenced by a solid-state ^{11}B{^{1}H} RSHE/MAS NMR study, but the system dissociates in solution, leading to 3-coordinate borole species.

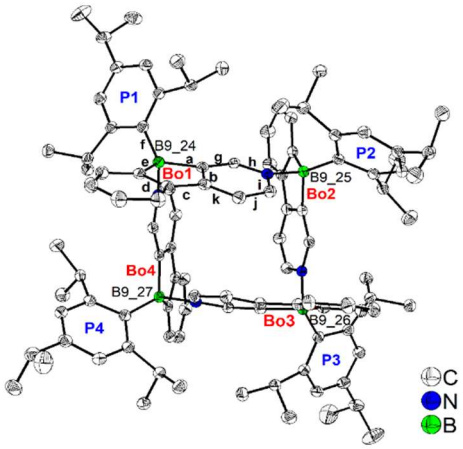

Figure 6.3 Molecular structure of **[TipPBB1]**$_4$ in the solid state at 100 K.

[TipPBB1]$_4$ exhibits two reduction processes which are attributed to the phenylpyridyl cores. **TipPBB2** also exhibits two reduction processes with the first half-reduction potential of $E_{1/2}^{red}$ = –1.94 V. The electron accepting ability of **TipPBB2** is largely enhanced and comparable to that of ^{F}**MesBf**. This enhanced electron accepting ability is attributed to the electron withdrawing property of the pyridyl group.

TipPBB2 exhibits concentration- and temperature-dependent dual fluorescence in solution. With the temperature is lowered, the emission intensity decreases (Figure 6.4, left). We suggested that the dual fluorescence is caused by an equilibrium between 3-coordinate **TipPBB2** and a weak intermolecular adduct of **TipPBB2** via a B–N bond. This hypothesis was further supported by lifetime measurements at different concentrations, low temperature excitation spectra (Figure 6.4, right), low temperature ^{1}H NMR spectra and lifetime measurements upon addition of DMAP to a solution of **TipPBB2** to simulate the 4-coordiante **TipPBB2** species. Interestingly, the ratio of the relative percentages of the two lifetimes shows a linear relationship with temperature; thus, **TipPBB2** could serve as a fluorescent thermometer.

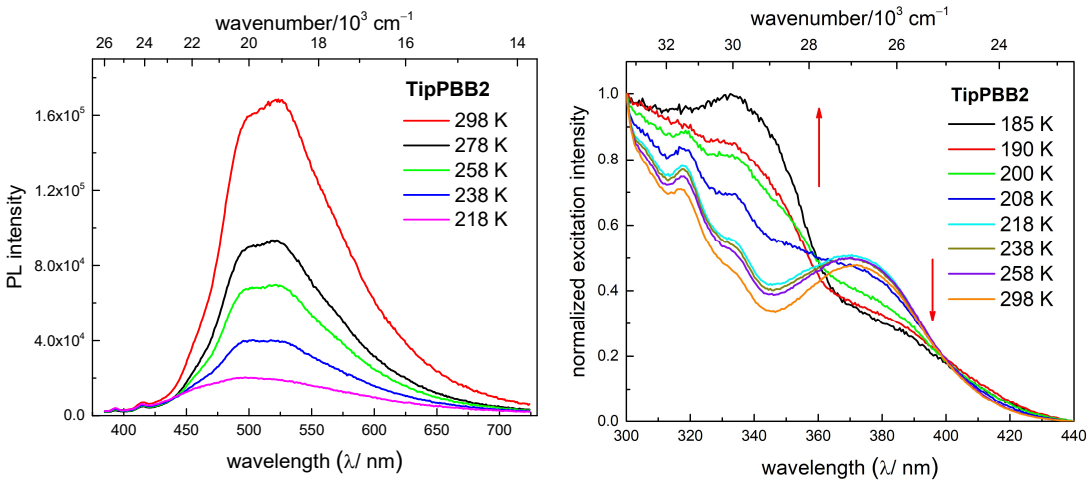

Figure 6.4. Temperature dependence of the emission spectra in 2-methyl-THF (left) and temperature dependence of excitation spectra (right) with emission at 520 nm in CH_2Cl_2.

Furthermore, theoretical studies were carried out on **TipPBB2**, and two models, (**(BMe$_3$)TipPBB1(NMe$_3$)** and **(BMe$_3$)TipPBB2(NMe$_3$)**), which utilize a BMe_3 group as the Lewis acid coordinated to pyridine and an NMe_3 group as the Lewis base coordinated to the boron center of the borole, were used to simulate the **[TipPBB1]$_4$** and intermolecular 4-coordinate **TipPBB2**, respectively. Theoretical studies indicate that the HOMO of **TipPBB2** is located at the Tip group, which is in contrast to its borafluorene derivatives for which the HOMOs are located on the borafluorene cores.

6.1.4 Chapter 4

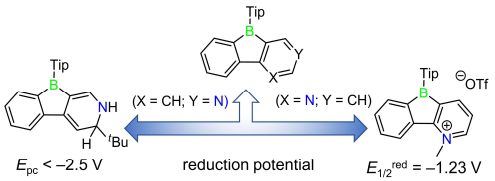

Two derivatives of phenylpyridyl-fused boroles were prepared via functionalization of the pyridyl groups in two different directions, namely an electron-rich dihydropyridine moiety (compound **10**) and an electron-deficient *N*-methylpyridinium cation (compound **11**). Both compounds were fully characterized. The ^{11}B NMR signal of compound **10** was observed at 58.8 ppm in $CDCl_3$, which suggests strong conjugation between the boron atom and dihydropyridine moiety. Compound **11** shows a reversible coordination to THF which was confirmed by NMR studies. Compared to other 2,4,6-tri*iso*propylphenyl protected 9-borafluorenes which only coordinate to CH_3CN or DMF, the coordination of the weaker and bulkier THF to compound **11** indicates an extremely electron-deficient boron center in compound **11**.

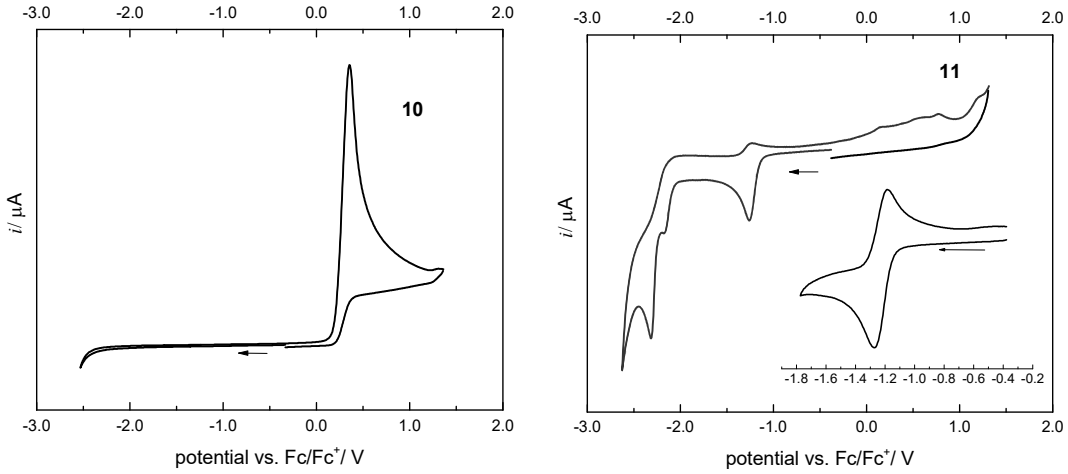

Figure 6.5. Cyclic voltammograms of compounds **10** (left) and **11** (right). Measured in CH_2Cl_2 in the presence of 0.1 M $TBAPF_6$, scan rates of 250 mV s^{-1} and potentials given vs. the Fc/Fc^+ couple.

The electron-rich property of the dihydropyridine moiety of compound **10** was confirmed by its oxidation potential (E_{pc} = +0.37 V). Due to the strong conjugation of

the dihydropyridine moiety with the boron atom, the reduction potential of compound **10** shifts cathodically and is more negative than –2.5 V (Figure 6.5, left). Compound **11** exhibits three reduction processes with the first reversible reduction potential at $E_{red}^{1/2}$ = –1.23 V (Figure 6.5, right), which is significantly anodically shifted compared to that of its precursor (**TipPBB2**) or its framework 1-methyl-2-phenylpyridin-1-ium triflate (**12**). This significantly anodically shifted reduction potential confirms an extremely electron-deficient property of compound **11**.

Photophysical studies indicate that the lowest energy transition of compound **10** is more likely a locally-excited (LE) transition and compound **11** exhibits a polarized ground state (Figure 6.6).

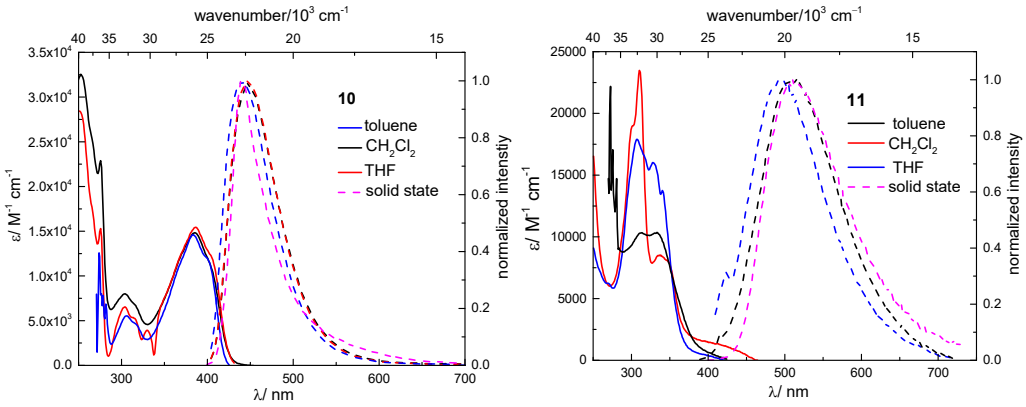

Figure 6.6. UV-vis absorption (solid line) and emission (dashed line) spectra of compounds **10** (left) and **11** (right) in toluene, CH_2Cl_2, THF and the solid state.

Furthermore, we performed theoretical studies for both compounds. The electron cloud distribution of the HOMO of compound **10** supports the strong conjugation between the boron atom and the dihydropyridine moiety in the ground state. An extremely low LUMO energy was determined by theoretical studies which confirmed the extremely electron-deficient property of compound **11**.

6.1.5 Chapter 5

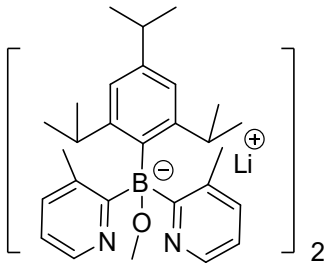

Inspired by the enhancement of electron accepting ability with increasing numbers of electron withdrawing groups at boron, we tried to study the properties of a bis(pyridyl)arylboranes. In our attempt to synthesize a bis(pyridyl)arylborane, we obtained a bis(2-pyridyl)methoxyborate Li^+ complex which is as a dimer both in solution and the solid state (Scheme 6.3).

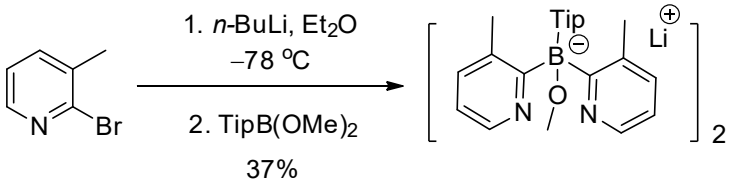

Scheme 6.3. Synthesis of bis(2-pyridyl)methoxyborate Li^+ complex **[16]**$_2$.

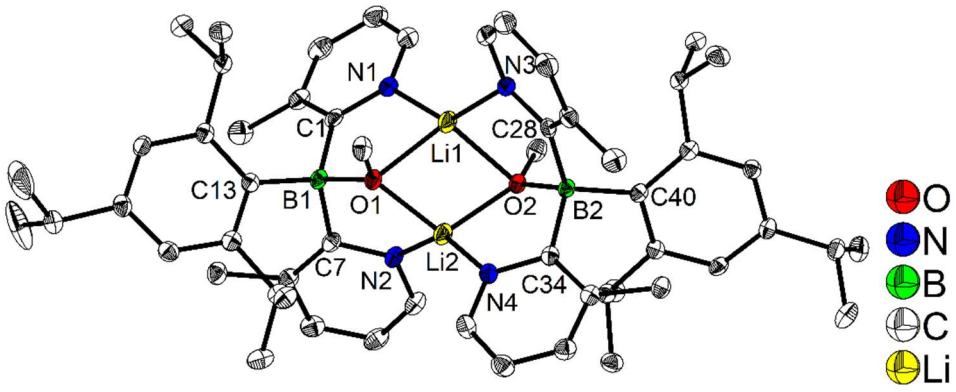

Figure 6.7. Molecular structure of **[16]**$_2$ from single-crystal X-ray diffraction data in the solid state at 100 K.

In the solid state, compound **[16]**$_2$ is a dimer containing two bis(2-pyridyl)methoxyborate which are linked by two lithium cations. Each lithium cation coordinates to one methoxy group and two pyridyl groups, one from each of the two bis(2-pyridyl)methoxyborate anions (Figure 6.7). The parameters of **[16]**$_2$ were compared with other bis(2-pyridyl)methoxyborate stabilized Pt(IV) complex, bis(2-pyridyl)hydroxylborate stabilized Ru(II) complex and the dimer of EtAl(OMe)(2-pyridyl)$_2$Li.

To confirm the coordination mode in solution, ^{1}H DOSY spectroscopy was carried out in CD_2Cl_2. The van der Waals radius obtained by ^{1}H DOSY nicely matches with the result from the solid state and thus proves the dimer of **16** is persistent in solution.

Finally, different Lewis acids (e.g., TMSCl, BF_3•Et_2O, $AlCl_3$, HCl) were used to attempt to detach the methoxy group of **[16]**$_2$. However, we observed either decomposition or selective cleavage of the Tip group, or no reaction at all, rather than cleavage of the methoxy group from boron.

6.2 Zusammenfassung

6.2.1 Kapitel 1

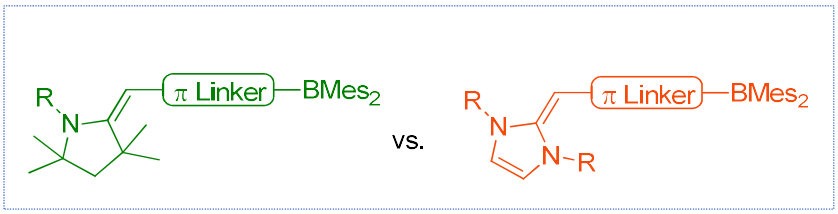

N-Heterocyclische Olefine (NHOs) sind Verwandte der *N*-heterocyclischen Carbene (NHCs) und weisen eine hohe Nukleophilie sowie einen weichen Lewis-Grundcharakter auf. Um ihre Fähigkeit als π-Elektronendonor zu untersuchen, wurden diese NHOs an π-Triarylboran-Akzeptoren (A) gebunden, wodurch die Donor(D)-π-A-Verbindungen **1**-**3** erhalten wurden. Zusätzlich wurde zum Vergleich das Enamin π-Donoranalogon (**4**) synthetisiert (Schema 6.1).

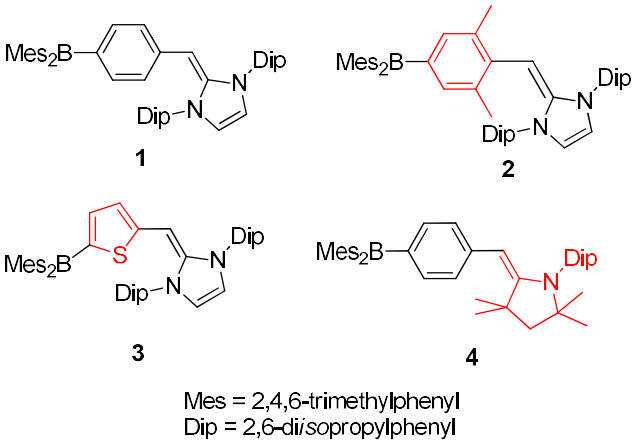

Schema 6.1. Die in dieser Studie entwickelten dreifach koordinierten Borane **1**-**4**.

Studien zur UV/Vis-Absorption zeigen für die NHO-haltigen Borane eine stärkere Rotverschiebung als für das Enamin-Analogon, welches ein Verwandter von CAACs ist. Die rotverschobene Absorption der NHO-haltigen Borane weist auf kleinere Energielücken bei den NHO-haltigen Boranen als bei den CAAC-haltigen Boranen hin. Des Weiteren zeigen Lösungsmittel-abhängige Emissionsstudien, dass die Verbindungen **1**-**4** ein moderates intramolekulares Ladungstransfer(ICT)-Verhalten aufweisen (Abbildung 6.1).

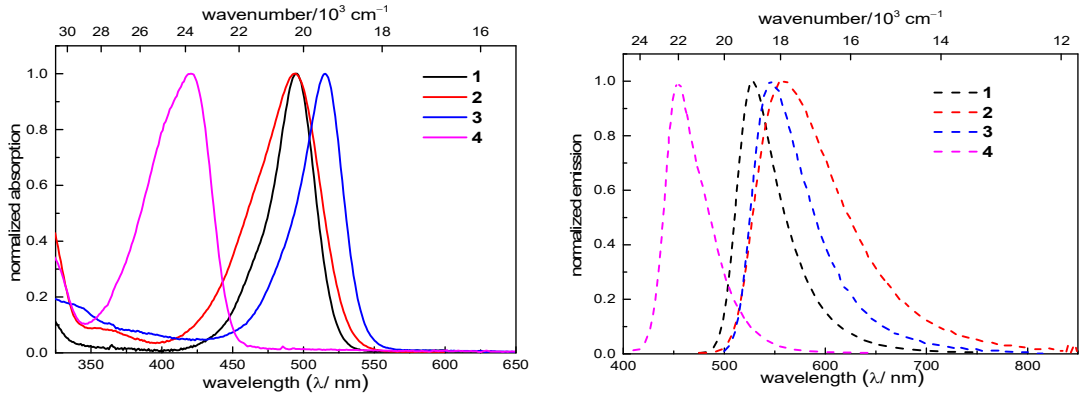

Abbildung 6.1. UV/Vis-Absorptionen- (links) und Emissionsspektren (rechts) der Borane **1**-**4** in Toluol.

Elektrochemische Untersuchungen zeigen, dass die NHO-haltigen Borane extrem niedrige reversible Oxidationspotentiale aufweisen (z.B. für **3**, $E_{1/2}^{ox}$ = –0,40 V vs. Fc/Fc^+ in THF), was auf die elektronenreiche Eigenschaft der NHOs hinweist (Abbildung 6.2).

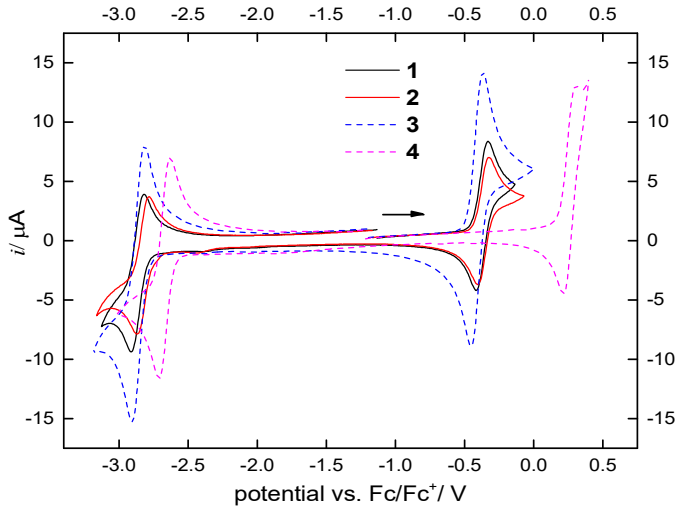

Abbildung 6.2. Zyklische Voltammogramme von **1** (schwarz, durchgezogene Linie), **2** (rot, durchgezogene Linie), **3** (blau, gestrichelte Linie) und **4** (rosa, gestrichelte Linie).

Darüber hinaus wurden TD-DFT-Berechnungen für diese vier D-π-A-Borane durchgeführt. Die Ergebnisse zeigen, dass die jeweiligen LUMOs von **1**-**4** nur einen geringen Unterschied zueinander aufweisen, die HOMOs von **1**-**3** jedoch viel stärker

destabilisiert sind als die des enaminhaltigen **4**, was mit den elektrochemischen Untersuchungen übereinstimmt und die stärkere Donorfähigkeit der NHOs bestätigt.

6.2.2 Kapitel 2

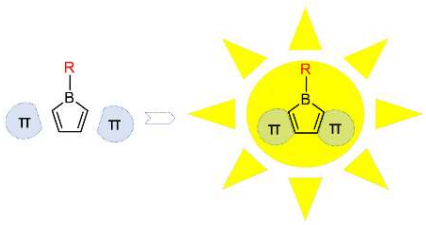

Seit Beginn dieses Jahrhunderts hat die Chemie von (Hetero)aren-kondensierten Borolen zunehmendes Interesse geweckt. (Hetero)aren-kondensierte Borole weisen eine starke Lewis-Acidität, ausgeprägte Fluoreszenzeigenschaften, starke Elektronenakzeptor-fähigkeiten, etc. auf. Ihre Chemie wurde jedoch bislang nur wenig untersucht und es gibt kaum Übersichten zu ihren Eigenschaften, entweder als Teil von Übersichtsarbeiten über "freie" Borole oder über bordotierte polyzyklische aromatische Kohlenwasserstoffe (PAK). In diesem Kapitel wird die Chemie von (Hetero)aren-kondensierten Borolen von den Grundlagen bis zu ihren sehr unterschiedlichen Anwendungen behandelt. Es umfasst:

1) Synthetische Methoden ⇒ Sowohl historische als auch kürzlich entwickelte Strategien für die Synthese von kondensierten Borolen.
2) Stabilitäten ⇒ Ein Vergleich verschiedener kinetischer Schutzstrategien.
3) 9-Borafluorene mit fluoriertem Rückgrat ⇒ Anwendung als Lewis-Säure, Bildung von Ionenpaaren mit $Cp_2Zr(CH_3)_2$ und Anwendung als Aktivatoren für die Polymerisation, Aktivatoren von H_2 und andere verwandte Anwendungen.
4) Donor-Akzeptor 9-Borafluorene ⇒ mögliche Anwendungen als F^- "Einschalt"-Sensoren, als elektronenakzeptierende Einheit für die organische (Opto-)Elektronik, bipolare Transportmaterialien, TADF-Materialien und verschiedene Funktionalisierungsstrategien.
5) Heteroaren-kondensierte Borole ⇒ Gesteigerte Antiaromatizität, einzigartiger Koordinationsmodus und interessante Eigenschaften.
6) Intramolekulare dative Bindung in 9-Borafluorenen ⇒ Bindungsbruch-induzierter

intramolekularer Ladungstransfer (BICT), BICT-induzierte große Stokes-Verschiebungen und duale Emissionen, Anwendung als ratiometrischer Sensor.

7) 9-Borafluoren-basierte Hauptkettenpolymere ⇒ Anwendung in der Polymerchemie und deren charakteristische Eigenschaften, z.B. als Sensoren für gasförmiges NH_3.
8) Elektrochemie ⇒ Ein Vergleich der Elektronenakzeptorfähigkeit unterschiedlicher funktionalisierter kondensierter Borole durch elektrochemische Untersuchungen.
9) Chemische Reduktion von kondensierten Borolen ⇒ Stabile Radikalanionen und Dianionen von kondensierten Borolen und deren Eigenschaften.
10) Dreifach koordinierte Borafluorenium-Kationen ⇒ Kationische 9-Borafluorene und ihre spannenden Eigenschaften, wie z.B. die reversible thermische Schaltbarkeit durch Farbe in THF.

Am Ende des Kapitels werden Schlussfolgerungen gezogen und ein Ausblick zur weiteren Chemie, etwaigen Eigenschaften sowie möglichen Anwendungen gegeben. Ferner werden Vorschläge zu Feldern gemacht, die weitere Untersuchungen bedürfen.

6.2.3 Kapitel 3

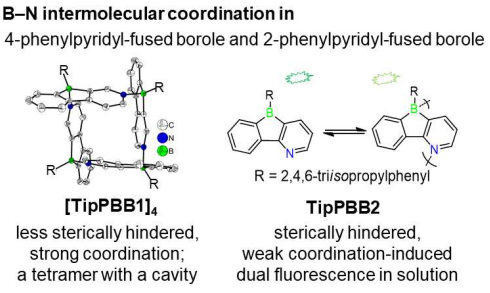

Um elektronenarme Arene mit Borolen zu kondensieren, wurden zwei elektronenarme Phenylpyridyl-kondensierte Borole, **[TipPBB1]**$_4$ und **TipPBB2**, hergestellt. **[TipPBB1]**$_4$ ist ein weißer Feststoff, der einen einzigartigen Koordinationsmodus aufweist. Sowohl im Festkörper (Abbildung 6.3) als auch in Lösung (^{1}H DOSY) liegt ein Tetramer mit einem Hohlraum vor. Das Borzentrum von **TipPBB2** ist im Festkörper 4-fach koordiniert, was durch ein Festkörper ^{11}B{^{1}H} nachgewiesen wurde. RSHE/MAS-NMR-Studien zeigten aber, dass das System in Lösung dissoziiert, was zu einer 3-fach koordinierten-

Borolspezies führt.

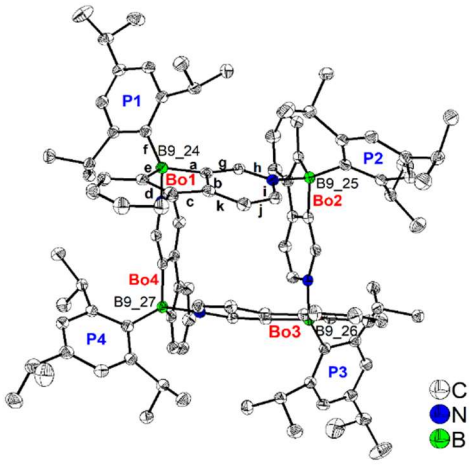

Abbildung 6.3 Molekülstruktur von **[TipPBBI]**$_4$ im Festkörper bei 100 K.

[TipPBBI]$_4$ zeigt zwei Reduktionsprozesse, die den Phenylpyridylkernen zugeschrieben werden. **TipPBB2** zeigt ebenfalls zwei Reduktionsprozesse mit dem ersten Halb-Reduktionspotential von $E_{1/2}^{red.}$ = –1,94 V. Die Elektronenakzeptorfähigkeit von **TipPBB2** ist somit weitgehend verbessert und mit der von ^{F}**MesBf** vergleichbar. Diese verbesserte Elektronenakzeptorfähigkeit ist auf den elektronenziehenden Effekt der Pyridylgruppe zurückzuführen.

TipPBB2 zeigt konzentrations- und temperaturabhängige duale Fluoreszenz in Lösung. Mit sinkender Temperatur nimmt die Emissionsintensität ab (Abbildung 6.4, links). Es liegt die Vermutung nahe, dass die duale Fluoreszenz durch ein Gleichgewicht zwischen 3-fach koordinierten-**TipPBB2** und einem schwachen intermolekularen Addukt von **TipPBB2** über eine B–N-Bindung verursacht wird. Diese Hypothese wurde durch Lebenszeitmessungen bei verschiedenen Konzentrationen, Niedrigtemperatur-Anregungsspektren (Abbildung 6.4 rechts), Niedrigtemperatur-^{1}H-NMR-Spektren und Lebenszeitmessungen nach Zugabe von DMAP zu einer Lösung von **TipPBB2** zur Simulation der 4-fach koordinierten-**TipPBB2**-Spezies weiter untermauert. Interessanterweise zeigt das Verhältnis der relativen Prozentsätze der beiden Lebenszeiten eine lineare Beziehung mit der Temperatur; daher könnte **TipPBB2** als

Fluoreszenzthermometer dienen.

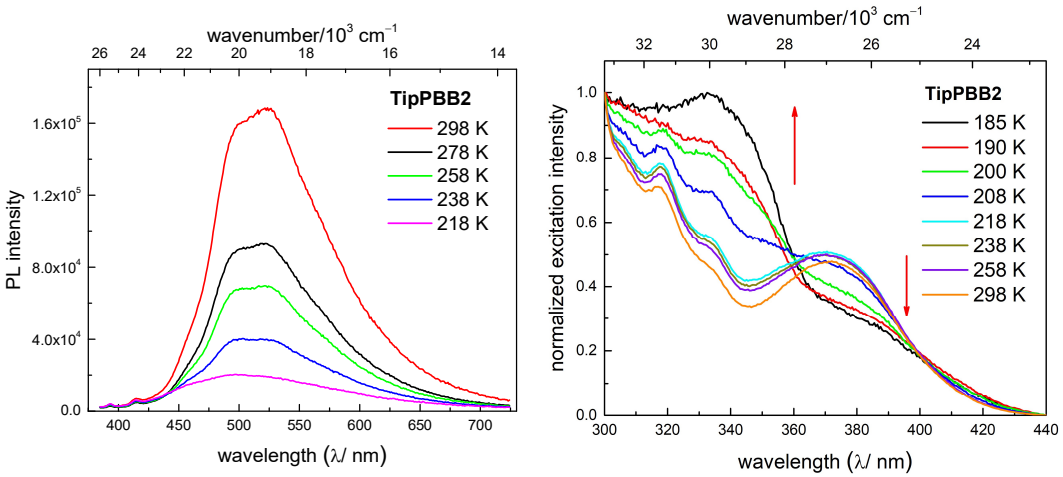

Abbildung 6.4. Temperaturabhängigkeit der Emissionsspektren in 2-Methyl-THF (links) und Temperaturabhängigkeit der Anregungsspektren (rechts) mit Emission bei 520 nm in CH_2Cl_2.

Darüber hinaus wurden theoretische Studien zu **TipPBB2** durchgeführt und zwei Modellverbindungen (**(BMe$_3$)TipPBB1(NMe$_3$)** und **(BMe$_3$)TipPBB2(NMe$_3$)**) wurden untersucht, um **[TipPBB1]$_4$** bzw. das intermolekular-4-fach koordinierte **TipPBB2** zu simulieren. Die BMe$_3$-Gruppe koordiniert als Lewis-Säure an Pyridin und die NMe$_3$-Gruppe als Lewis-Base an das Borzentrum des Borols. Die theoretischen Studien weisen darauf hin, dass das HOMO von **TipPBB2** an der Tip-Gruppe lokalisiert ist, was im Gegensatz zu den entsprechenden Borafluoren-Derivaten steht, bei denen sich die HOMOs auf den Borafluoren-Kernen befinden.

6.2.4 Kapitel 4

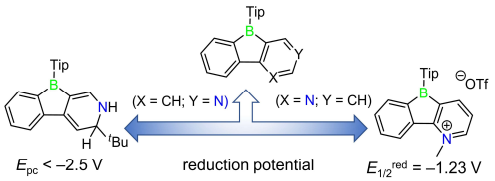

Zwei Derivate von Phenylpyridyl-kondensierten Borolen wurden durch Funktionalisierung der Pyridylgruppe an zwei unterschiedlichen Positionen hergestellt, zum einen eine elektronenreiche Dihydropyridin-Einheit (Verbindung **10**) und zum anderen ein elektronenarmes *N*-Methylpyridinium-Kation (Verbindung **11**). Beide Verbindungen wurden vollständig charakterisiert. Das ^{11}B-NMR-Signal von Verbindung **10** wurde bei 58,8 ppm in $CDCl_3$ beobachtet, was auf eine starke Konjugation zwischen dem Boratom und der Dihydropyridin-Einheit schließen lässt. Verbindung **11** zeigt eine reversible Koordination zu THF, was durch NMR-Studien bestätigt wurde. Im Vergleich zu anderen 2,4,6-Tri*iso*propylphenyl-geschützten 9-Borafluorenen, die nur an CH_3CN oder DMF koordinieren, weist die Koordination des schwächeren und voluminöseren THF zu Verbindung **11** auf ein extrem elektronenarmes Borzentrum in Verbindung **11** hin.

Der Elektronenreichtum der Dihydropyridin-Einheit von Verbindung **10** wurde durch sein Oxidationspotential (E_{pc} = +0,37 V) bestätigt. Aufgrund der starken Konjugation des Dihydropyridinteils mit dem Boratom verschiebt sich das Reduktionspotential von Verbindung **10** kathodisch und ist negativer als –2,5 V (Abbildung 6.5, links). Verbindung **11** zeigt drei Reduktionsprozesse mit dem ersten reversiblen Reduktionspotential bei $E_{red}^{1/2}$ = –1,23 V (Abbildung 6.5, rechts), das im Vergleich zu dem der Vorstufe (**TipPBB2**) oder ihres Gerüstes 1-Methyl-2-phenylpyridin-1-ium-Triflat (**12**) signifikant anodisch verschoben ist. Dieses signifikant anodisch verschobene Reduktionspotential bestätigt das Elektronendefizit von Verbindung **11**.

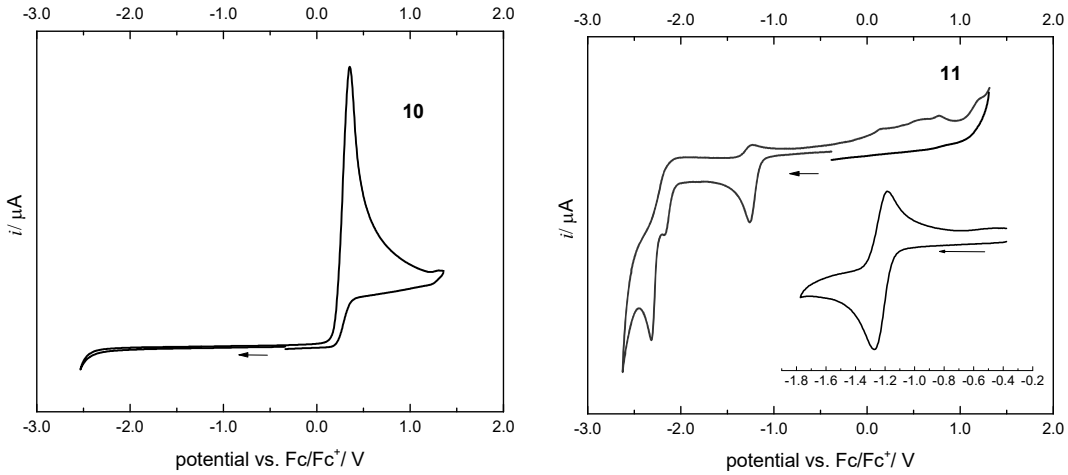

Abbildung 6.5. Zyklische Voltammogramme der Verbindungen **10** (links) und **11** (rechts). Gemessen in CH_2Cl_2 in Gegenwart von 0,1 M $TBAPF_6$, Scan-Raten von 250 mV s^{-1} und gegebene Potentiale referenziert auf das Fc/Fc^+-Paar.

Photophysikalische Studien zeigen, dass der niedrigste Energieübergang von Verbindung **10** eher ein lokal angeregter (LE) Übergang ist und Verbindung **11** einen polarisierten Grundzustand aufweist (Abbildung 6.6).

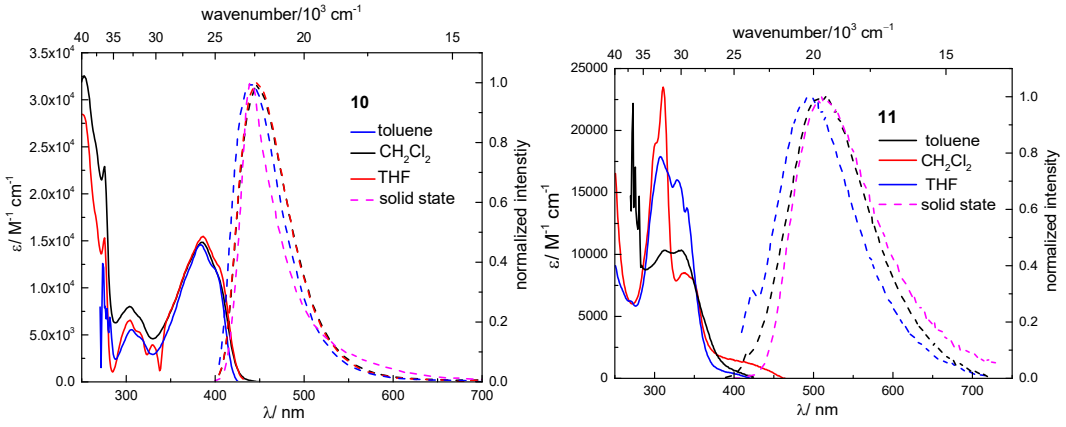

Abbildung 6.6. UV/Vis-Absorptionsspektren (durchgezogene Linie) und Emissionsspektren (gestrichelte Linie) der Verbindungen **10** (links) und **11** (rechts) in Toluol, CH_2Cl_2, THF und im Festkörper.

Darüber hinaus wurden für beide Verbindungen theoretische Studien durchgeführt. Die

Elektronenverteilung des HOMO von Verbindung **10** belegt die starke Konjugation zwischen dem Boratom und der Dihydropyridin-Einheit im Grundzustand. Eine sehr niedrige LUMO-Energie wurde durch theoretische Studien ermittelt, die das Elektronendefizit von Verbindung **11** bestätigt.

6.2.5 Kapitel 5

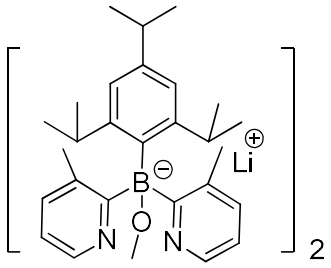

Inspiriert durch die zunehmende Elektronenakzeptorfähigkeit mit wachsender Anzahl elektronenziehender Gruppen am Boratom versuchten wir, die Eigenschaften eines Bis(pyridyl)arylborans zu untersuchen. Bei unserem Versuch, ein Bis(pyridyl)arylboran zu synthetisieren, erhielten wir jedoch einen Bis(2-pyridyl)methoxyborat-Li^+-Komplex, der als Dimer sowohl in Lösung als auch im festen Zustand vorliegt (Schema 6.3).

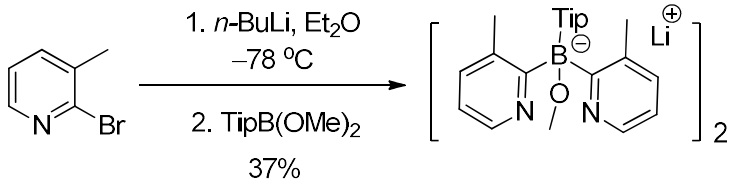

Schema 6.3. Synthese des Bis(2-pyridyl)methoxyborat-Li^+-Komplexes **[16]**$_2$.

Im Festkörper ist die Verbindung **[16]**$_2$ ein Dimer, das zwei Bis(2-pyridyl)methoxyborat-Einheiten enthält welche durch zwei Lithiumkationen verbunden sind. Jedes Lithiumkation koordiniert an eine Methoxygruppe und an zwei Pyridylgruppen, jeweils eine von jedem der beiden Bis(2-pyridyl)methoxyborat-Anionen (Abbildung 6.7). Die Parameter von **[16]**$_2$ wurden mit anderen Bis(2-pyridyl)methoxyborat-stabilisierten Pt(IV)-Komplexen, Bis(2-pyridyl)hydroxylborat-stabilisierten Ru(II)-Komplexen und

dem Dimer von EtAl(OMe)(2-pyridyl)$_2$Li verglichen.

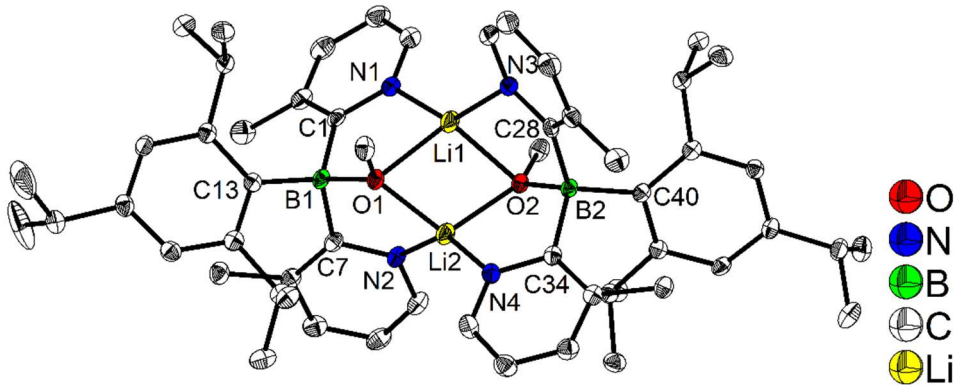

Abbildung 6.7. Molekülstruktur von **[16]**$_2$ im Festkörper bei 100 K.

Um den Koordinationsmodus in Lösung zu bestätigen, wurde eine ^{1}H-DOSY-Studie in CD_2Cl_2 durchgeführt. Der aus den Daten ermittelte van-der-Waals-Radius stimmt gut mit dem Ergebnis aus den Festkörperuntersuchungen überein und beweist somit, dass das Dimer von **16** in Lösung persistent ist.

Schließlich wurde mit verschiedenen Lewis-Säuren (z.B. TMSCl, BF_3•Et_2O, $AlCl_3$, HCl) versucht, die Methoxygruppe von **[16]**$_2$ abzuspalten. Wir beobachteten jedoch entweder eine Zersetzung oder selektive Abspaltung der Tip-Gruppe oder gar keine Reaktion und nicht die Abspaltung der Methoxy-Gruppe von Bor.

7 Experimental

7.1 Synthesis

Unless otherwise noted, the following conditions apply. All starting materials were purchased from commercial sources or prepared following reported procedure, used without further purification. All solvents for synthetic reactions and for photophysical and electrochemical measurements were HPLC grade, further treated to remove trace water using an Innovative Technology Inc. Pure-Solv Solvent Purification System and deoxygenated using the freeze-pump-thaw method. All synthetic reactions were performed in an Innovative Technology Inc. glovebox or under an argon atmosphere using standard Schlenk techniques.

Reactions were monitored using thin layer chromatography (TLC) plates pre-coated with a layer of silica (Polygram® Sil G/UV254) with fluorescent indicator UV254. Column chromatography was performed using either Silica Gel 60 (40-63 microns) or aluminiumoxide 90 neutral as the stationary phase and the solvent system indicated.

^{1}H, ^{13}C{^{1}H}, ^{11}B{^{1}H} ^{19}F{^{1}H}, ^{7}Li{^{1}H}, ^{1}H-^{15}N heteronuclear correlation and ^{1}H-^{1}H NOESY spectra were measured at 298 K using a Bruker Avance I 500 MHz (^{1}H, 500 MHz; ^{13}C, 125 MHz; ^{11}B, 160 MHz; ^{7}Li, 194 MHz) or a Bruker Avance III 400 MHz (^{1}H, 400 MHz; ^{13}C, 101 MHz; ^{11}B, 128 MHz; ^{19}F 376 MHz) NMR spectrometer or a Bruker Avance Neo 400 MHz (^{1}H, 400 MHz; ^{1}H DOSY NMR only (298 and 323 K)). Chemical shifts (δ) were referenced to solvent peaks as follows: ^{1}H NMR spectra were referenced to residual protonated solvent in $CDCl_3$ (7.26 ppm), CD_2Cl_2 (5.32 ppm), C_6D_6 (7.16 ppm), d_6-DMSO (2.50 ppm) or d_8-THF (1.72 and 3.58 ppm); ^{13}C{^{1}H} spectra were referenced to $CDCl_3$ (77.26 ppm), CD_2Cl_2 (53.84 ppm), d_6-DMSO (39.52 ppm) or C_6D_6 (128.06 ppm); ^{11}B{^{1}H} NMR signals were referenced to external $BF_3{\cdot}OEt_2$ and ^{19}F{^{1}H} NMR signals were referenced to $CFCl_3$. Solid-state magic angle spinning (MAS) NMR spectra was recorded using a Bruker Avance Neo WB 400 solid state NMR spectrometer 4 mm (o. d.) ZrO_2 rotor (^{11}B: 128 MHz). Elemental analyses were performed on an Elementar vario MICRO cube elemental analyzer in our institute. Carbon analysis of **TipPBB2** was up to 1.8%

and compound **10** was up to 1.4% below the calculated value, while hydrogen and nitrogen were satisfactory. This may be ascribed to the formation of boron carbide.[294] Due to the instability and high percentage of element weight of fluorine atoms (10.72%), the elemental analysis of compound **11** was not measured. High resolution mass spectrometry (HRMS) and LIFDI was performed with a Thermo Fisher Scientific Exactive Plus Orbitrap MS System with either an atmospheric pressure chemical ionization (APCI) or a heated-electrospray ionization (HESI) probe.

***Tert*-butyl(4-(dimesitylboryl)benzyloxy)dimethylsilane (6a)**

To a solution of (4-bromobenzyloxy)(*tert*-butyl)dimethylsilane (301 mg, 1.0 mmol) in THF (6.0 mL) was added *n*-BuLi (1.2 mmol) at –78 °C. The resulting yellow solution was stirred at –78 °C for 1 h. $FBMes_2$ (268 mg, 1.0 mmol) in THF (2.0 mL) was added dropwise and then the reaction was slowly warmed to r.t. over 3 h and then stirred at r.t. overnight. The reaction was quenched with water, extracted with CH_2Cl_2 and washed with brine. The organic layers were dried over Na_2SO_4, combined and purified using a short silica gel column. Compound **6a** was obtained in 87% yield as a white solid. ^1H NMR (500 MHz, $CDCl_3$, ppm): δ 7.51-7.47 (m, 2H), 7.32-7.28 (m, 2H), 6.82 (s, 4H), 4.80 (s, 2H), 2.31 (s, 6H), 2.01 (s, 12H), 0.94 (s, 9H), 0.10 (s, 6H); $^{13}C\{^1H\}$ NMR (125 MHz, $CDCl_3$, ppm): δ 145.9, 144.5 (br), 141.9 (br), 140.9, 138.6, 136.7, 128.2, 125.6, 65.1, 26.1, 23.6, 21.4, 18.6, –5.1; $^{11}B\{^1H\}$ NMR (160 MHz, $CDCl_3$, ppm): δ 74.4 (br). HRMS ($APCI^-$): m/z calcd for $[C_{31}H_{43}BOSi]^-$: 470.3182; Found: 470.3183 $[M]^-$; Elem. Anal. Calcd (%) for $C_{31}H_{43}BOSi$: C, 79.12; H, 9.21; Found: C, 79.19; H, 9.41.

(4-(Bromomethyl)phenyl)dimesitylborane (7a)

To a solution of **6a** (470 mg, 1.0 mmol) in CH_2Cl_2 (20 mL) was added PBr_3 (271 mg, 1.0 mmol) dropwise at 0 °C. The resulting mixture was kept stirring at 0 °C for 2 h, then tetrabutylammonium bromide (TBAB, 483 mg, 1.5 mmol) was added and the solution was slowly warmed to r.t. over 3 h and stirred at r.t overnight. Ice water was added and the mixture was extracted with CH_2Cl_2. The organic layers were dried over Na_2SO_4,

concentrated and purified using a short silica gel column. Compound **7a** was obtained in 71% yield as a white solid. ^{1}H NMR (500 MHz, $CDCl_3$, ppm): δ 7.52-7.48 (m, 2H), 7.39-7.35 (m, 2H), 6.83 (s, 4H), 4.51 (s, 2H), 2.32 (s, 6H), 2.01 (s, 12H); ^{13}C{^{1}H} NMR (125 MHz, $CDCl_3$, ppm): δ 146.1 (br), 141.7 (br), 141.5, 140.9, 138.9, 136.8, 128.7, 128.4, 33.4, 23.6, 21.4; ^{11}B{^{1}H} NMR (160 MHz, $CDCl_3$, ppm): δ 75.4 (br). HRMS (APCI$^-$): m/z calcd for $[C_{25}H_{28}BBr–Br]^-$: 339.2290; Found: 339.2291 $[M–Br]^-$; Elem. Anal. Calcd (%) for $C_{25}H_{28}BBr$: C, 71.63; H, 6.73; Found: C, 71.99; H, 7.04.

1,3-Bis(2,6-di*iso*propylphenyl)-2-(4-(dimesitylboryl)benzylidene)-2,3-dihydro-1H-imidazole (1)

To a solution of **7a** (209 mg, 0.5 mmol) in THF (4 mL) was added 1,3-bis-(2,6-di*iso*propylphenyl)imidazol-2-ylidene[295] (IPr, 388mg, 1.0 mmol). The solution turned orange reddish immediately. The mixture was stirred at r.t. overnight. The solid was filtered and washed by hexane. The volatiles were removed under reduced pressure and an orange reddish foamy solid was obtained. Then hexane (3.0 mL) was added and orange-reddish metallic crystals **1** precipitated in 90% yield. ^{1}H NMR (500 MHz, CD_2Cl_2, ppm): δ 7.41 (t, *J* = 7.7 Hz, 2H), 7.25 (d, *J* = 7.7 Hz, 4H), 6.74 (s, 4H), 6.66 (d, *J* = 8.5 Hz, 2H), 6.41 (s, 2H), 5.91 (d, *J* = 8.5 Hz, 2H), 4.00 (s, 1H), 3.10 (quint, *J* = 6.8 Hz, 4H), 2.26 (s, 6H), 1.93 (s, 12H), 1.22 (d, *J* = 6.8 Hz, 12H), 1.17 (d, *J* = 6.8 Hz, 12H); ^{13}C{^{1}H} NMR (125 MHz, CD_2Cl_2, ppm): δ 147.8, 146.9, 144.3, 143.0, 141.0, 137.6, 137.4, 135.0, 134.5, 129.9, 128.0, 124.6, 123.2, 117.7, 73.0, 29.0, 24.5, 23.6, 23.1, 21.2; ^{11}B{^{1}H} NMR (160 MHz, CD_2Cl_2, ppm): δ 69.6 (br). HRMS (APCI$^+$): m/z calcd for $[C_{52}H_{63}BN+H]^+$: 727.5157; Found: 727.5124 $[M+H]^+$; Elem. Anal. Calcd (%) for $C_{52}H_{63}BN_2$: C, 85.92; H, 8.74; N, 3.85; Found: C, 86.38; H, 8.86; N, 3.97.

(*E*)-1-(2,6-di*iso*propylphenyl)-5-(4-(dimesitylboryl)benzylidene)-2,2,4,4-tetramethylpyrrolidine (4)

To a solution of **7a** (209 mg, 0.5 mmol) in THF (4 mL) was added 1-(2,6-di*iso*propylphenyl)-3,3,5,5-tetramethylpyrrolidin-2-ylidene[296] (cyclic (alkyl) (amino)

carbene (CAAC), 285 mg, 1.0 mmol). The solution turned yellow immediately and was stirred at r.t. overnight. The solid was filtered and the volatiles were removed under reduced pressure. Crystallization from hexane gave a yellow solid **4** in 45% yield. ^{1}H NMR (500 MHz, CD_2Cl_2, ppm): δ 7.33 (dd, *J* = 7.1, 8.3 Hz, 1H), 7.28-7.22 (m, 4H), 7.06 (d, *J* = 8.3 Hz, 2H), 6.80 (s, 4H), 4.50 (s, 1H), 3.18 (sept, *J* = 6.8 Hz, 2H), 2.22 (s, 6H), 2.20 (s, 12H), 1.78 (s, 2H), 1.44 (s, 6H), 1.26 (d, *J* = 6.8 Hz, 6H), 1.23 (d, *J* = 6.8 Hz, 6H), 1.08 (s, 6H); ^{13}C{^{1}H} NMR (125 MHz, CD_2Cl_2, ppm): δ 159.8, 150.5, 145.2, 142.4, 141.0, 140.5, 138.4, 136.9, 134.2, 128.8, 128.6, 128.4, 128.3, 124.9, 94.1, 63.6, 57.8, 41.8, 30.1, 29.7, 28.8, 26.6, 23.7, 23.6, 21.3; ^{11}B{^{1}H} NMR (160 MHz, CD_2Cl_2, ppm): δ 73.3 (br). HRMS (APCI^{+}): m/z calcd for $[C_{45}H_{58}BN+H]^{+}$: 624.4735; Found: 624.4721 $[M+H]^{+}$; Elem. Anal. Calcd (%) for $C_{45}H_{58}BN$: C, 86.65; H, 9.37; N, 2.25; Found: C, 86.67; H, 9.82; N, 2.18.

(4-Bromo-2,6-dimethylbenzyloxy)(*tert*-butyl)dimethylsilane

To a solution of (4-bromo-2,6-dimethylphenyl)methanol (215 mg, 1.0 mmol) and imidazole (136 mg, 2.0 mmol) in CH_2Cl_2 (5 mL) was added TBDMSCl (227 mg, 1.5 mmol) portionwise at 0 °C. The solution was slowly warmed to r.t. and then stirred at r.t. overnight. The mixture was poured into aqueous HCl (1 N, 4 mL), extracted with CH_2Cl_2 and washed with sat. $NaHCO_3$. The organic layers were dried over Na_2SO_4, combined and purified using a short silica gel column. A white solid was obtained in 93% yield. ^{1}H NMR (400 MHz, $CDCl_3$, ppm): δ 7.16 (s, 2H), 4.64 (s, 2H), 2.36 (s, 6H), 0.91 (s, 9H), 0.10 (s, 6H); ^{13}C{^{1}H} NMR (100 MHz, $CDCl_3$, ppm): δ 139.6, 136.0, 131.0, 121.2, 59.3, 26.1, 19.5, 18.5, –5.2; HRMS (APCI^{+}): m/z calcd for $[C_{15}H_{25}BrOSi–H]^{+}$: 327.0774; Found: 327.0774 $[M–H]^{+}$; Elem. Anal. Calcd (%) for $C_{15}H_{25}BrOSi$: C, 54.70; H, 7.65; Found: C, 54.89; H, 7.65.

***Tert*-butyl(4-(dimesitylboryl)-2,6-dimethylbenzyloxy)dimethylsilane (6b)**

To a solution of (4-bromo-2,6-dimethylbenzyloxy)(*tert*-butyl)dimethylsilane (1316 mg, 4.0 mmol) in THF (40 mL) was added *n*-BuLi (4.8 mmol) at –78 °C. The resulting yellow solution was stirred at –78 °C for 1 h. $FBMes_2$ (1072 mg, 4.0 mmol) in THF (5.0 mL) was

added dropwise and the solution was slowly warmed to r.t. over 3 h and then stirred at r.t. overnight. The reaction was quenched with water and extracted with CH_2Cl_2 and washed with brine. The organic layers were dried over Na_2SO_4, combined and purified using a short silica gel column. Compound **6b** was obtained in 84% yield as a white solid. ^{1}H NMR (500 MHz, $CDCl_3$, ppm): δ 7.16 (s, 2H), 6.81 (br, 4H), 4.76 (s, 2H), 2.35 (s, 6H), 2.32 (s, 6H), 2.00 (s, 12H), 0.91 (s, 9H), 0.08 (s, 6H); ^{13}C{^{1}H} NMR (125 MHz, $CDCl_3$, ppm): δ 145.0, 142.1, 141.0, 140.9, 138.4, 136.8, 136.4, 128.2, 60.1, 26.1, 23.6, 21.4, 19.7, 18.6, –5.0; ^{11}B{^{1}H} NMR (160 MHz, $CDCl_3$, ppm): δ 75.3 (br). HRMS (APCI$^-$): m/z calcd for $[C_{33}H_{47}BOSi]^-$: 498.3495; Found: 498.3506 $[M]^-$; Elem. Anal. Calcd (%) for $C_{33}H_{47}BOSi$: C, 79.49; H, 9.50; Found: C, 79.73; H, 9.77.

(4-(Bromomethyl)-3,5-dimethylphenyl)dimesitylborane (7b)

To a solution of **6b** (470 mg, 1.0 mmol) in CH_2Cl_2 (5 mL) was added PBr_3 (271 mg, 1.0 mmol) dropwise at 0 °C. The resulting mixture was stirred at 0 °C for 2 h, then tetrabutylammonium bromide (TBAB, 483 mg, 1.5 mmol) was added and the reaction was slowly warmed to r.t. over 3 h and stirred at r.t overnight. Ice water mixture was added, and the mixture was extracted with CH_2Cl_2. The organic layers were dried over Na_2SO_4, concentrated and purified using a short silica gel. Compound **7b** was obtained in 90% yield as a white solid. ^{1}H NMR (500 MHz, $CDCl_3$, ppm): δ 7.17 (s, 2H), 6.81 (s, 4H), 4.58 (s, 2H), 2.38-2.35 (m, 6H), 2.31 (s, 6H), 1.99 (s, 12H); ^{13}C{^{1}H} NMR (125 MHz, $CDCl_3$, ppm): δ 146.2 (br), 141.9 (br), 141.0, 138.7, 138.0, 136.9, 136.2, 128.3, 29.3, 23.6, 21.4, 19.3; ^{11}B{^{1}H} NMR (160 MHz, $CDCl_3$, ppm): δ 74.8 (br). HRMS (APCI$^+$): m/z calcd for $[C_{27}H_{32}BBr–Br]^+$: 367.2592; Found: 367.2588 $[M–Br]^+$; Elem. Anal. Calcd (%) for $C_{27}H_{32}BBr$: C, 72.51; H, 7.21; Found: C, 72.42; H, 7.15.

1,3-Bis(2,6-di*iso*propylphenyl)-2-(4-(dimesitylboryl)-2,6-dimethylbenzylidene)-2,3-dihydro-1H-imidazole (2)

To a solution of **6a** (223 mg, 0.5 mmol) in THF (4 mL) was added 1,3-bis-(2,6-di*iso*propylphenyl)imidazole-2-ylidene[295] (IPr, 388 mg, 1.0 mmol). The solution turned

orange reddish immediately and was stirred at r.t. overnight. The precipitate was removed by filtration and washed with THF. The filtrate was evaporated to dryness under reduced pressure resulting in an orange reddish foamy solid. After dissolving it in 1.0 mL THF, hexane (5 mL) was added and a yellow solid precipitated from the solution. The pure solid product **2** was obtained in 87% yield by filtration and washing with hexane. ^{1}H NMR (500 MHz, CD_2Cl_2, ppm): δ 7.21 (br, 2H), 7.10 (br, 4H), 6.74 (s, 4H), 6.67 (s, 2H), 6.33 (s, 2H), 3.69 (s, 1H), 3.31(br, 4H), 2.23 (s, 6H), 1.93 (s, 6H), 1.89 (s, 12H), 1.27 (d, *J* = 6.5 Hz, 12H), 1.15 (d, *J* = 6.2 Hz, 12H); ^{13}C{^{1}H} NMR (125 MHz, CD_2Cl_2, ppm): δ 147.4 (br), 145.7, 143.3, 142.8, 141.0, 138.8, 137.8, 136.1, 134.5, 134.3, 129.0 (br), 128.1, 124.2, 117.0 (br), 67.6, 28.6, 25.7 (br), 23.8, 22.9 (br), 22.1, 21.2; ^{11}B{^{1}H} NMR (160 MHz, CD_2Cl_2, ppm): δ 71.9 (br). HRMS (APCI^{+}): m/z calcd for $[C_{54}H_{67}BN_2–H]^{+}$: 755.5470; Found: 755.5451 $[M–H]^{+}$; Elem. Anal. Calcd (%) for $C_{54}H_{67}BN_2$: C, 85.91; H, 8.95; N, 3.71; Found: C, 85.33; H, 9.03; N, 3.67.

***Tert*-butyl((5-(dimesitylboryl)thiophen-2-yl)methoxy)dimethylsilane (6c)**

To a solution of ((5-bromothiophen-2-yl)methoxy)(*tert*-butyl)dimethylsilane (307 mg, 1.0 mmol) in THF (5 mL) was added *n*-BuLi (1.2 mmol) at –78 °C. The resulting solution was stirred at –78 °C for 1 h. $FBMes_2$ (268 mg, 1.0 mmol) in THF (2 mL) was added dropwise and then the reaction mixture was slowly warmed to r.t. over 3 h and then stirred at r.t. overnight. The reaction was quenched with water and extracted with CH_2Cl_2 and washed with brine. The organic layers were dried over Na_2SO_4, combined and purified using a short silica gel column. Compound **6c** was obtained in 74% yield as a colorless foamy oil. ^{1}H NMR (500 MHz, $CDCl_3$, ppm): δ 7.29-7.33 (m, 1H), 7.04-7.08 (m, 1H), 6.81 (s, 4H), 4.91 (s, 2H), 2.30 (s, 6H), 2.11 (s, 12H), 0.82-0.97 (m, 9H), 0.07-0.09 (m, 6H); ^{13}C{^{1}H} NMR (125 MHz, $CDCl_3$, ppm): δ 159.0, 149.1, 141.4, 141.0, 140.9, 138.5, 128.2, 126.4, 61.3, 26.0, 23.6, 21.4, 18.5, 1.2, –5.1; ^{11}B{^{1}H} NMR (160 MHz, $CDCl_3$, ppm): δ 66.2 (br). HRMS (APCI^{+}): m/z calcd for $[C_{23}H_{29}BOSi–OTBDMS]^{+}$: 345.1843; Found: 345.1829 $[M–OTBDMS]^{+}$; Elem. Anal. Calcd (%) for $C_{29}H_{41}BOSi$: C, 73.08; H, 8.67; S, 6.73; Found: C, 73.27; H, 8.80; S, 6.45.

(5-(Bromomethyl)thiophen-2-yl)dimesitylborane (7c)

To a solution of **6c** (238 mg, 0.5 mmol) in CH_2Cl_2 (5 mL) at 0 °C was added PBr_3 (271 mg, 1.0 mmol) dropwise. The resulting mixture was stirred at 0 °C for 2 h, then tetrabutylammonium bromide (TBAB, 483 mg, 1.5 mmol) was added and the reaction was slowly warmed to r.t. over 3 h and stirred at r.t overnight. Ice water was added and the mixture was extracted with CH_2Cl_2. The organic layers were dried over Na_2SO_4, concentrated and the product was crystalized from CH_2Cl_2/hexane. Compound **7c** was obtained in 31% yield as a white solid. ^{1}H NMR (500 MHz, $CDCl_3$, ppm): δ 7.30 (d, *J* = 3.6 Hz, 1H), 7.21 (d, *J* = 3.6 Hz, 1H), 6.83 (s, 4H), 4.73 (s, 2H), 2.31 (s, 6H), 2.12 (s, 12H); ^{13}C{^{1}H} NMR (125 MHz, $CDCl_3$, ppm): δ 153.1, 151.8 (br), 141.1 (br), 140.9, 140.5, 138.9, 130.3, 128.3, 26.3, 23.6, 21.4; ^{11}B{^{1}H} NMR (160 MHz, $CDCl_3$, ppm): δ 67.0 (br). HRMS (APCI$^+$): m/z calcd for $[C_{23}H_{26}BSBr–Br]^+$: 345.1843; Found: 345.1829 $[M–Br]^+$; Elem. Anal. Calcd (%) for $C_{23}H_{26}BBrS$: C, 64.96; H, 6.16; S, 7.54; Found: C, 65.15; H, 6.21; S, 7.20.

1,3-Bis(2,6-di*iso*propylphenyl)-2-((5-(dimesitylboryl)thiophen-2-yl)methylene)-2,3-dihydro-1H-imidazole (3)

To a solution of **7c** (106 mg, 0.25 mmol) in THF (4 mL) was added 1,3-bis-(2,6-di*iso*propylphenyl)imidazole-2-ylidene[295] (IPr, 194mg, 0.5 mmol). The solution turned red immediately. The mixture was kept stirred at r.t. overnight. The solid was removed by filtration and washed with hexane. The volatiles were removed under reduced pressure and a reddish orange foamy solid was obtained. Hexane (3 mL) was added and the product was crystalized by cooling to –30 °C. Reddish orange crystals were obtained in 85% yield. ^{1}H NMR (500 MHz, CD_2Cl_2, ppm): δ 7.21 (br, 6H), 6.72 (s, 4H), 6.60 (d, *J* = 4.1 Hz, 1H), 6.42 (s, 2H), 5.20 (d, *J* = 4.1 Hz, 1H), 4.38 (s, 1H), 2.99 (br, 4H), 2.29 (s, 3H), 2.22 (s, 3H), 2.03 (s, 12H), 1.21 (d, *J* = 6.9 Hz, 12H), 1.16 (br, 12H); ^{13}C{^{1}H} NMR (125 MHz, CD_2Cl_2, ppm): δ 159.8, 148.2, 145.9, 143.3, 142.4 (br), 141.2, 140.4, 138.2, 136.9, 136.7, 130.4, 128.1, 127.9, 124.8, 124.3, 120.5, 118.8, 117.5, 68.0, 29.1, 24.4, 23.7, 23.5, 23.2 (br), 21.2, 21.1; ^{11}B{^{1}H} NMR (160 MHz, CD_2Cl_2, ppm): δ 57.5 (br). HRMS (ESI$^+$): m/z calcd for

$[C_{50}H_{61}BN_2S]^+$: 732.4643; Found: 732.4644 $[M]^+$; Elem. Anal. Calcd (%) for $C_{50}H_{61}BN_2S$: C, 81.94; H, 8.39; N, 3.82; S, 4.38; Found: C, 81.97; H, 8.71; N, 3.65; S, 4.02.

[9-(2,4,6-tri*iso*propylphenyl)-9H-benzo[4,5]borolo[2,3-c]pyridine]$_4$ ([TipPBBI]$_4$)

To a solution of 3-bromo-4-(2-bromophenyl)pyridine[232] (310 mg, 1.0 mmol) in THF (15.0 mL), was added *t*-BuLi (4.0 mmol) at –78 °C. The resulting orange solution was stirred at –78 °C for 1 h. Dimethyl (2,4,6-tri*iso*propylphenyl)boronate (TipB(OMe)$_2$, 1 mmol, 276 mg) in THF (2.0 mL) was added dropwise and then the reaction was slowly warmed to r.t. and stirred at r.t. overnight. The volatiles were removed under vacuum, and the product was purified by rapid column chromatography on Al_2O_3 in air eluting with CH_2Cl_2/MeOH = 20/1. The light-yellow solid was then dissolved in CH_2Cl_2, crystalized by slow diffusion of hexane under an argon atmosphere as it slowly decomposes in the air. Compound **[TipPBBI]$_4$** was obtained in 22% yield (81 mg) as a white solid. ^{1}H NMR (400 MHz, $CDCl_3$, ppm): δ 7.78-7.72 (m, 1H), 7.60-7.56 (m, 1H), 7.56-7.52 (m, 1H), 7.39 (dt, *J* = 7, 1 Hz, 1H), 7.34 (dt, *J* = 7, 1 Hz, 1H), 7.23 (s, 1H), 7.15-7.10 (m, 1H), 6.99 (d, *J* = 2 Hz), 6.83 (d, *J* = 2 Hz), 2.84 (sept, *J* = 7 Hz, 1H), 2.62 (sept, *J* = 6 Hz, 1H), 2.38 (sept, *J* = 6 Hz, 1H), 1.26 (d, *J* = 7 Hz, 3H), 1.25 (d, *J* = 7 Hz, 3H), 1.18 (d, *J* = 6 Hz, 3H), 0.95 (d, *J* = 6 Hz, 3H), 0.77 (d, *J* = 6 Hz, 3H), 0.30 (d, *J* = 6 Hz, 3H); ^{13}C{^{1}H} NMR (125 MHz, $CDCl_3$, ppm): δ 159.8, 158.4, 157.2, 154.0, 153.1, 145.8, 144.0, 143.3, 140.6, 139.3, 133.4, 131.5, 128.2, 122.4, 121.6, 120.3, 115.2, 33.7, 32.7, 32.5, 28.3, 26.3, 24.2, 24.1, 23.8, 23.8; ^{11}B{^{1}H} NMR (160 MHz, $CDCl_3$, ppm): δ 2.9 (br). LIFDI (APCI$^+$): m/z calcd for $[C_{104}H_{120}B_4N_4]^+$: 1468.9880; Found: 1468.9920 $[M]^+$; Elem. Anal. Calcd (%) for $C_{26}H_{30}BN$: C, 85.01; H, 8.23; N, 3.81; Found: C, 84.87; H, 8.25; N, 3.98.

5-(2,4,6-tri*iso*propylphenyl)-5H-benzo[4,5]borolo[3,2-b]pyridine (TipPBB2)

To a solution of 3-bromo-2-(2-bromophenyl)pyridine[232] (310 mg, 1.0 mmol) in THF (15.0 mL), was added *t*-BuLi (4.0 mmol) at –78 °C. The resulting green solution was stirred at –78 °C for 1 h. Dimethyl (2,4,6-tri*iso*propylphenyl)boronate (TipB(OMe)$_2$, 1 mmol, 276 mg) in THF (2.0 mL) was added dropwise and then the reaction was slowly warmed to r.t. and stirred at r.t. overnight. The volatiles were removed under vacuum,

and the product was purified by rapid column chromatography on Al_2O_3 in air eluting with CH_2Cl_2/MeOH = 20/1. The yellow solid was then dissolved in CH_2Cl_2 and precipitated with hexane under an argon atmosphere as it slowly decomposes in the air. The light yellow solid was collected by fractions in 27% yield (99 mg). ^{1}H NMR (500 MHz, $CDCl_3$, ppm): δ 8.43 (dd, *J* = 5, 2 Hz, 1H), 7.78-7.73 (m, 1H), 7.64 (dd, *J* = 7, 2 Hz, 1H), 7.48-7.42 (m, 2H), 7.24-7.19 (m, 1H), 7.03 (s, 2H), 6.97 (dd, *J* = 7, 5 Hz, 1H), 2.94 (sept, *J* = 7 Hz, 1H), 2.43 (sept, *J* = 7 Hz, 2H), 1.31 (d, *J* = 7 Hz, 6H), 1.14 (d, *J* = 7 Hz, 6H), 1.13 (d, *J* = 7 Hz, 6H); ^{13}C{^{1}H}MR (125 MHz, $CDCl_3$, ppm): δ 172.7, 153.4, 151.9, 150.0, 149.5, 143.6 (br), 141.3, 137.2 (br), 135.2, 135.0, 133.8 (br), 130.5, 123.2, 120.8, 120.4, 36.2, 34.5, 24.9, 24.8, 24.2; ^{11}B{^{1}H} NMR (160 MHz, $CDCl_3$, ppm): δ 72.8 (br). HRMS (APCI$^+$): m/z calcd for $[C_{26}H_{30}BN+H]^+$: 368.2544; Found: 368.2535 $[M+H]^+$; Elem. Anal. Calcd (%) for $C_{26}H_{30}BN$: C, 85.01; H, 8.23; N, 3.81; Found: C, 83.20; H, 8.09; N, 3.93.

3-(*Tert*-butyl)-9-(2,4,6-tri*iso*propylphenyl)-3,9-dihydro-2H-benzo[4,5]borolo[2,3-c]pyridine (10)

To a solution of 3-bromo-4-(2-bromophenyl)pyridine[232] (626 mg, 2 mmol) in THF (30.0 mL), *n*-BuLi (2 mmol) was added at –78 °C. The resulting solution was stirred at –78 °C for 1 h then $B(OMe)_3$ (4 mmol, 0.44 mL) was added. The reaction was allowed to warm to r.t. and was stirred at r.t. for 6 h. The volatiles were removed under vacuum and the residue was extracted with CH_2Cl_2 (2 × 5 mL). The CH_2Cl_2 was removed under vacuum and the resulting solid was dissolved in THF (15.0 mL) and cooled to 0 °C. TipMgBr (2 mmol)[255] was added at 0 °C and then the mixture was warmed to 75 °C for 3 h. After cooling to r.t. and stirring at for another 6 h, the volatiles were removed under vacuum. The resulting solid was extracted with hexane and then the hexane was removed under vacuum. The crude ^{1}H NMR indicated a ca. 50% yield of product formed (the side products are Tip$B(OMe)_2$ and 1,3,5-tri*iso*propylbenzene, and the yield is based on the integration of aromatic protons of the Tip group among these three compounds). Then, the light yellow oil was dissolved in THF, cooled to –78 °C, and *t*-BuLi (2.0 eq, 2 mmol) was added. The mixture was stirred at –78 °C for 2 h and then slowly warmed to

r.t and stirred at r.t for another 6 h. The volatiles were removed again and the residue was extracted with CH_2Cl_2 (2 × 5 mL). The solution was concentrated, hexane was added, and cooling to –30 °C gave compound **10** in 10% yield (86 mg) as a light yellow solid. ^{1}H NMR (500 MHz, $CDCl_3$, ppm): δ 7.76-7.72 (m, 1H), 7.58-7.54 (m, 1H), 7.44 (dt, *J* = 7, 1 Hz, 1H), 7.34-7.31 (m, 1H), 7.26 (dt, *J* = 7, 1 Hz, 1H), 7.01-6.96 (m, 2H), 6.00-5.96 (m, 1H), 5.17-5.06 (m, 1H), 4.01 (dd, *J* = 4, 2 Hz, 1H), 2.93 (sept, *J* = 7 Hz, 1H), 2.65 (sept, *J* = 7 Hz, 1H), 2.63 (sept, *J* = 7 Hz, 1H), 1.31 (d, *J* = 7 Hz, 6H), 1.12 (d, *J* = 7 Hz, 3H), 1.10-1.06 (m, 9H), 0.99 (s, 1H); ^{13}C{^{1}H} NMR (125 MHz, $CDCl_3$, ppm): δ 150.7, 150.5, 149.7 (br), 148.4, 147.5, 147.4, 143.1, 136.6 (br), 132.3, 130.2, 127.5, 120.2, 119.6, 119.5, 113.1 (br), 104.4, 62.7, 38.6, 34.9, 34.8, 34.3, 34.28, 25.3, 25.0, 24.9, 24.8, 24.3, 24.27, 24.25; ^{11}B{^{1}H} NMR (160 MHz, $CDCl_3$, ppm): δ 58.8 (br). HRMS (APCI$^+$): m/z calcd for $[C_{30}H_{40}BN+H]^+$: 426.3327; Found: 426.3318 $[M+H]^+$; Elem. Anal. Calcd (%) for $C_{30}H_{40}BN$: C, 84.69; H, 9.48; N, 3.29; Found: C, 83.28; H, 9.58; N, 3.11.

1-Methyl-5-(2,4,6-tri*iso*propylphenyl)-5H-benzo[4,5]borolo[3,2-b]pyridin-1-ium triflate (11)

To a solution of **TipPBB2** (74 mg, 0.2 mmol) in CH_2Cl_2 (2.0 mL), MeOTf (30 mg, 0.2 mmol) in 0.5 mL CH_2Cl_2 was added at –30 °C. The resulting solution was warmed to r.t. and stirred at r.t. for 3 h. Hexane (ca. 6 mL) was added and the mixture was concentrated under vacuum until a yellow solid precipitated. The solid was collected by filtration, washed with ca. 20 mL hexane, and dried under vacuum. Compound **11** was obtained in 39% yield (40 mg) as a yellow solid. ^{1}H NMR (400 MHz, CD_2Cl_2, ppm): δ 8.78-8.67 (m, 1H), 8.23-8.13 (m, 1H), 8.09-7.99 (m, 1H), 7.80-7.71 (m, 2H), 7.71-7.64 (m, 1H), 7.64-7.54 (m, 1H), 7.10 (s, 2H), 4.67 (s, 3H), 2.95 (sept, *J* = 7 Hz, 1H), 2.27 (sept, *J* = 7 Hz, 2H), 1.30 (d, *J* = 7 Hz, 6H), 1.17-1.09 (m, 12H); ^{13}C{^{1}H} NMR (100 MHz, CD_2Cl_2, ppm): δ 166.7, 151.7, 151.1, 149.1, 147.6, 143.6, 137.9, 137.1, 135.1, 128.0, 127.2, 121.4, 48.3, 37.6, 34.9, 25.0, 24.9, 24.1; ^{11}B{^{1}H} NMR (128 MHz, CD_2Cl_2, ppm): δ 72.3 (br); ^{19}F{^{1}H} NMR (376 MHz, CD_2Cl_2, ppm): δ –79.0. HRMS (ESI$^+$): m/z calcd for $[C_{27}H_{33}BN]^+$: 382.2701; Found: 382.2692 $[M]^+$; HRMS (ESI$^-$): m/z calcd for $[CF_3O_3S]^-$: 148.9526; Found: 148.9519 $[M]^-$.

1-Methyl-2-phenylpyridin-1-ium triflate (12)[259]

To a solution of 2-phenylpyridine (78 mg, 0.5 mmol) in CH_2Cl_2 (2.0 mL), MeOTf (82 mg, 0.5 mmol) in 0.5 mL CH_2Cl_2 was added at –30 °C. The resulting solution was warmed to r.t. and stirred at r.t. for 3 h. The solvent was removed under reduced pressure, the resulting residue was washed with Et_2O in an ultrasound bath. A white sold was obtained in 58% (92 mg) yield. ^{1}H NMR (400 MHz, DMSO, ppm): δ 9.17-9.09 (m, 1H), 8.68-8.59 (m, 1H), 8.19-8.12 (m, 1H), 8.11-8.06 (m, 1H), 7.73-7.62 (m, 5H), 4.12 (s, 3H); ^{13}C{^{1}H} NMR (100 MHz, DMSO, ppm): δ 155.0, 146.7, 145.4, 131.8, 131.1, 129.8, 129.2, 129.1, 126.6, 120.7 (q, *J* = 322 Hz), 47.1; ^{19}F{^{1}H} NMR (376 MHz, DMSO, ppm): δ –77.7. HRMS (ESI$^+$): m/z calcd for $[C_{12}H_{12}N]^+$: 170.0964; Found: 170.0961 $[M]^+$; HRMS (ESI$^-$): m/z calcd for $[CF_3O_3S]^-$: 148.9526; Found: 148.9513 $[M]^-$.

The data nicely matches that previously reported.[259]

Determination of the selectivity of bromine-lithium exchange reaction: For convenience of purification, we transformed the air sensitive compound **13** into air stable compound **14**.

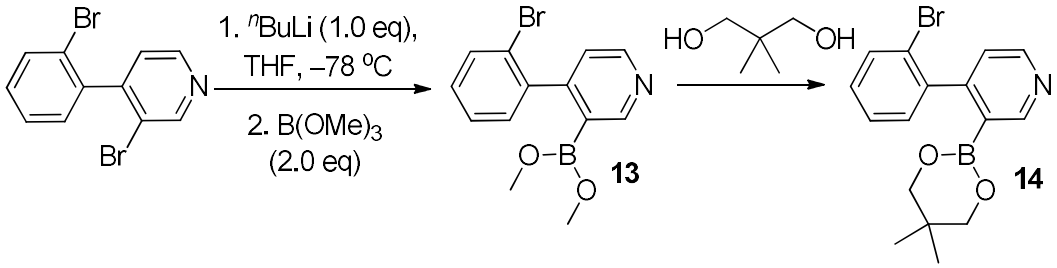

4-(2-Bromophenyl)-3-(5,5-dimethyl-1,3,2-dioxaborinan-2-yl)pyridine (14)

To a solution of 3-bromo-4-(2-bromophenyl)pyridine[232] (313 mg, 1 mmol) in THF (15.0 mL), *n*-BuLi (1 mmol) was added at –78 °C. The resulting solution was stirred at –78 °C for 1 h then $B(OMe)_3$ (2 mmol, 0.22 mL) was added. The reaction was allowed to warm to r.t. and stirred at r.t. for 6 h. The compound 2,2-dimethylpropane-1,3-diol (3 mmol) was added and the reaction kept stirring at r.t. for another 6 h. All volatiles were removed under vacuum and the residue was extracted with hexane. Then the hexane

was removed under vacuum and compound **14** was obtained as a white solid in 81% (280 mg) yield. ^{1}H NMR (500 MHz, $CDCl_3$, ppm): δ 8.96 (d, *J* = 1 Hz, 1H), 8.65 (d, *J* = 5 Hz, 1H), 7.62-7.58 (m, 1H), 7.36-7.31 (m, 1H), 7.23-7.18 (m, 2H), 7.12 (dd, *J* = 5, 1 Hz, 1H), 3.52 (s, 2H), 3.51 (s, 2H), 0.92 (s, 6H); ^{13}C{^{1}H} NMR (125 MHz, CD_2Cl_2, ppm): δ 154.8, 154.4, 150.6, 142.2, 132.2, 130.2, 129.0, 126.9, 124.14, 122.4, 72.4, 31.8, 22.0; ^{11}B{^{1}H} NMR (160 MHz, $CDCl_3$, ppm): δ 26.8. HRMS (APCI^{+}): m/z calcd for $[C_{16}H_{17}BBrNO_2+H]^{+}$: 346.0608; Found: 346.0602 $[M+H]^{+}$; Elem. Anal. Calcd (%) for $C_{16}H_{17}BBrNO_2$: C, 55.54; H, 4.95; N, 4.05; Found: C, 55.12; H, 5.00; N, 3.71.

Synthesis of [16]$_2$

The compound 3-Methyl-2-bromopyridiene (688 mg, 4.0 mmol) was dissolved in Et_2O (30 mL) and cooled to –78 °C, then *n*-BuLi (4.8 mmol) was added dropwise. The resulting yellow solution was stirred at –78 °C for 90 mins. Dimethyl (2,4,6-triisopropylphenyl)boronate (TipB(OMe)$_2$, 552 mg, 2 mmol) in Et_2O (5.0 mL) was added dropwise. Afterwards, the reaction was slowly warmed to r.t. and stirred at r.t. overnight. The volatiles were removed under vacuum and then the residue was extracted with hexane (2 × 20 mL). The hexane was removed under vacuum and the resulting solid was dissolved in CH_2Cl_2 and crystalized at –30 °C. Compound **[16]$_2$** was collected as a white solid in 37% yield. ^{1}H NMR (500 MHz, CD_2Cl_2, ppm): δ 8.05 (s, br, 2H), 7.20 (m, 2H), 7.02 (s, 2H), 6.80 (s, br, 2H), 3.51 (s, 3H), 3.06 (s, br, 2H), 2.91 (sept, *J* = 7 Hz, 1H), 1.98 (s, 6H), 1.31 (d, *J* = 7 Hz, 6H), 1.12-1.03 (m, 6H), 0.97-0.88 (m, 6H); ^{13}C{^{1}H} NMR (125 MHz, CD_2Cl_2, ppm): δ 182.2 (br), 154.8, 149.2, 146.7, 145.5, 137.8 (br), 122.4, 120.7, 119.5, 53.6, 34.4, 31.9, 27.9, 24.4, 24.0, 23.4; ^{11}B{^{1}H} NMR (160 MHz, CD_2Cl_2, ppm): δ 3.5; ^{7}Li{^{1}H} NMR (194 MHz, CD_2Cl_2, ppm): δ 2.9. HRMS (APCI^{-}): m/z calcd for $[C_{28}H_{38}BN_2OLi]^{-}$: 429.3083; Found: 429.3080 $[M–Li]^{-}$.

7.2 Single-crystal X-ray diffraction

Crystals suitable for single-crystal X-ray diffraction were selected, coated in perfluoropolyether oil (for **2**, **3**, **7b** and **7c**) or polybutyl oil (for **1**, **4, 7a** and **[TipPBBI]**$_4$), mounted on a polyimide microloop (MicroMounts from MiTeGen) and transferred to a stream of cold nitrogen (Bruker Kryoflex2 or Oxford Cryostream 700 or 800). Diffraction data were collected on Bruker Apex II 4-circle diffractometers with CCD area detectors using Mo-K_α radiation monochromated by graphite (for **1**, **3** and **7b**) or multi-layer focusing mirrors (for **2**, **4**, and **7a**) at 100 K. Diffraction data of **7c**, **[TipPBBI]**$_4$ and **[16]**$_2$ were collected on a Rigaku Oxford Diffraction XtaLAB Synergy diffractometer with a semiconductor HPA-detector (HyPix-6000) and multi-layer mirror monochromated Mo-Kα radiation. The crystal was cooled using an Oxford Cryostreams 800 low-temperature device. Data were collected at 100 K. The images were processed and corrected for Lorentz-polarization effects and absorption as implemented in the Bruker software packages (**1**, **2**, **3**, **4**, **7a**, and **7b**) or using the CrysAlisPro software from Rigaku Oxford Diffraction (**7c**, **[TipPBBI]**$_4$ and **[16]**$_2$). The structures were solved using the intrinsic phasing method (SHELXT)[297] and Fourier expansion technique. All non-hydrogen atoms were refined in anisotropic approximation, with hydrogen atoms "riding" in idealized positions, by full-matrix least squares against F^2 of all data, using SHELXL[298] software and the SHELXLE graphical user interface.[299] Diamond[300]software was used for graphical representation.[301] Crystal data and experimental details are listed in tables below; full structural information has been deposited with the Cambridge Crystallographic Data Centre. CCDC-1926413 (**1**), 1926414 (**2**), 1926415 (**3**), 1926416 (**4**), 1926417 (**7a**), 1926418 (**7b**), 1926419 (**7c**), 2013331 (**[TipPBBI]**$_4$).

Table 7.2-1. Single-crystal X-ray diffraction data and structure refinements of **1**-**4**.

Data	**1**	**2**	**3**	**4**
CCDC number	1926413	1926414	1926415	1926416
Empirical formula	$C_{52}H_{63}BN_2$	$C_{54}H_{67}BN_2$	$C_{50}H_{61}BN_2S$	$C_{45}H_{58}BN$
Formula weight/ g·mol^{-1}	726.85	754.90	732.87	623.73
T/ K	100(2)	100(2)	100(2)	100(2)
λ/ Å, radiation	MoK_α 0.71073	MoK_α 0.71073	MoK_α 0.71073	MoK_α 0.71073
Crystal size/ mm^3	0.35×0.46×0.51	0.11×0.25×0.30	0.16×0.26×0.54	0.33×0.48×0.61
Crystal color, habit	orange block	red block	orange plate	colorless plate
μ/ mm^{-1}	0.061	0.063	0.111	0.060
Crystal system	monoclinic	monoclinic	monoclinic	monoclinic
Space group	$P2_1/c$	$P2_1/n$	$P2_1/c$	$P2_1/n$
a/ Å	15.0679(5)	11.8087(11)	13.549(5)	15.925(8)
b/ Å	16.9030(7)	30.881(3)	15.791(9)	14.679(7)
c/ Å	19.0516(7)	12.3539(11)	20.162(12)	33.324(14)
α/ °	90	90	90	90
β/ °	111.937(2)	90.185(3)	94.841(13)	97.522(16)
γ/ °	90	90	90	90
Volume/ Å^3	4501.0(3)	4505.0(7)	4298(4)	7723(6)
Z	4	4	4	8
ρ_{calc}/ g·cm^{-3}	1.073	1.113	1.132	1.073
F(000)	1576	1640	1584	2720
θ range/ °	2.220-28.729	1.319-26.822	1.985-26.093	1.501-28.000
Reflections collected	69450	51996	48138	89344
Unique reflections	11633	9635	8518	18443
Parameters/ restraints	509 / 0	530 / 0	501 / 0	907 / 14
GooF on F^2	1.003	1.076	1.020	1.076
R_1 [I>2σ(I)]	0.0552	0.0600	0.0463	0.0689
wR^2 (all data)	0.1358	0.1383	0.1176	0.1949
Max./ min. residual electron density/ e·Å^{-3}	0.315 / −0.272	0.427 / −0.242	0.305 / −0.272	0.378 / −0.265

Table 7.2-2. Single-crystal X-ray diffraction data and structure refinements of **7a**, **7b**, and **7c**.

Data	**7a**	**7b**	**7c**
CCDC number	1926417	1926418	1926419
Empirical formula	$C_{25}H_{28}BBr$	$C_{27}H_{32}BBr$	$C_{23}H_{26}BBrS$
Formula weight/ $g{\cdot}mol^{-1}$	419.19	447.24	425.22
T/ K	100(2)	100(2)	100(2)
λ/ Å, radiation	MoK_α 0.71073	MoK_α 0.71073	MoK_α 0.71073
Crystal size/ mm^3	0.16×0.24×0.38	0.20×0.20×0.30	0.13×0.19×0.26
Crystal color, habit	colorless block	colorless block	colorless block
μ/ mm^{-1}	1.919	1.800	2.082
Crystal system	triclinic	triclinic	monoclinic
Space group	$P\bar{1}$	$P\bar{1}$	$P2_1/n$
a/ Å	8.3027(5)	8.5736(10)	13.4521(6)
b/ Å	10.9354(7)	11.3480(13)	11.6902(4)
c/ Å	12.2373(8)	12.6370(15)	14.0318(6)
α/ °	85.481(2)	84.066(4)	90
β/ °	75.990(2)	88.530(4)	109.591(5)
γ/ °	89.998(2)	69.964(4)	90
Volume/ $Å^3$	1074.46(12)	1148.8(2)	2078.87(17)
Z	2	2	4
ρ_{calc}/ $g{\cdot}cm^{-3}$	1.296	1.293	1.359
F(000)	436	468	880
θ range/ °	1.721-26.348	1.620-26.797	2.326-26.372
Reflections collected	16859	13106	26853
Unique reflections	4383	4894	4253
Parameters/ restraints	250 / 0	270 / 0	241 / 0
GooF on F^2	1.029	1.022	1.040
RI [I>2σ(I)]	0.0324	0.0390	0.0288
wR^2 (all data)	0.0777	0.1012	0.0721
Max./ min. residual electron density/ $e{\cdot}Å^{-3}$	0.366 / −0.461	0.735 / −0.688	0.621 / −0.323

Table 7.2-3. Single-crystal X-ray diffraction data and structure refinements of **[TipPBBI]$_4$**.

Data	**[TipPBBI]$_4$**
CCDC number	20133
Empirical formula	$C_{104}H_{120}B_4N_4 \cdot 5.115(C_6D_6)$
Formula weight/ g·mol^{-1}	1868.79
T/ K	100(2)
Radiation, λ/ Å	CuK_α 1.54184
Crystal color, habit	Colorless block
Crystal size/ mm³	0.357 × 0.353 × 0.153
Crystal system	Triclinic
Space group	$P\bar{1}$
Unit cell dimensions	
a/ Å	14.53964(16)
b/ Å	17.2926(2)
c/ Å	26.1078(3)
α/ °	103.9023(10)
β/ °	96.1424(9)
γ/ °	114.6288(11)
Volume (Å^3)	5630.42(11)
Z	2
ρcalc/ g·cm^{-3}	1.102
μ/ mm^{-1}	0.464
F(000)	2014
θ range/ °	2.94-77.53
Reflections collected	118762
Unique reflections	2351
Parameters / restraints	1457 / 469
GooF on F^2	1.04
R1 [I>2σ(I)]	0.0457
wR^2	0.1197
Max./min. residual electron density (e·Å^{-3})	0.328 / –0.283

Table 7.2-4. Single-crystal X-ray diffraction data and structure refinements of **[16]**$_2$.

Data	**[16]**$_2$
CCDC number	
Empirical formula	$C_{56}H_{76}B_2Li_2N_4O_2 \cdot 4(CH_2Cl_2)$
Formula weight/ g·mol^{-1}	1212.41
T/ K	100.0(1)
λ/ Å, radiation	CuK_α 1.54184
Crystal color, habit	Colorless block
Crystal size/ mm^3	0.176×0.332×0.432
Crystal system	Triclinic
Space group	$P\bar{1}$
Unit cell dimensions	
a/ Å	13.2416(3)
b/ Å	14.1880(2)
c/ Å	17.9154(3)
α/ °	87.6193(13)
β/ °	70.6309(17)
γ/ °	89.4391(14)
Volume (Å^3)	3172.55(10)
Z	2
Calculated density (Mg·m^{-3})	1.269
Absorption coefficient (mm^{-1})	3.578
F(000)	1280
θ range (°)	2.616-67.076
Reflections collected	33506
Unique reflections	11204
Minimum/maximum transmission	0.307/0.572
parameters / restraints	749 / 18
GooF F^2	1.069
R_1 [I>2σ(I)]	0.0503
wR^2 (all data)	0.1420
Maximum/minimum residual electron density (e·Å^{-3})	0.741 / –0.734

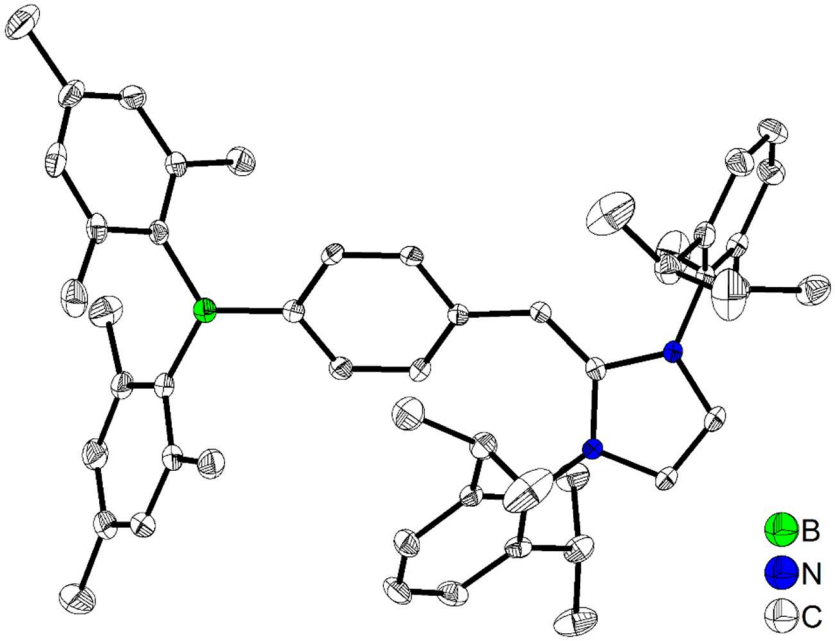

Figure 7.2-1. The solid-state molecular structure of **1** determined by single-crystal X-ray diffraction at 100 K. All ellipsoids are drawn at the 50% probability level, and H atoms are omitted for clarity.

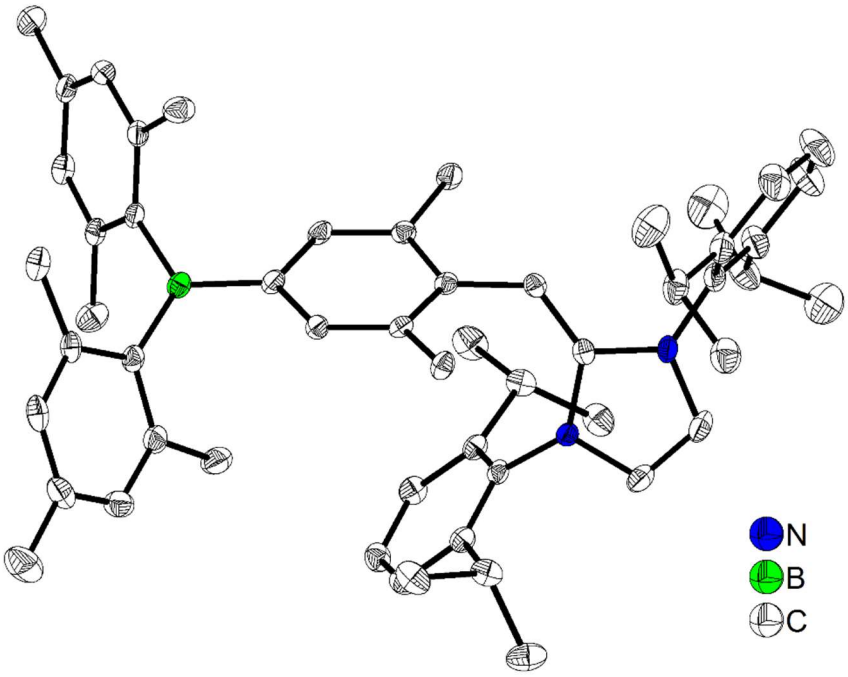

Figure 7.2-2. The solid-state molecular structure of **2** determined by single-crystal X-ray diffraction at 100 K. All ellipsoids are drawn at the 50% probability level, and H atoms are omitted for clarity.

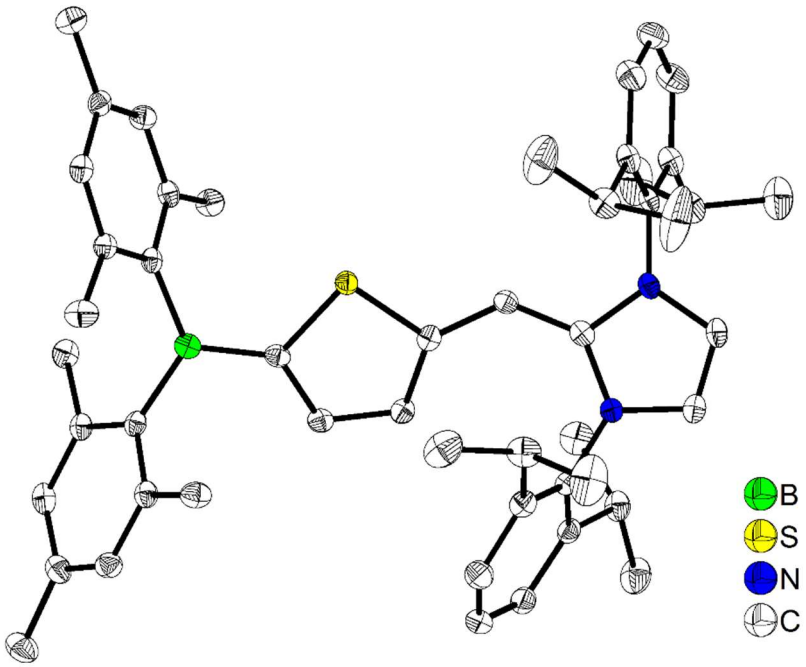

Figure 7.2-3. The solid-state molecular structure of **3** determined by single-crystal X-ray diffraction at 100 K. All ellipsoids are drawn at the 50% probability level, and H atoms are omitted for clarity.

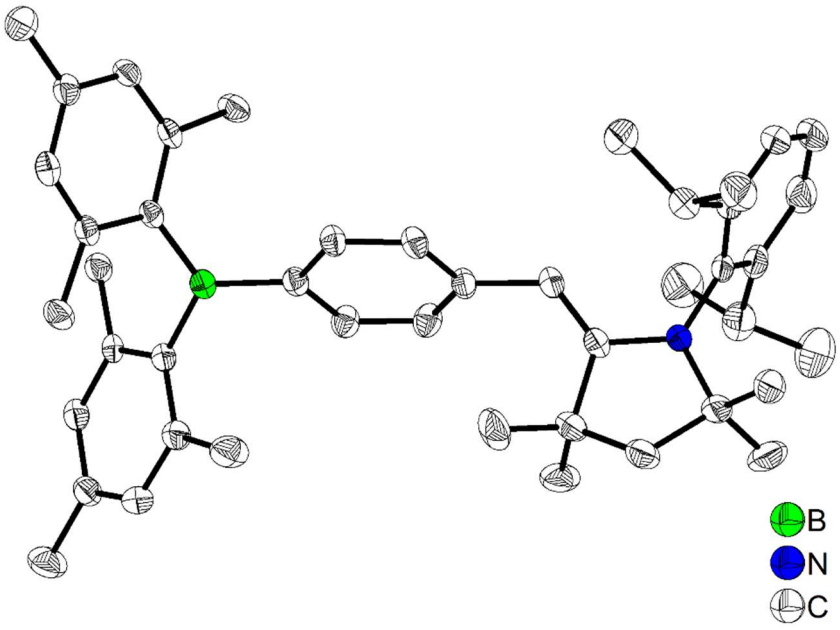

Figure 7.2-4. The solid-state molecular structure of **4** determined by single-crystal X-ray diffraction at 100 K. All ellipsoids are drawn at the 50% probability level, and H atoms are omitted for clarity. Only one of two symmetrically independent molecules are shown. The pyrrolidine moiety of this molecule is disordered and only the part with 87% occupancy is shown.

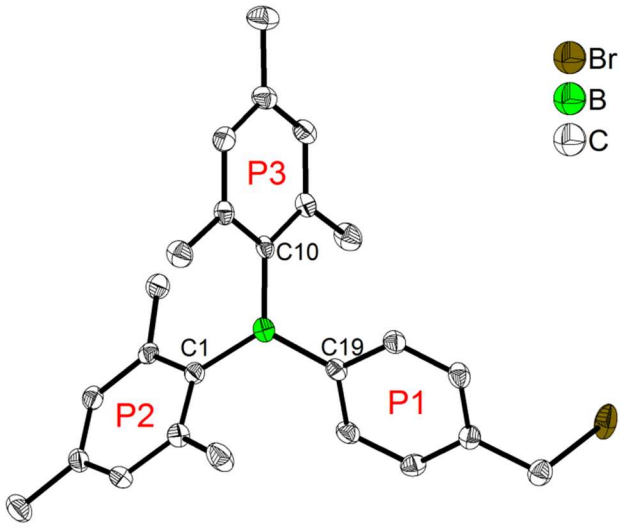

Figure 7.2-5. The solid-state molecular structure of **7a** determined by single-crystal X-ray diffraction at 100 K. All ellipsoids are drawn at the 50% probability level, and H atoms are omitted for clarity.

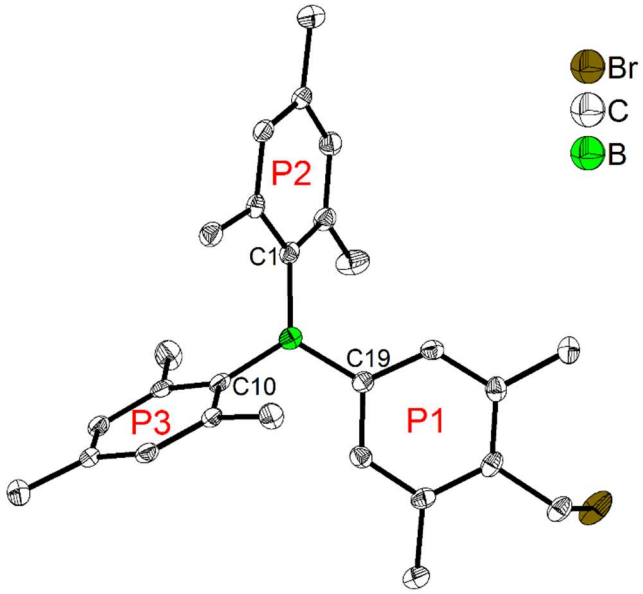

Figure 7.2-6. The solid-state molecular structure of **7b** determined by single-crystal X-ray diffraction at 100 K. All ellipsoids are drawn at the 50% probability level, and H atoms are omitted for clarity.

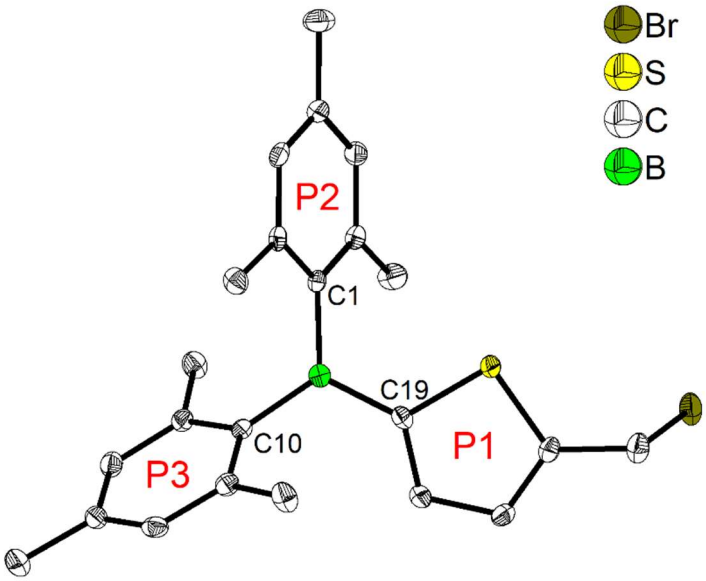

Figure 7.2-7. The solid-state molecular structure of **7c** determined by single-crystal X-ray diffraction at 100 K. All ellipsoids are drawn at the 50% probability level, and H atoms are omitted for clarity.

Table 7.2-5. Selected bond lengths (Å) and angles (°) of **7a**, **7b**, and **7c**. Rings are labeled P1, P2, and P3 according to Figures 6.2-1-6.2-7.

	7a	**7b**	**7c**
B–C19	1.571(3)	1.568(3)	1.545(3)
B–C1	1.578(3)	1.582(3)	1.584(3)
B–C10	1.574(3)	1.578(3)	1.582(3)
∠BC_3-P1	28.46(11)	21.02(14)	15.27(8)
∠BC_3-P2	51.00(7)	47.78(10)	57.53(8)
∠BC_3-P3	56.95(8)	67.15(8)	56.82(7)
Sum ∠CBC	359.9(2)	360.0(2)	360.00(15)

Table 7.2-6. Selected bond lengths (Å) of **1**-**4**.

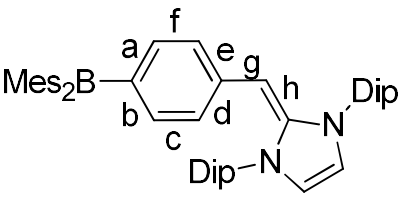

1

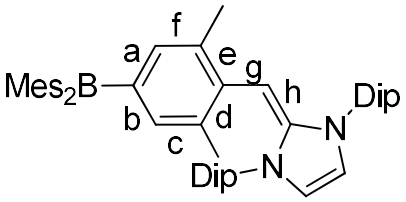

2

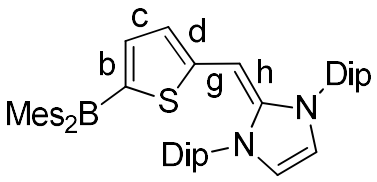

3

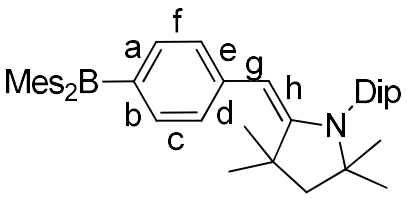

4

Mes = 2,4,6-trimethylphenyl
Dip = 2,6-di*iso*propylphenyl

Bond	**1**	**2**	**3**	**4**	
				molecule 1	molecule 2
B1–C (P1)	1.547(2)	1.552(3)	1.512(3)	1.564(3)	1.558(3)
a	1.408(2)	1.406(3)		1.402(3)	1.401(3)
b	1.408(2)	1.406(3)	1.388(3)	1.403(3)	1.403(3)
c	1.376(2)	1.385(3)	1.383(3)	1.386(3)	1.385(3)
d	1.412(2)	1.419(3)	1.395(3)	1.402(3)	1.397(3)
e	1.410(2)	1.416(3)		1.388(3)	1.396(3)
f	1.379(2)	1.383(3)		1.388(3)	1.385(3)
g	1.444(2)	1.462(3)	1.427(3)	1.486(3)	1.486(3)
h	1.379(2)	1.361(3)	1.382(3)	1.337(3)	1.334(3)
C–S			1.745(2)		
			1.742(2)		

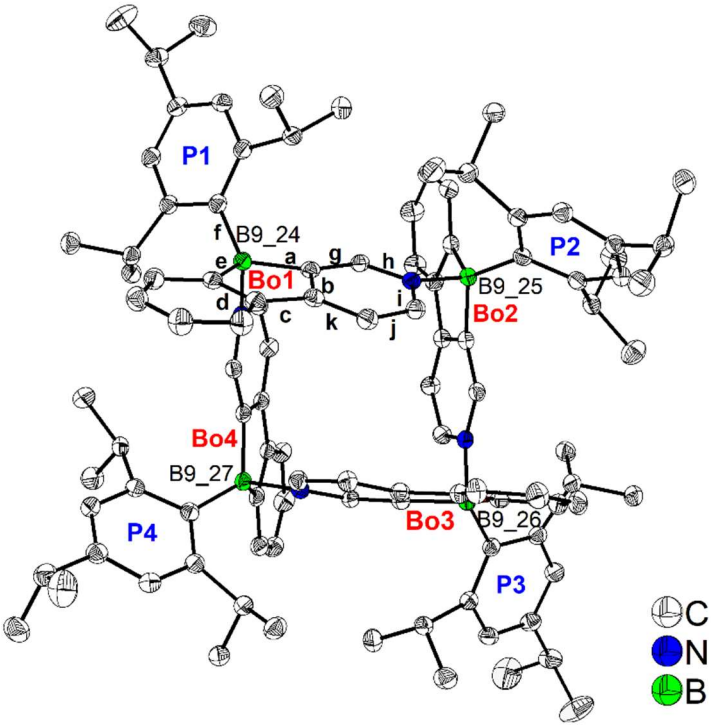

Figure 7.2-8. Molecular structure of **[TipPBBI]**$_4$ in the solid state at 100 K. Atomic displacement ellipsoids are drawn at the 50% probability level, and H atoms as well as C_6D_6 solvent molecules are omitted for clarity. 'Bo' and 'P' denote the planes of phenylpyridyl-fused borole and the Tip phenyl groups, respectively. Selected B–C and C–C bond distances are labelled with letters.

Table 7.2-7. Selected bond lengths (Å) and angles (°) (according to Figure 7.2-8) of **[TipPBBI]**$_4$.

	Bo1	Bo2	Bo3	Bo4
g: C10–C1 (Bo)	1.381(2)	1.379 (2)	1.380(2)	1.383(2)
h: C1–N2 (Bo)	1.357(2)	1.359(2)	1.358(2)	1.361(2)
i: N2–C3 (Bo)	1.351(2)	1.350(2)	1.352(2)	1.347(2)
j: C3–C4 (Bo)	1.378(2)	1.383(2)	1.381(2)	1.385(2)
k: C4–C11 (Bo)	1.392(2)	1.395(2)	1.391(2)	1.396(2)
∠$C10_{Bo}$–B–$C13_{Bo}$	97.49(9)	98.00(9)	97.24(9)	97.80(9)
∠$C10_{Bo}$–B–Cl_{Tip}	123.90(10)	119.58(10)	124.46(10)	119.20(9)
∠$C13_{Bo}$–B–Cl_{Tip}	116.16(10)	121.69(10)	115.32(10)	119.67(10)
∠Cl_{Tip}–B–N	111.50(9)	108.33(9)	110.48(9)	109.10(9)

7.3 Photophysical measurements

All measurements (except for **4**) were performed under an argon atmosphere using standard cuvettes (1 cm × 1 cm cross-section). UV-visible absorption spectra were recorded using an Agilent 8453 diode array UV-visible spectrophotometer (for **1**, **2**, **3**, **4** and **[TipPBB1]$_4$**) or LAMBDA 465 (**TipPBB2**, **10** and **11**) diode array UV-visible spectrophotometer. Molar extinction coefficients were calculated from three independently prepared samples. Excitation and emission spectra were recorded using an Edinburgh Instruments FLS920 spectrometer equipped with a double monochromator for both excitation and emission, operating in right-angle geometry mode, and all spectra were fully corrected for the spectral response of the instrument. The concentration of **1**, **2**, **3**, **4, [TipPBB1]$_4$** and **10** were lower than 10^{-5} M to minimize inner filter effects during fluorescence measurements. Due to the weak absorption of **TipPBB2** and compound **11**, the solutions for fluorescence measurements were measured at a concentration of ca. 2×10^{-5} M.

Fluorescence quantum yield measurements

Fluorescence quantum yields were measured using a calibrated integrating sphere (150 mm inner diameter) from Edinburgh Instruments combined with the FLS920 spectrometer described above. For solution-state measurements, the longest wavelength absorption maximum of the compound in the respective solvent was chosen for excitation. For solid-state measurements, excitation near the longest-wavelength absorption in hexane was selected.

Lifetime measurements

Fluorescence lifetimes were recorded via the time-correlated single photon counting (TCSPC) method using an Edinburgh Instruments FLS920 spectrometer equipped with a high-speed photomultiplier tube positioned after a single emission monochromator. Measurements were made in right-angle geometry mode, and the emission was

collected through a polarizer set to the magic angle. Both solutions and solids were excited with either pulsed diode lasers at wavelengths of 316 nm, 377 nm, 473 nm or 508 nm at repetition rates of 0.5, 10 or 20 MHz, as appropriate. The full-width-at-half-maximum (FWHM) of the pulse from the diode laser was ca. 90 ps with an instrument response function (IRF) of ca. 1 ns FWHM, respectively. The IRFs were measured from the scatter from either pure solvent or from the solid sample at the excitation wavelength. Decays were recorded to 10000 counts in the peak channel with a record length of at least 1000 channels. The band pass of the emission monochromator and a variable neutral density filter on the excitation side were adjusted to give a signal count rate of <60 kHz. Iterative reconvolution of the IRF with one decay function and non-linear least-squares analysis were used to analyze the data. The quality of decay fits was judged to be satisfactory based on the calculated values of the reduced χ^2 and Durbin-Watson parameters and visual inspection of the weighted residuals.

UV-vis and emission spectra

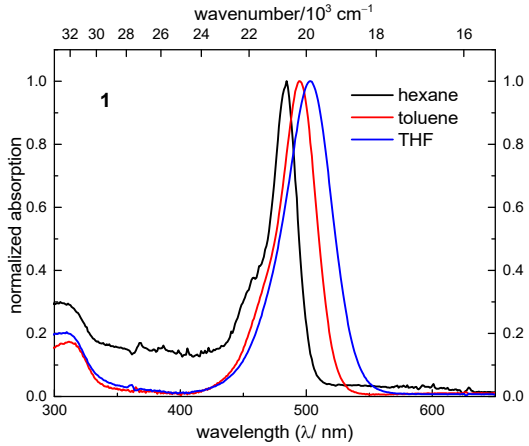

Figure 7.3-1. UV-vis absorption spectra of **1** in different solvents.

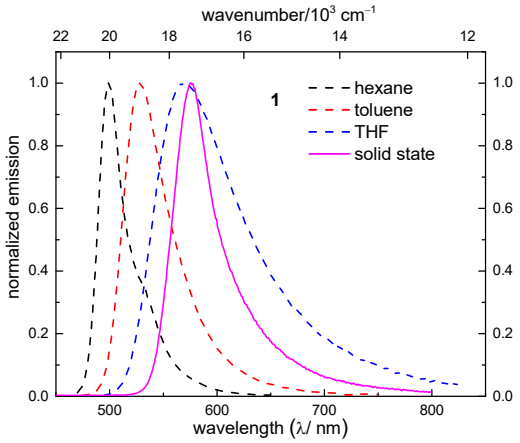

Figure 7.3-2. Emission spectra of **1** in different solvents and the solid state.

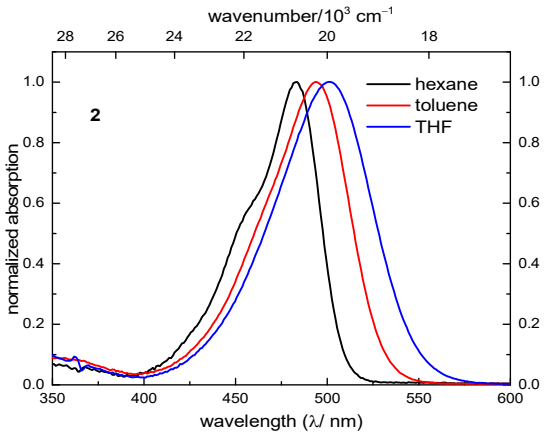

Figure 7.3-3. UV-vis absorption spectra of **2** in different solvents.

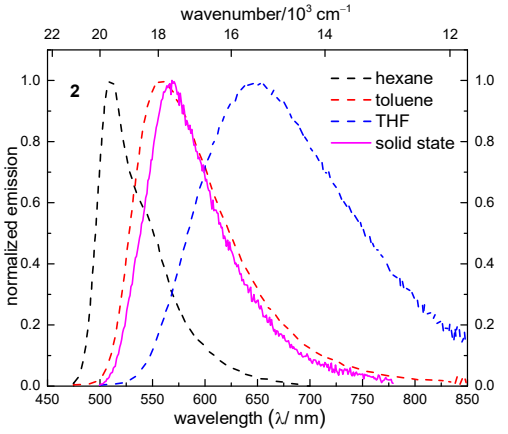

Figure 7.3-4. Emission spectra of **2** in different solvents and the solid state.

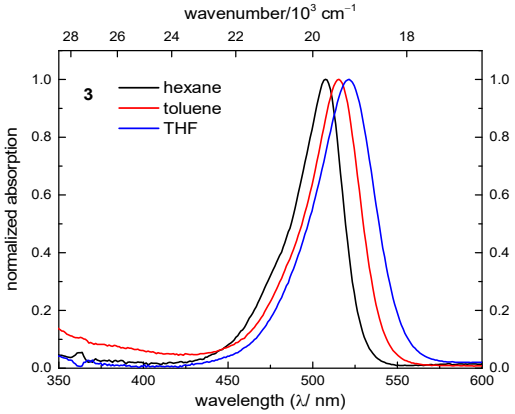

Figure 7.3-5. UV-vis absorption spectra of **3** in different solvents.

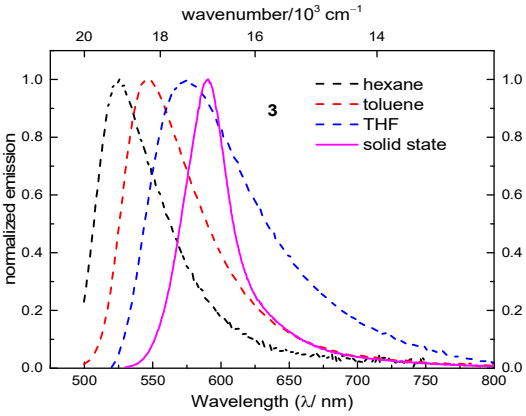

Figure 7.3-6. Emission spectra of **3** in different solvents and the solid state.

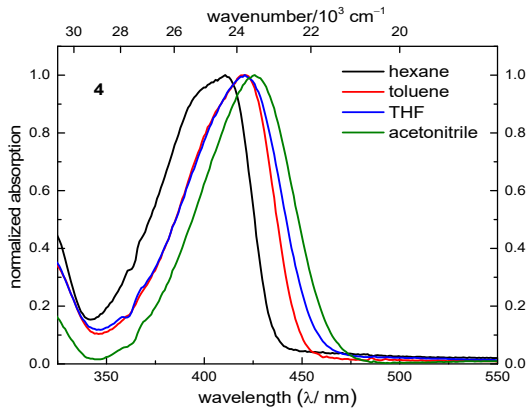

Figure 7.3-7. UV-vis absorption spectra of **4** in different solvents.

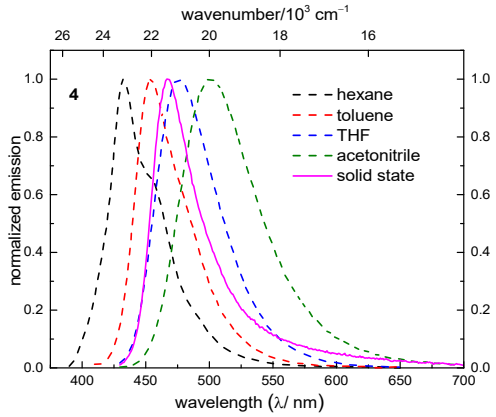

Figure 7.3-8. Emission spectra of **4** in different solvents and the solid state.

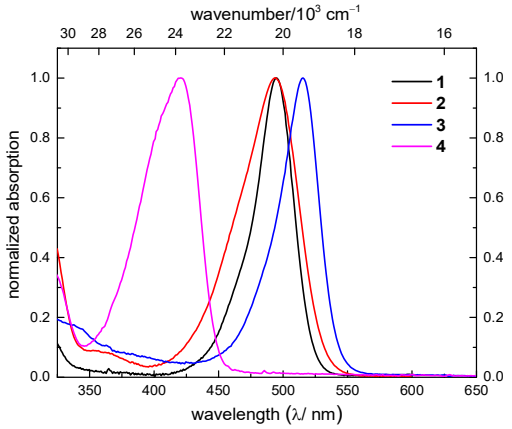

Figure 7.3-9. UV-vis absorption spectra of compounds **1**-**4** in toluene.

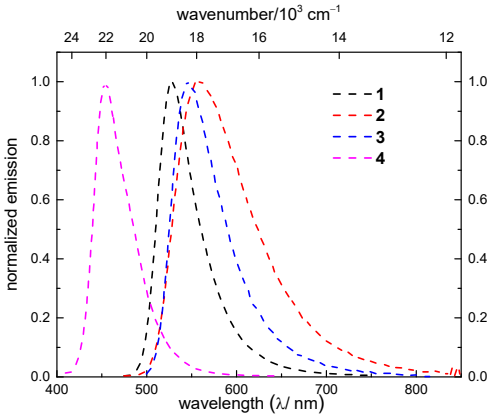

Figure 7.3-10. Emission spectra of compounds **1**-**4** in toluene.

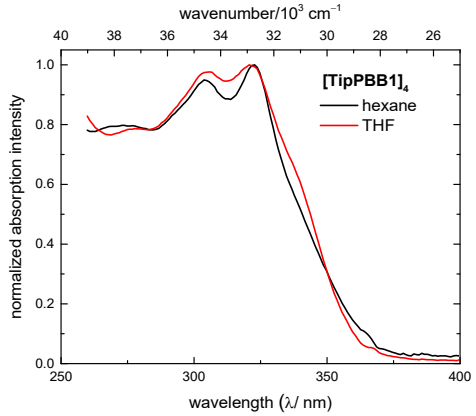

Figure 7.3-11. UV-vis absorption spectra of **[TipPBB1]**$_4$ in hexane and THF.

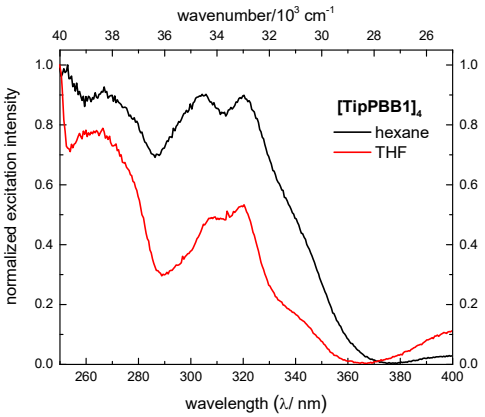

Figure 7.3-12. Excitation spectra of **[TipPBB1]**$_4$ in hexane and THF.

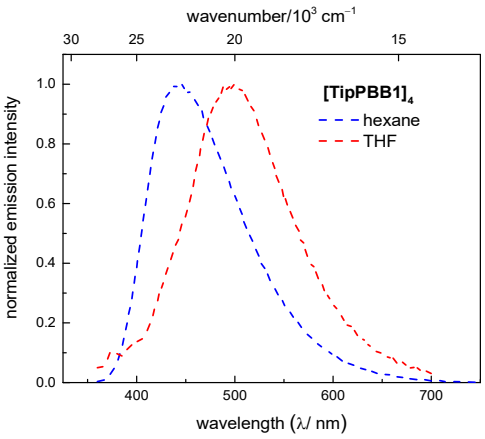

Figure 7.3-13. Emission spectra of **[TipPBB1]$_4$** in hexane and THF.

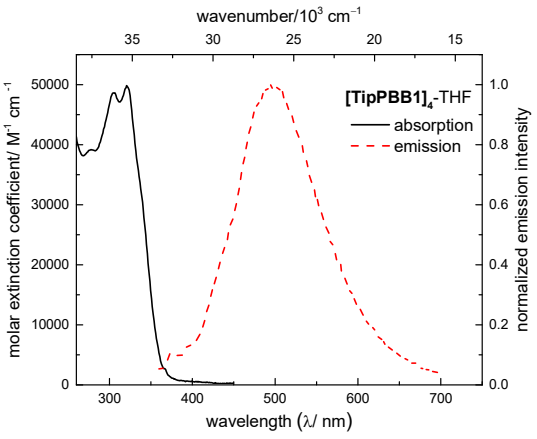

Figure 7.3-14. UV-vis absorption and emission spectra of **[TipPBB1]$_4$** in THF.

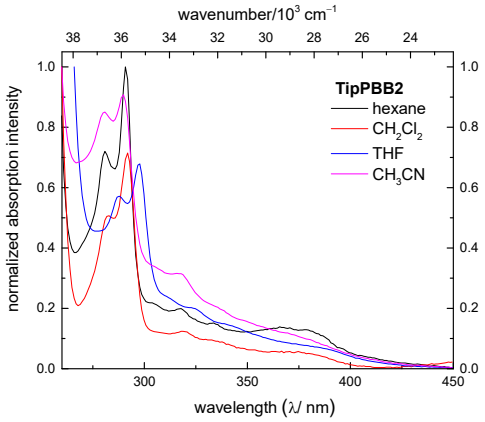

Figure 7.3-15. UV-vis absorption of **TipPBB2** in different solvents.

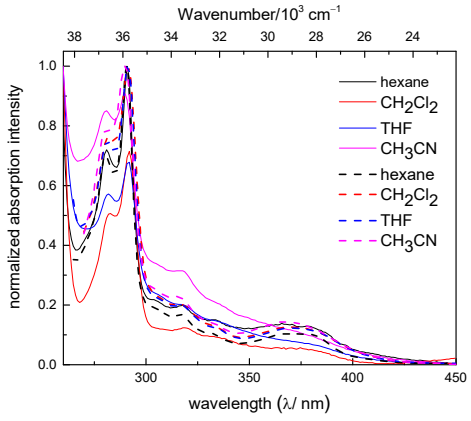

Figure 7.3-16. UV-vis absorption (solid line) and excitation spectra (dashed line) of **TipPBB2** in different solvents.

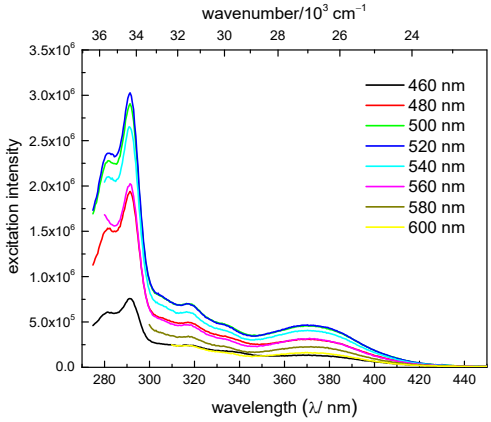

Figure 7.3-17. Excitation spectra of **TipPBB2** in CH_2Cl_2 at different emission wavelengths.

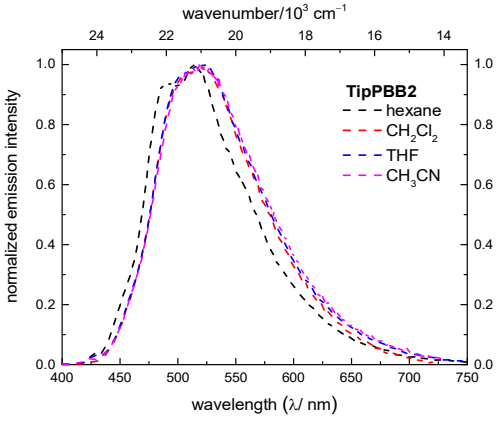

Figure 7.3-18. Emission spectra of **TipPBB2** in different solvents.

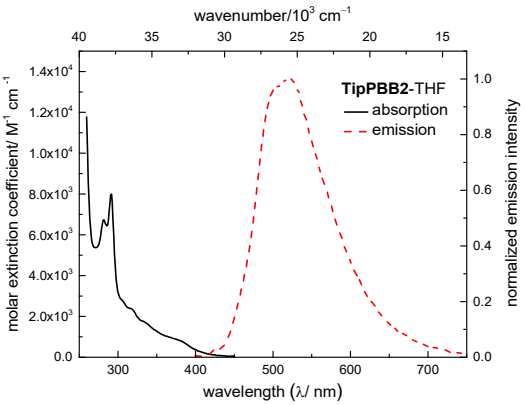

Figure 7.3-19. UV-vis absorption and emission spectra of **TipPBB2** in THF.

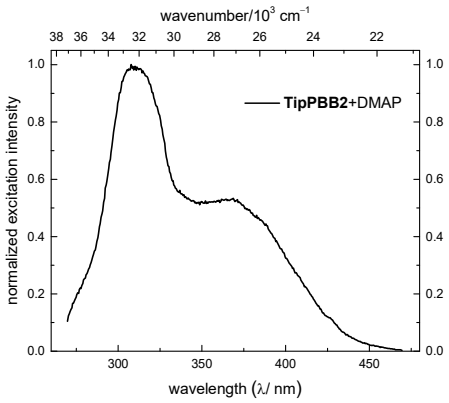

Figure 7.3-20. Excitation spectrum of **TipPBB2** + DMAP in THF.

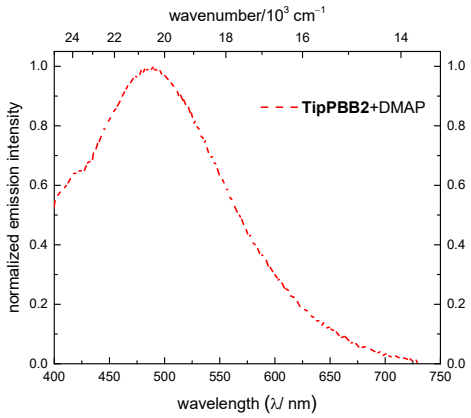

Figure 7.3-21. Emission spectrum of **TipPBB2** + DMAP in THF.

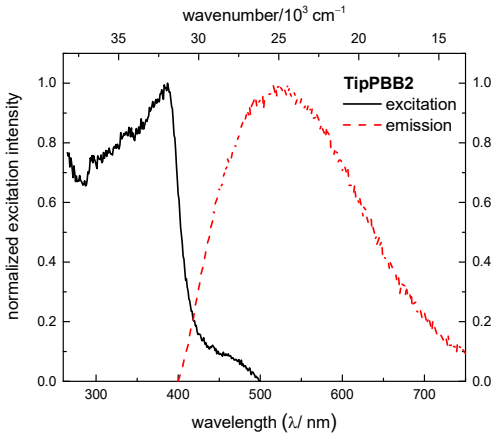

Figure 7.3-22. Excitation and emission spectra of **TipPBB2** in the solid state.

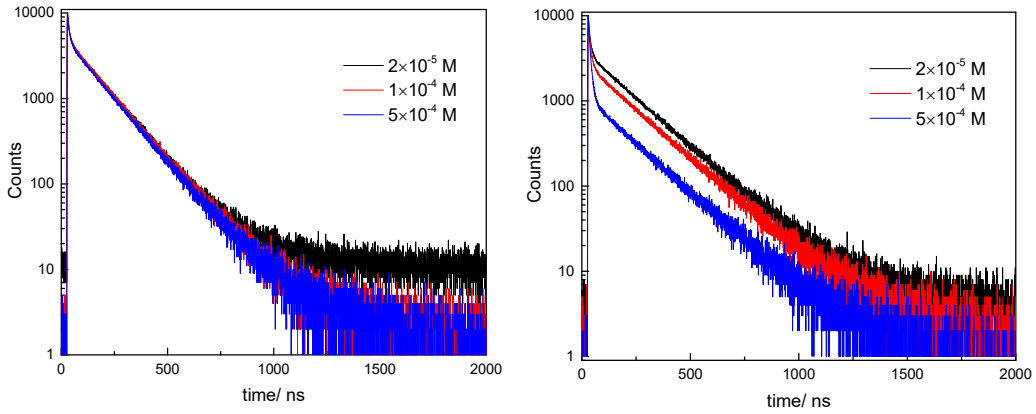

Figure 7.3-23. Lifetime measurements of **TipPBB2** at different concentrations at 298 K (left) and 213 K (right), measured in CH_2Cl_2.

Table 7.3-1. Lifetimes (ns) and corresponding relative percentages (in brackets) of **TipPBB2** at different concentrations at 298 K and 213 K, measured in CH_2Cl_2. τ_{LT} and τ_{ST} are the long and the short lifetimes, respectively.

Concentration (mol L^{-1})	298 K		213 K	
	τ_{LT} (rel.%)	τ_{ST} (rel.%)	τ_{LT} (rel.%)	τ_{LT} (rel.%)
2×10^{-5}	145 (93.4%)	7.3 (6.6%)	191 (91.0%)	8.4 (9.0%)
1×10^{-4}	146 (93.4%)	7.5 (6.6%)	188 (86.7%)	8.4 (13.3%)
5×10^{-4}	144 (93.0%)	7.3 (7.0%)	183 (69.3%)	8.5 (30.7%)

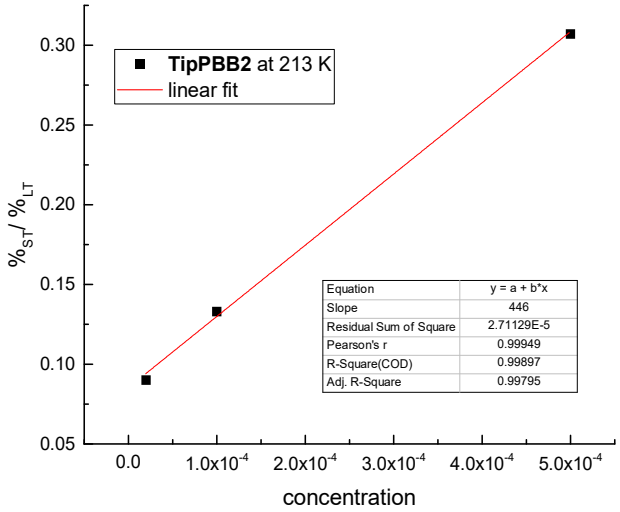

Figure 7.3-24. Plot of $\%_{ST}/\%_{LT}$ ($\%_{ST}$ and $\%_{LT}$ are the relative percentages of the long lifetime and the short lifetime components, respectively) vs. concentration (M) of **TipPBB2** in CH_2Cl_2 at 213 K.

Table 7.3-2. Lifetimes of **TipPBB2** at different temperature and pre-exponential fitting parameters of τ_{ST} and τ_{LT}, measured in 2-methyl-THF.

T. (K)	B_{ST}	τ_{ST}(ns)	B_{LT}	τ_{LT} (ns)
288	0.16	6.852	0.113	154.8
268	0.178	6.918	0.097	166.3
248	0.206	7.067	0.071	175.5
228	0.226	7.351	0.047	181.9
208	0.246	7.857	0.025	184.8
198	0.262	8.483	0.005	168.7

The $\%_{LT}/\%_{ST}$ can be calculated by equation (1) at different temperature from Table 7.3-2.[302]

$$\frac{\%_{LT}}{\%_{ST}} = \frac{\tau_{LT} * B_{LT}}{\tau_{ST} * B_{ST}} \quad (1)$$

$\%_{LT}$ is the relative value of the long lifetime component and $\%_{ST}$ is the relative value of the short lifetime component (Figure 3.5).

7.4 Electrochemical measurements

Cyclic voltammetry experiments were performed using a Gamry Instruments Reference 600 potentiostat. A standard three-electrode cell configuration was employed using a platinum disk working electrode, a platinum wire counter electrode, and a silver wire, separated by a Vycor tip, serving as the reference electrode. Formal redox potentials are referenced to the ferrocene/ferrocenium redox couple. Tetra-*n*-butylammonium hexafluorophosphate ([*n*-Bu_4N][PF_6]) was employed as the supporting electrolyte. Compensation for resistive losses (*iR* drop) was employed for all measurements.

Cyclic voltammetry diagrams

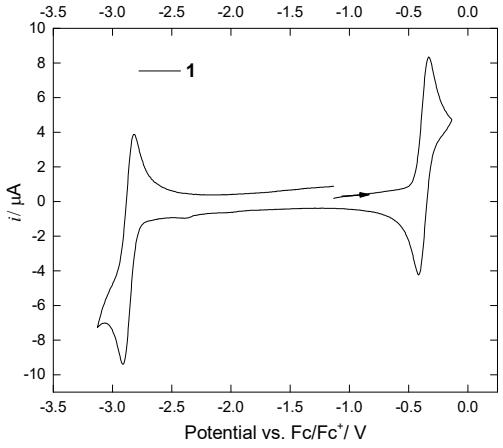

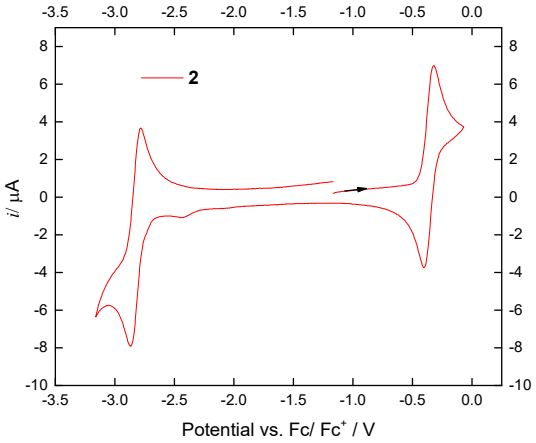

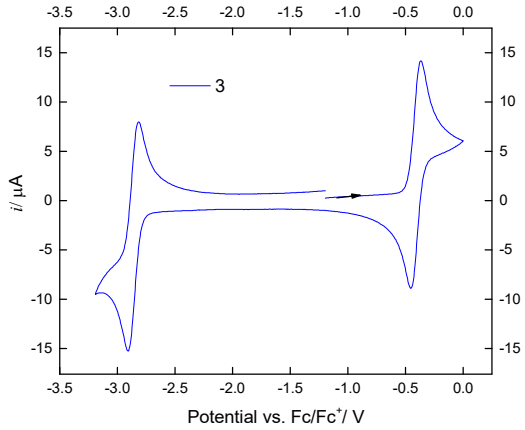

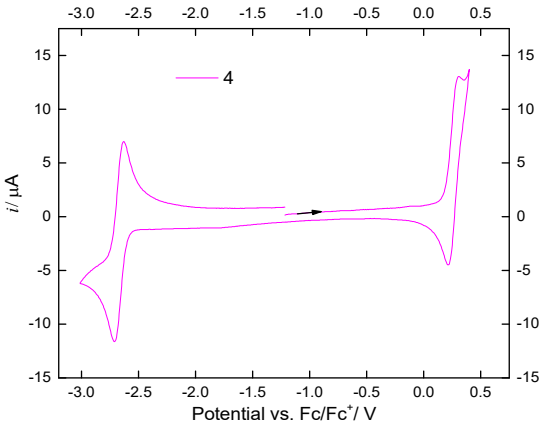

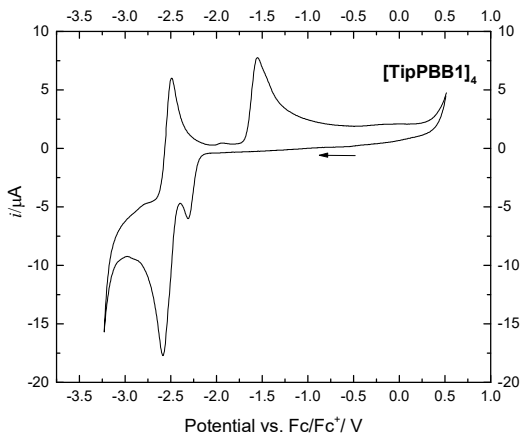

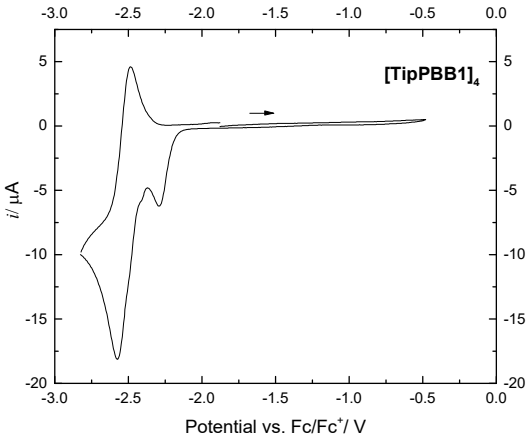

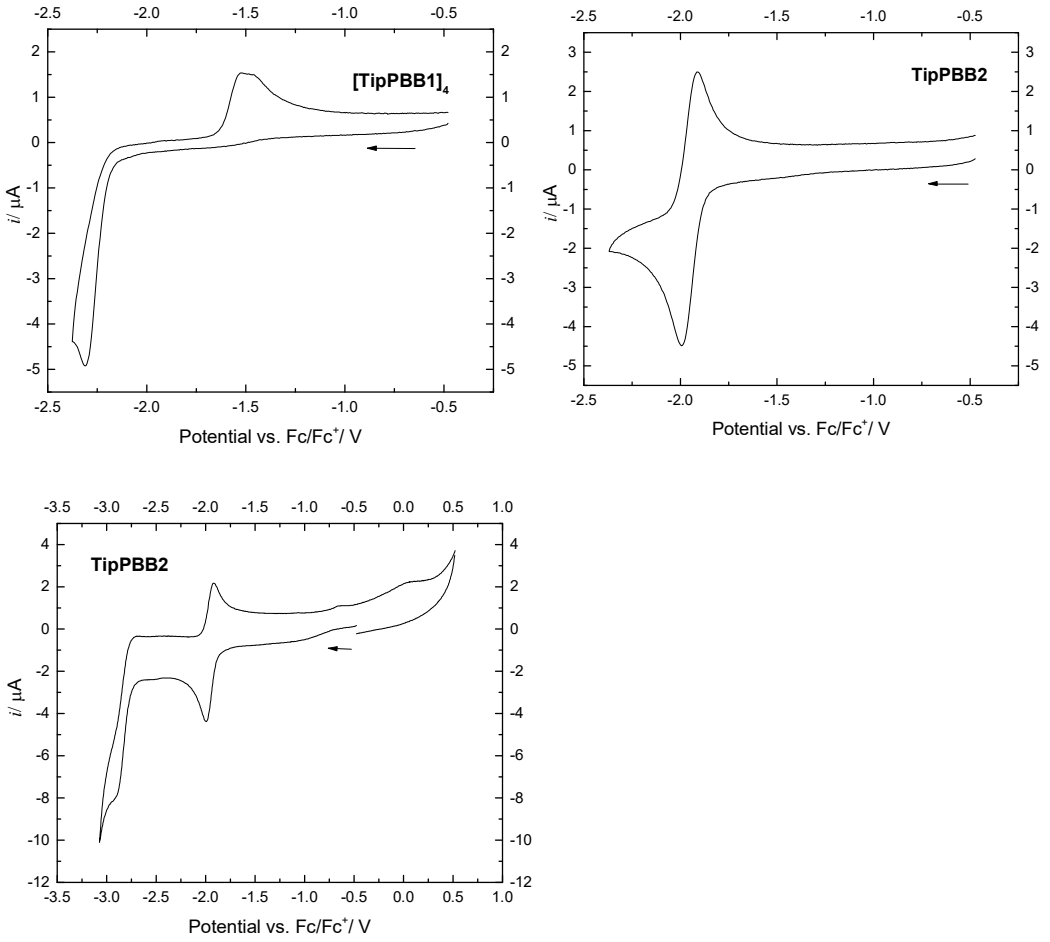

Figure 7.4-1. Cyclic voltammograms of **1**, **2**, **3**, **4**, **[TipPBB1]$_4$** and **TipPBB2** measured in THF in the presence of 0.1 M $TBAPF_6$, scan rates of 250 mV s^{-1} with potential given vs. the ferrocene/ ferrocenium (Fc/Fc^+) couple.

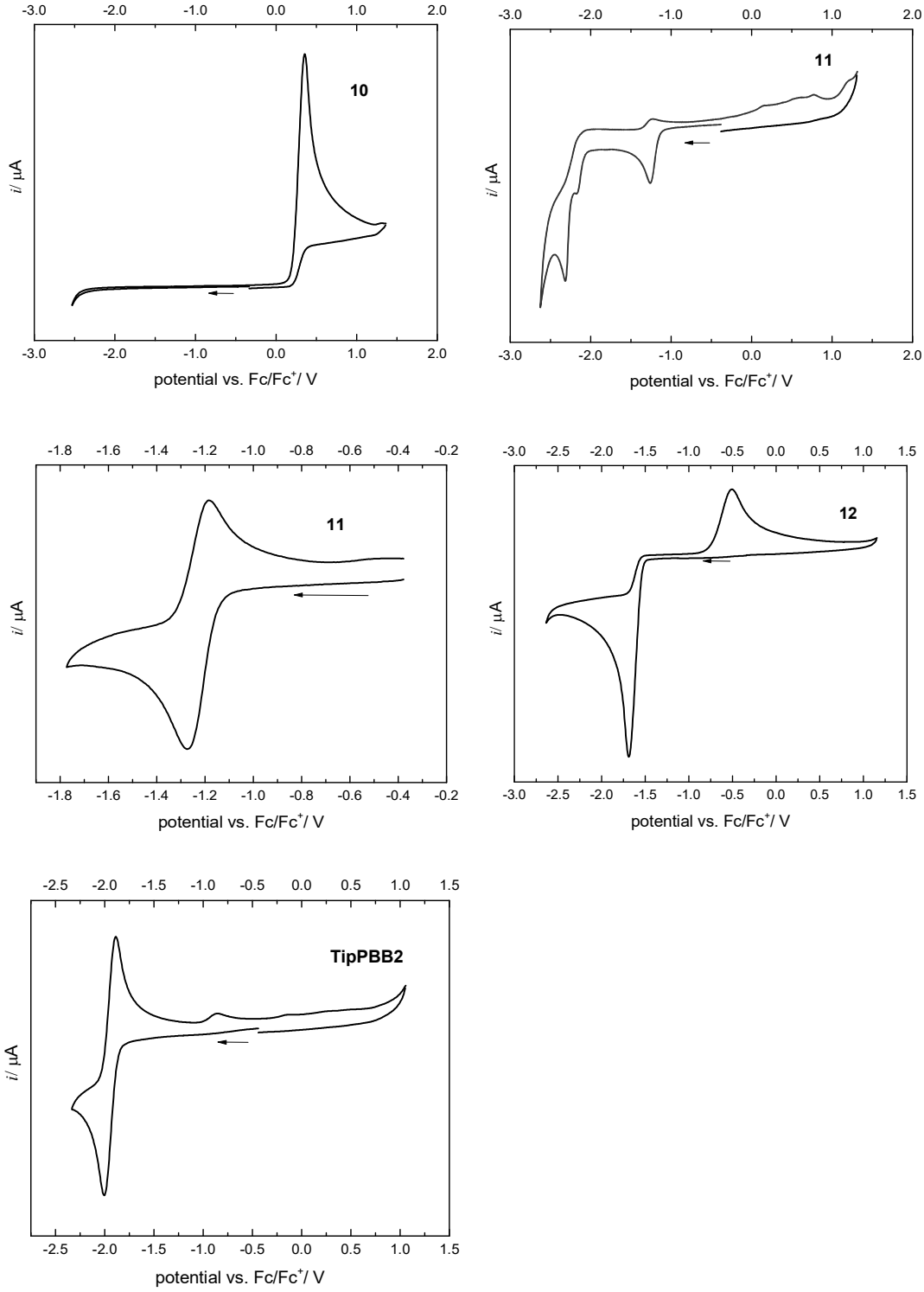

Figure 7.4-2. Cyclic voltammograms of compounds **10**, **11**, **12** and **TipPBB2** measured in CH_2Cl_2 in the presence of 0.1 M $TBAPF_6$, scan rates of 250 mV s^{-1} with potential given vs. the ferrocene/ ferrocenium (Fc/Fc^+) couple.

7.5 Theoretical studies

DFT and TD-DFT calculations were carried out with the program package Gaussian 09 (9.E.01)[303] and were performed on a parallel cluster system. GaussView (6.0.16), Avogadro (1.2.0)[304] and multiwfn[305] were used to visualize the results, to measure calculated structural parameters, and to plot orbital surfaces (isovalue: ± 0.020 [eÅ^{-3}]$^{1/2}$). The ground-state geometries were optimized using the B3LYP functional[306] in combination with the 6-31+G(d) basis set.[247, 248] The D3 dispersion correction of Grimme and coworkers was used.[307] The polarizable continuum model (PCM)[308] was used to include solvent effects for the ground state structure. Frequency calculation were performed on the optimized structures to confirm them to be local minima showing no negative (imaginary) frequencies. Λ indices were calculated according to literature[77] using multiwfn.[305] Based on these optimized structures, the lowest-energy vertical transitions (gas-phase and solvent correction using the polarizable continuum model) were calculated (singlets, 25 states) by TD-DFT, using the Coulomb attenuated functional CAM-B3LYP[76] as well as B3LYP in combination with the 6-31++G(d, p) basis set.[247, 248] The CAM-B3LYP has been shown to more accurately describe ICT systems in comparison to B3LYP. In our case, even though designed as ICT systems, the TD-DFT calculations using B3LYP more accurately reproduce the experimental results (**1**, **2**, **3** and **4**). An ultrafine integration grid and no symmetry constraints were used for all molecules.

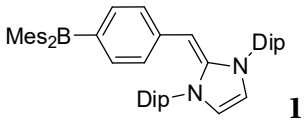

1

Calculated absorption spectra	Orbitals relevant to the $S_1 \leftarrow S_0$ transition
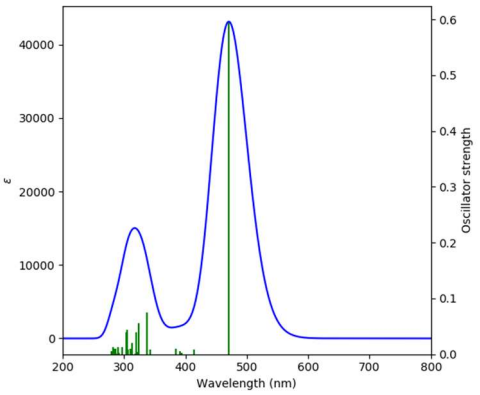 TD-DFT B3LYP/6-31+G(d), gas phase	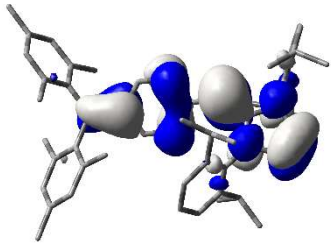 HOMO –4.42 eV (gas phase, B3LYP) –5.59 eV (gas phase CAM-B3LYP) –4.42 eV (toluene solution, B3LYP) –4.45 eV (THF solution, B3LYP)
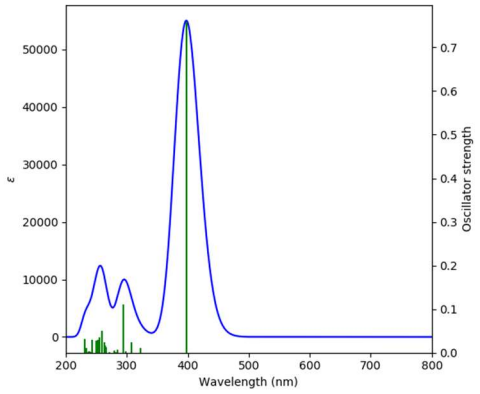 TD-DFT CAM-B3LYP/6-31+G(d), gas phase	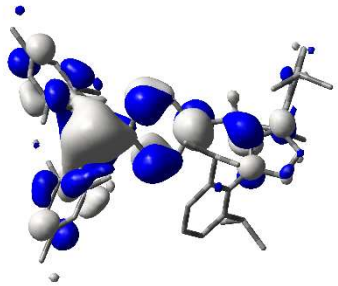 LUMO –1.45 eV (gas phase, B3LYP) –0.37 eV (gas phase, CAM-B3LYP) –1.53 eV (toluene solution, B3LYP) –1.64 eV (THF solution, B3LYP)
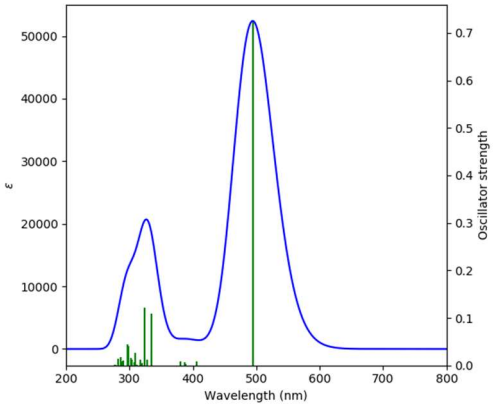 TD-DFT B3LYP/6-31+G(d), toluene solution	

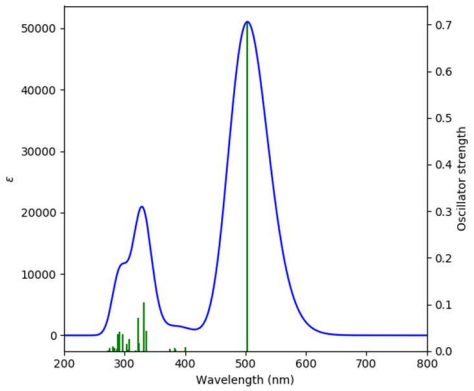

TD-DFT B3LYP/6-31+G(d), THF solution

Table 7.5-1. Lowest energy singlet electronic transitions of **1** (TD-DFT B3LYP/6-31+G(d), gas phase).

State	*E*/ eV	λ/ nm	*f*	Major contributions	Λ
1	2.63	470.68	0.5947	H→L (98%)	0.54
2	3.00	413.69	0.0079	H→L+1 (98%)	0.24
3	3.15	393.91	0.021	H→L+2 (71%), H→L+3 (28%)	0.30
4	3.17	391.45	0.0054	H→L+2 (25%), H→L+3 (67%)	0.31
5	3.22	384.77	0.0094	H→L+4 (94%)	0.25
6	3.62	342.83	0.0087	H→L+5 (97%)	0.25
7	3.68	337.07	0.0750	H-1→L (97%)	0.48
8	3.83	324.10	0.0550	H-2→L (74%), H→L+6 (21%)	0.54

Table 7.5-2. Lowest energy singlet electronic transitions of **1** (TD-DFT CAM-B3LYP/6-31+G(d), gas phase).

State	*E*/ eV	λ/ nm	*f*	Major contributions	Λ
1	3.12	394.41	0.7598	H→L (89%)	0.51
2	3.85	322.23	0.0115	H→L+1 (37%), H→L+2 (53%)	0.23
3	4.03	308.04	0.025	H→L+2 (14%), H→L+3 (63%), H→L+7 (11%)	0.32
4	4.04	306.91	0.0248	H→L+2 (12%), H→L+3 (41%), H→L+5 (23%)	0.25
5	4.16	298.01	0.0040	H→L+3 (29%), H→L+5 (35%), H→L+6 (18%)	0.24
6	4.21	294.37	0.1107	H–1→L (88%)	0.48
7	4.35	285.28	0.0071	H→L+1 (35%), H→L+2 (22%), H→L+3 (15%)	0.25
8	4.39	282.29	0.0006	H-5→L (11%), H→L+18 (11%), H→L+23 (16%)	0.33

Table 7.5-3. Lowest energy singlet electronic transitions of **1** (TD-DFT B3LYP/6-31+G(d), toluene).

State	*E*/ eV	λ/ nm	*f*	Major contributions
1	2.51	494.27	0.7236	H→L (99%)
2	3.05	406.39	0.0090	H→L+1 (99%)
3	3.19	388.65	0.0025	H→L+3 (97%)
4	3.21	386.73	0.0061	H→L+2 (88%), H→L+4 (10%)
5	3.26	380.01	0.0078	H→L+2 (10%), H→L+4 (88%)
6	3.70	335.05	0.0296	H-1→L (10%), H→L+5 (85%)
7	3.71	334.53	0.1097	H-1→L (87%), H→L+5 (10%)
8	3.78	328.02	0.0121	H→L+6 (22%), H→L+8 (35%), H→L+12 (11%)

Table **7.5-4**. Lowest energy singlet electronic transition of **1** (TD-DFT B3LYP/6-31+G(d), THF).

State	*E*/ eV	λ/ nm	*f*	Major contributions
1	2.46	503.13	0.7049	H→L (99%)
2	3.10	400.33	0.0089	H→L+1 (99%)
3	3.22	384.77	0.0029	H→L+2 (70%), H→L+3 (26%)
4	3.24	382.40	0.0060	H→L+3 (20%), H→L+4 (69%)
5	3.31	374.52	0.0053	H→L+4 (89%)
6	3.70	335.57	0.0432	H→L+5 (60%)
7	3.73	332.28	0.1042	H-1→L (95%)
8	3.74	331.15	0.0580	H→L+5 (10%), H→L+6 (27%), H→L+7 (25%), H→L+9 (16%)

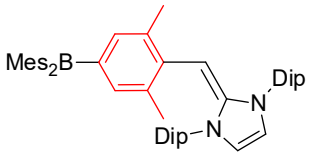

(2)

Calculated absorption spectra	Orbitals relevant to the $S_1 \leftarrow S_0$ transition
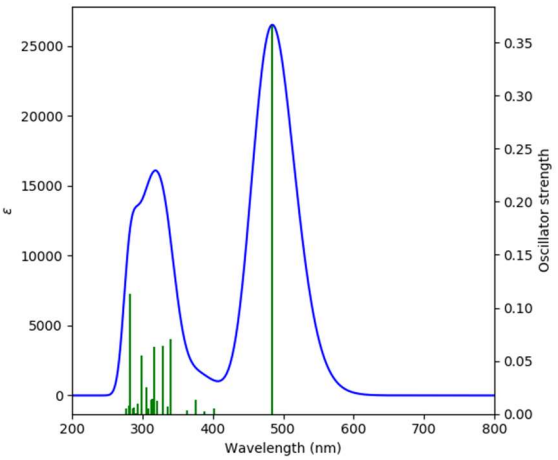 TD-DFT B3LYP/6-31+G(d), gas phase	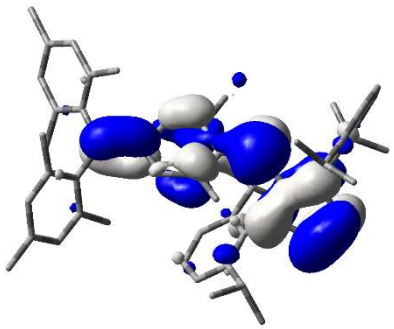 HOMO –4.47 eV (gas phase, B3LYP) –5.69 eV (gas phase, CAM-B3LYP)
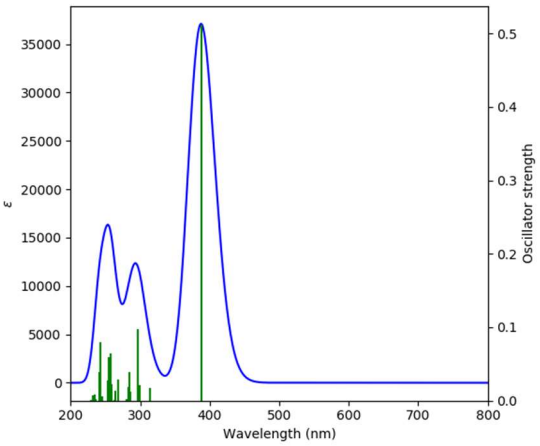 TD-DFT CAM-B3LYP/6-31+G(d), gas phase	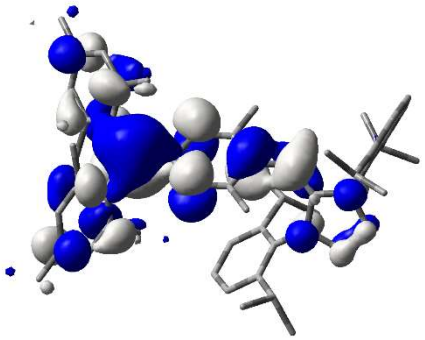 LUMO –1.49 eV (gas phase, B3LYP) –0.39 eV (gas phase, CAM-B3LYP)

Table 7.5-5. Lowest energy singlet electronic transitions of **2** (TD-DFT B3LYP/6-31+G(d), gas phase).

State	*E*/ eV	λ/ nm	*f*	Major contributions
1	2.56	484.51	0.3658	H→L (99%)
2	3.09	401.50	0.0054	H→L+1 (99%)
3	3.20	387.88	0.0024	H→L+2 (97%)
4	3.30	376.13	0.0137	H→L+3 (95%)
5	3.42	362.70	0.0032	H→L+4 (98%)
6	3.65	339.46	0.0709	H-1→L (98%)
7	3.69	336.14	0.0074	H→L+5 (95%)
8	3.78	328.33	0.0645	H-2→L (94%)

Table 7.5-6. Lowest energy singlet electronic transitions of **2** (TD-DFT CAM/B3LYP/6-31+G(d), gas phase).

State	*E*/ eV	λ/ nm	*f*	Major contributions
1	3.20	387.58	0.5120	H→L (87%)
2	3.95	314.01	0.0175	H→L+1 (11%), H→L+2 (73%)
3	4.14	299.86	0.0207	H→L+3 (20%), H→L+4 (15%), H→L+6 (37%)
4	4.16	297.80	0.0065	H→L+1 (13%), H→L+2 (12%), H→L+3 (60%)
5	4.18	269.52	0.0972	H-1→L (86%)
6	4.34	285.53	0.120	H-5→L (10%), H-4→L (28%), H-3→L (19%)
7	4.37	283.85	0.390	H-2→L (37%), H→L+7 (43%)
8	4.38	283.17	0.0189	H-2→L (33%), H→L+1 (15%), H→L+7 (22%)

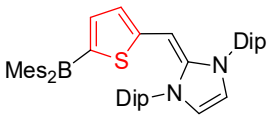

(**3**)

Calculated absorption spectra	Orbitals relevant to the $S_1 \leftarrow S_0$ transition
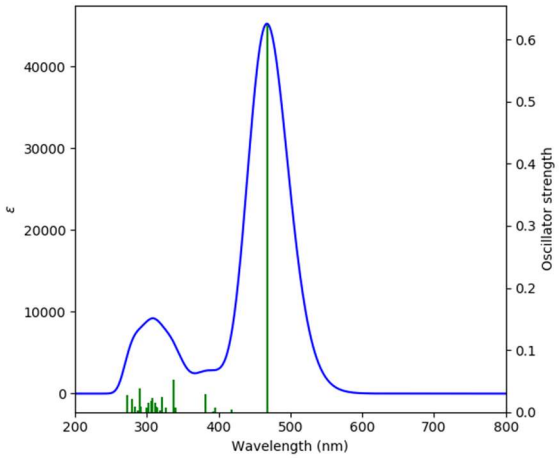 TD-DFT B3LYP/6-31+G(d), gas phase	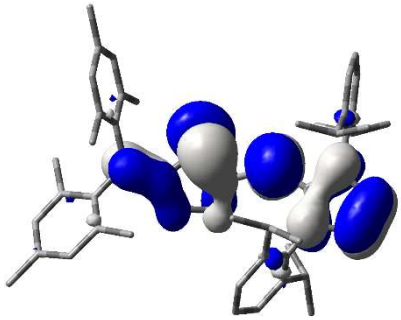 HOMO –4.45 eV (gas phase, B3LYP) –5.62 eV (gas phase, CAM-B3LYP)
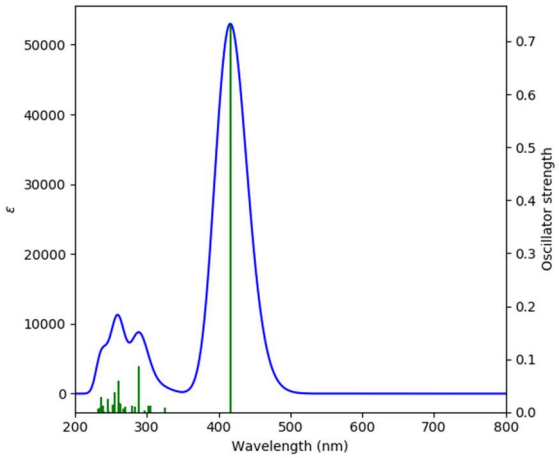 TD-DFT CAM-B3LYP/6-31+G(d), gas phase	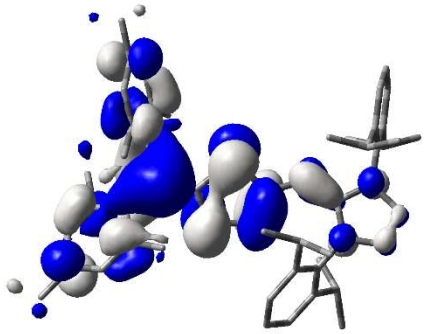 LUMO –1.45 eV (gas phase, B3LYP) –0.40 eV (gas phase, CAM-B3LYP)

Table 7.5-7. Lowest energy singlet electronic transitions of **3** (TD-DFT B3LYP/6-31+G(d), gas phase).

State	*E*/ eV	λ/ nm	*f*	Major contributions
1	2.65	467.30	0.6239	H→L (98%)
2	2.97	417.51	0.0045	H→L+1 (99%)
3	3.14	394.65	0.0076	H→L+2 (91%)
4	3.17	391.72	0.0011	H→L+3 (91%)
5	3.24	382.17	0.0284	H→L+4 (99%)
6	3.64	340.35	0.0067	H→L+5 (97%)
7	3.67	337.68	0.0523	H-1→L (97%)
8	3.80	325.90	0.0073	H-2→L (93%)

Table 7.5-8. Lowest energy singlet electronic transitions of **3** (TD-DFT CAM-B3LYP/6-31+G(d), gas phase).

State	*E*/ eV	λ/ nm	*f*	Major contributions
1	2.98	416.18	0.7314	H→L (93%)
2	3.81	325.06	0.0084	H→L+1 (61%), H→L+2 (31%)
3	4.07	304.33	0.0119	H→L+3 (28%), H→L+4 (39%)
4	4.11	301.51	0.0122	H→L+2 (14%), H→L+3 (12%), H→L+4 (45%), H→L+5 (11%)
5	4.17	297.29	0.0024	H→L+3 (50%), H→L+5 (30%)
6	4.29	289.32	0.0873	H-1→L (82%)
7	4.37	283.86	0.0110	H→L+1 (17%), H→L+2 (35%), H→L+5 (18%)
8	4.45	278.90	0.0125	H-2→L (55%)

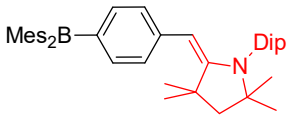

(4)

Calculated absorption spectra	Orbitals relevant to the $S_1 \leftarrow S_0$ transition
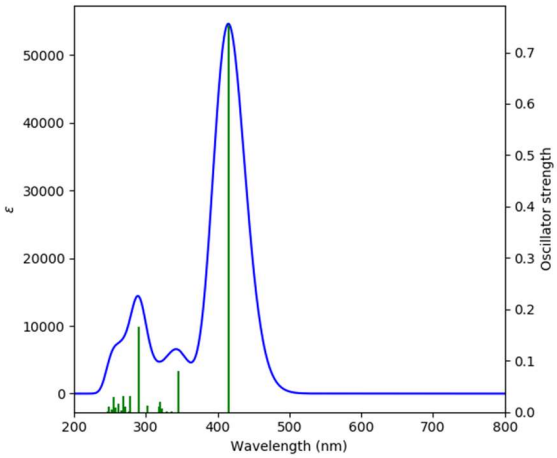 TD-DFT B3LYP/6-31+G(d), gas phase	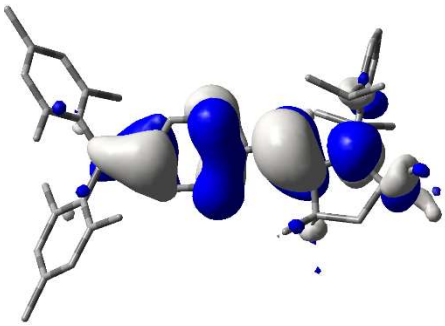 HOMO –4.99 eV (gas phase, B3LYP) –6.24 eV (gas phase, CAM-B3LYP)
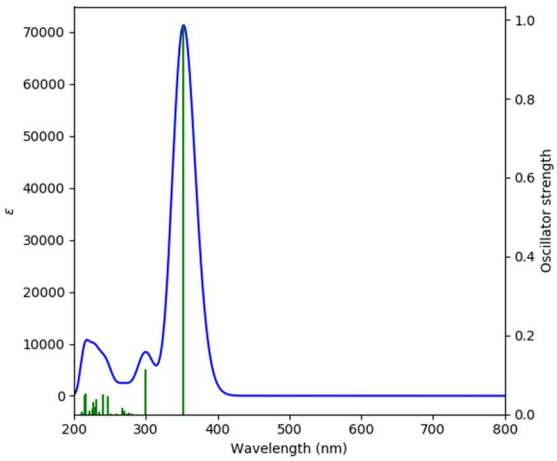 TD-DFT CAM-B3LYP/6-31+G(d), gas phase	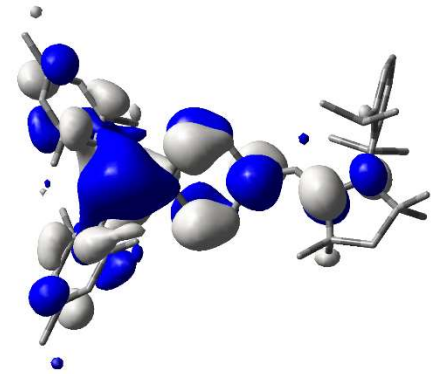 LUMO –1.66 eV (gas phase, B3LYP) –0.56 eV (gas phase, CAM-B3LYP)

Table 7.5-9. Lowest energy singlet electronic transitions of **4** (TD-DFT B3LYP/6-31+G(d), gas phase).

State	*E*/ eV	*λ*/ nm	*f*	Major contributions
1	2.99	414.86	0.754	H→L (98%)
2	3.59	345.16	0.0806	H-1→L (98%)
3	3.69	336.25	0.0008	H→L+1 (96%)
4	3.77	328.67	0.0011	H-2→L (92%)
5	3.85	321.68	0.0061	H→L+2 (94%)
6	3.88	319.81	0.0192	H-3→L (89%)
7	3.89	318.50	0.0102	H-4→L (94%)
8	4.10	302.45	0.013	H-5→L (28%), H→L+3 (13%), H→L+5 (32%), H→L+6 (17%)

Table 7.5-10. Lowest energy singlet electronic transitions of **4** (TD-DFT CAM-B3LYP/6-31+G(d), gas phase).

State	*E*/ eV	*λ*/ nm	*f*	Major contributions
1	3.52	352.44	0.9841	H→L (89%)
2	4.14	299.74	0.1149	H-1→L (88%)
3	4.42	280.66	0.0022	H-2→L (76%)
4	4.49	276.20	0.0049	H→L+2 (48%), H→L+4 (20%)
5	4.52	274.12	0.0014	H-6→L (36%), H→L+11 (12%)
6	4.60	269.55	0.008	H-3→L (76%)
7	4.63	267.69	0.0155	H-4→L (69%)
8	4.79	258.60	0.0029	H→L+3 (12%), H→L+5 (63%)

Theoretical calculations: Selected parameters

Table 7.5-11. Selected bond lengths in (Å) indicating the quinoidal distortion of the spacer.

Compound	**1**	**2**	**3**	**4**
B1–C (P1)	1.543	1.548	1.519	1.549
a	1.413	1.410		1.410
b	1.416	1.410	1.394	1.413
c	1.385	1.392	1.404	1.389
d	1.421	1.421	1.399	1.419
e	1.415	1.422		1.413
f	1.386	1.391		1.386
g	1.442	1.457	1.433	1.455
h	1.378	1.372	1.381	1.366
C–S				1.765
				1.758

Table 7.5-12. Selected bond lengths (Å) and angles (°).

Compound	**1**	**2**	**3**	**4**
B1–C (P1)	1.543	1.548	1.519	1.549
B1–C (P3)	1.580	1.578	1.582	1.577
B1–C (P4)	1.579	1.579	1.581	1.576
∠BIC_3-P1	21.59	18.57	14.04	23.01
∠BIC_3-P3	55.47	57.06	59.44	54.91
∠BIC_3-P4	55.18	54.64	56.86	54.43
Sum ∠CB1C	360	360	360	360
h (C=C)	1.378	1.372	1.381	1.366
C–N1	1.395	1.398	1.390	1.389
C–N2	1.400	1.404	1.396	
∠P1-P2	34.93	58.73	33.67	33.55

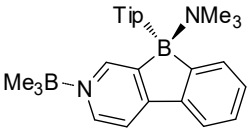

((BMe$_3$)TipPBBI(NMe$_3$))

Calculated absorption spectrum	Orbital	Energy/ eV
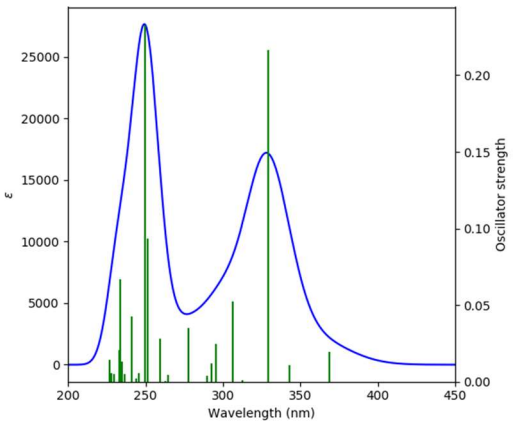 TD-DFT B3LYP/6-31+G(d), gas phase	L+4	–0.34
	L+3	–0.46
	L+2	–0.58
	L+1	–1.37
	LUMO	–2.07
	HOMO	–6.05
	H-1	–6.22
	H-2	–6.35
	H-3	–6.70
	H-4	–6.85

Orbitals relevant to the $S_1 \leftarrow S_0$ transition	Other relevant orbitals	
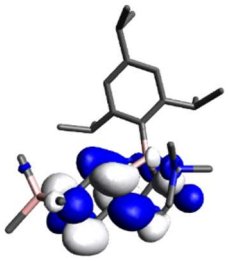 LUMO	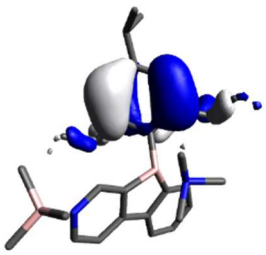 HOMO-1	
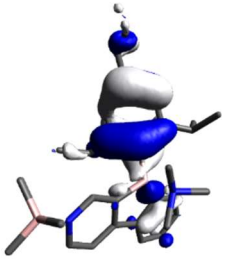 HOMO	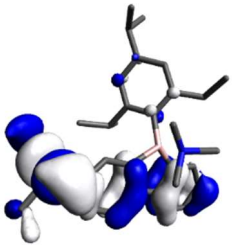 HOMO-2	

Table 7.5-13. Lowest energy singlet electronic transitions of **(BMe$_3$)TipPBBI(NMe$_3$)** (TD-DFT B3LYP/6-31+G(d), gas phase).

State	*E*/ eV	λ/ nm	*f*	Symmetry	Major contributions	Λ
1	3.36	368.51	0.0195	A	H→L (99%)	0.31
2	3.62	342.76	0.0108	A	H-1→L (99%)	0.20
3	3.77	329.13	0.2167	A	H-2→L (96%)	0.63
4	3.96	312.75	0.0012	A	H-3→L (99%)	0.15
5	4.04	306.62	0.0522	A	H→L+1 (95%)	0.37
6	4.19	295.71	0.0244	A	H-4→L (65%), H-2→L+1 (17%)	0.60
7	4.24	292.48	0.0121	A	H-4→L (27%), H-2→L+1 (33%), H-1→L+1 (26%)	0.47
8	4.28	289.48	0.0039	A	H-2→L+1 (23%), H-1→L+1 (67%)	0.31
9	4.47	277.50	0.0353	A	H-5→L (64%), H-2→L+1 (10%)	0.53
10	4.69	264.40	0.0043	A	H-1→L+2 (41%), H-1→L+4 (10%), H→L+5 (29%)	0.60
11	4.72	262.86	0.0002	A	H-3→L+1 (96%)	0.11
12	4.78	259.32	0.0281	A	H-6→L (47%), H-4→L+1 (34%), H-2→L+1 (11%)	0.62
13	4.93	251.26	0.0934	A	H-6→L (11%), H-4→L+1 (17%), H→L+2 (48%)	0.65
14	4.96	249.78	0.2328	A	H-6→L (11%), H-5→L (10%), H-4→L+1 (33%), H→L+2 (29%)	0.61
15	5.05	245.47	0.0057	A	H-7→L (80%)	0.47
16	5.08	243.85	0.0022	A	H→L+3 (95%)	0.23
17	5.14	241.02	0.0427	A	H→L+4 (67%)	0.63
18	5.24	236.64	0.0053	A	H-1→L+2 (10%), H-1→L+3 (74%)	0.26
19	5.24	236.45	0.0019	A	H-8→L (40%), H-2→L+2 (38%)	0.52
20	5.28	234.95	0.0133	A	H-1→L+2 (20%), H-1→L+3 (17%), H-1→L+4 (50%)	0.44
21	5.30	233.86	0.0666	A	H-5→L+1 (74%)	0.63
22	5.32	232.96	0.0209	A	H-8→L (31%), H-2→L+2 (42%)	0.50
23	5.40	229.42	0.0053	A	H-2→L+3 (74%), H→L+6 (14%)	0.20
24	5.43	228.13	0.0057	A	H-6→L+1 (14%), H-2→L+4 (11%), H→L+5 (12%), H→L+8 (23%), H→L+9 (14%)	0.49
25	5.47	226.82	0.0144	A	H-2→L+3 (12%), H→L+6 (45%), H→L+8 (25%)	0.27

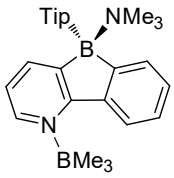

((BMe$_3$)TipPBB2(NMe$_3$))

Calculated absorption spectrum	Orbital	Energy/ eV
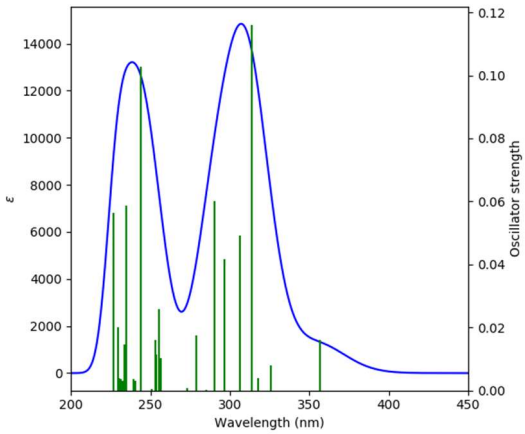 TD-DFT B3LYP/6-31+G(d), gas phase	L+4	–0.21
	L+3	–0.38
	L+2	–0.59
	L+1	–1.32
	LUMO	–1.91
	HOMO	–6.02
	H-1	–6.25
	H-2	–6.39
	H-3	–6.55
	H-4	–6.77

Orbitals relevant to the $S_1 \leftarrow S_0$ transition	Other relevant orbitals	
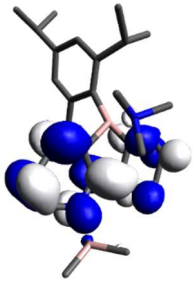 LUMO	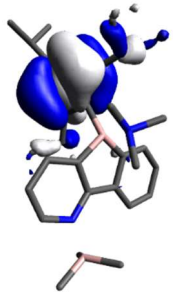 HOMO-1	
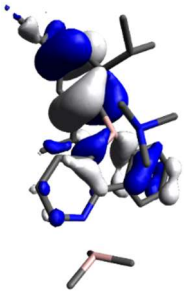 HOMO	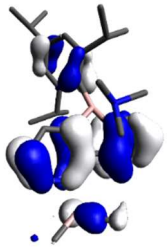 HOMO-2	

Table 7.5-14. Lowest energy singlet electronic transitions of **(BMe_3)TipPBB2(NMe_3)** (TD-DFT B3LYP/6-31+G(d), gas phase).

State	*E*/ eV	λ/ nm	*f*	Symmetry	Major contributions	Λ
1	3.47	356.87	0.016	A	H→L (98%)	0.36
2	3.81	325.70	0.008	A	H-1→L (99%)	0.20
3	3.90	317.99	0.0039	A	H-3→L (97%)	0.18
4	3.95	313.59	0.1161	A	H-2→L (74%), H→L+1 (16%)	0.64
5	4.05	306.45	0.0492	A	H-2→L (14%), H→L+1 (80%)	0.43
6	4.18	296.70	0.0418	A	H-4→L (75%), H-2→L+1 (11%)	0.45
7	4.27	290.48	0.0602	A	H-5→L (72%), H-4→L (10%)	0.50
8	4.35	284.92	0.0003	A	H-1→L+1 (97%)	0.20
9	4.44	279.05	0.0174	A	H-2→L+1 (80%)	0.60
10	4.54	273.31	0.0008	A	H-3→L+1 (97%)	0.17
11	4.83	256.64	0.0102	A	H-1→L+4 (18%), H→L+2 (16%), H→L+3 (19%), H→L+7 (12%)	0.53
12	4.86	255.18	0.0257	A	H-6→L (18%), H-4→L+1 (68%)	0.48
13	4.88	253.91	0.0113	A	H-7→L (25%), H-6→L (47%), H-4→L+1 (23%)	0.56
14	4.89	253.40	0.0161	A	H-5→L+1 (75%)	0.47
15	4.94	250.77	0.0006	A	H→L+2 (81%)	0.26
16	5.08	244.26	0.1027	A	H→L+3 (62%)	0.55
17	5.15	240.58	0.003	A	H-1→L+2 (92%)	0.20
18	5.17	239.65	0.0038	A	H-7→L (48%), H-6→L (24%)	0.57
19	5.28	234.76	0.0587	A	H-2→L+2 (33%), H→L+4 (24%), H→L+5 (11%)	0.49
20	5.30	233.75	0.0147	A	H-2→L+2 (45%), H-1→L+3 (15%), H→L+4 (14%), H→L+6 (13%)	0.40
21	5.33	232.55	0.0031	A	H-8→L (57%)	0.51
22	5.35	231.58	0.0037	A	H-1→L+3 (30%), H→L+4 (15%), H→L+5 (18%), H→L+7 (15%)	0.53
23	5.39	230.09	0.004	A	H-2→L+2 (12%), H→L+5 (14%), H→L+6 (64%)	0.32
24	5.40	229.81	0.0201	A	H-1→L+3 (29%), H→L+5 (23%), H→L+7 (13%)	0.51
25	5.46	226.90	0.0563	A	H-6→L+1 (40%), H-2→L+3 (36%)	0.64

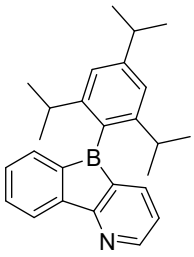

(TipPBB2)

Calculated absorption spectrum	Orbital	Energy/ eV
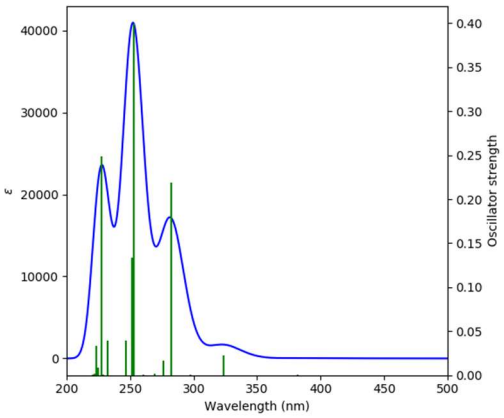 TD-DFT B3LYP/6-31+G(d), gas phase	L+4	–0.21
	L+3	–0.32
	L+2	–0.38
	L+1	–1.46
	LUMO	–2.53
	HOMO	–6.28
	H-1	–6.30
	H-2	–6.44
	H-3	–7.07
	H-4	–7.13

Orbitals relevant to the $S_1 \leftarrow S_0$ transition	Other relevant orbitals	
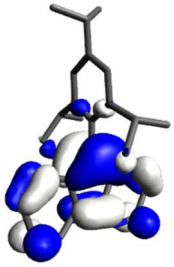 LUMO	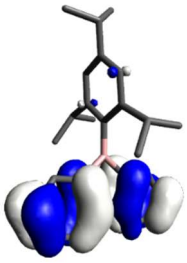 HOMO-1	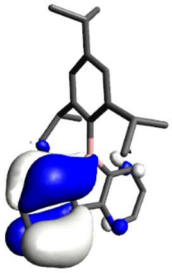 HOMO-3
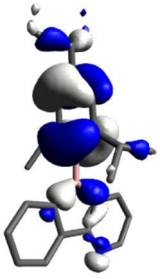 HOMO	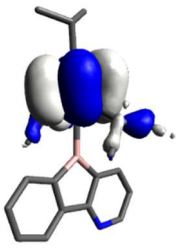 HOMO-2	

Table 7.5-15. Lowest energy singlet electronic transitions of **TipPBB2** (TD-DFT B3LYP/6-31+G(d), gas phase).

State	*E*/ eV	λ/ nm	*f*	Major contributions	Λ
1	2.92	423.94	0.0	H→L (98%)	0.27
2	2.95	419.96	0.0002	H-1→L (98%)	0.65
3	3.25	381.98	0.0004	H-2→L (99%)	0.21
4	3.59	345.24	0.0001	H-4→L (97%)	0.33
5	3.84	323.30	0.0229	H-3→L (74%), H-1→L+1 (22%)	0.61
6	4.17	297.62	0.0005	H-4→L+1 (10%), H→L+1 (88%)	0.21
7	4.40	282.08	0.2188	H-5→L (20%), H-3→L (17%), H-1→L+1 (47%)	0.66
8	4.48	276.46	0.0166	H-2→L+1 (94%)	0.18
9	4.60	269.62	0.0019	H-4→L+1 (86%), H→L+1 (10%)	0.42
10	4.76	260.55	0.0008	H-7→L (87%)	0.37
11	4.90	252.93	0.3998	H-5→L (65%), H-1→L+1 (18%)	0.69
12	4.93	251.26	0.1333	H-6→L (44%), H-3→L+1 (35%)	0.63
13	4.98	249.12	0.0002	H-2→L+3 (45%), H→L+4 (46%)	0.66
14	5.03	246.40	0.0393	H-6→L (35%), H-3→L+1 (43%), H-1→L+2 (13%)	0.63
15	5.22	237.50	0.0002	H-9→L (59%), H→L+2 (15%)	0.36
16	5.27	235.32	0.0002	H-9→L (12%), H→L+2 (78%)	0.29
17	5.34	232.09	0.0392	H-8→L (73%), H-1→L+2 (11%)	0.37
18	5.42	228.92	0.0008	H-1→L+3 (94%)	0.27
19	5.45	227.57	0.2487	H-2→L+4 (14%), H-1→L+2 (15%), H→L+3 (51%)	0.79
20	5.52	224.77	0.0066	H→L+5 (82%)	0.26
21	5.52	224.56	0.0083	H-2→L+2 (56%), H-1→L+2 (12%), H→L+5 (12%)	0.33
22	5.56	223.18	0.0334	H-2→L+2 (34%), H-1→L+2 (11%), H-1→L+4 (17%)	0.41
23	5.59	221.98	0.0015	H-1→L+4 (75%)	0.34
24	5.61	220.87	0.0001	H-10→L (34%), H-1→L+5 (40%)	0.28
25	5.62	220.71	0.0012	H-10→L (45%), H-1→L+5 (34%)	0.30

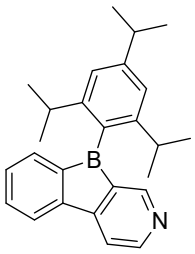

(TipPBBl)

<table>
<tr><th>Calculated absorption spectrum</th><th>Orbital</th><th>Energy/ eV</th></tr>
<tr><td rowspan="11"> 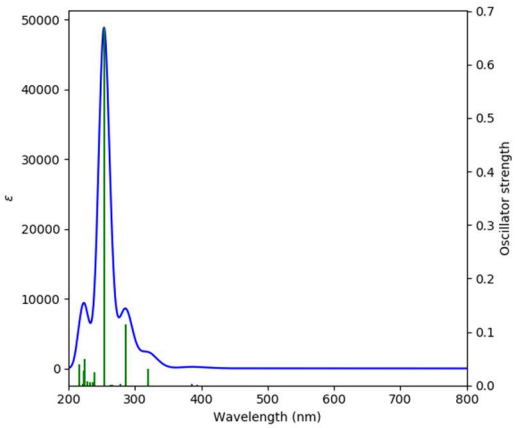

TD-DFT B3LYP/6-31+G(d), gas phase</td><td>L+4</td><td>–0.17</td></tr>
<tr><td>L+3</td><td>–0.27</td></tr>
<tr><td>L+2</td><td>–0.34</td></tr>
<tr><td>L+1</td><td>–1.46</td></tr>
<tr><td>LUMO</td><td>–2.58</td></tr>
<tr><td>HOMO</td><td>–6.29</td></tr>
<tr><td>H-1</td><td>–6.43</td></tr>
<tr><td>H-2</td><td>–6.59</td></tr>
<tr><td>H-3</td><td>–7.15</td></tr>
<tr><td>H-4</td><td>–7.17</td></tr>
<tr><td colspan="3"></td></tr>
<tr><td>Orbitals relevant to the $S_1 \leftarrow S_0$ transition</td><td colspan="2">Other relevant orbitals</td></tr>
<tr><td rowspan="2"> 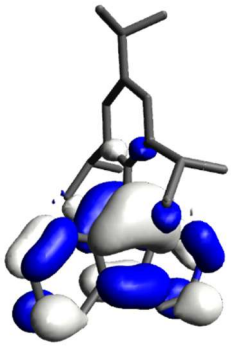
LUMO
 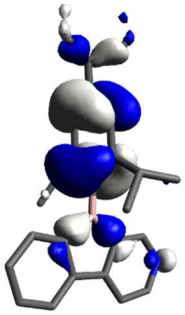
HOMO</td><td> 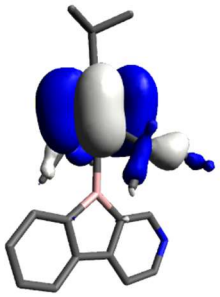
HOMO-1
 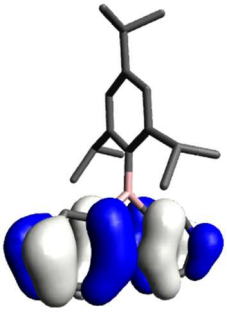
HOMO-2</td><td> 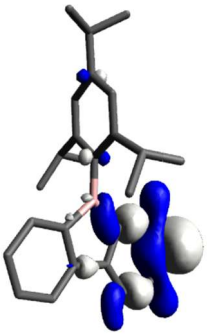
HOMO-3</td></tr>
</table>

Table 7.5-16. Lowest energy singlet electronic transitions of **TipPBB1** (TD-DFT B3LYP/6-31+G(d), gas phase).

State	*E*/ eV	λ/ nm	*f*	Symmetry	Major contributions	Λ
1	2.90	427.05	0.0001	A	H→L (98%)	0.25
2	3.15	393.85	0.0008	A	H-2→L (60%), H-1→L (39%)	0.49
3	3.21	386.27	0.0024	A	H-2→L (39%), H-1→L (60%)	0.39
4	3.63	341.57	0.0003	A	H-3→L (97%)	0.33
5	3.88	319.74	0.0308	A	H-4→L (80%), H-2→L+1 (18%)	0.65
6	4.20	295.23	0.0001	A	H→L+1 (95%)	0.16
7	4.34	285.92	0.1143	A	H-5→L (89%)	0.71
8	4.45	278.32	0.0029	A	H-1→L+1 (97%)	0.15
9	4.67	265.59	0.0014	A	H-3→L+1 (89%)	0.38
10	4.70	263.55	0.0007	A	H-6→L (89%)	0.36
11	4.89	253.40	0.6673	A	H-4→L (18%), H-2→L+1 (75%)	0.68
12	5.02	247.19	0.0002	A	H-1→L+3 (46%), H→L+4 (44%)	0.65
13	5.12	242.08	0.0001	A	H-10→L (13%), H-9→L (72%)	0.40
14	5.18	239.43	0.0252	A	H-7→L (44%), H-5→L+1 (23%), H-4→L+1 (19%)	0.63
15	5.26	235.84	0.0063	A	H-7→L (19%), H-4→L+1 (71%)	0.71
16	5.33	232.48	0.0	A	H→L+2 (90%)	0.34
17	5.34	232.03	0.0056	A	H-8→L (73%), H-7→L (15%)	0.61
18	5.44	227.89	0.0078	A	H-7→L (12%), H-5→L+1 (33%), H-2→L+2 (27%)	0.70
19	5.52	224.54	0.0502	A	H-1→L+2 (10%), H-1→L+4 (16%), H→L+3 (42%), H→L+5 (17%)	0.64
20	5.54	223.74	0.0181	A	H→L+5 (68%)	0.30
21	5.58	222.36	0.0284	A	H-1→L+2 (78%)	0.41
22	5.60	221.51	0.0023	A	H-11→L (16%), H-10→L (60%), H-9→L (20%)	0.41
23	5.65	219.38	0.0001	A	H-1→L+5 (82%), H-1→L+6 (14%)	0.23
24	5.73	216.40	0.003	A	H-2→L+3 (85%)	0.26
25	5.74	215.98	0.0391	A	H-11→L (51%), H-10→L (14%)	0.47

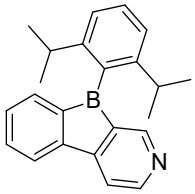

(DipPBBl)

Calculated absorption spectrum	Orbital	Energy/ eV
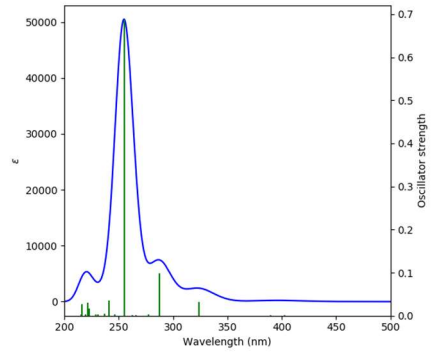 TD-DFT B3LYP/6-31+G(d), gas phase	L+4	–0.25
	L+3	–0.38
	L+2	–0.41
	L+1	–1.51
	LUMO	–2.66
	HOMO	–6.48
	H-1	–6.50
	H-2	–6.59
	H-3	–7.16
	H-4	–7.20

Orbitals relevant to the $S_1 \leftarrow S_0$ transition	Other relevant orbitals	
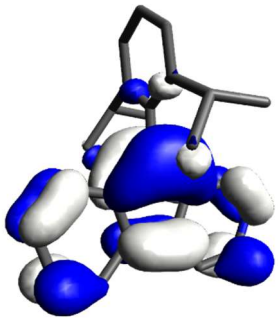 LUMO	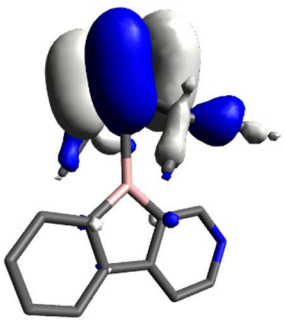 HOMO	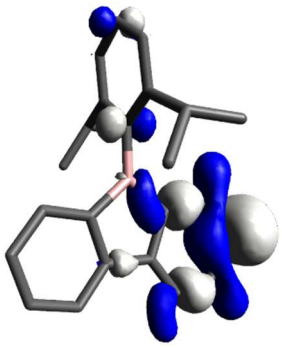 HOMO-3
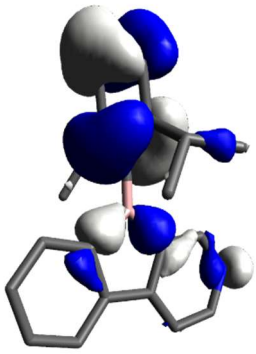 HOMO-1	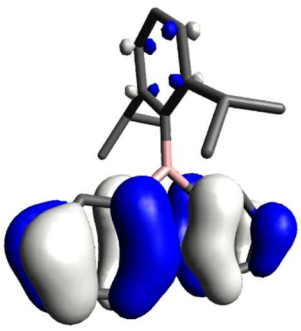 HOMO-2	

Table 7.5-17. Lowest energy singlet electronic transitions of **DipPBBI** (TD-DFT B3LYP/6-31+G(d), gas phase).

State	*E*/ eV	λ/ nm	*f*	Symmetry	Major contributions	Λ
1	3.01	412.55	0.0001	A	H-1→L (98%)	0.28
2	3.08	402.27	0.0016	A	H-2→L (78%), H→L (21%)	0.57
3	3.18	389.54	0.0015	A	H-2→L (21%), H→L (79%)	0.33
4	3.58	346.69	0.0003	A	H-3→L (97%)	0.33
5	3.83	323.57	0.0322	A	H-4→L (80%), H-2→L+1 (18%)	0.65
6	4.31	287.77	0.0003	A	H-3→L+1 (11%), H-1→L+1 (87%)	0.20
7	4.31	287.40	0.0989	A	H-5→L (89%)	0.72
8	4.47	277.54	0.0027	A	H→L+1 (97%)	0.20
9	4.67	265.67	0.0011	A	H-3→L+1 (82%), H-1→L+1 (12%)	0.36
10	4.72	262.70	0.0007	A	H-6→L (93%)	0.39
11	4.86	254.99	0.6867	A	H-4→L (18%), H-2→L+1 (74%)	0.68
12	5.03	246.44	0.0023	A	H-1→L+4 (37%), H→L+2 (55%)	0.64
13	5.14	241.12	0.0001	A	H-10→L (11%), H-9→L (83%)	0.45
14	5.15	240.92	0.0355	A	H-7→L (60%), H-5→L+1 (20%), H-4→L+1 (12%)	0.70
15	5.23	237.05	0.0044	A	H-7→L (13%), H-4→L+1 (77%)	0.75
16	5.37	231.00	0.0037	A	H-8→L (75%), H-2→L+3 (13%)	0.47
17	5.42	228.86	0.0033	A	H-8→L (15%), H-5→L+1 (40%), H-2→L+3 (19%)	0.68
18	5.46	226.96	0.0	A	H-1→L+3 (87%)	0.36
19	5.57	222.68	0.017	A	H-1→L+2 (35%), H→L+3 (44%), H→L+4 (12%)	0.61
20	5.59	221.67	0.0002	A	H-2→L+2 (94%)	0.26
21	5.60	221.41	0.0299	A	H-1→L+2 (21%), H→L+3 (50%), H→L+4 (24%)	0.60
22	5.65	219.31	0.0026	A	H-10→L (85%)	0.35
23	5.70	217.36	0.0	A	H→L+5 (75%), H→L+6 (21%)	0.22
24	5.73	216.32	0.0265	A	H-11→L (80%)	0.40
25	5.75	215.64	0.0021	A	H-1→L+5 (82%), H-1→L+6 (16%)	0.20

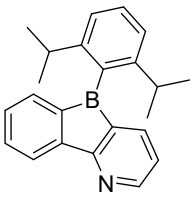

(DipPBB2)

<table>
<tr><th>Calculated absorption spectrum</th><th>Orbital</th><th>Energy/ eV</th></tr>
<tr><td rowspan="10"> 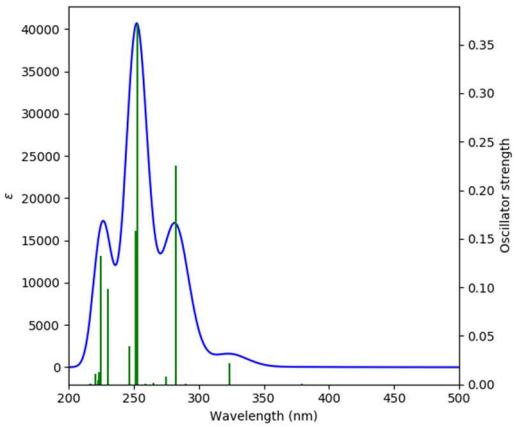

TD-DFT B3LYP/6-31+G(d), gas phase</td><td>L+4</td><td>–0.26</td></tr>
<tr><td>L+3</td><td>–0.41</td></tr>
<tr><td>L+2</td><td>–0.41</td></tr>
<tr><td>L+1</td><td>–1.48</td></tr>
<tr><td>LUMO</td><td>–2.57</td></tr>
<tr><td>HOMO</td><td>–6.33</td></tr>
<tr><td>H-1</td><td>–6.49</td></tr>
<tr><td>H-2</td><td>–6.50</td></tr>
<tr><td>H-3</td><td>–7.10</td></tr>
<tr><td>H-4</td><td>–7.18</td></tr>
<tr><td>Orbitals relevant to the $S_1 \leftarrow S_0$ transition</td><td colspan="2">Other relevant orbitals</td></tr>
<tr><td> 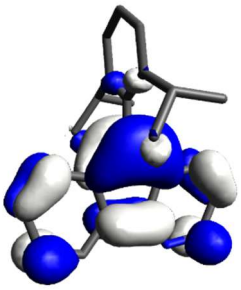
LUMO

 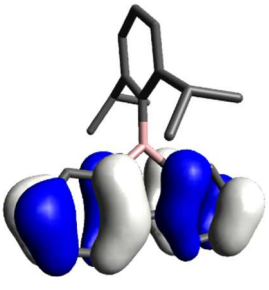
HOMO</td><td> 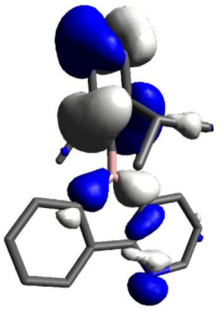
HOMO-1

 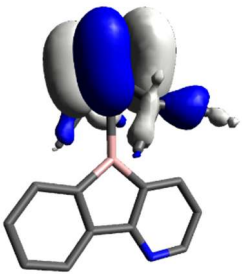
HOMO-2</td><td> 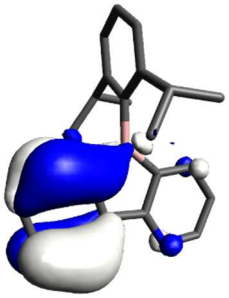
HOMO-3

 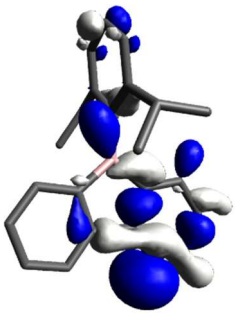
HOMO-4</td></tr>
</table>

Table 7.5-18. Lowest energy singlet electronic transitions of **DipPBB2** (TD-DFT B3LYP/6-31+G(d), gas phase).

State	*E*/ eV	λ/ nm	*f*	Symmetry	Major contributions	Λ
1	2.95	420.91	0.0001	A	H→L (99%)	0.65
2	3.07	404.46	0.0	A	H-1→L (97%)	0.28
3	3.27	379.02	0.0004	A	H-2→L (99%)	0.19
4	3.61	343.27	0.0	A	H-4→L (97%)	0.33
5	3.83	323.63	0.0217	A	H-3→L (74%), H→L+1 (22%)	0.61
6	4.27	290.04	0.0009	A	H-4→L+1 (20%), H-1→L+1 (78%)	0.25
7	4.40	281.99	0.225	A	H-5→L (21%), H-3→L (17%), H→L+1 (48%)	0.68
8	4.52	274.51	0.0084	A	H-2→L+1 (97%)	0.15
9	4.67	265.41	0.0014	A	H-4→L+1 (77%), H-1→L+1 (21%)	0.39
10	4.80	258.57	0.0009	A	H-7→L (92%)	0.41
11	4.90	253.01	0.3712	A	H-5→L (64%), H→L+1 (17%)	0.69
12	4.93	251.38	0.158	A	H-6→L (45%), H-3→L+1 (32%)	0.63
13	5.03	246.51	0.0389	A	H-6→L (32%), H-3→L+1 (45%), H→L+3 (14%)	0.63
14	5.03	246.39	0.002	A	H-2→L+2 (53%), H-1→L+4 (41%)	0.64
15	5.32	233.08	0.0001	A	H-9→L (78%)	0.44
16	5.35	231.96	0.0	A	H→L+2 (94%)	0.21
17	5.40	229.72	0.0981	A	H-8→L (55%), H→L+3 (26%)	0.49
18	5.41	229.22	0.0	A	H-1→L+3 (83%)	0.29
19	5.52	224.71	0.1327	A	H-8→L (15%), H-2→L+4 (14%), H-1→L+2 (39%), H→L+3 (14%)	0.69
20	5.55	223.34	0.0125	A	H-2→L+3 (16%), H→L+4 (68%)	0.28
21	5.56	222.82	0.0046	A	H-2→L+3 (77%), H→L+4 (20%)	0.23
22	5.63	220.35	0.0111	A	H-8→L (21%), H-2→L+4 (21%), H-1→L+2 (22%), H→L+3 (10%)	0.62
23	5.64	219.88	0.0001	A	H→L+5 (87%)	0.20
24	5.71	217.22	0.0007	A	H-2→L+5 (85%)	0.24
25	5.73	216.30	0.0004	A	H-1→L+5 (92%)	0.24

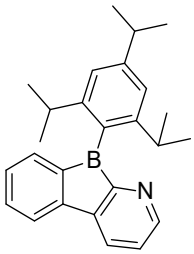

(TipPBB3)

<table>
<tr><th>Calculated absorption spectrum</th><th>Orbital</th><th>Energy/ eV</th></tr>
<tr><td rowspan="11"> 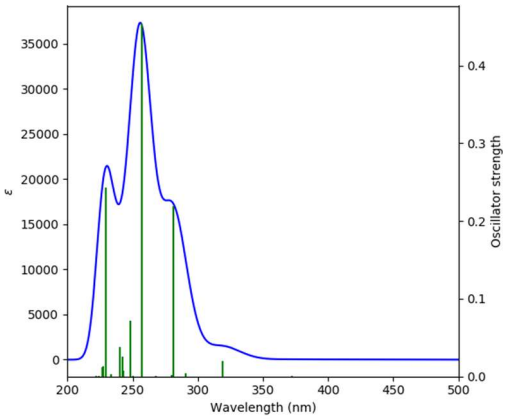

TD-DFT B3LYP/6-31+G(d), gas phase</td><td>L+4</td><td>–0.10</td></tr>
<tr><td>L+3</td><td>–0.18</td></tr>
<tr><td>L+2</td><td>–0.41</td></tr>
<tr><td>L+1</td><td>–1.50</td></tr>
<tr><td>LUMO</td><td>–2.58</td></tr>
<tr><td>HOMO</td><td>–6.10</td></tr>
<tr><td>H-1</td><td>–6.25</td></tr>
<tr><td>H-2</td><td>–6.32</td></tr>
<tr><td>H-3</td><td>–6.95</td></tr>
<tr><td>H-4</td><td>–7.18</td></tr>
<tr><td colspan="3">Orbitals relevant to the $S_1 \leftarrow S_0$ transition</td></tr>
<tr><td colspan="3"> 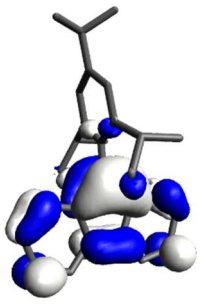
LUMO
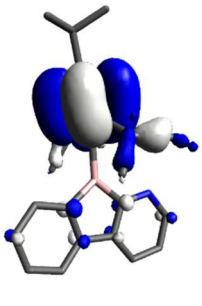
HOMO-1
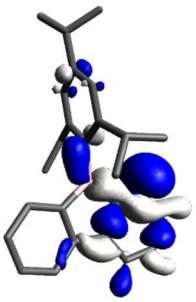
HOMO-3
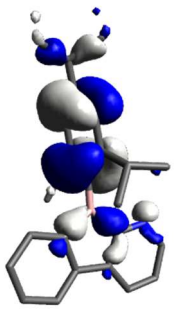
HOMO
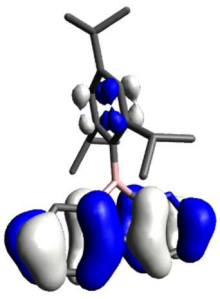
HOMO-2</td></tr>
</table>

Table 7.5-19. Lowest energy singlet electronic transitions of **TipPBB3** (TD-DFT B3LYP/6-31+G(d), gas phase).

State	*E*/ eV	λ/ nm	*f*	Major contributions	Λ
1	2.68	461.78	0.0001	H→L (97%)	0.27
2	2.91	426.40	0.0001	H-2→L (79%), H-1→L (20%)	0.57
3	3.01	411.28	0.0002	H-2→L (21%), H-1→L (79%)	0.36
4	3.33	372.10	0.0005	H-3→L (97%)	0.41
5	3.88	319.29	0.02	H-4→L (72%), H-2→L+1	0.60
6	3.97	312.46	0.0002	H→L+1 (91%)	0.18
7	4.26	290.85	0.0046	H-1→L+1 (94%)	0.25
8	4.41	281.23	0.2193	H-5→L (28%), H-4→L (17%), H-2→L+1 (43%)	0.68
9	4.42	280.29	0.0024	H-3→L+1 (88%)	0.39
10	4.63	267.99	0.0005	H-6→L (89%)	0.35
11	4.83	256.88	0.4541	H-5→L (61%), H-2→L+1 (24%)	0.68
12	4.96	250.21	0.0004	H-1→L+3 (43%), H→L+5 (43%)	0.62
13	4.99	248.24	0.0717	H-7→L (13%), H-4→L+1 (49%), H-2→L+2 (12%)	0.59
14	5.04	245.84	0.0	H→L+2 (84%)	0.25
15	5.10	242.92	0.0072	H-9→L (43%), H-7→L (25%)	0.43
16	5.11	242.48	0.0251	H-9→L (24%), H-7→L (47%)	0.55
17	5.17	240.02	0.0376	H-8→L (71%), H-4→L+1 (17%)	0.47
18	5.31	233.38	0.0029	H-1→L+2 (94%)	0.30
19	5.40	229.43	0.2431	H-4→L+1 (13%), H-2→L+2 (23%), H→L+3 (38%)	0.74
20	5.45	227.70	0.0028	H-11→L (59%), H-9→L (17%)	0.39
21	5.45	227.65	0.0136	H-11→L (11%), H→L+4 (43%), H→L+6 (15%)	0.35
22	5.46	227.01	0.0122	H-10→L (19%), H-1→L+5 (11%), H→L+3 (24%), H→L+4 (21%)	0.53
23	5.54	224.00	0.0005	H-2→L+3 (23%), H-2→L+4 (53%), H-1→L+4 (14%)	0.28
24	5.58	222.39	0.0002	H-2→L+3 (67%), H-2→L+4 (13%), H-1→L+4 (11%)	0.30
25	5.59	221.89	0.0003	H-2→L+4 (21%), H-1→L+4 (39%), H-1→L+6 (31%)	0.25

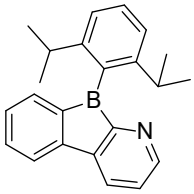

(DipPBB3)

<table>
<tr><th>Calculated absorption spectrum</th><th>Orbital</th><th>Energy/ eV</th></tr>
<tr><td rowspan="11"> 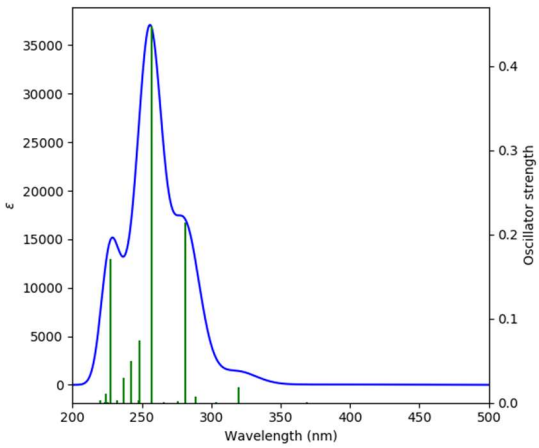

TD-DFT B3LYP/6-31+G(d), gas phase</td><td>L+4</td><td>–0.12</td></tr>
<tr><td>L+3</td><td>–0.26</td></tr>
<tr><td>L+2</td><td>–0.44</td></tr>
<tr><td>L+1</td><td>–1.52</td></tr>
<tr><td>LUMO</td><td>–2.62</td></tr>
<tr><td>HOMO</td><td>–6.30</td></tr>
<tr><td>H-1</td><td>–6.30</td></tr>
<tr><td>H-2</td><td>–6.35</td></tr>
<tr><td>H-3</td><td>–7.00</td></tr>
<tr><td>H-4</td><td>–7.21</td></tr>
<tr><td>Orbitals relevant to the $S_1 \leftarrow S_0$ transition</td><td colspan="2">Other relevant orbitals</td></tr>
<tr><td> 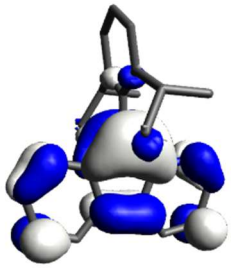
LUMO

 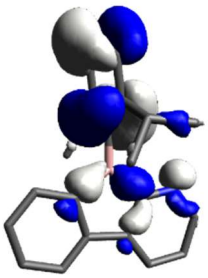
HOMO</td><td> 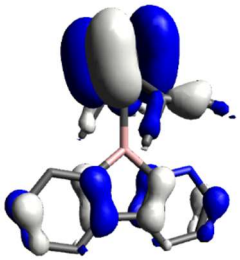
HOMO-1

 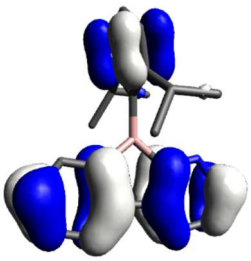
HOMO-2</td><td> 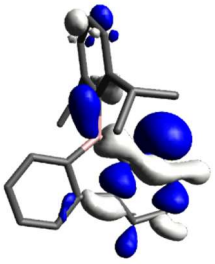
HOMO-3</td></tr>
</table>

Table 7.5-20. Lowest energy singlet electronic transitions of **DipPBB3** (TD-DFT B3LYP/6-31+G(d), gas phase).

State	*E*/ eV	λ/ nm	*f*	Symmetry	Major contributions	Λ
1	2.82	440.24	0.0002	A	H→L (97%)	0.30
2	2.90	427.28	0.0001	A	H-2→L (66%), H-1→L (33%)	0.54
3	3.04	408.27	0.0002	A	H-2→L (33%), H-1→L (67%)	0.46
4	3.36	369.00	0.0004	A	H-3→L (96%)	0.40
5	3.88	319.58	0.0185	A	H-4→L (72%), H-2→L+1 (18%)	0.59
6	4.08	303.70	0.0005	A	H-3→L+1 (16%), H→L+1 (83%)	0.22
7	4.29	288.79	0.0075	A	H-2→L+1 (11%), H-1→L+1 (86%)	0.39
8	4.41	281.19	0.2145	A	H-5→L (28%), H-4→L (17%), H-2→L+1 (43%)	0.66
9	4.49	276.15	0.0015	A	H-3→L+1 (81%), H→L+1 (16%)	0.36
10	4.66	265.79	0.0005	A	H-6→L (93%)	0.39
11	4.83	256.94	0.4481	A	H-5→L (61%), H-2→L+1 (21%)	0.66
12	5.00	248.20	0.0743	A	H-7→L (21%), H-4→L+1 (48%), H-2→L+2 (10%)	0.59
13	5.01	247.48	0.0025	A	H-1→L+3 (47%), H→L+5 (40%)	0.61
14	5.11	242.40	0.0498	A	H-7→L (61%), H-4→L+1 (15%), H-2→L+2 (10%)	0.62
15	5.17	239.61	0.0	A	H→L+2 (75%)	0.27
16	5.23	237.17	0.0297	A	H-8→L (79%), H-4→L+1 (13%)	0.41
17	5.24	236.66	0.0002	A	H-12→L (10%), H-11→L (16%), H-9→L (49%), H→L+2 (18%)	0.34
18	5.34	232.06	0.003	A	H-2→L+2 (16%), H-1→L+2 (83%)	0.44
19	5.45	227.64	0.1712	A	H-4→L+1 (15%), H-2→L+2 (30%), H→L+3 (16%)	0.63
20	5.50	225.47	0.0003	A	H-2→L+3 (77%), H-1→L+3 (18%)	0.43
21	5.53	224.17	0.0108	A	H-10→L (22%), H-1→L+5 (19%), H→L+3 (47%)	0.69
22	5.53	224.09	0.0044	A	H-11→L (61%), H-9→L (32%)	0.39
23	5.55	223.42	0.0003	A	H-2→L+4 (64%), H-1→L+4 (28%)	0.26
24	5.64	219.99	0.0	A	H-2→L+4 (19%), H-1→L+4 (39%), H-1→L+6 (29%)	0.24
25	5.64	219.78	0.0031	A	H→L+4 (75%), H→L+6 (20%)	0.19

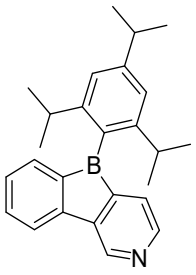

(TipPBB4)

<table>
<tr><th>Calculated absorption spectrum</th><th>Orbital</th><th>Energy/ eV</th></tr>
<tr><td rowspan="10"> 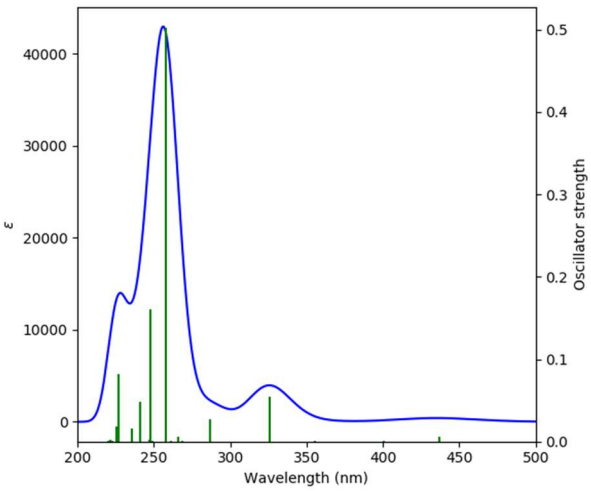

TD-DFT B3LYP/6-31+G(d), gas phase</td><td>L+4</td><td>–0.26</td></tr>
<tr><td>L+3</td><td>–0.38</td></tr>
<tr><td>L+2</td><td>–0.49</td></tr>
<tr><td>L+1</td><td>–1.32</td></tr>
<tr><td>LUMO</td><td>–2.73</td></tr>
<tr><td>HOMO</td><td>–6.35</td></tr>
<tr><td>H-1</td><td>–6.37</td></tr>
<tr><td>H-2</td><td>–6.48</td></tr>
<tr><td>H-3</td><td>–7.13</td></tr>
<tr><td>H-4</td><td>–7.19</td></tr>
<tr><td colspan="2">Orbitals relevant to the $S_1 \leftarrow S_0$ transition</td><td colspan="2">Other relevant orbitals</td></tr>
<tr><td colspan="2"> 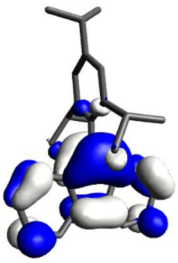
LUMO
 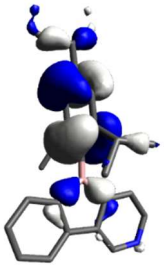
HOMO</td><td> 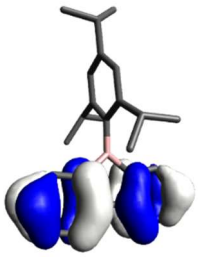
HOMO-1
 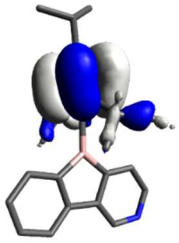
HOMO-2</td><td> 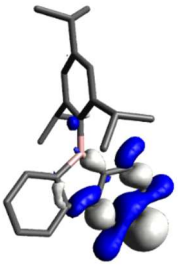
HOMO-3</td></tr>
</table>

Table 7.5-21. Lowest energy singlet electronic transitions of **TipPBB4** (TD-DFT B3LYP/6-31+G(d), gas phase).

State	*E*/ eV	λ/ nm	*f*	Major contributions	Λ
1	2.82	439.93	0.0001	H→L (98%)	0.26
2	2.84	436.78	0.0054	H-1→L (99%)	0.64
3	3.10	400.36	0.0008	H-2→L (99%)	0.17
4	3.49	355.69	0.0011	H-3→L (98%)	0.39
5	3.81	325.61	0.0545	H-4→L (84%), H-1→L+1 (13%)	0.63
6	4.33	286.42	0.0266	H-5→L (86%)	0.70
7	4.42	280.22	0.0	H→L+1 (92%)	0.15
8	4.62	268.52	0.0006	H-6→L (90%)	0.36
9	4.66	265.89	0.0055	H-2→L+1 (96%)	0.14
10	4.75	261.24	0.0004	H-3→L+1 (87%)	0.32
11	4.81	257.96	0.5025	H-7→L (13%), H-4→L (11%), H-1→L+1 (62%)	0.72
12	4.98	249.18	0.0004	H-2→L+3 (47%), H→L+4 (44%)	0.65
13	5.01	247.39	0.1602	H-7→L (68%), H-1→L+2 (16%)	0.73
14	5.02	246.82	0.002	H-10→L (11%), H-9→L (70%)	0.39
15	5.15	240.91	0.0477	H-8→L (20%), H-4→L+1 (25%), H-1→L+2 (36%)	0.64
16	5.25	236.25	0.0	H→L+2 (92%)	0.30
17	5.26	235.76	0.0156	H-8→L (67%), H-4→L+1 (21%)	0.42
18	5.44	227.92	0.0001	H-1→L+3 (96%)	0.18
19	5.46	227.01	0.0823	H-4→L+1 (11%), H-2→L+2 (47%), H→L+3 (26%)	0.51
20	5.47	226.70	0.0695	H-4→L+1 (25%), H-2→L+2 (32%), H-1→L+2 (15%)	0.50
21	5.49	225.88	0.0034	H-11→L (14%), H-10→L (63%), H-9→L (18%)	0.41
22	5.51	225.17	0.0181	H-2→L+2 (18%), H-2→L+4 (20%), H→L+3 (36%)	0.66
23	5.56	223.08	0.0004	H→L+5 (93%)	0.23
24	5.60	221.21	0.0027	H-1→L+4 (95%)	0.22
25	5.63	220.40	0.0015	H-1→L+5 (72%), H-1→L+6 (24%)	0.19

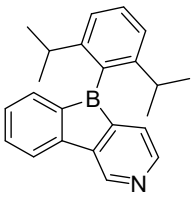

(DipPBB4)

<table>
<tr><th>Calculated absorption spectrum</th><th>Orbital</th><th>Energy/ eV</th></tr>
<tr><td rowspan="10"> 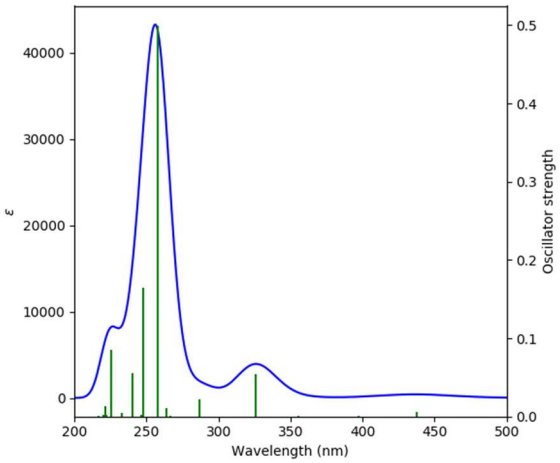

TD-DFT B3LYP/6-31+G(d), gas phase</td><td>L+4</td><td>–0.31</td></tr>
<tr><td>L+3</td><td>–0.47</td></tr>
<tr><td>L+2</td><td>–0.52</td></tr>
<tr><td>L+1</td><td>–1.35</td></tr>
<tr><td>LUMO</td><td>–2.76</td></tr>
<tr><td>HOMO</td><td>–6.40</td></tr>
<tr><td>H-1</td><td>–6.54</td></tr>
<tr><td>H-2</td><td>–6.57</td></tr>
<tr><td>H-3</td><td>–7.16</td></tr>
<tr><td>H-4</td><td>–7.22</td></tr>
<tr><td>Orbitals relevant to the $S_1 \leftarrow S_0$ transition</td><td colspan="2">Other relevant orbitals</td></tr>
<tr><td> 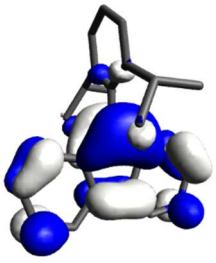
LUMO</td><td> 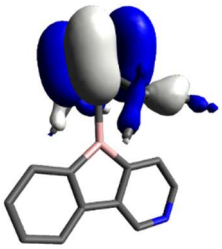
HOMO-1</td><td> 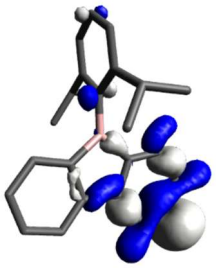
HOMO-3</td></tr>
<tr><td> 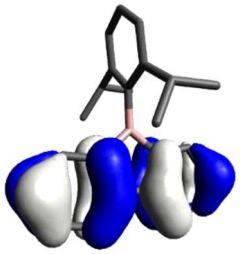
HOMO</td><td> 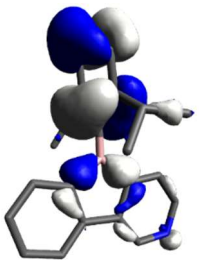
HOMO-2</td><td></td></tr>
</table>

Table 7.5-22. Lowest energy singlet electronic transitions of **DipPBB4** (TD-DFT B3LYP/6-31+G(d), gas phase).

State	*E*/ eV	λ/ nm	*f*	Symmetry	Major contributions	Λ
1	2.83	437.89	0.0055	A	H→L (99%)	0.64
2	2.97	416.85	0.0001	A	H-2→L (98%)	0.28
3	3.12	397.02	0.0007	A	H-1→L (100%)	0.16
4	3.49	355.36	0.001	A	H-3→L (98%)	0.38
5	3.80	326.00	0.0541	A	H-4→L (84%), H→L+1 (13%)	0.63
6	4.33	286.60	0.0216	A	H-5→L (86%)	0.70
7	4.56	272.15	0.0001	A	H-3→L+1 (22%), H-2→L+1 (75%)	0.19
8	4.65	266.39	0.0007	A	H-7→L (94%)	0.40
9	4.70	263.94	0.0102	A	H-1→L+1 (96%)	0.13
10	4.80	258.52	0.0002	A	H-3→L+1 (72%), H-2→L+1 (24%)	0.28
11	4.81	257.91	0.4997	A	H-6→L (13%), H-4→L (11%), H→L+1 (61%)	0.72
12	5.01	247.48	0.1644	A	H-6→L (68%), H→L+1 (10%), H→L+2 (18%)	0.74
13	5.03	246.41	0.0024	A	H-2→L+4 (39%), H-1→L+3 (56%)	0.65
14	5.11	242.82	0.0002	A	H-10→L (10%), H-9→L (81%)	0.45
15	5.16	240.33	0.0552	A	H-4→L+1 (32%), H→L+2 (36%)	0.69
16	5.33	232.59	0.0042	A	H-8→L (73%), H-4→L+1 (21%)	0.45
17	5.37	231.05	0.0	A	H→L+3 (96%)	0.15
18	5.41	229.29	0.0	A	H-2→L+2 (88%)	0.31
19	5.49	225.74	0.0849	A	H-8→L (11%), H-5→L+1 (13%), H-4→L+1 (34%), H→L+2 (19%)	0.66
20	5.50	225.30	0.001	A	H-1→L+2 (96%)	0.24
21	5.58	222.32	0.0024	A	H-2→L+3 (14%), H→L+4 (73%)	0.36
22	5.60	221.55	0.0139	A	H-2→L+3 (36%), H-1→L+4 (28%), H→L+4 (24%)	0.65
23	5.60	221.52	0.0039	A	H-10→L(85%)	0.35
24	5.64	219.82	0.0017	A	H→L+5 (81%), H→L+6 (15%)	0.20
25	5.72	216.82	0.0008	A	H-1→L+5 (82%)	0.23

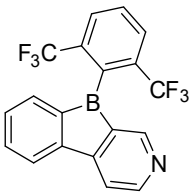

(**^{F}XylPBBl**)

<table>
<tr><th>Calculated absorption spectrum</th><th>Orbital</th><th>Energy/ eV</th></tr>
<tr><td rowspan="10"> 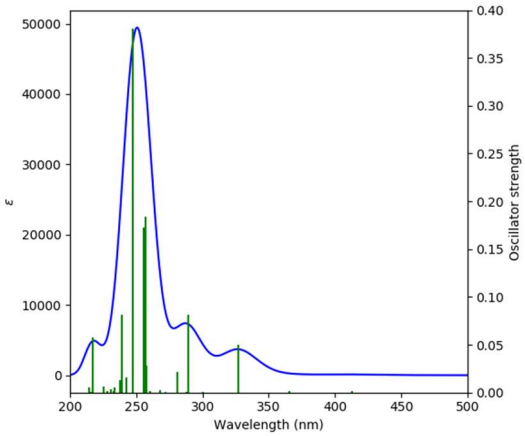

TD-DFT B3LYP/6-31+G(d), gas phase</td><td>L+4</td><td>–0.38</td></tr>
<tr><td>L+3</td><td>–1.50</td></tr>
<tr><td>L+2</td><td>–1.72</td></tr>
<tr><td>L+1</td><td>–1.98</td></tr>
<tr><td>LUMO</td><td>–2.79</td></tr>
<tr><td>HOMO</td><td>–6.63</td></tr>
<tr><td>H-1</td><td>–7.11</td></tr>
<tr><td>H-2</td><td>–7.26</td></tr>
<tr><td>H-3</td><td>–7.71</td></tr>
<tr><td>H-4</td><td>–7.96</td></tr>
<tr><td>Orbitals relevant to the $S_1 \leftarrow S_0$ transition</td><td colspan="2">Other relevant orbitals</td></tr>
<tr><td> 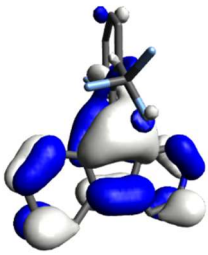
LUMO
 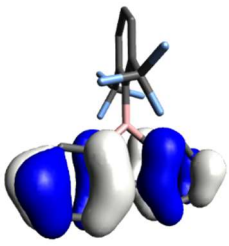
HOMO</td><td> 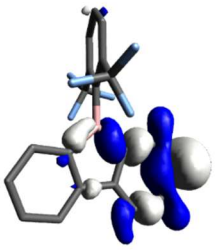
HOMO-1
 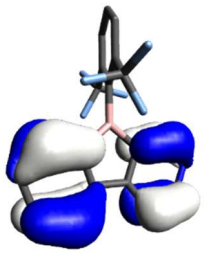
HOMO-2</td><td> 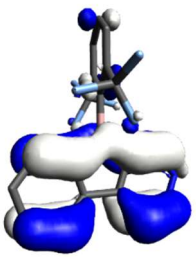
HOMO-3</td></tr>
</table>

Table 7.5-23. Lowest energy singlet electronic transitions of **^{F}XylPBBI** (TD-DFT B3LYP/6-31+G(d), gas phase).

State	*E*/ eV	λ/ nm	*f*	Symmetry	Major contributions	Λ
1	3.00	413.14	0.0015	A	H→L (99%)	0.64
2	3.39	365.43	0.0014	A	H-1→L (98%)	0.35
3	3.79	326.97	0.0502	A	H-2→L (82%), H→L+3 (17%)	0.65
4	4.13	300.03	0.0007	A	H→L+1 (100%)	0.06
5	4.29	289.26	0.0814	A	H-4→L (37%), H-3→L (58%)	0.65
6	4.31	287.55	0.0008	A	H→L+2 (98%)	0.24
7	4.41	281.07	0.0218	A	H-4→L (58%), H-3→L (33%)	0.59
8	4.56	271.81	0.001	A	H-1→L+3 (91%)	0.38
9	4.62	268.08	0.0028	A	H-1→L+1 (91%)	0.14
10	4.76	260.48	0.0019	A	H-2→L+1 (99%)	0.08
11	4.81	257.91	0.0285	A	H-5→L (76%)	0.25
12	4.82	256.99	0.1837	A	H-2→L+2 (12%), H-1→L+2 (47%), H→L+3 (23%)	0.38
13	4.86	255.28	0.1727	A	H-2→L+2 (26%), H-1→L+2 (45%), H→L+3 (20%)	0.36
14	5.02	247.01	0.3809	A	H-2→L+2 (58%), H→L+3 (29%)	0.40
15	5.12	242.27	0.0158	A	H-5→L (10%), H-5→L+2 (20%), H-4→L+1 (25%), H-3→L+1 (42%)	0.41
16	5.19	238.73	0.0814	A	H-6→L (79%)	0.73
17	5.22	237.56	0.0127	A	H-4→L+1 (36%), H-3→L+1 (52%)	0.41
18	5.30	233.79	0.0051	A	H-2→L+3 (88%)	0.77
19	5.33	232.54	0.0021	A	H-3→L+2 (73%)	0.47
20	5.37	230.82	0.004	A	H-8→L (11%), H-7→L (76%)	0.52
21	5.44	227.86	0.0017	A	H-8→L (83%)	0.54
22	5.50	225.48	0.0067	A	H-3→L+2 (14%), H-3→L+3 (43%), H→L+4 (24%)	0.69
23	5.70	217.33	0.0576	A	H-5→L+1 (27%), H-4→L+2 (63%)	0.81
24	5.74	215.85	0.0006	A	H-4→L+3 (49%), H-1→L+4 (37%)	0.35
25	5.79	214.04	0.0055	A	H-4→L+3 (37%), H-1→L+4 (49%)	0.35

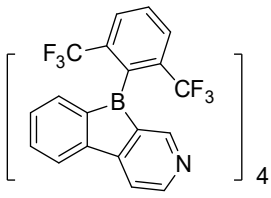

([^{F}XylPBBI]$_4$)

Calculated absorption spectrum	Orbital	Energy/ eV
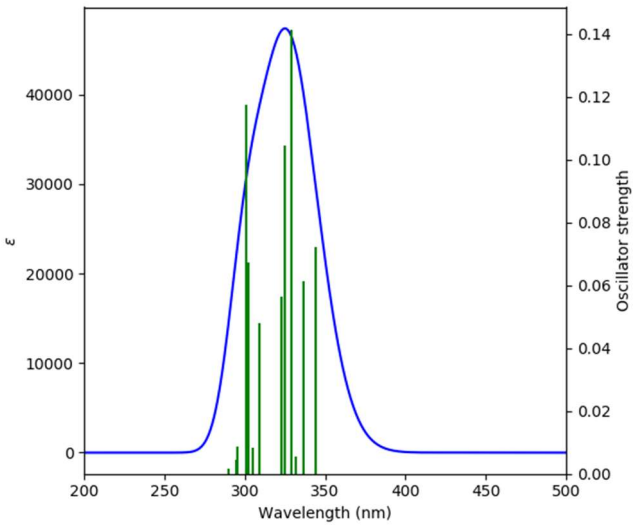	L+4	–1.62
	L+3	–2.10
	L+2	–2.28
	L+1	–2.37
	LUMO	–2.37
	HOMO	–6.49
	H-1	–6.63
	H-2	–6.63
	H-3	–6.70
	H-4	–7.02
TD-DFT B3LYP/6-31+G(d), gas phase		

Orbitals relevant to the $S_1 \leftarrow S_0$ transition	Other relevant orbitals
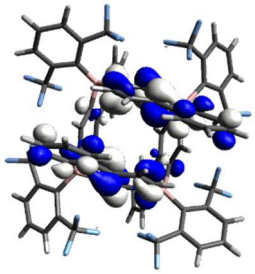	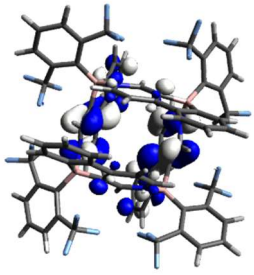
LUMO	LUMO+1
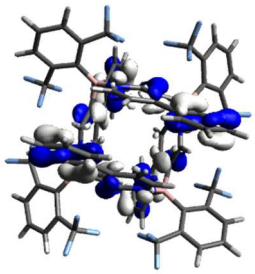	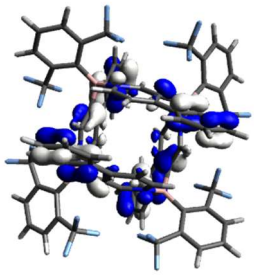
HOMO	HOMO-1

Table 7.5-24. Lowest energy singlet electronic transitions of [^{F}**XylPBBI**]$_4$ (TD-DFT B3LYP/6-31+G(d), gas phase).

State	*E*/ eV	λ/ nm	*f*	Major contributions	Λ
1	3.60	344.06	0.0721	H→L (96%)	0.69
2	3.60	344.06	0.0721	H→L+1 (96%)	0.69
3	3.68	336.53	0.0612	H-2→L+1 (10%), H-1→L (10%), H→L+2 (60%)	0.72
4	3.72	333.57	0.0	H-2→L+1 (37%), H-1→L (37%)	0.63
5	3.73	332.05	0.0056	H-2→L+1 (38%), H-1→L (38%), H→L+2 (23%)	0.65
6	3.74	331.15	0.0	H-2→L (38%), H-2→L+1 (10%), H-1→L+1 (38%)	0.67
7	3.77	329.12	0.1414	H-2→L (40%), H-1→L+1 (40%), H→L+2 (15%)	0.70
8	3.81	325.14	0.1045	H-3→L (57%), H-2→L+2 (14%), H-1→L+2 (22%)	0.66
9	3.81	325.13	0.1046	H-3→L+1 (57%), H-2→L+2 (22%), H-1→L+2 (14%)	0.66
10	3.84	322.86	0.0563	H-3→L+1 (27%), H-1→L+2 (56%)	0.68
11	3.84	322.86	0.0564	H-3→L (27%), H-2→L+2 (56%)	0.68
12	3.88	319.48	0.0	H→L+3 (81%)	0.73
13	3.91	317.18	0.0	H-3→L+2 (84%)	0.70
14	4.01	309.06	0.0479	H-2→L+3 (65%), H-1→L+3 (10%)	0.66
15	4.01	309.06	0.0479	H-2→L+3 (10%), H-1→L+3 (65%)	0.66
16	4.07	305.00	0.0084	H-6→L (13%), H-5→L+1 (13%), H-4→L+2 (10%), H-3→L+3 (54%)	0.61
17	4.10	302.16	0.0672	H-4→L (46%)	0.51
18	4.10	302.16	0.0672	H-4→L+1 (46%)	0.51
19	4.12	300.79	0.1174	H-6→L (10%), H-5→L+1 (10%), H-4→L+2 (12%), H-3→L+3 (41%)	0.56
20	4.15	298.76	0.0	H-7→L+2 (10%), H-6→L (28%), H-5→L+1 (28%)	0.50
21	4.20	295.38	0.0085	H-7→L (57%), H-4→L (10%), H-4→L+1 (14%)	0.46
22	4.20	295.38	0.0085	H-7→L+1 (57%), H-4→L (14%), H-4→L+1 (10%)	0.46
23	4.20	294.91	0.0046	H-6→L (15%), H-6→L+1 (25%), H-5→L (25%), H-5→L+1 (15%), H-4→L+2 (14%)	0.39
24	4.21	294.74	0.0	H-6→L (10%), H-6→L+1 (32%), H-5→L (32%), H-5→L+1 (10%)	0.36
25	4.28	289.60	0.0018	H-6→L+1 (15%), H-5→L (15%), H-4→L+2 (42%)	0.44

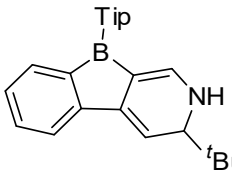

(10)

<table>
<tr><th>Calculated absorption spectra</th><th>Orbital</th><th>Energy/ eV</th></tr>
<tr><td rowspan="11"> 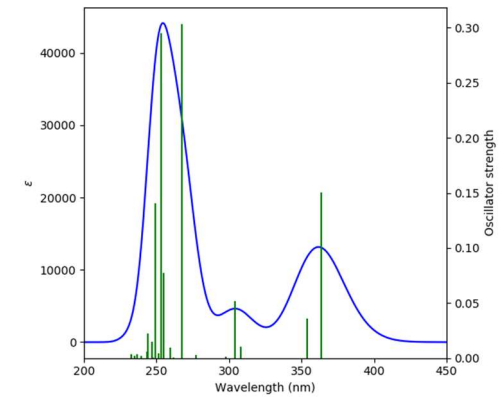

TD-DFT B3LYP/6-31+G(d, p), gas phase</td><td>L+4</td><td>0.07</td></tr>
<tr><td>L+3</td><td>0.01</td></tr>
<tr><td>L+2</td><td>–0.46</td></tr>
<tr><td>L+1</td><td>–1.18</td></tr>
<tr><td>LUMO</td><td>–1.47</td></tr>
<tr><td>HOMO</td><td>–5.33</td></tr>
<tr><td>H-1</td><td>–5.98</td></tr>
<tr><td>H-2</td><td>–6.15</td></tr>
<tr><td>H-3</td><td>–6.22</td></tr>
<tr><td>H-4</td><td>–6.83</td></tr>
<tr><td>Orbitals relevant to the $S_1 \leftarrow S_0$ transition</td><td colspan="2">other relevant orbitals</td></tr>
<tr><td> 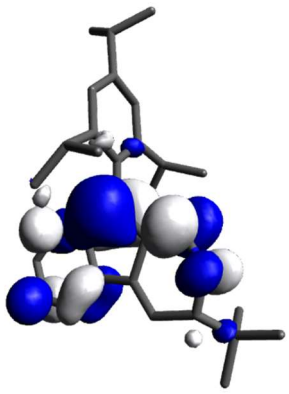
LUMO
 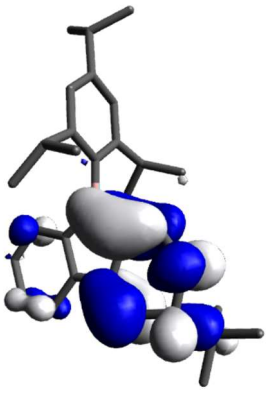
HOMO</td><td> 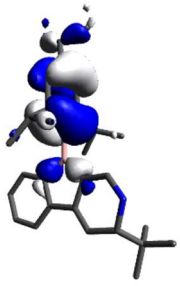
HOMO-1
 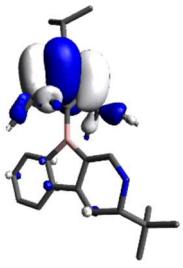
HOMO-2
 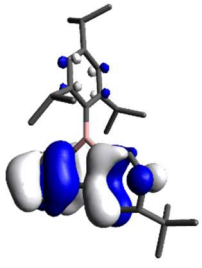
HOMO-3</td><td> 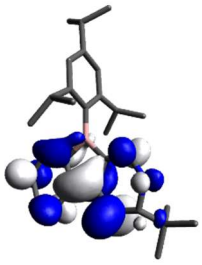
LUMO+1
 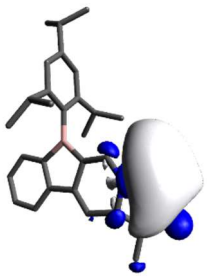
LUMO+2
 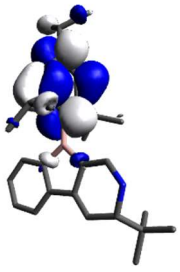
LUMO+3</td></tr>
</table>

Table 7.5-25.Lowest energy singlet electronic transitions of compound **10** (TD-DFT B3LYP/6-31+G(d), gas phase).

State	*E*/ eV	λ/ nm	*f*	Symmetry	Major contributions	Λ
1	3.41	363.49	0.1505	A	H→L (91%)	0.66
2	3.50	353.91	0.0358	A	H→L+1 (95%)	0.67
3	3.72	333.31	0.0001	A	H-1→L (98%)	0.22
4	4.02	308.30	0.0103	A	H-2→L (94%)	0.24
5	4.08	304.11	0.052	A	H-3→L (86%)	0.58
6	4.16	298.06	0.0016	A	H→L+2 (98%)	0.27
7	4.21	294.48	0.0001	A	H-1→L+1 (99%)	0.15
8	4.48	277.04	0.0029	A	H-2→L+1 (97%)	0.25
9	4.63	267.73	0.3035	A	H-4→L (35%), H-3→L+1 (50%)	0.72
10	4.73	261.98	0.0003	A	H→L+3 (97%)	0.18
11	4.78	259.45	0.0097	A	H→L+5 (89%)	0.26
12	4.86	255.13	0.0773	A	H-4→L (14%), H→L+6 (60%)	0.33
13	4.90	252.88	0.2951	A	H-4→L (25%), H-3→L+1 (19%), H→L+6 (31%)	0.49
14	4.93	251.29	0.004	A	H→L+4 (82%)	0.17
15	4.98	249.19	0.1408	A	H-4→L+1 (45%), H→L+8 (22%)	0.58
16	5.01	247.52	0.0005	A	H-2→L+3 (41%), H-1→L+6 (43%)	0.64
17	5.02	246.77	0.0147	A	H→L+7 (63%), H→L+8 (17%)	0.40
18	5.08	244.05	0.0225	A	H-1→L+2 (91%)	0.09
19	5.09	243.49	0.0056	A	H-4→L (12%), H-4→L+1 (32%), H→L+8 (40%)	0.54
20	5.18	239.52	0.0023	A	H→L+9 (67%), H→L+12 (18%)	0.21
21	5.24	236.49	0.0032	A	H-3→L+2 (53%), H-2→L+2 (42%)	0.15
22	5.27	235.08	0.0022	A	H-3→L+2 (41%), H-2→L+2 (53%)	0.14
23	5.33	232.80	0.0019	A	H→L+9 (16%), H→L+12 (42%), H→L+13 (15%)	0.23
24	5.33	232.50	0.0039	A	H-5→L (80%)	0.35
25	5.34	232.39	0.0034	A	H→L+10 (63%), H→L+12 (13%)	0.25

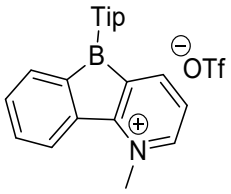

(**11**)

<table>
<tr><th>Calculated absorption spectra</th><th>Orbital</th><th>Energy/ eV</th></tr>
<tr><td rowspan="10"> 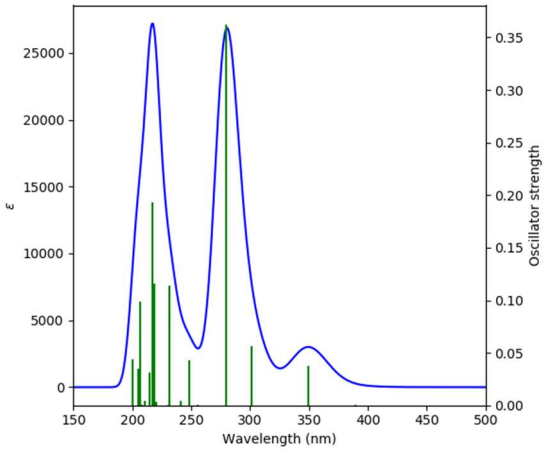

TD-DFT B3LYP/6-31++G(d, p), gas phase</td><td>L+4</td><td>–2.10</td></tr>
<tr><td>L+3</td><td>–2.53</td></tr>
<tr><td>L+2</td><td>–2.86</td></tr>
<tr><td>L+1</td><td>–4.69</td></tr>
<tr><td>LUMO</td><td>–4.97</td></tr>
<tr><td>HOMO</td><td>-10.18</td></tr>
<tr><td>H-1</td><td>–10.23</td></tr>
<tr><td>H-2</td><td>–11.45</td></tr>
<tr><td>H-3</td><td>–11.91</td></tr>
<tr><td>H-4</td><td>–12.24</td></tr>
<tr><td>Orbitals relevant to the $S_1 \leftarrow S_0$ transition</td><td colspan="2">other relevant orbitals</td></tr>
<tr><td> 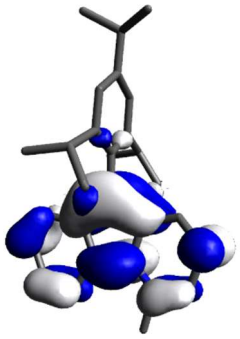
LUMO
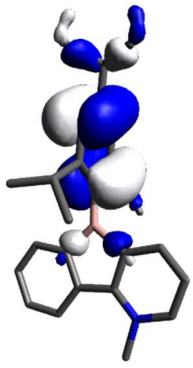
HOMO</td><td> 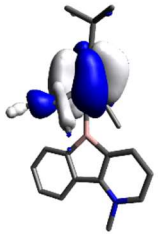
HOMO-1
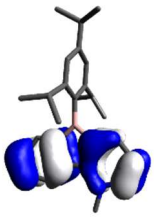
HOMO-2

HOMO-3</td><td> 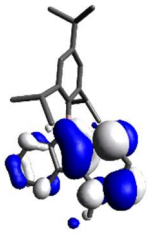
LUMO+1
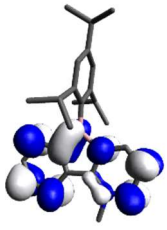
LUMO+2
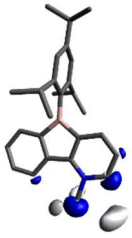
LUMO+3</td></tr>
</table>

Table 7.5-26: Lowest energy singlet electronic transitions of compound **11** (TD-DFT B3LYP/6-31+G(d), gas phase).

State	*E*/ eV	λ/ nm	*f*	Symmetry	Major contributions	Λ
1	2.78	445.31	0	A	H→L (73%), H→L+1 (14%)	0.17
2	3.19	389.20	0.0009	A	H-1→L (78%), H-1→L+1 (13%)	0.13
3	3.55	349.52	0.0376	A	H-2→L (84%)	0.67
4	3.55	349.26	0.0037	A	H→L (14%), H→L+1 (68%)	0.18
5	3.80	325.99	0.0001	A	H-1→L (14%), H-1→L+1 (79%)	0.10
6	4.11	301.31	0.0564	A	H-3→L (46%), H-2→L+1 (44%)	0.60
7	4.43	279.99	0.3624	A	H-3→L (43%), H-2→L+1 (46%)	0.59
8	4.85	255.63	0.0005	A	H-12→L (20%), H-4→L (51%)	0.23
9	5.00	248.14	0.0429	A	H-3→L+1 (93%)	0.41
10	5.15	240.87	0.0041	A	H-1→L+8 (28%), H-1→L+9 (13%), H-1→L+10 (11%), H→L+11 (27%)	0.47
11	5.30	233.83	0.0001	A	H-17→L (22%), H-16→L (10%), H-14→L (16%), H-6→L (17%)	0.29
12	5.36	231.30	0.1137	A	H-7→L (43%), H-5→L (30%)	0.31
13	5.37	230.80	0.0002	A	H→L+2 (84%)	0.14
14	5.64	220.02	0.003	A	H-1→L+2 (85%)	0.11
15	5.67	218.72	0.0018	A	H-4→L (11%), H-4→L+1 (61%)	0.17
16	5.68	218.47	0.116	A	H-13→L (12%), H-9→L (23%)	0.46
17	5.70	217.50	0.1933	A	H-2→L+2 (13%), H-1→L+11 (10%), H→L+8 (20%)	0.56
18	5.77	214.72	0.0314	A	H-9→L (13%), H-7→L+1 (11%), H-5→L (18%), H-2→L+2 (12%)	0.41
19	5.89	210.42	0.0045	A	H-14→L (14%), H-8→L (22%), H-6→L (33%)	0.20
20	5.96	208.03	0.0007	A	H-17→L+1 (20%), H-14→L+1 (12%), H-6→L+1 (20%)	0.24
21	6.00	206.66	0.0987	A	H-7→L+1 (22%), H-5→L+1 (32%), H-2→L+2 (15%)	0.38
22	6.02	206.00	0.0081	A	H-12→L (16%), H-10→L (18%), H-4→L (11%)	0.26
23	6.05	204.98	0.0346	A	H-15→L+1 (10%), H-13→L (38%), H-2→L+2 (10%)	0.60
24	6.18	200.59	0.0012	A	H-17→L (13%), H-10→L (40%)	0.25
25	6.20	200.03	0.0441	A	H-5→L+1 (12%), H-2→L+2 (11%), H→L+3 (19%), H→L+6 (11%)	0.31

8 References

[1] J. He, F. Rauch, A. Friedrich, D. Sieh, T. Ribbeck, I. Krummenacher, H. Braunschweig, M. Finze, T. B. Marder, *Chem. Eur. J.* **2019**, *25*, 13777–13784.

[2] H. C. Brown, V. H. Dodson, *J. Am. Chem. Soc.* **1957**, *79*, 2302–2306.

[3] T. W. Hudnall, C. -W. Chiu, F. P. Gabbaï, *Acc. Chem. Res.* **2009**, *42*, 388–397.

[4] C. R. Wade, A. E. Broomsgrove, S. Aldridge, F. P. Gabbaï, *Chem. Rev.* **2010**, *110*, 3958–3984.

[5] F. Jäkle, *Chem. Rev.* **2010**, *110*, 3985–4022.

[6] Z. M. Hudson, S. Wang, *Acc. Chem. Res.* **2009**, *42*, 1584–1596.

[7] Z. Yuan, N. J. Taylor, T. B. Marder, I. D. Williams, S. K. Kurtz, L. -T. Cheng, *J. Chem. Soc., Chem. Commun.* **1990**, 1489–1492.

[8] M. Lequan, R. M. Lequan, K. C. Ching, *J. Mater. Chem.* **1991**, *1*, 997–999.

[9] M. Lequan, R. M. Lequan, K. C. Ching, A. -C. Callier, M. Barzoukas, A. Fort, *Adv. Mater. Opt. Electron.* **1992**, *1*, 243–247.

[10] M. Lequan, R. M. Lequan, K. C. Ching, M. Barzoukas, A. Fort, H. Lahoucine, G. Bravic, D. Chasseau, J. Gaultier, *J. Mater. Chem.* **1992**, *2*, 719–725.

[11] Z. Yuan, N. J. Taylor, Y. Sun, T. B. Marder, I. D. Williams, L. -T. Cheng, *J. Organomet. Chem.* **1993**, *449*, 27–37.

[12] Z. Yuan, N. J. Taylor, R. Ramachandran, T. B. Marder, *Appl. Organomet. Chem.* **1996**, *10*, 305–316.

[13] C. Branger, M. Lequan, R. M. Lequan, M. Barzoukas, A. Fort, *J. Mater. Chem.* **1996**, *6*, 555–558.

[14] Z. Yuan, J. C. Collings, N. J. Taylor, T. B. Marder, C. Jardin, J. -F. Halet, *J. Solid State Chem.* **2000**, *154*, 5–12.

[15] Z. Yuan, C. D. Entwistle, J. C. Collings, D. A. Jové, A. S. Batsanov, J. A. Howard, N. J. Taylor, H. M. Kaiser, D. E. Kaufmann, S. Y. Poon, , W. -Y. Wong, C. Jardin, S. Fathallah, A. Boucekkine, J. -F. Halet, T. B. Marder, *Chem. Eur. J.* **2006**, *12*, 2758–2771.

[16] Z. -Q. Liu, Q. Fang, D. Wang, G. Xue, W. -T. Yu, Z. -S. Shao, M. -H. Jiang, *Chem. Commun.* **2002**, 2900–2901.

[17] Z. -Q. Liu, Q. Fang, D. Wang, D. X. Cao, G. Xue, W. -T. Yu, H. Lei, *Chem. Eur. J.* **2003**, *9*, 5074–5084.

[18] M. Charlot, L. Porrès, C. D. Entwistle, A. Beeby, T. B. Marder, M. Blanchard-Desce, *Phy. Chem. Chem. Phy.* **2005**, *7*, 600–606.

[19] J. C. Collings, S. -Y. Poon, C. L. Droumaguet, M. Charlot, C. Katan, L. -O. Pålsson, A. Beeby, J. A. Mosely, H. M. Kaiser, D. Kaufmann, W.-Y. Wong, M. Blanchard-Desce, T. B. Marder, *Chem. Eur. J.* **2009**, *15*, 198–208.

[20] L. Ji, R. M. Edkins, L. J. Sewell, A. Beeby, A. S. Batsanov, K. Fucke, M. Drafz, J. A. Howard, O. Moutounet, F. Ibersiene, A. Boucekkine, E. Furet, Z. Liu, J. -F. Halet, C. Katan, T. B. Marder, *Chem. Eur. J.* **2014**, *20*, 13618–13635.

[21] S. Griesbeck, Z. Zhang, M. Gutmann, T. Lühmann, R. M. Edkins, G. Clermont, A. N. Lazar, M. Haehnel, K. Edkins, A. Eichhorn, M. Blanchard-Desce, L. Meinel, T. B. Marder, *Chem. Eur. J.* **2016**, *22*, 14701–14706.

[22] S. Griesbeck, E. Michail, C. Wang, H. Ogasawara, S. Lorenzen, L. Gerstner, T. Zang, J. Nitsch, Y. Sato, R. Bertermann, M. Taki, C. Lambert, S. Yamaguchi, T. B. Marder, *Chem. Sci.* **2019**, *10*, 5405–5422.

[23] S. Griesbeck, M. Ferger, C. Czernetzi, C. Wang, R. Bertermann, A. Friedrich, M. Haehnel, D. Sieh, M. Taki, S. Yamaguchi, T. B. Marder, *Chem. Eur. J.* **2019**, *25*, 7679–7688.

[24] C. D. Entwistle, T. B. Marder, *Angew. Chem. Int. Ed.* **2002**, *41*, 2927–2931.

[25] C. D. Entwistle, T. B. Marder, *Chem. Mater.* **2004**, *16*, 4574–4585.

[26] S. Yamaguchi, A. Wakamiya, *Pure Appl. Chem.* **2006**, *78*, 1413–1424.

[27] F. Jäkle, *Coord. Chem. Rev.* **2006**, *250*, 1107–1121.

[28] Z. M. Hudson, S. Wang, *Dalton Trans.* **2011**, *40*, 7805–7816.

[29] A. Wakamiya, S. Yamaguchi, *Bull. Chem. Soc. Jpn.* **2015**, *88*, 1357–1377.

[30] L. Ji, S. Griesbeck, T. B. Marder, *Chem. Sci.* **2017**, *8*, 846–863.

[31] S. -Y. Li, Z. -B. Sun, C. -H. Zhao, *Inorg. Chem.* **2017**, *56*, 8705–8717.

[32] G. Turkoglu, M. E. Cinar, T. Ozturk, *Molecules* **2017**, *22*, 1522.

[33] Y. Ren, F. Jäkle, *Dalton Trans.* **2016**, *45*, 13996–14007.

[34] J. Doty, B. Babb, P. Grisdale, M. Glogowski, J. Williams, *J. Organomet. Chem.* **1972**, *38*,

229–236.

[35] S. M. Cornet, K. B. Dillon, C. D. Entwistle, M. A. Fox, A. E. Goeta, H. P. Goodwin, T. B. Marder, A. L. Thompson, *Dalton Trans.* **2003**, *23*, 4395–4405.

[36] X. Yin, J. Chen, R. A. Lalancette, T. B. Marder, F. Jäkle, *Angew. Chem. Int. Ed.* **2014**, *53*, 9761–9765.

[37] Z. Zhang, R. M. Edkins, J. Nitsch, K. Fucke, A. Steffen, L. E. Longobardi, D. W. Stephan, C. Lambert, T. B. Marder, *Chem. Sci.* **2015**, *6*, 308–321.

[38] Z. Zhang, R. M. Edkins, M. Haehnel, M. Wehner, A. Eichhorn, L. Mailänder, M. Meier, J. Brand, F. Brede, K. Müller-Buschbaum, H. Braunschweig, T. B. Marder, *Chem. Sci.* **2015**, *6*, 5922–5927.

[39] Z. Zhang, R. M. Edkins, J. Nitsch, K. Fucke, A. Eichhorn, A. Steffen, Y. Wang, T. B. Marder, *Chem. Eur. J.* **2015**, *21*, 177–190.

[40] J. Wang, Y. Wang, T. Taniguchi, S. Yamaguchi, S. Irle, *J. Phys. Chem. A* **2012**, *116*, 1151–1158.

[41] T. Taniguchi, J. Wang, S. Irle, S. Yamaguchi, *Dalton Trans.* **2013**, *42*, 620–624.

[42] X. Yin, F. Guo, R. A. Lalancette, F. Jäkle, *Macromolecules* **2016**, *49*, 537–546.

[43] D. -T. Yang, S. K. Mellerup, J. -B. Peng, X. Wang, Q. -S. Li, S. Wang, *J. Am. Chem. Soc.* **2016**, *138*, 11513–11516.

[44] X. Yin, K. Liu, Y. Ren, R. A. Lalancette, Y. -L. Loo, F. Jäkle, *Chem. Sci.* **2017**, *8*, 5497–5505.

[45] M. F. Smith, S. J. Cassidy, I. A. Adams, M. Vasiliu, D. L. Gerlach, D. A. Dixon, P. A. Rupar, *Organometallics* **2016**, *35*, 3182–3191.

[46] S. -B. Zhao, P. Wucher, Z. M. Hudson, T. M. McCormick, X. -Y. Liu, S. Wang, X. -D. Feng, Z. -H. Lu, *Organometallics* **2008**, *27*, 6446–6456.

[47] A. G. Crawford, A. D. Dwyer, Z. Liu, A. Steffen, A. Beeby, L. -O. Pålsson, D. J. Tozer, T. B. Marder, *J. Am. Chem. Soc.* **2011**, *133*, 13349–13362.

[48] A. G. Crawford, Z. Liu, I. A. Mkhalid, M. H. Thibault, N. Schwarz, G. Alcaraz, A. Steffen, J. C. Collings, A. S. Batsanov, J. A. Howard, T. B. Marder, *Chem. Eur. J.* **2012**, *18*, 5022–5035.

[49] L. Ji, R. M. Edkins, A. Lorbach, I. Krummenacher, C. Brückner, A. Eichhorn, H.

Braunschweig, B. Engels, P. J. Low, T. B. Marder, *J. Am. Chem. Soc.* **2015**, *137*, 6750–6753.

[50] R. Kurata, A. Ito, M. Gon, K. Tanaka, Y. Chujo, *J. Org. Chem.* **2017**, *82*, 5111–5121.

[51] J. Merz, J. Fink, A. Friedrich, I. Krummenacher, H. H. Al Mamari, S. Lorenzen, M. Haehnel, A. Eichhorn, M. Moos, M. Holzapfel, H. Braunschweig, C. Lambert, A. Steffen, L. Ji, T. B. Marder, *Chem. Eur. J.* **2017**, *23*, 13164–13180.

[52] N. Yuan, W. Wang, Y. Fang, J. Zuo, Y. Zhao, G. Tan, X. Wang, *Organometallics* **2017**, *36*, 2498–2501.

[53] L. Ji, I. Krummenacher, A. Friedrich, A. Lorbach, M. Haehnel, K. Edkins, H. Braunschweig, T. B. Marder, *J. Org. Chem.* **2018**, *83*, 3599–3606.

[54] T. E. Stennett, P. Bissinger, S. Griesbeck, S. Ullrich, I. Krummenacher, M. Auth, A. Sperlich, M. Stolte, K. Radacki, C. -J. Yao, F. Würthner, A. Steffen, T. B. Marder, H. Braunschweig, *Angew. Chem. Int. Ed.* **2019**, *58*, 6449–6454.

[55] O. Kwon, S. Barlow, S. A. Odom, L. Beverina, N. J. Thompson, E. Zojer, J. -L. Brédas, S. R. Marder, *J. Phys. Chem. A* **2005**, *109*, 9346–9352.

[56] Y. Shirota, M. Kinoshita, T. Noda, K. Okumoto, T. Ohara, *J. Am. Chem. Soc.* **2000**, *122*, 11021–11022.

[57] H. Doi, M. Kinoshita, K. Okumoto, Y. Shirota, *Chem. Mater.* **2003**, *15*, 1080–1089.

[58] D. Mutaguchi, K. Okumoto, Y. Ohsedo, K. Moriwaki, Y. Shirota, *Org. Electron.* **2003**, *4*, 49–59.

[59] W. L. Jia, D. R. Bai, T. McCormick, Q. D. Liu, M. Motala, R. Y. Wang, C. Seward, Y. Tao, S. Wang, *Chem. Eur. J.* **2004**, *10*, 994–1006.

[60] W. L. Jia, X. D. Feng, D. R. Bai, Z. H. Lu, S. Wang, G. Vamvounis, *Chem. Mater.* **2005**, *17*, 164–170.

[61] W. L. Jia, M. J. Moran, Y. -Y. Yuan, Z. H. Lu, S. Wang, *J. Mater. Chem.* **2005**, *15*, 3326–3333.

[62] F. Li, W. Jia, S. Wang, Y. Zhao, Z. H. Lu, *J. Appl. Phys.* **2008**, *103*, 034509.

[63] Z. Chen, X. K. Liu, C. -J. Zheng, J. Ye, C. -L. Liu, F. Li, X. -M. Ou, C. -S. Lee, X. -H. Zhang, *Chem. Mater.* **2015**, *27*, 5206–5211.

[64] R. Bertermann, H. Braunschweig, C. K. L. Brown, A. Damme, R. D. Dewhurst, C. Hörl, T.

Kramer, I. Krummenacher, B. Pfaffinger, K. Radacki, *Chem. Commun.* **2014**, *50*, 97–99.

[65] C. J. Berger, G. He, C. Merten, R. McDonald, M. J. Ferguson, E. Rivard, *Inorg. Chem.* **2014**, *53*, 1475–1486.

[66] C. E. Knappke, A. J. Arduengo, H. Jiao, J. -M. Neudörfl, A. J. v. Wangelin, *Synthesis* **2011**, *23*, 3784–3795.

[67] Y. -B. Wang, Y. -M. Wang, W. -Z. Zhang, X. B. Lu, *J. Am. Chem. Soc.* **2013**, *135*, 11996–12003.

[68] M. M. Roy, E. Rivard, *Acc. Chem. Res.* **2017**, *50*, 2017–2025.

[69] S. M. I. Al-Rafia, A. C. Malcolm, S. K. Liew, M. J. Ferguson, R. McDonald, E. Rivard, *Chem. Commun.* **2011**, *47*, 6987–6989.

[70] A. Franzke, A. Pfaltz, *Synthesis* **2008**, *2*, 245–252.

[71] L. Weber, D. Eickhoff, T. B. Marder, M. A. Fox, P. J. Low, A. D. Dwyer, D. J. Tozer, S. Schwedler, A. Brockhinke, H. G. Stammler, B. Neumann, *Chem. Eur. J.* **2012**, *18*, 1369–1382.

[72] F. H. Allen, O. Kennard, D. G. Watson, L. Brammer, A. G. Orpen, R. Taylor, *J. Chem. Soc., Perkin Trans. II* **1987**, 1–19.

[73] R. Stahl, C. Lambert, C. Kaiser, R. Wortmann, R. Jakober, *Chem. Eur. J.* **2006**, *12*, 2358–2370.

[74] A. Ito, K. Kawanishi, E. Sakuda, N. Kitamura, *Chem. Eur. J.* **2014**, *20*, 3940–3953.

[75] Z. Yuan, N. J. Taylor, T. B. Marder, I. D. Williams, S. K. Kurtz, L. -T. Cheng in *Organic Materials for Non-linear Optics II* (Eds.: R. A. Hann, D. Bloor), The Royal Society of Chemistry, Cambridge, **1991**, pp. 190–196.

[76] T. Yanai, D. P. Tew, N. C. Handy, *Chem. Phys. Lett.* **2004**, *393*, 51–57.

[77] M. J. Peach, P. Benfield, T. Helgaker, D. J. Tozer, *J. Chem. Phys.* **2008**, *128*, 044118.

[78] S. Yamaguchi, S. Akiyama, K. Tamao, *J. Am. Chem. Soc.* **2001**, *123*, 11372–11375.

[79] K. Parab, K. Venkatasubbaiah, F. Jäkle, *J. Am. Chem. Soc.* **2006**, *128*, 12879–12885.

[80] C. D. Entwistle, J. C. Collings, A. Steffen, L. -O. Pålsson, A. Beeby, D. Albesa-Jové, J. M. Burke, A. S. Batsanov, J. A. Howard, J. A. Mosely, W. -Y. Wong, F. Ibersiene, S. Fathallah, A. Boucekkine, J. -F. Halet, T. B. Marder, *J. Mater. Chem.* **2009**, *19*, 7532–7544.

[81] S. Griesbeck, E. Michail, F. Rauch, H. Ogasawara, C. Wang, Y. Sato, R. M. Edkins, Z. Zhang, M. Taki, C. Lambert, S. Yamaguchi, T. B. Marder, *Chem. Eur. J.* **2019**, *25*, 13164–13175.

[82] Ž. Ban, S. Griesbeck, S. Tomić, J. Nitsch, T. B. Marder, I. Piantanida, *Chem. Eur. J.* **2020**, *26*, 2195–2203.

[83] H. Amini, Ž. Ban, M. Ferger, S. Lorenzen, F. Rauch, A. Friedrich, I. Crnolatac, A. Kenđel, S. Miljanić, I. Piantanida, T. B. Marder, *Chem. Eur. J.* **2020**, *26*, 6017–6028.

[84] X. Yin, J. Liu, F. Jäkle, *Chem. Eur. J.* **2020**, DOI: 10.1002/chem.202003481.

[85] R. Hoffmann, *J. Chem. Phys.* **1963**, *39*, 1397–1412.

[86] R. Breslow, *Chem. Eng. News* **1965**, *43*, 90–100.

[87] R. Breslow, *Acc. Chem. Res.* **1973**, *6*, 393–398.

[88] M. Saunders, R. Berger, A. Jaffe, J. McBride, J. O'Neill, R. Breslow, J. Hoffmann, C. Perchonock, E. Wasserman, *J. Am. Chem. Soc.* **1973**, *95*, 3017–3018.

[89] W. A. Yager, *J. Am. Chem. Soc.* **1963**, *85*, 2033–2034.

[90] E. P. Malar, K. Jug, *Tetrahedron* **1986**, *42*, 417–426.

[91] P. v. R. Schleyer, P. K. Freeman, H. Jiao, B. Goldfuss, *Angew. Chem. Int. Ed.* **1995**, *34*, 337–340.

[92] M. K. Cyranski, T. M. Krygowski, A. R. Katritzky, P. v. R. Schleyer, *J. Org. Chem.* **2002**, *67*, 1333–1338.

[93] J. J. Eisch, N. K. Hota, S. Kozima, *J. Am. Chem. Soc.* **1969**, *91*, 4575–4577.

[94] H. Braunschweig, I. Fernández, G. Frenking, T. Kupfer, *Angew. Chem. Int. Ed.* **2008**, *47*, 1951–1954.

[95] C. Fan, W. E. Piers, M. Parvez, *Angew. Chem. Int. Ed.* **2009**, *48*, 2955–2958.

[96] H. Braunschweig, V. Dyakonov, J. O. C. Jimenez-Halla, K. Kraft, I. Krummenacher, K. Radacki, A. Sperlich, J. Wahler, *Angew. Chem. Int. Ed.* **2012**, *51*, 2977–2980.

[97] J. J. Eisch, *Adv. Organomet. Chem.* **1996**, *39*, 355–392.

[98] A. Steffen, R. M. Ward, W. D. Jones, T. B. Marder, *Coord. Chem. Rev.* **2010**, *254*, 1950–1976.

[99] H. Braunschweig, T. Kupfer, *Chem. Commun*. **2011**, *47,* 10903–10914.

[100] H. Braunschweig, I. Krummenacher *in Organic Redox Systems: Synthesis, Properties, and Applications* (Ed.: T. Nishinaga), John Wiley & Sons, Hoboken (New Jersey), **2016** 503–522.

[101] H. Braunschweig, I. Krummenacher, J. Wahler, *Adv. Organomet. Chem.* **2013**, *61*, 1–53.

[102] A. Wakamiya *in Main Group Strategies towards Functional Hybrid Materials*, (Eds.: T. Baumgartner, F. Jäkle), John Wiley & Sons Ltd., Hoboken (New Jersey), **2018**, *1*, 1–26.

[103] J. H. Barnard, S. Yruegas, K. Huang, C. D. Martin, *Chem. Commun.* **2016**, *52*, 9985–9991.

[104] B. Su, R. Kinjo, *Synthesis* **2017**, *49*, 2985–3034.

[105] Y. Su, R. Kinjo, *Chem. Soc. Rev.* **2019**, *48*, 3613–3659.

[106] R. Köster, G. Benedikt, *Angew. Chem. Int. Ed.* **1963**, *6*, 323–324.

[107] A. Escande, M. J. Ingleson, *Chem. Commun.* **2015**, *51*, 6257–6274.

[108] E. v. Grotthuss, A. John, T. Kaese, M. Wagner, *Asian J. Org. Chem.* **2018**, *7*, 37–53.

[109] C. K. Narula, H. Nöth, *J. Organomet. Chem.* **1985**, *281*, 131–134.

[110] J. J. Eisch, J. E. Galle, S. Kozima, *J. Am. Chem. Soc.* **1986**, *108*, 379–385.

[111] P. A. Chase, W. E. Piers, B. O. Patrick, *J. Am. Chem. Soc.* **2000**, *122*, 12911–12912.

[112] S. Yruegas, J. J. Martinez, C. D. Martin, *Chem. Commun.* **2018**, *54*, 6808–6811.

[113] U. Gross, D. Kaufmann, *Chem. Ber.* **1987**, *120*, 991–994.

[114] H. Hong, T. Chung, *J. Organomet. Chem.* **2004**, *689*, 58–64.

[115] P. E. Romero, W. E. Piers, S. A. Decker, D. Chau, T. K. Woo, M. Parvez, *Organometallics* **2003**, *22*, 1266–1274.

[116] S. Yamaguchi, T. Shirasaka, S. Akiyama, K. Tamao, *J. Am. Chem. Soc.* **2002**, *124*, 8816–8817.

[117] R. -F. Chen, Q. -L. Fan, C. Zheng, W. Huang, *Org. Lett.* **2006**, *8*, 203–205.

[118] F. Rauch, S. Fuchs, A. Friedrich, D. Sieh, I. Krummenacher, H. Braunschweig, M. Finze, T. B. Marder, *Chem. Eur. J.* **2020**, *26*, 12794–12808.

[119] R. J. Wehmschulte, M. A. Khan, B. Twamley, B. Schiemenz, *Organometallics* **2001**, *20*, 844–849.

[120] R. J. Wehmschulte, A. A. Diaz, M. A. Khan, *Organometallics* **2003**, *22*, 83–92.

[121] A. Iida, S. Yamaguchi, *J. Am. Chem. Soc.* **2011**, *133*, 6952–6955.

[122] M. Urban, K. Durka, P. Górka, G. Wiosna-Sałyga, K. Nawara, P. Jankowski, S. Luliński, *Dalton Trans.* **2019**, *48*, 8642–8663.

[123] J. F. Araneda, B. Neue, W. E. Piers, M. Parvez, *Angew. Chem. Int. Ed.* **2012**, *51*, 8546–8550.

[124] J. F. Araneda, W. E. Piers, M. J. Sgro, M. Parvez, *Chem. Sci.* **2014**, *5*, 3189–3196.

[125] A. Hübner, Z. -W. Qu, U. Englert, M. Bolte, H. -W. Lerner, M. C. Holthausen, M. Wagner, *J. Am. Chem. Soc.* **2011**, *133*, 4596–4609.

[126] A. Das, A. Hübner, M. Weber, M. Bolte, H. -W. Lerner, M. Wagner, *Chem. Commun.* **2011**, *47*, 11339–11341.

[127] A. Hübner, M. Diefenbach, M. Bolte, H. -W. Lerner, M. C. Holthausen, M. Wagner, *Angew. Chem. Int. Ed.* **2012**, *51*, 12514–12518.

[128] A. Hübner, A. M. Diehl, M. Bolte, H. -W. Lerner, M. Wagner, *Organometallics* **2013**, *32*, 6827–6833.

[129] S. Biswas, I. M. Oppel, H. F. Bettinger, *Inorg. Chem*. **2010**, *49*, 4499–4506.

[130] Y. Shoji, N. Tanaka, S. Muranaka, N. Shigeno, H. Sugiyama, K. Takenouchi, F. Hajjaj, T. Fukushima, *Nat. Commun.* **2016**, *7*, 1–7.

[131] W. Zhang, G. Li, L. Xu, Y. Zhuo, W. Wan, N. Yan, G. He, *Chem. Sci*. **2018**, *9,* 4444–4450.

[132] S. Yruegas, J. H. Barnard, K. Al-Furaiji, J. L. Dutton, D. J. Wilson, C. D. Martin, *Organometallics* **2018**, *37*, 1515–1518.

[133] K. R. Bluer, L. E. Laperriere, A. Pujol, S. Yruegas, V. A. Adiraju, C. D. Martin, *Organometallics* **2018**, *37*, 2917–2927.

[134] F. Leroux, *ChemBioChem* **2004**, *5*, 644–649.

[135] M. Mantina, A. C. Chamberlin, R. Valero, C. J. Cramer, D. G. Truhlar, *J. Phys. Chem. A* **2009**, *113*, 5806–5812.

[136] R. J. Blagg, E. J. Lawrence, K. Resner, V. S. Oganesyan, T. J. Herrington, A. E. Ashley, G. G. Wildgoose, *Dalton Trans.* **2016**, *45*, 6023–6031.

[137] R. J. Blagg, T. R. Simmons, G. R. Hatton, J. M. Courtney, E. L. Bennett, E. J. Lawrence, G. G. Wildgoose, *Dalton Trans.* **2016**, *45*, 6032–6043.

[138] S. Toyota, M. Asakura, M. Oki, F. Toda, *Bull. Chem. Soc. Jpn*. **2000**, *73*, 2357–2362.

[139] F. Rauch, P. Endres, A. Friedrich, D. Sieh, M. Hähnel, I. Krummenacher, H. Braunschweig,

M. Finze, L. Ji, T. B. Marder, *Chem. Eur. J.* **2020**, DOI: 10.1002/chem.202001985.

[140] A. K. Narsaria, F. Rauch, J. Krebs, P. Endres, A. Friedrich, I. Krummenacher, H. Braunschweig, M. Finze, J. Nitsch, F. M. Bickelhaupt, T. B. Marder, *Adv. Funct. Mater.* **2020**, *30*, 2002064.

[141] F. Rauch, J. Krebs, J. Günther, A. Friedrich, M. Hähnel, I. Krummenacher, H. Braunschweig, M. Finze, T. B. Marder, *Chem. Eur. J.* **2020**, *26*, 10626–10633.

[142] A. Wakamiya, K. Mishima, K. Ekawa, S. Yamaguchi, *Chem. Commun.* **2008**, 579–581.

[143] L. Kaufmann, H. Vitze, M. Bolte, H. -W. Lerner, M. Wagner, *Organometallics* **2008**, *27*, 6215–6221.

[144] A. Iida, A. Sekioka, S. Yamaguchi, *Chem. Sci.* **2012**, *3*, 1461–1466.

[145] W. E. Piers, *Adv. Organomet. Chem.* **2005**, *52*, 1–76.

[146] G. Erker, *Dalton Trans.* **2005**, *11*, 1883–1890.

[147] W. E. Piers, T. Chivers, *Chem. Soc. Rev.* **1997**, *26*, 345–354.

[148] P. A. Chase, L. D. Henderson, W. E. Piers, M. Parvez, W. Clegg, M. R. Elsegood, *Organometallics* **2006**, *25*, 349–357.

[149] A. Y. Houghton, V. A. Karttunen, W. E. Piers, H. M. Tuononen, *Chem. Commun.* **2014**, *50*, 1295–1298.

[150] A. Y. Houghton, J. Hurmalainen, A. Mansikkamäki, W. E. Piers, H. M. Tuononen, *Nat. Chem.* **2014**, *6*, 983.

[151] V. C. Williams, W. E. Piers, W. Clegg, M. R. Elsegood, S. Collins, T. B. Marder, *J. Am. Chem. Soc.* **1999**, *121*, 3244–3245.

[152] V. C. Williams, G. J. Irvine, W. E. Piers, Z. Li, S. Collins, W. Clegg, M. R. Elsegood, T. B. Marder, *Organometallics* **2000**, *19*, 1619–1621.

[153] V. C. Williams, C. Dai, Z. Li, S. Collins, W. E. Piers, W. Clegg, M. R. Elsegood, T. B. Marder, *Angew. Chem. Int. Ed.* **1999**, *38*, 3695–3698.

[154] R. F. Childs, D. L. Mulholland, A. Nixon, *Can. J. Chem.* **1982**, *60*, 801–808.

[155] P. Laszlo, M. Teston, *J. Am. Chem. Soc.* **1990**, *112*, 8750–8754.

[156] P. A. Chase, P. E. Romero, W. E. Piers, M. Parvez, B. O. Patrick, *Can. J. Chem.* **2005**, *83*, 2098–2105.

[157] K. Köhler, W. E. Piers, A. P. Jarvis, S. Xin, Y. Feng, A. Bravakis, S. Collins, W. Clegg, G. P. A. Yap, T. B. Marder, *Organometallics* **1998**, *17*, 3557–3566.

[158] P. G. Hayes, W. E. Piers, M. Parvez, *Organometallics* **2005**, *24*, 1173–1183.

[159] S. P. Lewis, N. J. Taylor, W. E. Piers, S. Collins, *J. Am. Chem. Soc.* **2003**, *125*, 14686–14687.

[160] L. D. Henderson, W. E. Piers, G. J. Irvine, R. McDonald, *Organometallics* **2002**, *21*, 340–345.

[161] J. Chai, S. P. Lewis, S. Collins, T. J. Sciarone, L. D. Henderson, P. A. Chase, G. J. Irvine, W. E. Piers, M. R. Elsegood, W. Clegg, *Organometallics* **2007**, *26*, 5667–5679.

[162] C. Fan, L. G. Mercier, W. E. Piers, H. M. Tuononen, M. Parvez, *J. Am. Chem. Soc.* **2010**, *132*, 9604–9606.

[163] A. Y. Houghton, V. A. Karttunen, C. Fan, W. E. Piers, H. M. Tuononen, *J. Am. Chem. Soc.* **2013**, *135*, 941–947.

[164] D. J. Parks, W. E. Piers, *J. Am. Chem. Soc.* **1996**, *118*, 9440–9441.

[165] N. L. Allinger, J. H. Siefert, J. *Am. Chem. Soc.* **1975**, *97*, 752–760.

[166] D. -M. Chen, Q. Qin, Z. -B. Sun, Q. Peng, C. -H. Zhao, *Chem. Commun.* **2014**, *50*, 782–784.

[167] D. -M. Chen, S. Wang, H. -X. Li, X. -Z. Zhu, C. -H. Zhao, *Inorg. Chem.* **2014**, *53*, 12532–12539.

[168] J. He, F. Rauch, A. Friedrich, J. Krebs, I. Krummenacher, R. Bertermann, J. Nitsch, H. Braunschweig, M. Finze and T. B. Marder, *Angew. Chem. Int. Ed.* Submitted.

[169] Selected patents: (a) H. J. Lee, Y. J. Cho, H. J. Kwon, B. O. Kim, S. M. Kim and S. S. Yoon, CN. Pat., 102574871 A, **2010**; (b) C. S. Kim, Y. J. Cho, H. J. Kwon, B. O. Kim and S. M. Kim, KR Pat., 20110049012 A, **2011**; (c) Z. F. Xie, CN Pat., 108409762 A, **2018**; (d) Y. L. Wang, Z. Xue, H. Y. Li, J. P. Wang, C. X. Gao, Z. W. Chen, L. G. Li and W. J. Wang, CN Pat., 109293690 A, **2018**; (e) W. Gao, L. Zhang, W. P. Dai, J. H. Niu and H. Y. Zhu, CN Pat., 110003258 A, **2019**.

[170] A. D. Allen, T. T. Tidwell, *Chem. Rev.* **2001**, *101*, 1333–1348.

[171] T. B. Tai, V. T. T. Huong, M. T. Nguyen, *Chem. Commun.* **2013**, *49*, 11548–11550.

[172] Y. Sugihara, R. Miyatake, K. Takakura, S. Yano, *J. Chem. Soc., Chem. Commun.* **1994**,

1925–1926.

[173] Y. Sugihara, K. Takakura, T. Murafuji, R. Miyatake, K. Nakasuji, M. Kato, S. Yano, *J. Org. Chem.* **1996**, *61*, 6829–6834.

[174] S. Wakabayashi, S. Imamura, Y. Sugihara, M. Shimizu, T. Kitagawa, Y. Ohki, K. Tatsumi, *J. Org. Chem.* **2008**, *73*, 81–87.

[175] K. Ansorg, H. Braunschweig, C. -W. Chiu, B. Engels, D. Gamon, M. Hügel, T. Kupfer, K. Radacki, *Angew. Chem. Int. Ed.* **2011**, *50*, 2833–2836.

[176] K. Matsuo, S. Saito, S. Yamaguchi, *J. Am. Chem. Soc.* **2014**, *136*, 12580–12583.

[177] T. Matsumoto, K. Tanaka, K. Tanaka, Y. Chujo, *Dalton Trans.* **2015**, *44*, 8697–8707.

[178] T. Matsumoto, H. Takamine, K. Tanaka, Y. Chujo, *Mater. Chem. Front.* **2017**, *1*, 2368–2375.

[179] S. J. Cassidy, I. Brettell-Adams, L. E. McNamara, M. F. Smith, M. Bautista, H. Cao, M. Vasiliu, D. L. Gerlach, F. Qu, N. I. Hammer, *Organometallics* **2018**, *37*, 3732–3741.

[180] F. Vollmer, W. Rettig, E. Birckner, *J. Fluoresc.* **1994**, *4*, 65–69.

[181] J. D. Hoefelmeyer, S. Solé, F. P. Gabbaï, *Dalton Trans.* **2004**, *8*, 1254–1258.

[182] S. Bontemps, M. Devillard, S. Mallet-Ladeira, G. Bouhadir, K. Miqueu, D. Bourissou, *Inorg. Chem.* **2013**, *52*, 4714–4720.

[183] S. Bontemps, G. Bouhadir, K. Miqueu, D. Bourissou, *J. Am. Chem. Soc.* **2006**, *128*, 12056–12057.

[184] L. A. Essex, J. W. Taylor, W. H. Harman, *Tetrahedron* **2019**, *75*, 2255–2260.

[185] Y. Tokoro, A. Nagai, K. Tanaka, Y. Chujo, *Macromol. Rapid Commun*. **2012**, *33*, 550–555.

[186] V. D. Bonifácio, J. Morgado, U. Scherf, *J. Polym. Sci., Part A: Polym. Chem.* **2008**, *46*, 2878–2883.

[187] I. A. Adams, P. A. Rupar, *Macromol. Rapid Commun.* **2015**, *36*, 1336–1340.

[188] T. Matsumoto, S. Ito, K. Tanaka, Y. Chujo, *Polym. J.* **2018**, *50*, 197–202.

[189] A. Hübner, A. M. Diehl, M. Diefenbach, B. Endeward, M. Bolte, H. -W. Lerner, M. C. Holthausen, M. Wagner, *Angew. Chem. Int. Ed.* **2014**, *53*, 4832–4835.

[190] K. Okada, T. Sugawa, M. Oda, *J. Chem. Soc., Chem. Commun.* **1992**, 74–75.

[191] T. Noda, Y. Shirota, *J. Am. Chem. Soc.* **1998**, *120*, 9714–9715.

[192] Y. Sun, N. Ross, S. -B. Zhao, K. Huszarik, W. -L. Jia, R. -Y. Wang, D. Macartney, S. Wang, *J. Am. Chem. Soc.* **2007**, *129*, 7510–7511.

[193] N. G. Connelly, W. E. Geiger, *Chem. Rev.* **1996**, *96*, 877–910.

[194] W. J. Grigsby, P. P. Power, *J. Am. Chem. Soc.* **1996**, *118*, 7981–7988.

[195] A. Hübner, M. Bolte, H. -W. Lerner, M. Wagner, *Angew. Chem. Int. Ed.* **2014**, *53*, 10408–10411.

[196] T. Kaese, A. Hübner, M. Bolte, H. -W. Lerner, M. Wagner, *J. Am. Chem. Soc.* **2016**, *138*, 6224–6233.

[197] J. Gilmer, H. Budy, T. Kaese, M. Bolte, H. -W. Lerner, M. Wagner, *Angew. Chem. Int. Ed.* **2020**, *59*, 5621–5625.

[198] C. Narula, H. Nöth, *Inorg. Chem.* **1985**, *24*, 2532–2539.

[199] D. M. Adams, J. Chatt, J. M. Davidson, J. Gerratt, *J. Chem. Soc.* **1963**, 2189-2194.

[200] W. Yang, K. E. Krantz, L. A. Freeman, D. A. Dickie, A. Molino, A. Kaur, D. J. Wilson, R. J. Gilliard Jr, *Chem. Eur. J.* **2019**, *25*, 12512–12516.

[201] G. C. Welch, D. W. Stephan, *J. Am. Chem. Soc.* **2007**, *129*, 1880–1881.

[202] G. C. Welch, R. R. San Juan, J. D. Masuda, D. W. Stephan, *Science* **2006**, *314*, 1124–1126.

[203] D. W. Stephan, G. Erker, *Angew. Chem. Int. Ed.* **2015**, *54*, 6400–6441.

[204] D. W. Stephan, *J. Am. Chem. Soc.* **2015**, *137*, 10018–10032.

[205] H. Belaidi, F. Rauch, Z. Zhang, C. Latouche, A. Boucekkine, T. B. Marder, J. -F. Halet, *ChemPhotoChem* **2020**, *26*, 10626–10633.

[206] C. -W. So, D. Watanabe, A. Wakamiya, S. Yamaguchi, *Organometallics* **2008**, *27*, 3496–3501.

[207] W. Zhang, D. Yu, Z. Wang, B. Zhang, L. Xu, G. Li, N. Yan, E. Rivard, G. He, *Org. Lett.* **2018**, *21*, 109–113.

[208] N. Yuan, W. Wang, Z. Wu, S. Chen, G. Tan, Y. Sui, X. Wang, J. Jiang, P. P. Power, *Chem. Commun.* **2016**, *52*, 12714–12716.

[209] L. Wang, J. Li, L. Zhang, Y. Fang, C. Chen, Y. Zhao, Y. Song, L. Deng, G. Tan, X. Wang, *J. Am. Chem. Soc.* **2017**, *139*, 17723–17726.

[210] R. Feng, L. Zhang, C. Chen, Y. Fang, Y. Zhao, G. Tan, X. Wang, *Chem. Eur. J.* **2019**, *25*,

4031–4035.

[211] R. Feng, W. Yang, W. Wang, Y. Zhao, G. Tan, L. Zhang, X. Wang, *Chem. Commun.* **2019**, *55*, 12908–12911.

[212] C. -W. Chiu, F. P. Gabbaï, *Angew. Chem. Int. Ed.* **2007**, *46*, 1723–1725.

[213] C. -W. Chiu, F. P. Gabbaï, *Angew. Chem. Int. Ed.* **2007**, *46*, 6878–6881.

[214] D. L. Crossley, R. Kahan, S. Endres, A. Warner, R. Smith, J. Cid, J. Dunsford, J. Jones, I. Vitorica-Yrezabal, M. J. Ingleson, *Chem. Sci.* **2017**, *8*, 7969–7977.

[215] S. -B. Zhao, T. McCormick, S. Wang, *Inorg. Chem.* **2007**, *46*, 10965–10967.

[216] Y. Sun, S. Wang, *Inorg. Chem.* **2009**, *48*, 3755–3767.

[217] Y. -L. Rao, S. Wang, *Inorg. Chem.* **2009**, *48*, 7698–7713.

[218] Z. M. Hudson, S. -B. Zhao, R. Y. Wang, S. Wang, *Chem. Eur. J.* **2009**, *15*, 6131–6137.

[219] Z. M. Hudson, C. Sun, M. G. Helander, H. Amarne, Z. -H. Lu, S. Wang, *Adv. Funct. Mater.* **2010**, *20*, 3426–3439.

[220] Z. M. Hudson, M. G. Helander, Z. -H. Lu, S. Wang, *Chem. Commun.* **2011**, *47*, 755–757.

[221] X. Yang, Z. Huang, J. Dang, C. -L. Ho, G. Zhou, W. -Y. Wong, *Chem. Commun.* **2013**, *49*, 4406–4408.

[222] F. Juliá, D. Bautista, P. González-Herrero, *Chem. Commun.* **2016**, *52*, 1657–1660.

[223] N. Wang, M. Hu, S. K. Mellerup, X. Wang, F. O. Sauriol, T. Peng, S. Wang, *Inorg. Chem.* **2017**, *56*, 12783–12794.

[224] G. Zhou, C. -L. Ho, W. -Y. Wong, Q. Wang, D. Ma, L. Wang, Z. Lin, T. B. Marder, A. Beeby, *Adv. Funct. Mater.* **2008**, *18*, 499–511.

[225] X. Yang, N. Sun, J. Dang, Z. Huang, C. Yao, X. Xu, C. -L. Ho, G. Zhou, D. Ma, X. Zhao, W. -Y. Wong, *J. Mater. Chem. C* **2013**, *1*, 3317–3326.

[226] X. Xu, X. Yang, Y. Wu, G. Zhou, C. Wu, W. -Y. Wong, *Chem. Asian J.* **2015**, *10*, 252–262.

[227] B. Liu, F. Dang, Z. Feng, Z. Tian, J. Zhao, Y. Wu, X. Yang, G. Zhou, Z. Wu, W. -Y. Wong, *J. Mater. Chem. C* **2017**, *5*, 7871–7883.

[228] Y. -L. Rao, H. Amarne, S. -B. Zhao, T. M. McCormick, S. Martić, Y. Sun, R. -Y. Wang, S. Wang, *J. Am. Chem. Soc.* **2008**, *130*, 12898–12900.

[229] S. K. Mellerup, Y. -L. Rao, H. Amarne, S. Wang, *Org. Lett.* **2016**, *18*, 4436–4439.

[230] S. K. Mellerup, S. Wang, *Chem. Soc. Rev.* **2019**, *48*, 3537–3549.

[231] S. Xu, F. Haeffner, B. Li, L. N. Zakharov, S. Y. Liu, *Angew. Chem. Int. Ed.* **2014**, *53*, 6795–6799.

[232] S. Durben, T. Baumgartner, *Inorg. Chem.* **2011**, *50*, 6823–6836.

[233] R. E. Hoffman, E. Shabtai, M. Rabinovitz, V. S. Iyer, K. Müllen, A. K. Rai, E. Bayrd, L. T. Scott, *J. Chem. Soc., Perkin Trans. II* **1998**, 1659–1664.

[234] R. Evans, G. D. Poggetto, M. Nilsson, G. A. Morris, *Anal. Chem.* **2018**, *90*, 3987–3994.

[235] O. V. Dolomanov, L. J. Bourhis, R. J. Gildea, J. A. Howard, H. Puschmann, *J. Appl. Crystallogr.* **2009**, *42*, 339–341.

[236] H. Amarne, C. Baik, S. K. Murphy, S. Wang, *Chem. Eur. J.* **2010**, *16*, 4750–4761.

[237] K. M. M. Josef, *Lichtabsorption und Photochemie organischer Moleküle*, VCH, Weinheim; New York, **1989**.

[238] S. Strickler, R. A. Berg, *J. Chem. Phys.* **1962**, *37*, 814–822.

[239] S. Delmond, J. -F. Létard, R. Lapouyade, W. Rettig, *J. Photochemi. A* **1997**, *105*, 135–148.

[240] V. Volchkov, B. Uzhinov, *High Energ. Chem.* **2008**, *42*, 153–169.

[241] S. Sasaki, G. P. Drummen, G. -i. Konishi, *J. Mater. Chem. C* **2016**, *4*, 2731–2743.

[242] Y. Hong, J. W. Lam, B. Z. Tang, *Chem. Commun.* **2009**, *45*, 4332–4353.

[243] Y. Hong, J. W. Lam, B. Z. Tang, *Chem. Soc. Rev.* **2011**, *40*, 5361–5388.

[244] F. Würthner, *Angew. Chem. Int. Ed.* **2020**, *59*, 14192–14196.

[245] J. Feng, K. Tian, D. Hu, S. Wang, S. Li, Y. Zeng, Y. Li, G. Yang, *Angew. Chem. Int. Ed.* **2011**, *50*, 8072–8076.

[246] X. Liu, S. Li, J. Feng, Y. Li, G. Yang, *Chem. Commun.* **2014**, *50*, 2778–2780.

[247] G. Petersson, M. A. Al-Laham, *J. Chem. Phys.* **1991**, *94*, 6081–6090.

[248] G. Petersson, A. Bennett, T. G. Tensfeldt, M. A. Al-Laham, W. A. Shirley, J. Mantzaris, *J. Chem. Phys.* **1988**, *89*, 2193–2218.

[249] P. Bissinger, H. Braunschweig, A. Damme, C. Hörl, I. Krummenacher, T. Kupfer, *Angew. Chem. Int. Ed.* **2015**, *54*, 359–362.

[250] U. Eisner, J. Kuthan, *Chem. Rev.* **1972**, *72*, 1–42.

[251] R. Lavilla, *J. Chem. Soc., Perkin Trans. I* **2002**, 1141–1156.

[252] D. M. Stout, A. I. Meyers, *Chem. Rev.* **1982**, *82*, 223–243.

[253] C. L. Bird, A. T. Kuhn, *Chem. Soc. Rev.* **1981**, *10*, 49–82.

[254] C. -W. Chiu, Y. Kim, F. P. Gabbaï, *J. Am. Chem. Soc.* **2009**, *131*, 60–61.

[255] J. J. Murphy, D. Bastida, S. Paria, M. Fagnoni, P. Melchiorre, *Nature* **2016**, *532*, 218–222.

[256] S. A. Orr, A. R. Kennedy, J. J. Liggat, R. McLellan, R. E. Mulvey, S. D. Robertson, *Dalton Trans.* **2016**, *45*, 6234–6240.

[257] R. F. Francis, W. Davis, J. T. Wisener, *J. Org. Chem.* **1974**, *39*, 59–62.

[258] S. D. Robertson, A. R. Kennedy, J. J. Liggat, R. E. Mulvey, *Chem. Commun.* **2015**, *51*, 5452–5455.

[259] K. Leduskrasts, E. Suna, *RSC Adv.* **2019**, *9*, 460–465.

[260] Z. Yuan, C. D. Entwistle, J. C. Collings, D. Albesa-Jové, A. S. Batsanov, J. A. K. Howard, N. J. Taylor, H. M. Kaiser, D. E. Kaufmann, S. -Y. Poon, W. -Y. Wong, C. Jardin, S. Fathallah, A. Boucekkine, J. -F. Halet, T. B. Marder, *Chem. Eur. J.* **2006**, *12*, 2758–2771.

[261] R. Stahl, C. Lambert, C. Kaiser, R. Wortmann, R. Jakober, *Chem. Eur. J.* **2006**, *12*, 2358–2370.

[262] C. Lee, W. Yang, R. G. Parr, *Phys. Rev. B: Condens. Matter Mater. Phys.* **1988**, *37*, 785–789.

[263] J. L. Bredas, R. Silbey, D. S. Boudreaux, R. R. Chance, *J. Am. Chem. Soc.* **1983**, *105*, 6555–6559.

[264] D. Reitzenstein, T. Quast, F. Kanal, M. Kullmann, S. Ruetzel, M. S. Hammer, C. Deibel, V. Dyakonov, T. Brixner, C. Lambert, *Chem. Mater.* **2010**, *22*, 6641–6655.

[265] A. Pron, G. Zhou, H. Norouzi-Arasi, M. Baumgarten, K. Müllen, *Org. Lett.* **2009**, *11*, 3550–3553.

[266] P. Chen, F. Jäkle, *J. Am. Chem. Soc.* **2011**, *133*, 20142–20145.

[267] P. Chen, R. A. Lalancette, F. Jäkle, *Angew. Chem. Int. Ed.* **2012**, *51*, 7994–7998.

[268] P. Chen, X. Yin, N. Baser-Kirazli, F. Jäkle, *Angew. Chem. Int. Ed.* **2015**, *54*, 10768–10772.

[269] P. Chen, A. S. Marshall, S. H. Chi, X. Yin, J. W. Perry, F. Jäkle, *Chem. Eur. J.* **2015**, *21*, 18237–18247.

[270] A. Sengupta, A. Doshi, F. Jäkle, R. M. Peetz, *J. Polym. Sci., Part A: Polym. Chem.* **2015**, *53*,

1707–1718.

[271] A. Lik, L. Fritze, L. Müller, H. Helten, *J. Am. Chem. Soc.* **2017**, *139*, 5692–5695.

[272] A. Lik, S. Jenthra, L. Fritze, L. Müller, K. N. Truong, H. Helten, *Chem. Eur. J.* **2018**, *24*, 11961–11972.

[273] D. Li, G. Kagan, R. Hopson, P. G. Williard, *J. Am. Chem. Soc.* **2009**, *131*, 5627–5634.

[274] E. Khaskin, P. Y. Zavalij, A. N. Vedernikov, *J. Am. Chem. Soc.* **2006**, *128*, 13054–13055.

[275] E. Khaskin, P. Y. Zavalij, A. N. Vedernikov, *Angew. Chem. Int. Ed.* **2007**, *46*, 6309–6312.

[276] E. Khaskin, P. Y. Zavalij, A. N. Vedernikov, *J. Am. Chem. Soc.* **2008**, *130*, 10088–10089.

[277] E. Khaskin, D. L. Lew, S. Pal, A. N. Vedernikov, *Chem. Commun.* **2009**, 45, 6270–6272.

[278] S. Pal, A. N. Vedernikov, *Dalton Trans.* **2012**, *41*, 8116–8122.

[279] S. Pal, P. Zavalij, A. N. Vedernikov, *Chem. Commun.* **2014**, *50*, 5376–5378.

[280] S. Pal, P. Y. Zavalij, A. N. Vedernikov, *Organometallics* **2015**, *34*, 5183–5190.

[281] B. L. Conley, T. J. Williams, *J. Am. Chem. Soc.* **2010**, *132*, 1764–1765.

[282] B. L. Conley, D. Guess, T. J. Williams, *J. Am. Chem. Soc.* **2011**, *133*, 14212–14215.

[283] Z. Lu, B. Malinoski, A. V. Flores, B. L. Conley, D. Guess, T. J. Williams, *Catalysts* **2012**, *2*, 412–421.

[284] J. A. Celaje, M. K. Pennington-Boggio, R. W. Flaig, M. G. Richmond, T. J. Williams, *Organometallics* **2014**, *33*, 2019–2026.

[285] V. A. Krylova, P. I. Djurovich, B. L. Conley, R. Haiges, M. T. Whited, T. J. Williams, M. E. Thompson, *Chem. Commun.* **2014**, *50*, 7176–7179.

[286] S. Shi, P. I. Djurovich, M. E. Thompson, *Inorg. Chim. Acta* **2018**, *482*, 246–251.

[287] M. K. Pennington-Boggio, B. L. Conley, M. G. Richmond, T. J. Williams, *Polyhedron* **2014**, *84*, 24–31.

[288] T. G. Hodgkins, D. R. Powell, *Inorg. Chem.* **1996**, *35*, 2140–2148.

[289] K. Hensen, A. Lemke, T. Stumpf, M. Bolte, H. Fleischer, C. R. Pulham, R. O. Gould, S. Harris, *Inorg. Chem.* **1999**, 38, 4700–4704.

[290] R. García-Rodríguez, D. Wright, *Chem. Eur. J.* **2015**, *21*, 14949–14957.

[291] R. García-Rodríguez, S. Hanf, A. D. Bond, D. S. Wright, *Chem. Commun.* **2017**, *53*, 1225–1228.

[292] Á. García-Romero, A. J. Plajer, L. Álvarez-Miguel, A. D. Bond, D. S. Wright, R. García-Rodríguez, *Chem. Eur. J.* **2018**, *24*, 17019–17026.

[293] A. J. Plajer, S. Kopf, A. L. Colebatch, A. D. Bond, D. S. Wright, R. García-Rodríguez, *Dalton Trans.* **2019**, *48*, 5692–5697.

[294] S. -F. Liu, Q. Wu, H. L. Schmider, H. Aziz, N. -X. Hu, Z. Popović, S. Wang, *J. Am. Chem. Soc.* **2000**, *122*, 3671–3678.

[295] X. Bantreil, S. P. Nolan, *Nat. Protoc.* **2011**, *6*, 69.

[296] P. Bissinger, H. Braunschweig, A. Damme, I. Krummenacher, A. K. Phukan, K. Radacki, S. Sugawara, *Angew. Chem. Int. Ed.* **2014**, *53*, 7360–7363.

[297] G. M. Sheldrick, *Acta Crystallogr. Sect. A* **2015**, *71*, 3–8.

[298] G. M. Sheldrick, *Acta Crystallogr. Sect. A* **2008**, *64*, 112–122.

[299] C. B. Hübschle, G. M. Sheldrick, B. Dittrich, *J. Appl. Crystallogr.* **2011**, *44*, 1281–1284.

[300] K. Brandenburg, C. Diamond, M. S. Visualization, See also: *http://crystalimpact.com/diamond* ***2016***.

[301] C. F. Macrae, I. J. Bruno, J. A. Chisholm, P. R. Edgington, P. McCabe, E. Pidcock, L. Rodriguez-Monge, R. Taylor, J. Streek, P. A. Wood, *J. Appl. Crystallogr.* **2008**, *41*, 466–470.

[302] F. B. Dias, T. J. Penfold, A. P. Monkman, *Methods Appl. Fluoresc.* **2017**, *5*, 012001.

[303] M. J. Frisch, G. W. Trucks, H. B. Schlegel, G. E. Scuseria, M. A. Robb, J. R. Cheeseman, G. Scalmani, V. Barone, G. A. Petersson, H. Nakatsuji, X. Li, M. Caricato, A. V. Marenich, J. Bloino, B. G. Janesko, R. Gomperts, B. Mennucci, H. P. Hratchian, J. V. Ortiz, A. F. Izmaylov, J. L. Sonnenberg, Williams, F. Ding, F. Lipparini, F. Egidi, J. Goings, B. Peng, A. Petrone, T. Henderson, D. Ranasinghe, V. G. Zakrzewski, J. Gao, N. Rega, G. Zheng, W. Liang, M. Hada, M. Ehara, K. Toyota, R. Fukuda, J. Hasegawa, M. Ishida, T. Nakajima, Y. Honda, O. Kitao, H. Nakai, T. Vreven, K. Throssell, J. A. Montgomery Jr., J. E. Peralta, F. Ogliaro, M. J. Bearpark, J. J. Heyd, E. N. Brothers, K. N. Kudin, V. N. Staroverov, T. A. Keith, R. Kobayashi, J. Normand, K. Raghavachari, A. P. Rendell, J. C. Burant, S. S. Iyengar, J. Tomasi, M. Cossi, J. M. Millam, M. Klene, C. Adamo, R. Cammi, J. W. Ochterski, R. L. Martin, K. Morokuma, O. Farkas, J. B. Foresman, D. J. Fox, Computer Program, **2016**.

[304] M. D. Hanwell, D. E. Curtis, D. C. Lonie, T. Vandermeersch, E. Zurek, G. R. Hutchison, *J. Cheminformatics* **2012**, *4*, 17.

[305] T. Lu, F. Chen, *J. Comput. Chem.* **2012**, *33*, 580–592.

[306] C. Lee, W. Yang, R. G. Parr, *Rev. B: Condens. Matter Mater. Phys.* **1988**, *37*, 785.

[307] S. Grimme, *Chem. Eur. J.* **2004**, *10*, 3423–3429.

[308] J. Tomasi, B. Mennucci, R. Cammi, *Chem. Rev.* **2005**, *105*, 2999–3094.

9 Appendix

9.1 NMR spectra

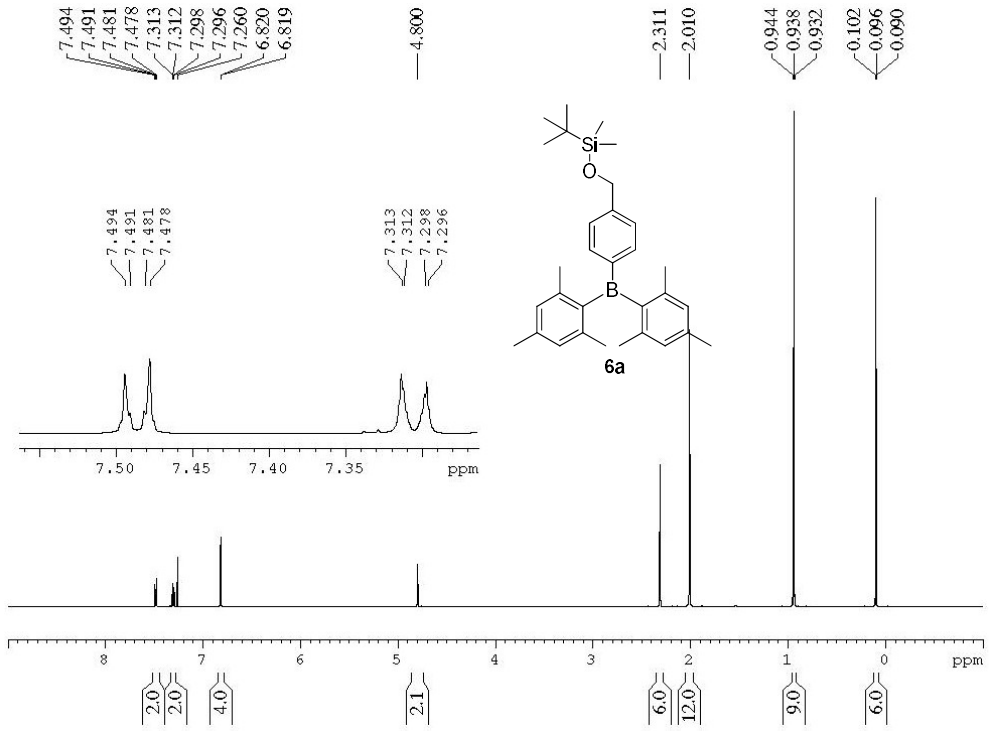

Figure 9.1-1. ^{1}H NMR spectrum of **6a** in $CDCl_3$ at 500 MHz.

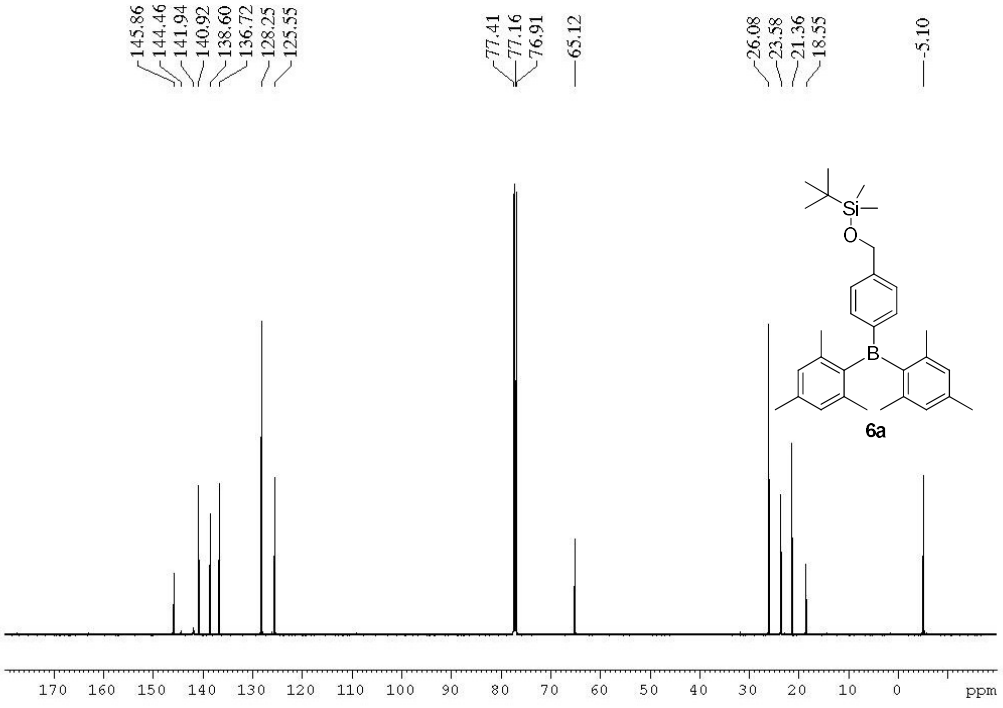

Figure 9.1-2. $^{13}C\{^{1}H\}$ NMR spectrum of **6a** in $CDCl_3$ at 125 MHz.

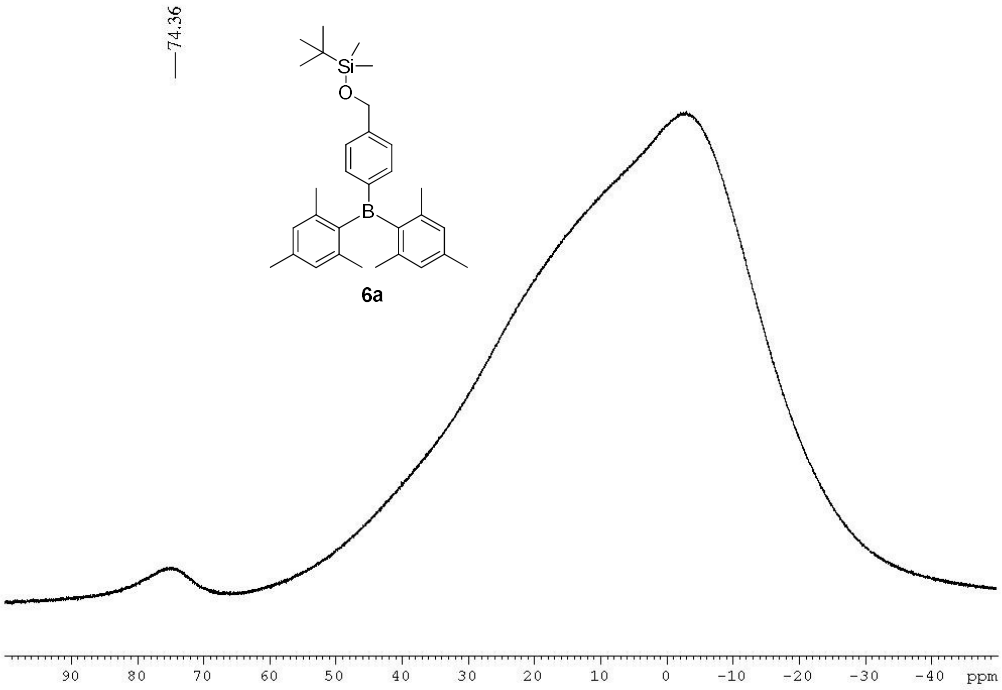

Figure 9.1-3. $^{11}B\{^{1}H\}$ NMR spectrum of **6a** in $CDCl_3$ at 160MHz.

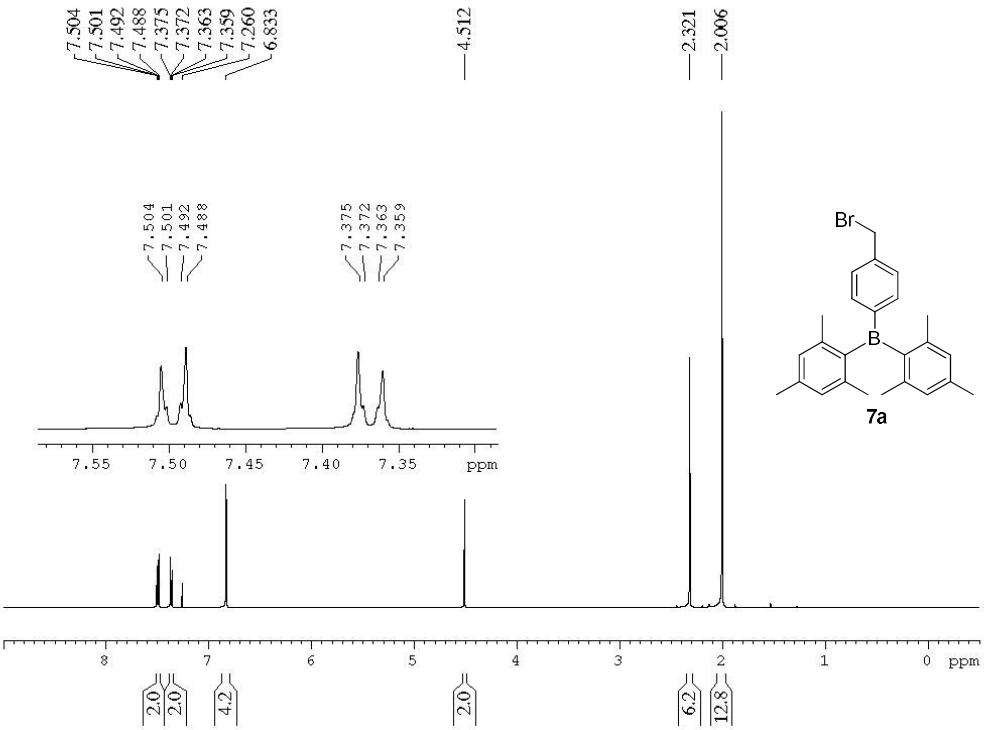

Figure 9.1-4. ^{1}H NMR spectrum of **7a** in $CDCl_3$ at 500 MHz.

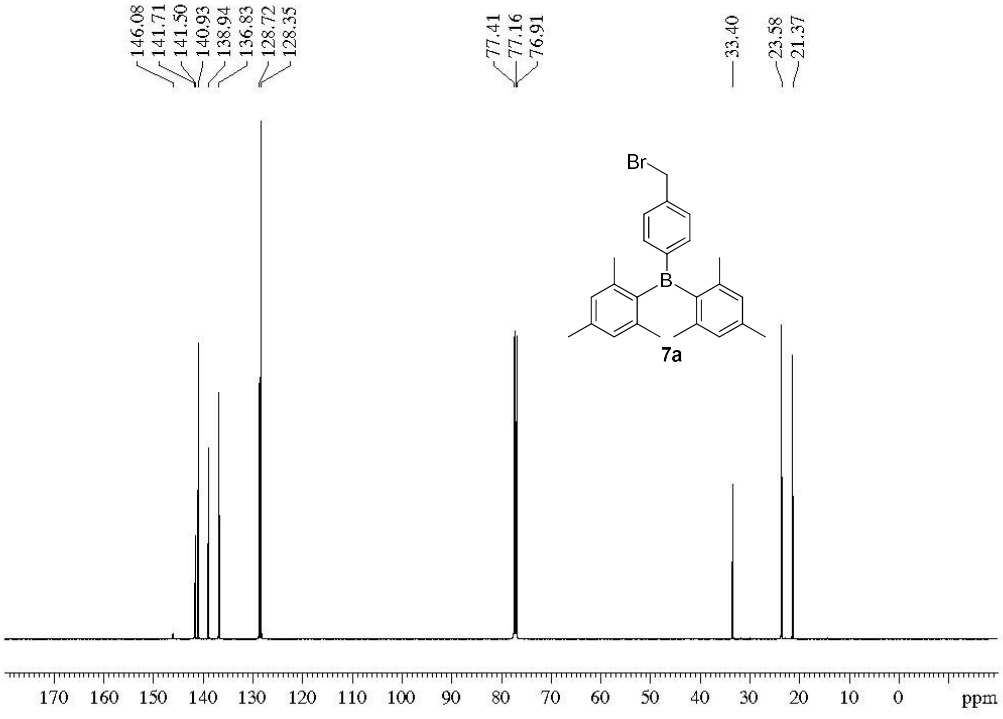

Figure 9.1-5. $^{13}C\{^{1}H\}$ NMR spectrum of **7a** in $CDCl_3$ at 125 MHz.

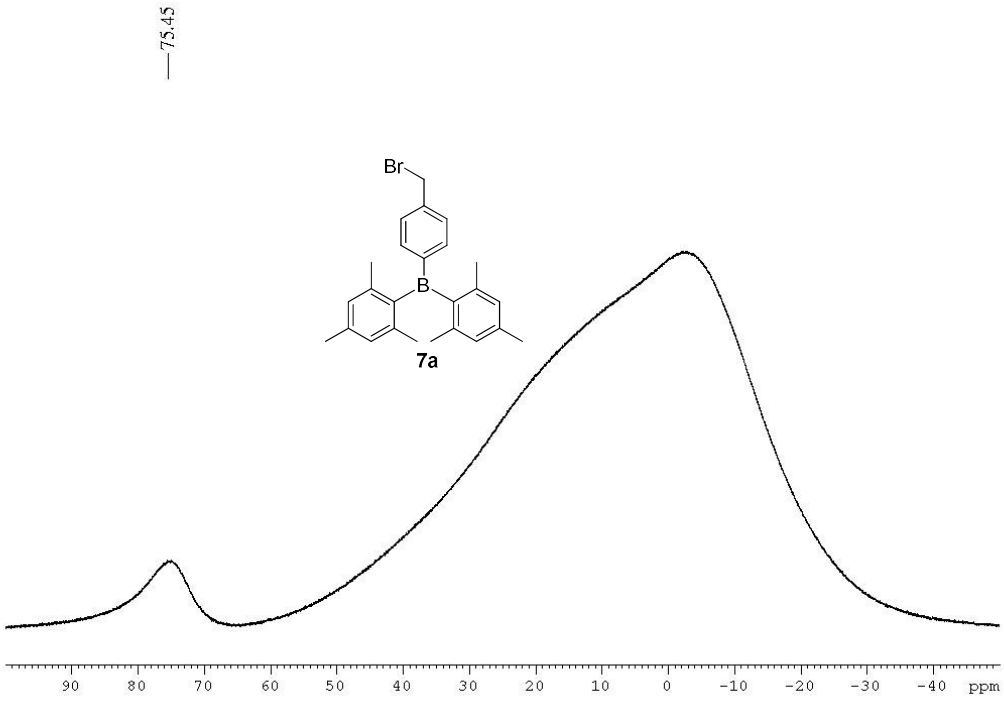

Figure 9.1-6. $^{11}B\{^{1}H\}$ NMR spectrum of **7a** in $CDCl_3$ at 160 MHz.

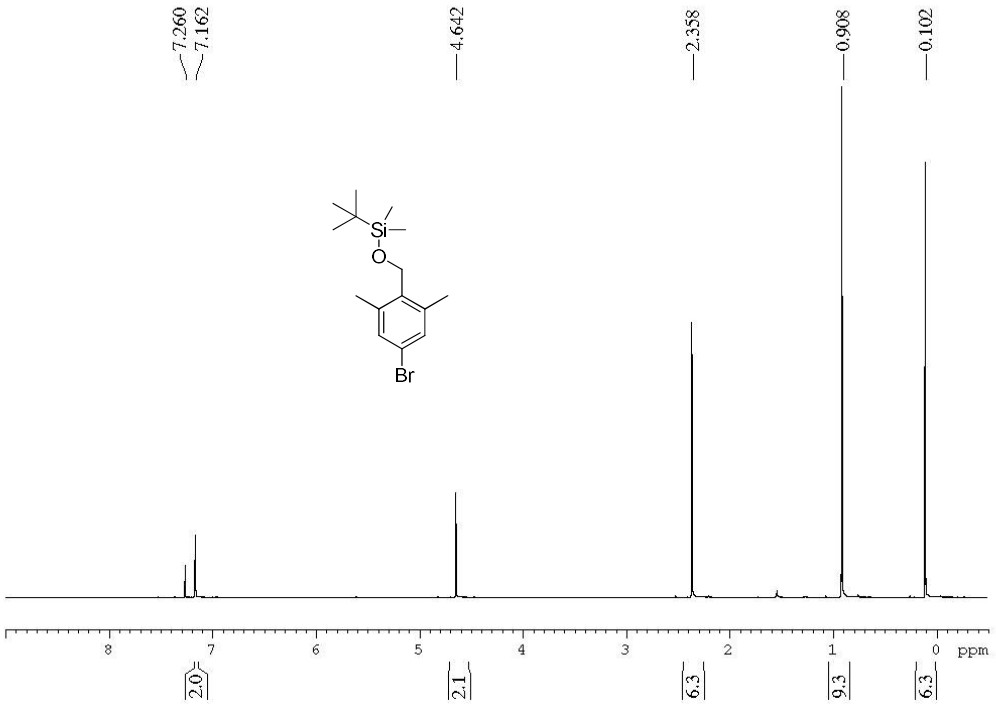

Figure 9.1-7. ^{1}H NMR spectrum of (4-bromo-2,6-dimethylbenzyloxy)(*tert*-butyl)dimethylsilane in $CDCl_3$ at 400 MHz.

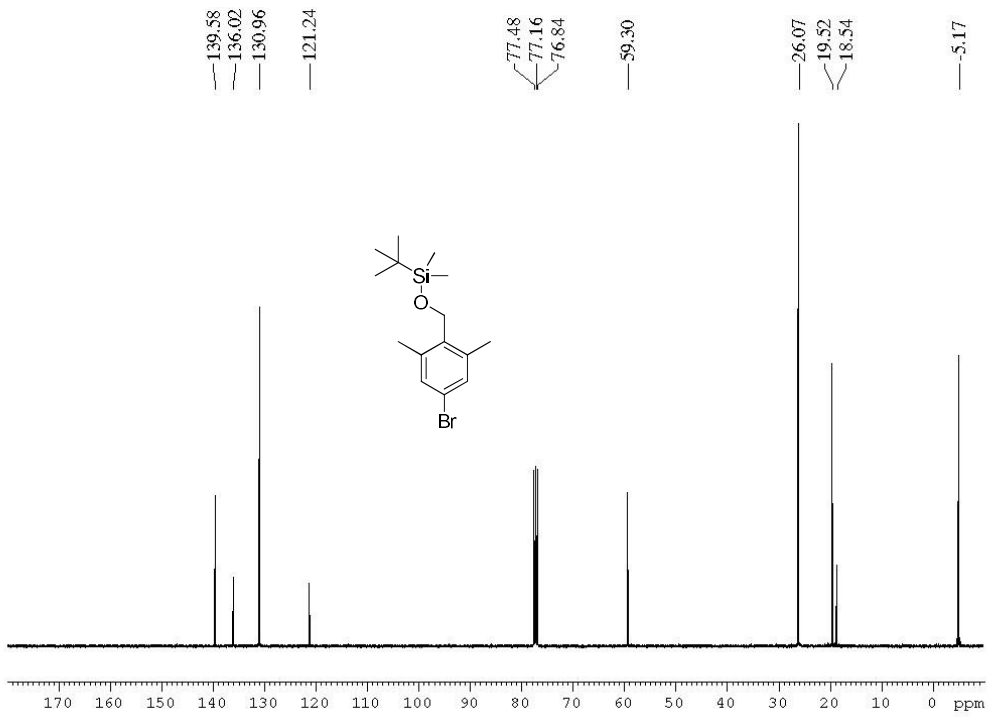

Figure 9.1-8. $^{13}C\{^{1}H\}$ NMR spectrum of (4-bromo-2,6-dimethylbenzyloxy)(*tert*-butyl) dimethylsilane in $CDCl_3$ at 100 MHz.

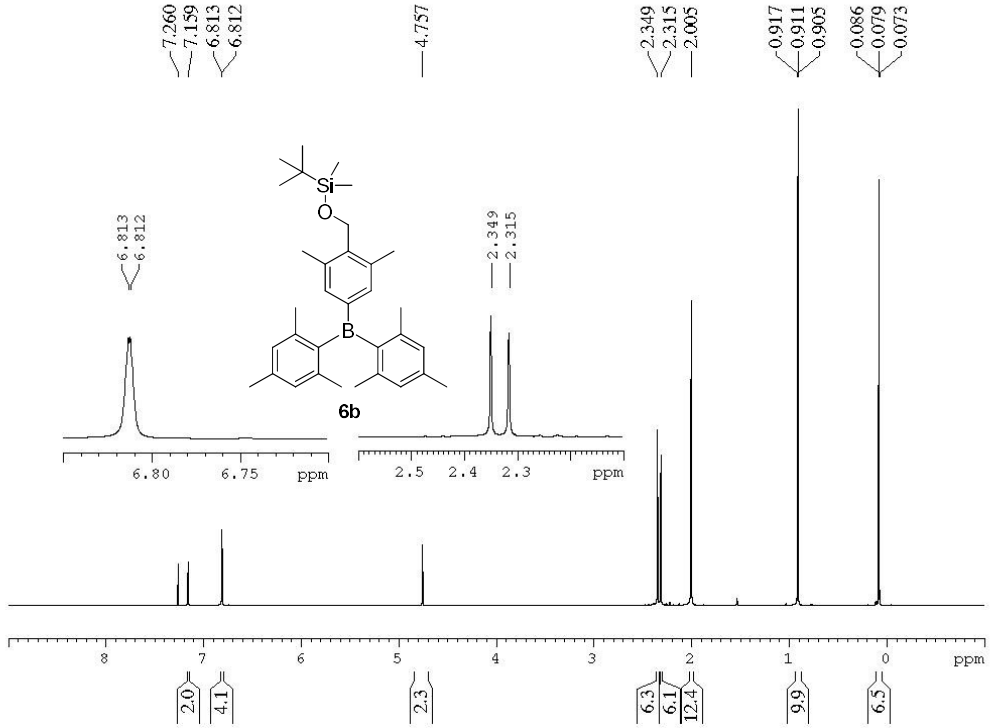

Figure 9.1-9. ^{1}H NMR spectrum of **6b** in $CDCl_3$ at 500 MHz.

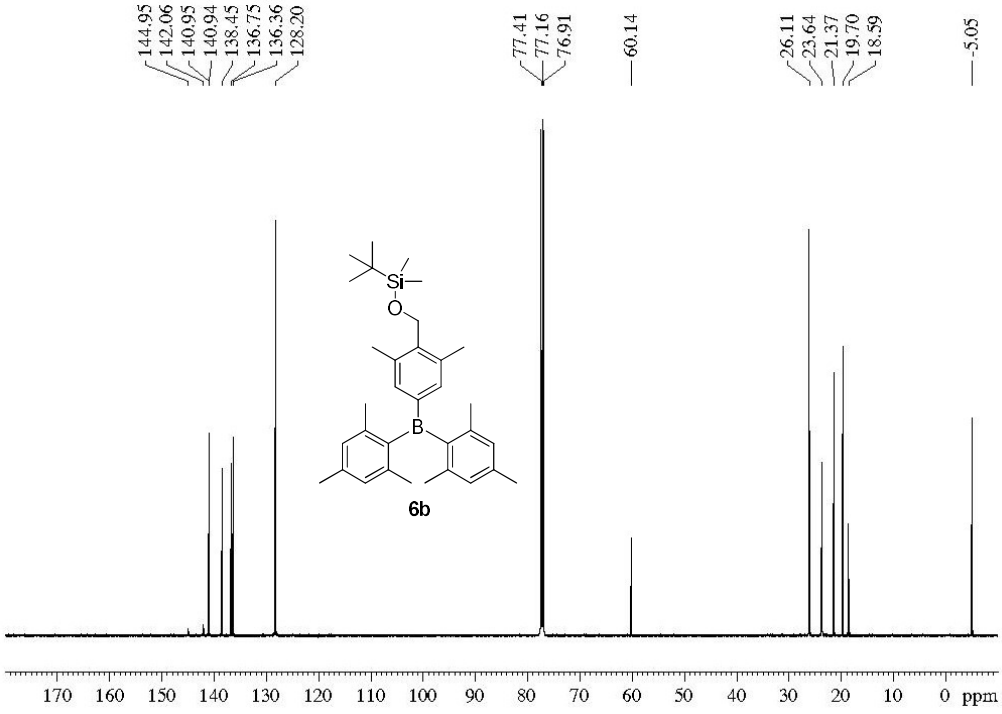

Figure 9.1-10. $^{13}C\{^{1}H\}$ NMR spectrum of **6b** in $CDCl_3$ at 125 MHz.

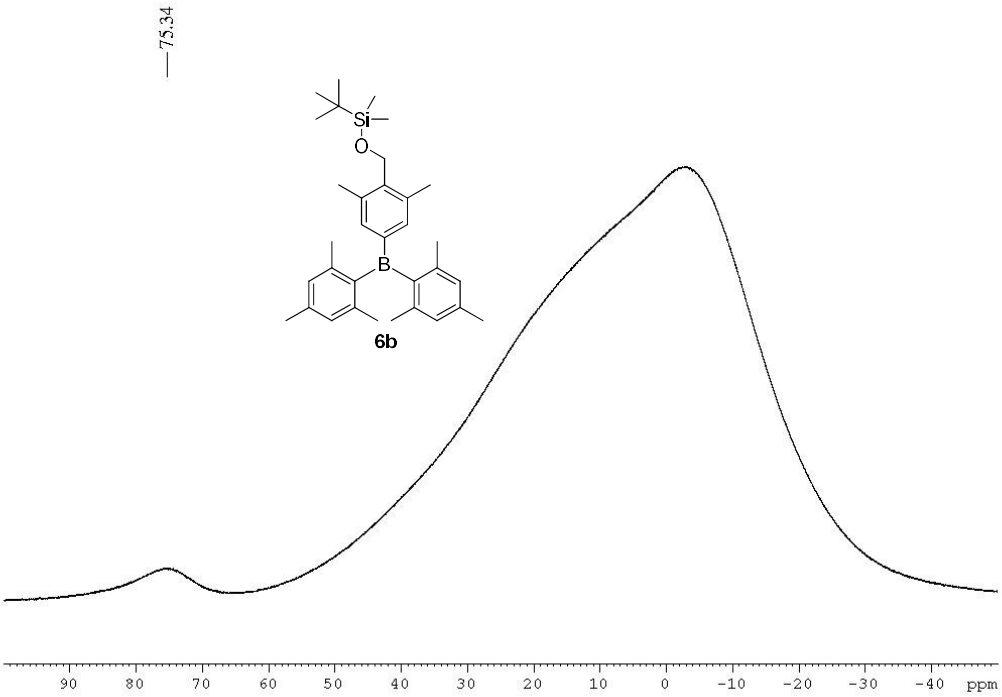

Figure 9.1-11. $^{11}B\{^{1}H\}$ NMR spectrum of **6b** in $CDCl_3$ at 160 MHz.

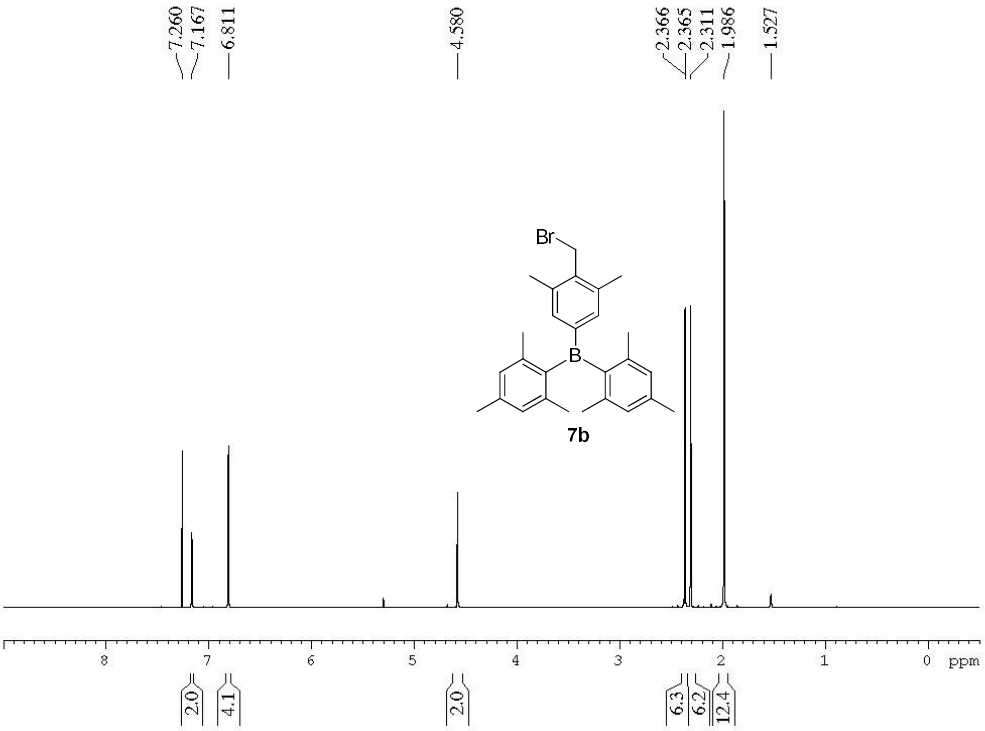

Figure 9.1-12. ^{1}H NMR spectrum of **7b** in $CDCl_3$ at 500 MHz.

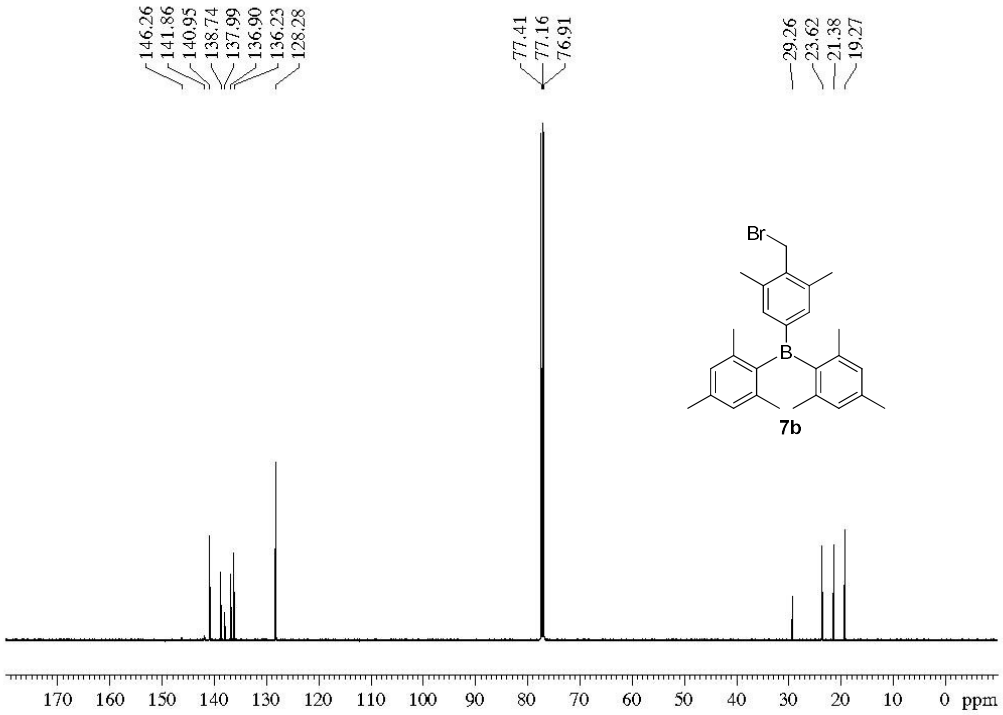

Figure 9.1-13. $^{13}C\{^{1}H\}$ NMR spectrum of **7b** in $CDCl_3$ at 125 MHz.

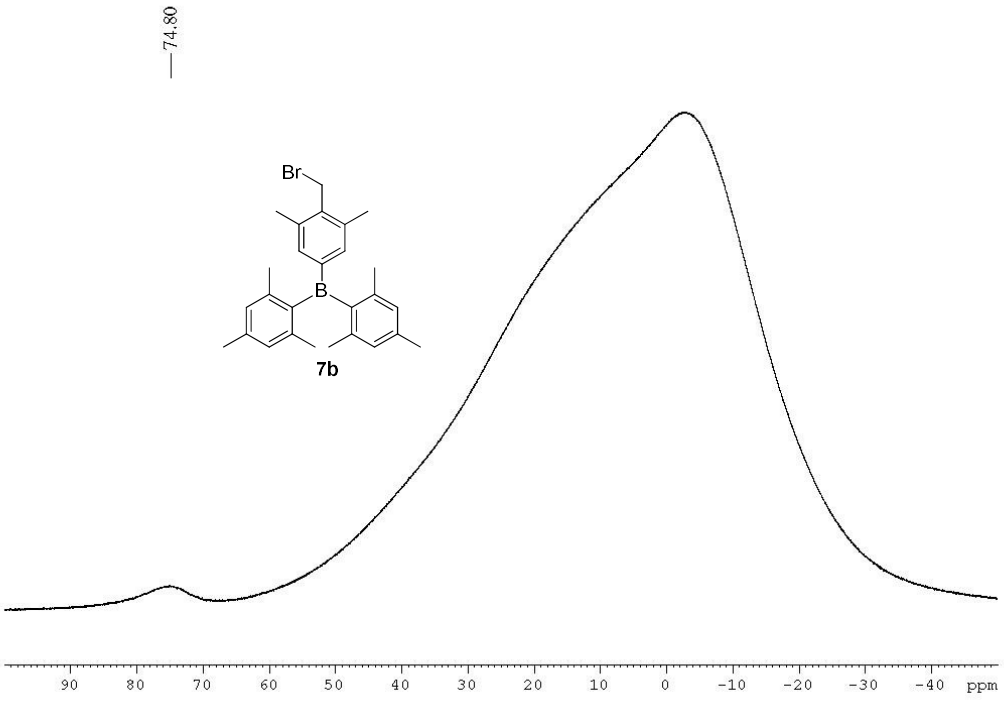

Figure 9.1-14. $^{11}B\{^{1}H\}$ NMR spectrum of **7b** in $CDCl_3$ at 160 MHz.

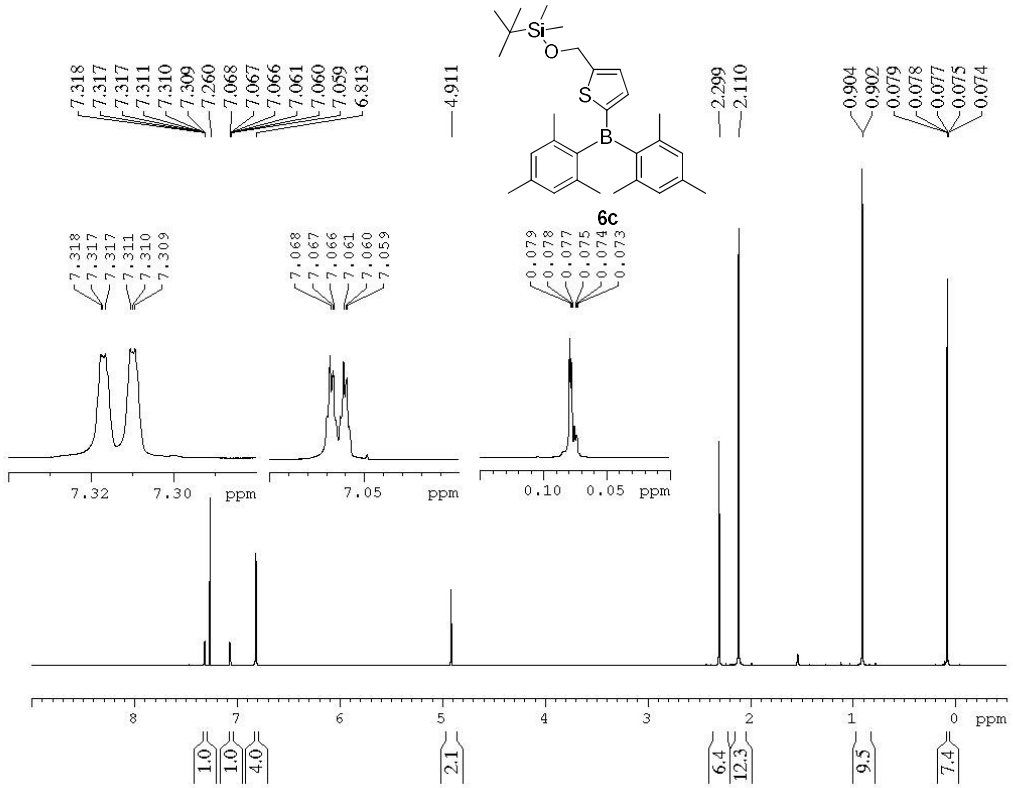

Figure 9.1-15. ^{1}H NMR spectrum of **6c** in $CDCl_3$ at 500 MHz.

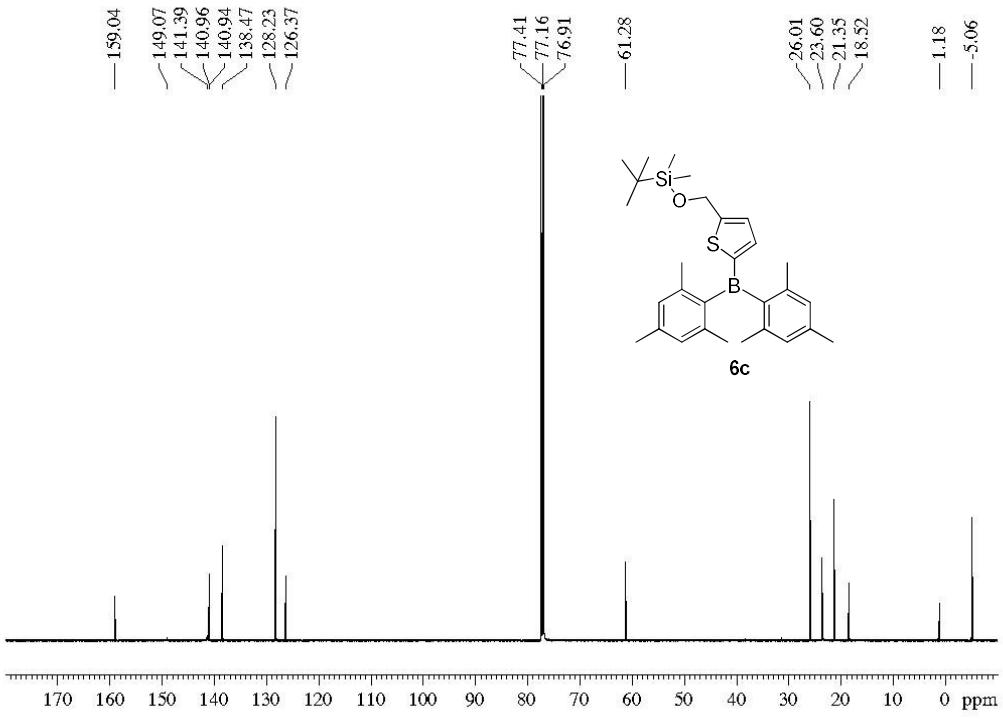

Figure 9.1-16. $^{13}C\{^{1}H\}$ NMR spectrum of **6c** in $CDCl_3$ at 125 MHz.

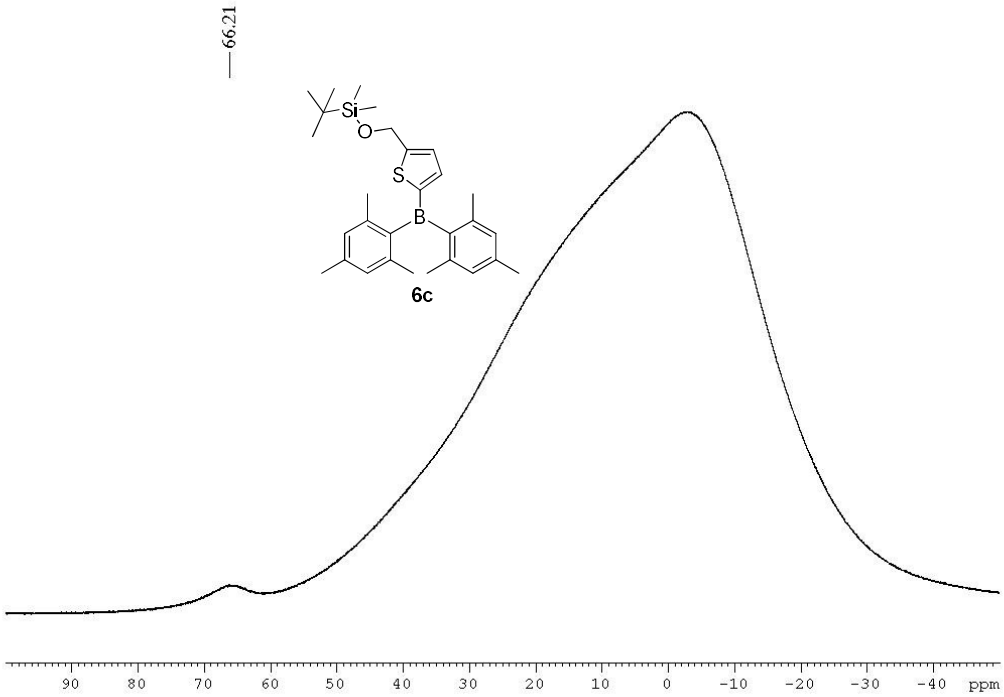

Figure 9.1-17. $^{11}B\{^{1}H\}$ NMR spectrum of **6c** in $CDCl_3$ at 160 MHz.

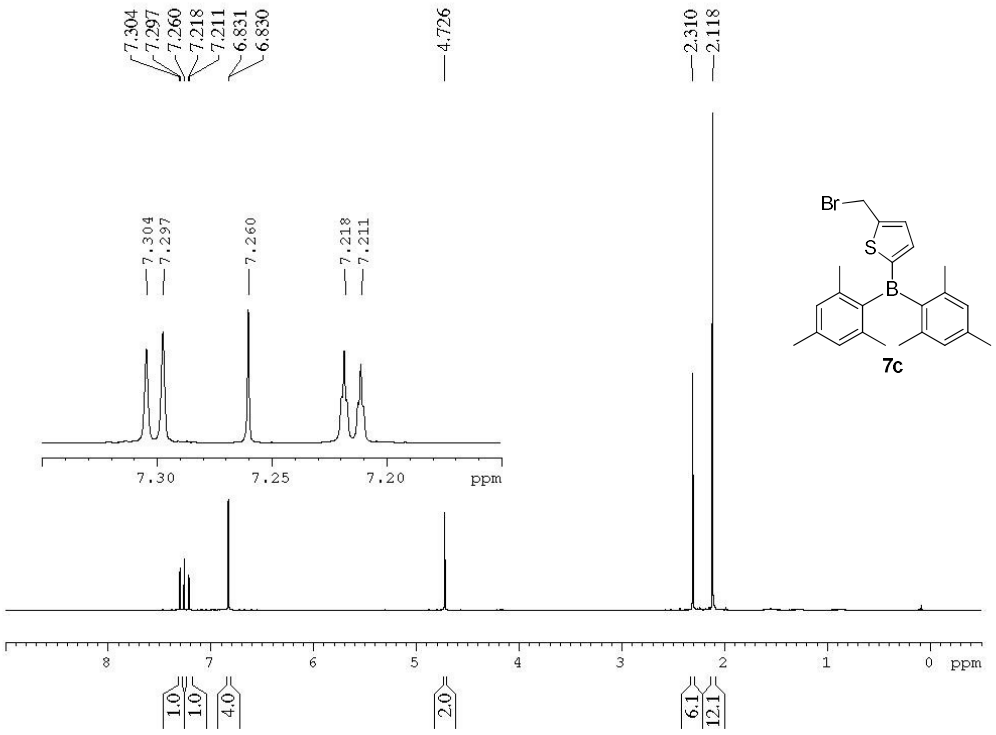

Figure 9.1-18. ^{1}H NMR spectrum of **7c** in $CDCl_3$ at 500 MHz.

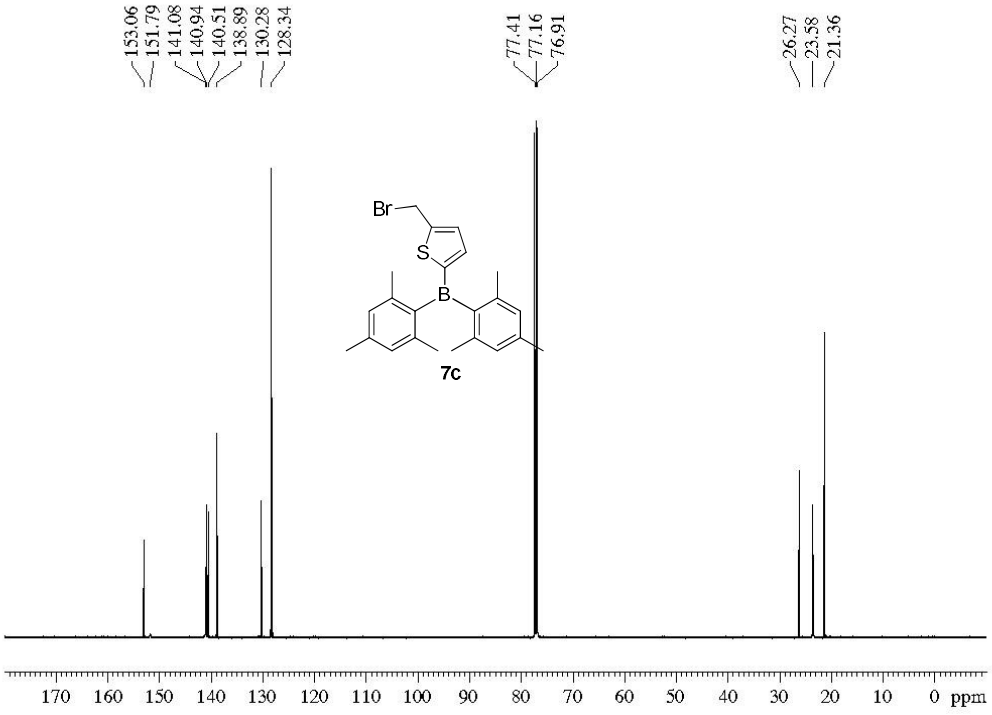

Figure 9.1-19. $^{13}C\{^{1}H\}$ NMR spectrum of **7c** in $CDCl_3$ at 125 MHz.

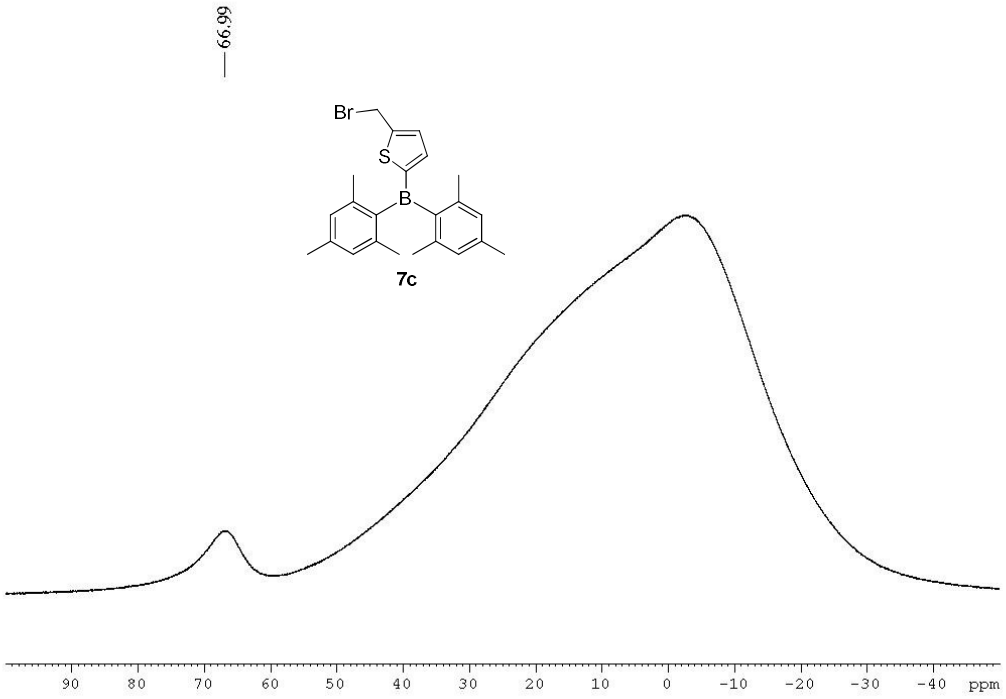

Figure 9.1-20. $^{11}B\{^{1}H\}$ NMR spectrum of **7c** in $CDCl_3$ at 160 MHz.

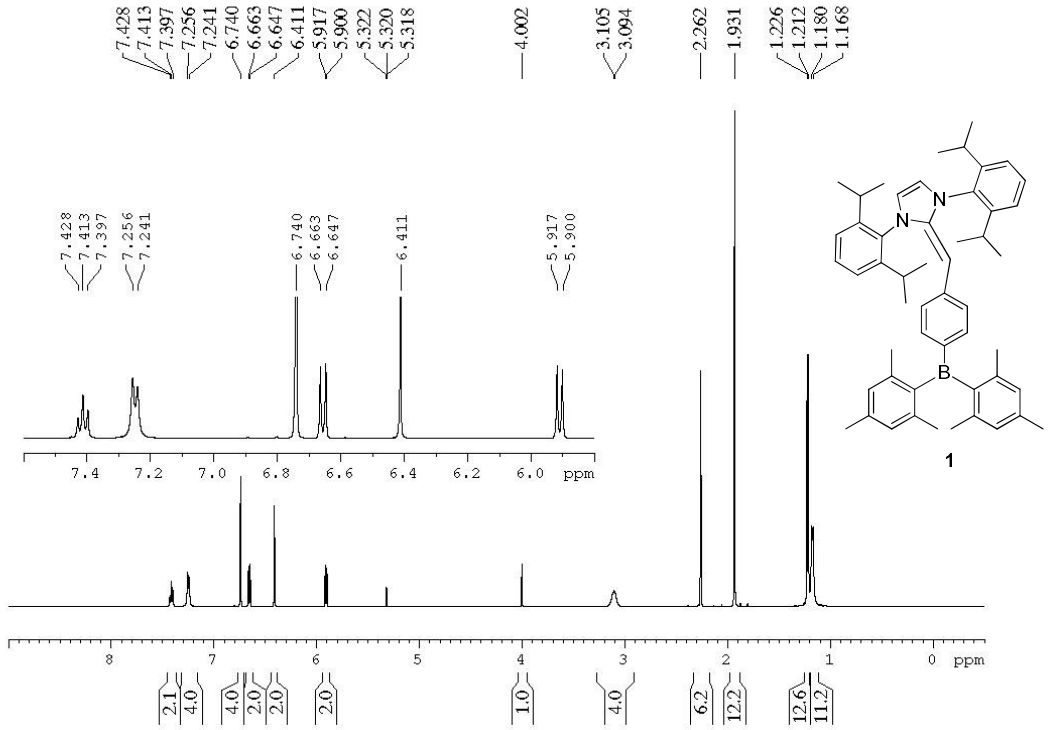

Figure 9.1-21. ^{1}H NMR spectrum of **1** in CD_2Cl_2 at 500 MHz.

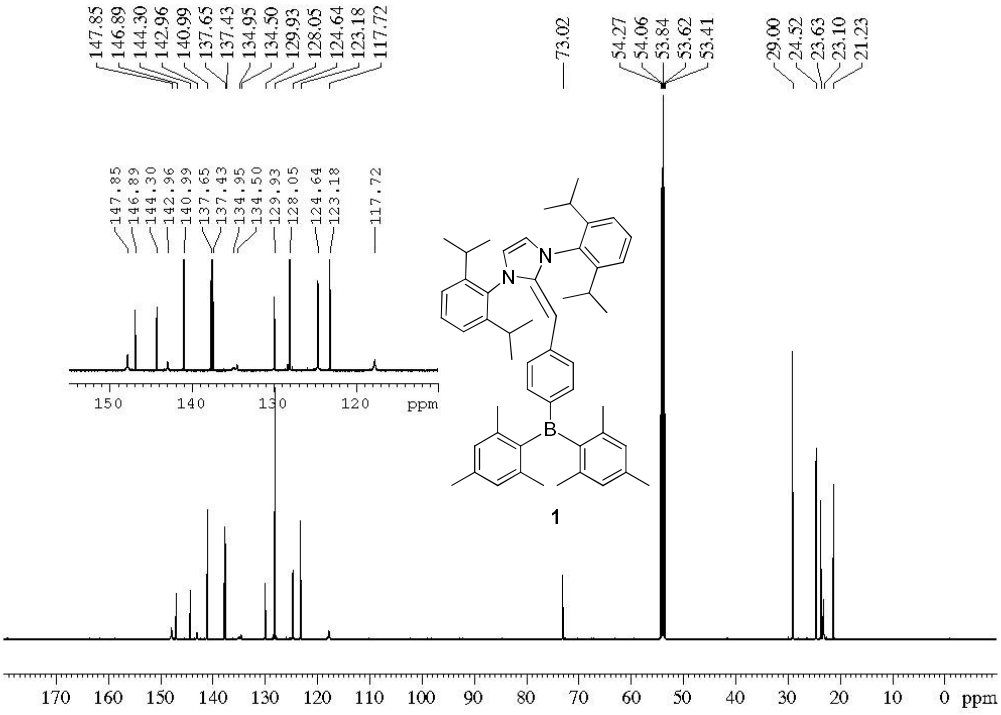

Figure 9.1-22. $^{13}C\{^{1}H\}$ NMR spectrum of **1** in CD_2Cl_2 at 125 MHz.

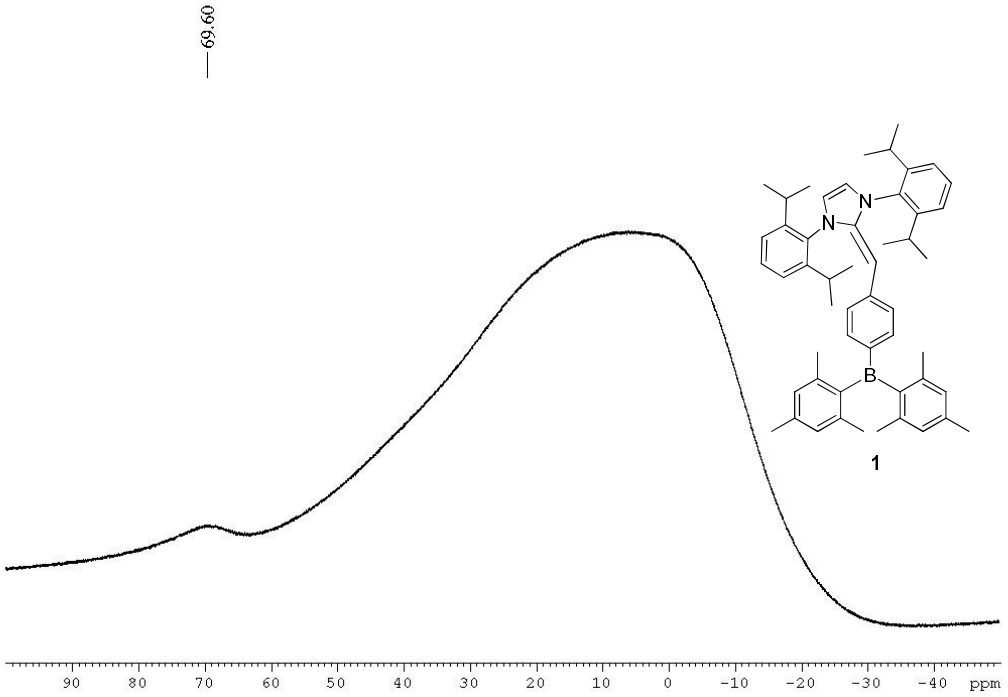

Figure 9.1-23. $^{11}B\{^1H\}$ NMR spectrum of **1** in CD_2Cl_2 at 160 MHz.

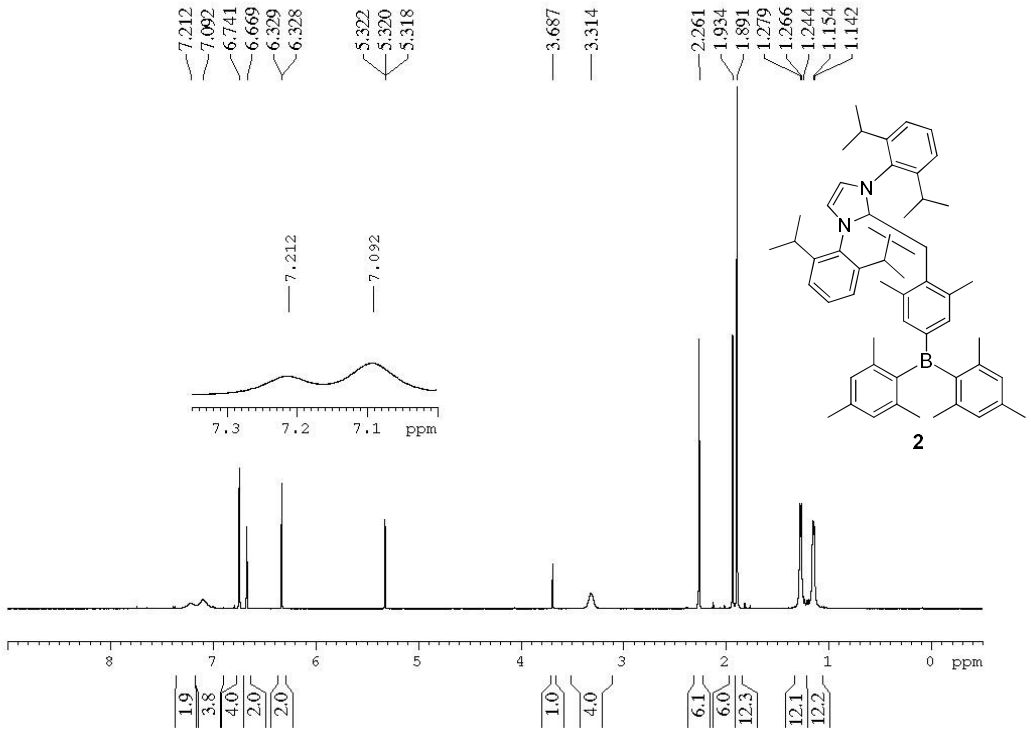

Figure 9.1-24. ^1H NMR spectrum of **2** in CD_2Cl_2 at 500 MHz.

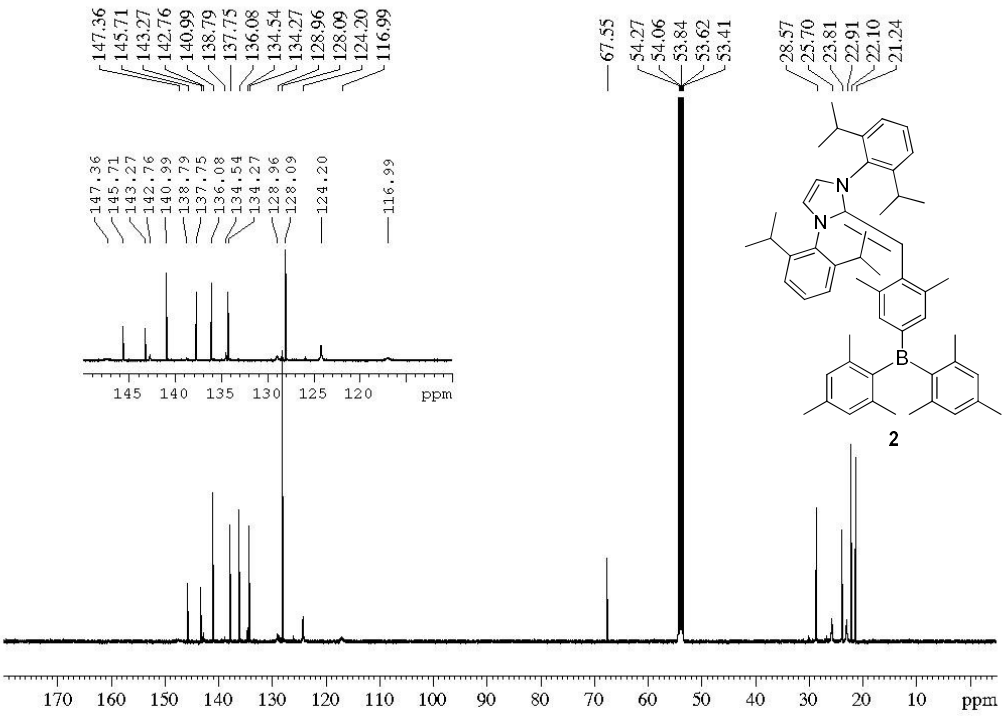

Figure 9.1-25. $^{13}C\{^{1}H\}$ NMR spectrum of **2** in CD_2Cl_2 at 125 MHz.

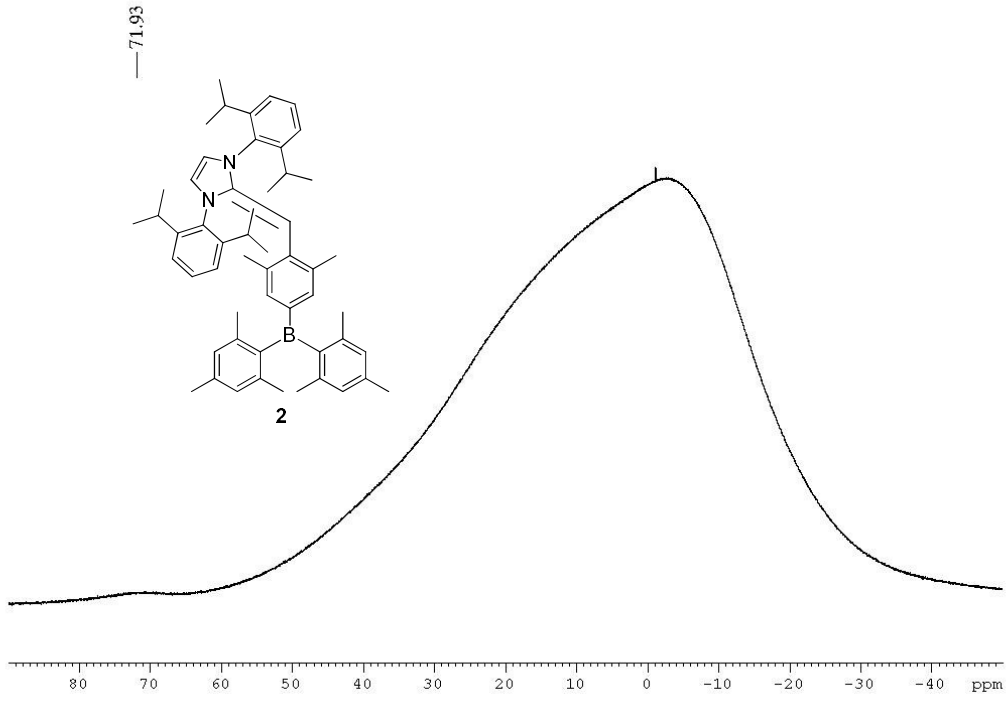

Figure 9.1-26. $^{11}B\{^{1}H\}$ NMR spectrum of **2** in CD_2Cl_2 at 160 MHz.

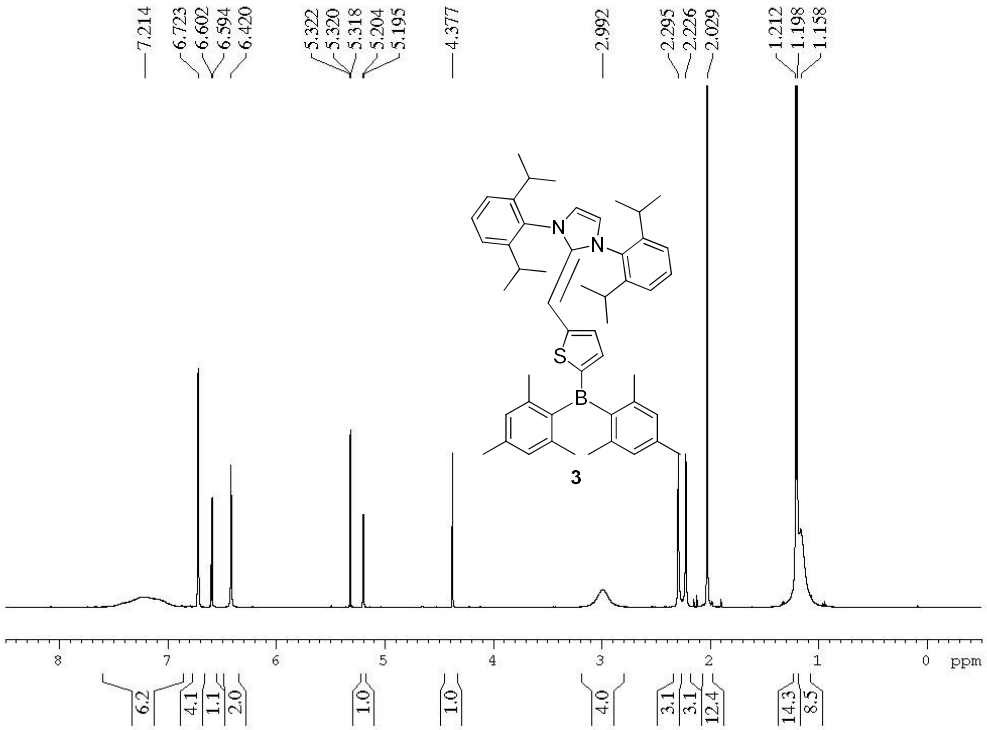

Figure 9.1-27. ^{1}H NMR spectrum of **3** in CD_2Cl_2 at 500 MHz.

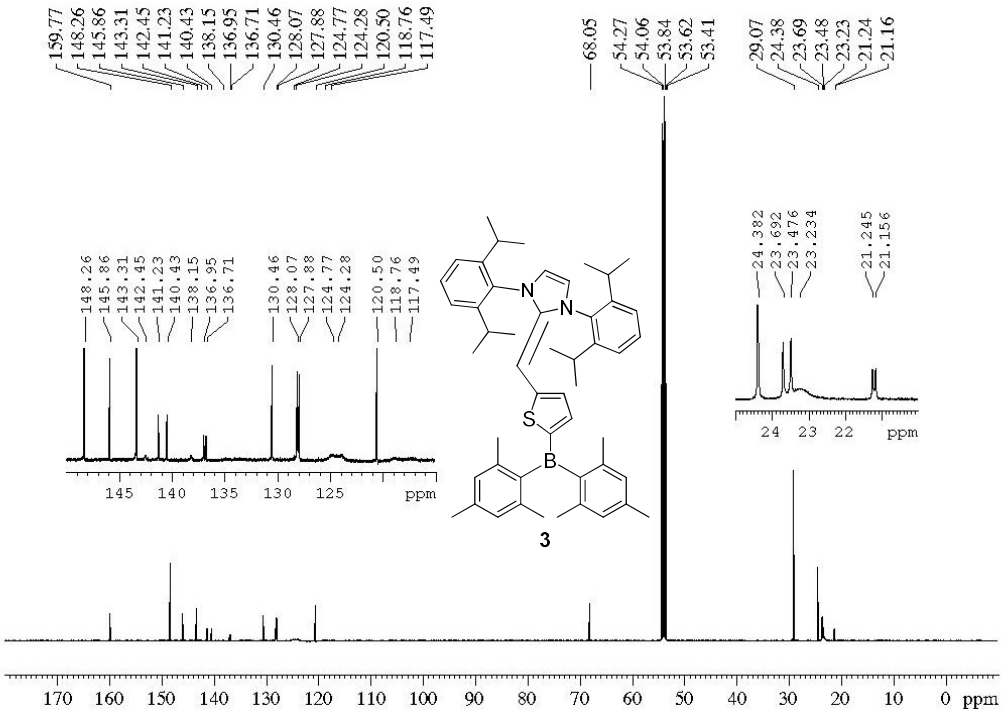

Figure 9.1-28. $^{13}C\{^{1}H\}$ NMR spectrum of **3** in CD_2Cl_2 at 125 MHz.

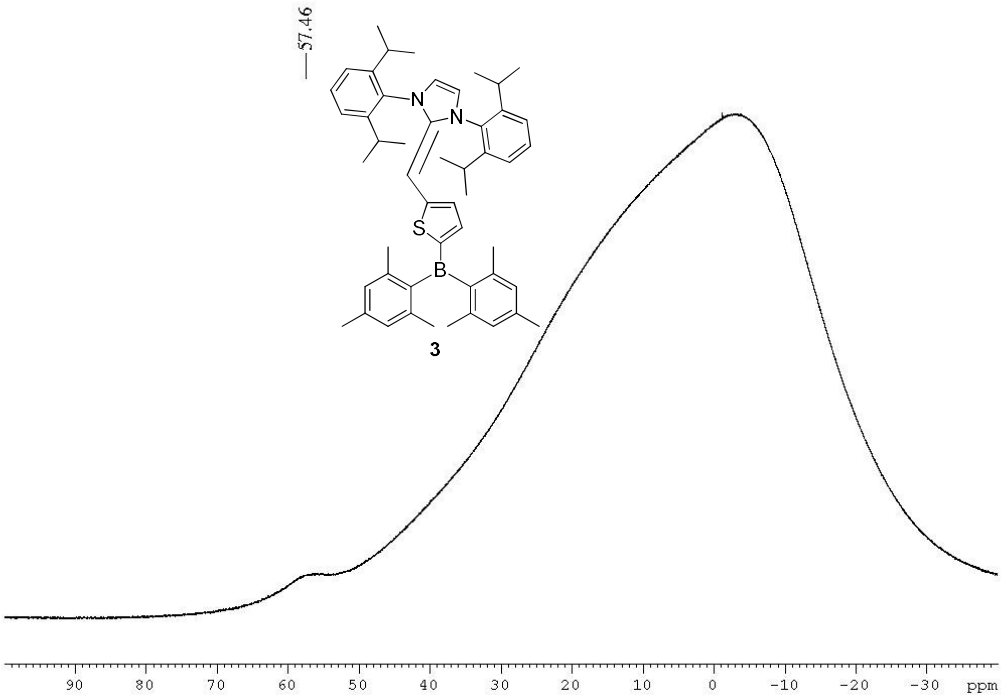

Figure 9.1-29. $^{11}B\{^1H\}$ NMR spectrum of **3** in CD_2Cl_2 at 160 MHz.

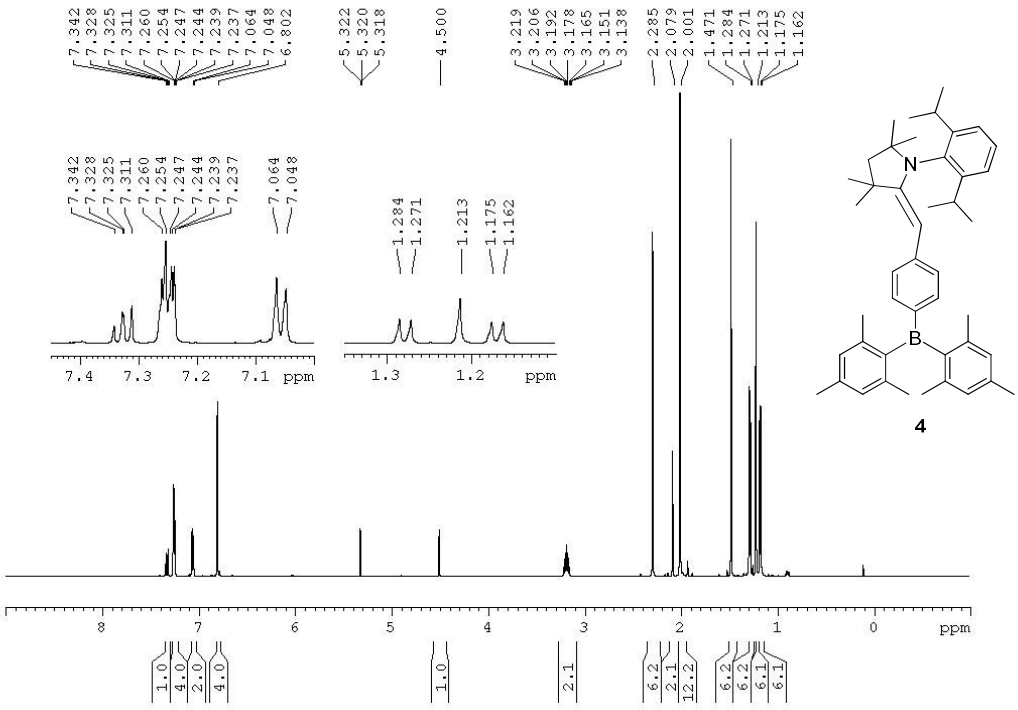

Figure 9.1-30. ^1H NMR spectrum of **4** in CD_2Cl_2 at 500 MHz.

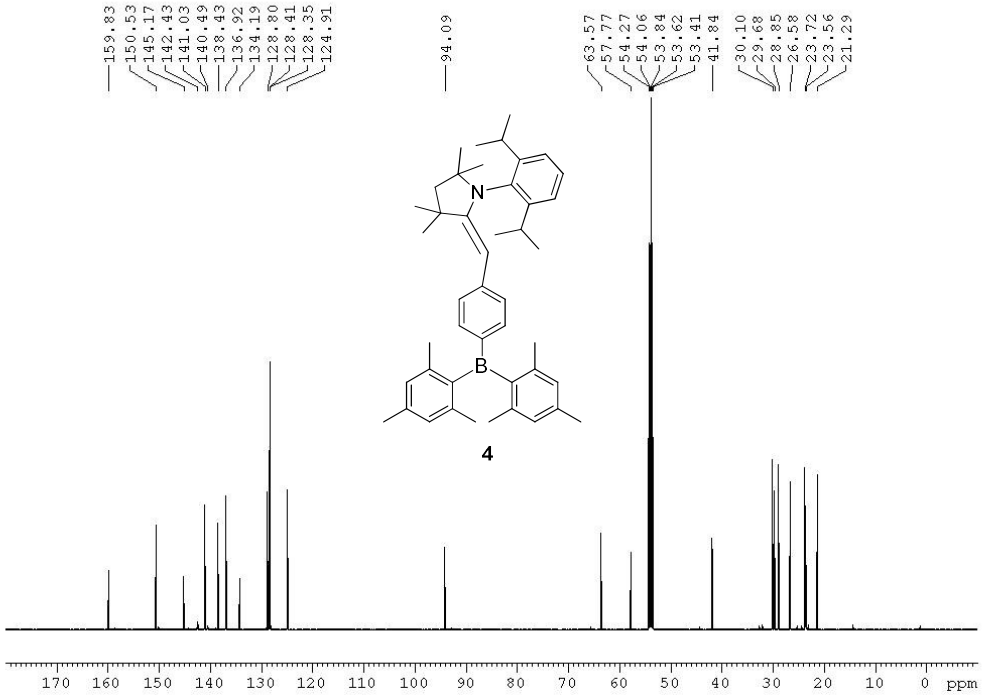

Figure 9.1-31. $^{13}C\{^{1}H\}$ NMR spectrum of **4** in CD_2Cl_2 at 125 MHz.

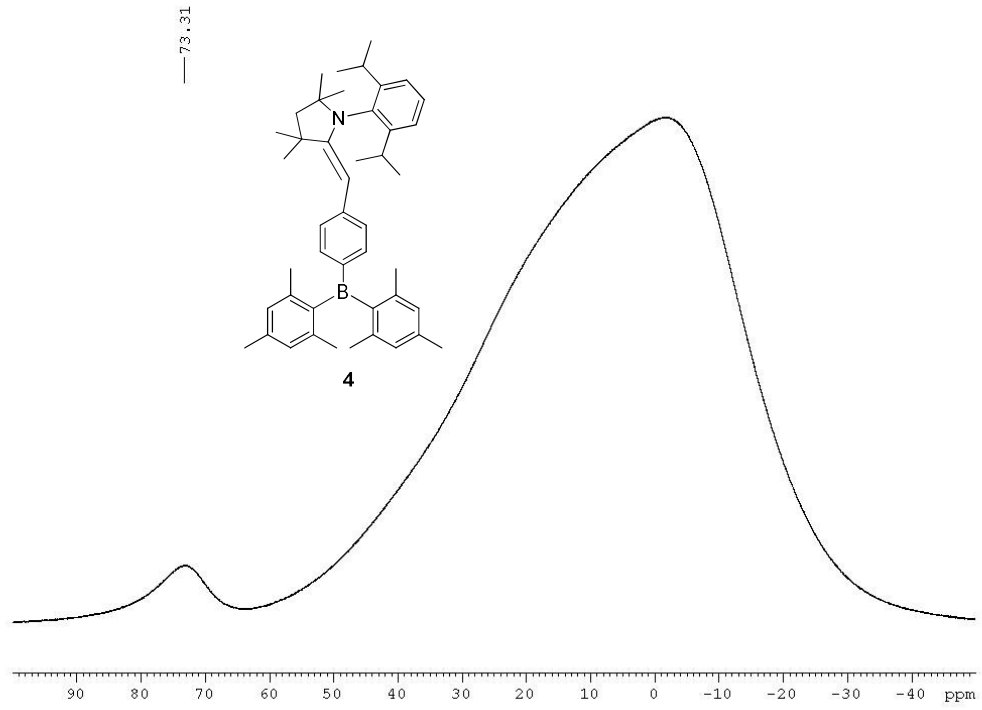

Figure 9.1-32. $^{11}B\{^{1}H\}$ NMR spectrum of **4** in CD_2Cl_2 at 160 MHz.

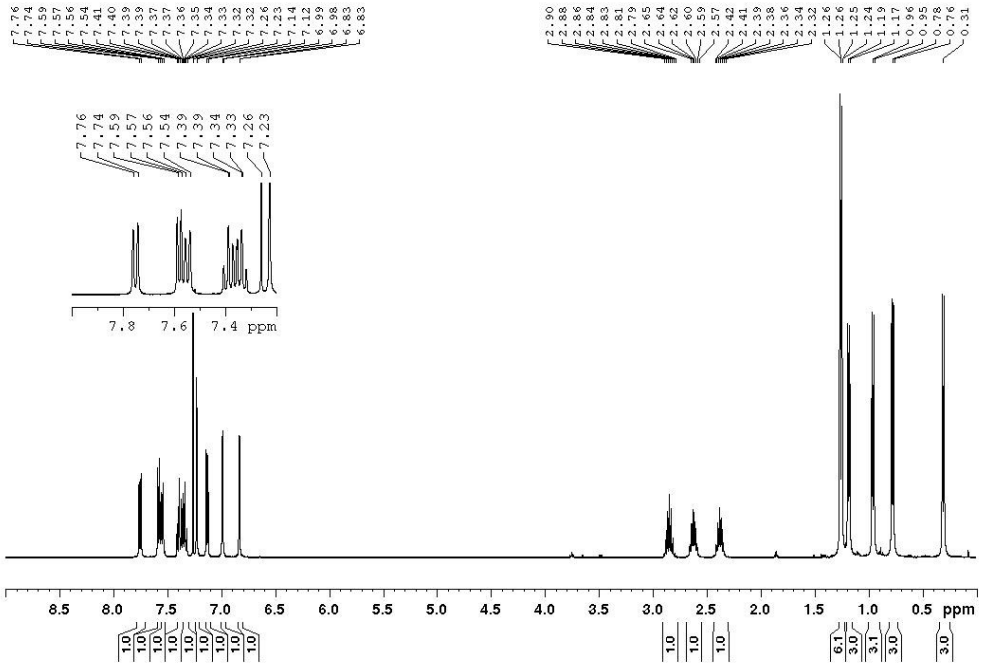

Figure 9.1-33. ^{1}H NMR spectrum of **[TipPBBI]$_4$** in $CDCl_3$ at 400 MHz.

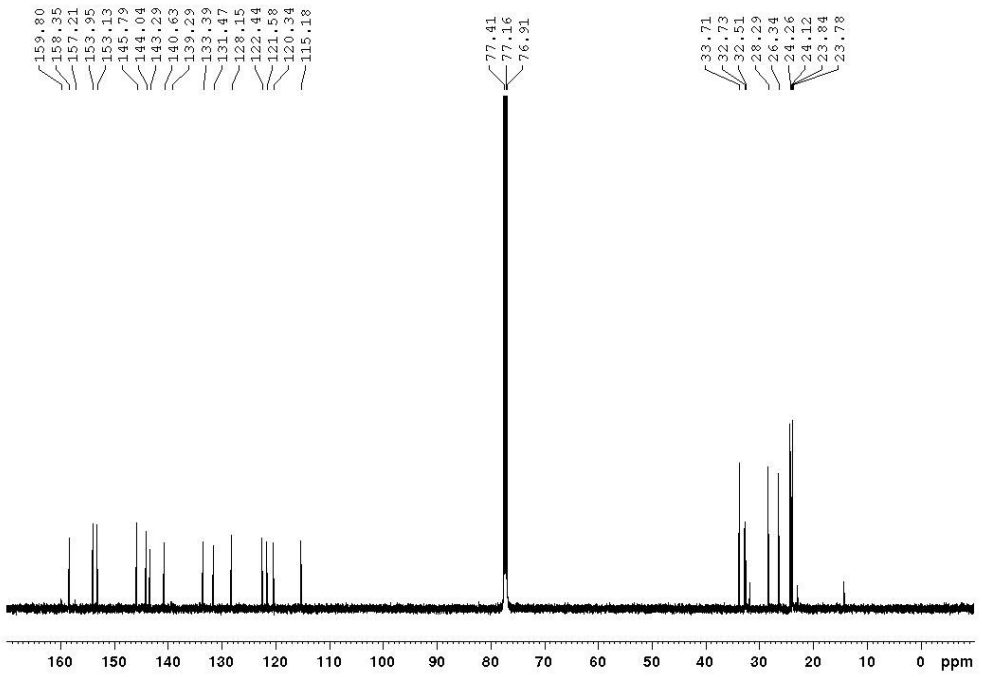

Figure 9.1-34. $^{13}C\{^{1}H\}$ NMR spectrum of **[TipPBBI]$_4$** in $CDCl_3$ at 125 MHz.

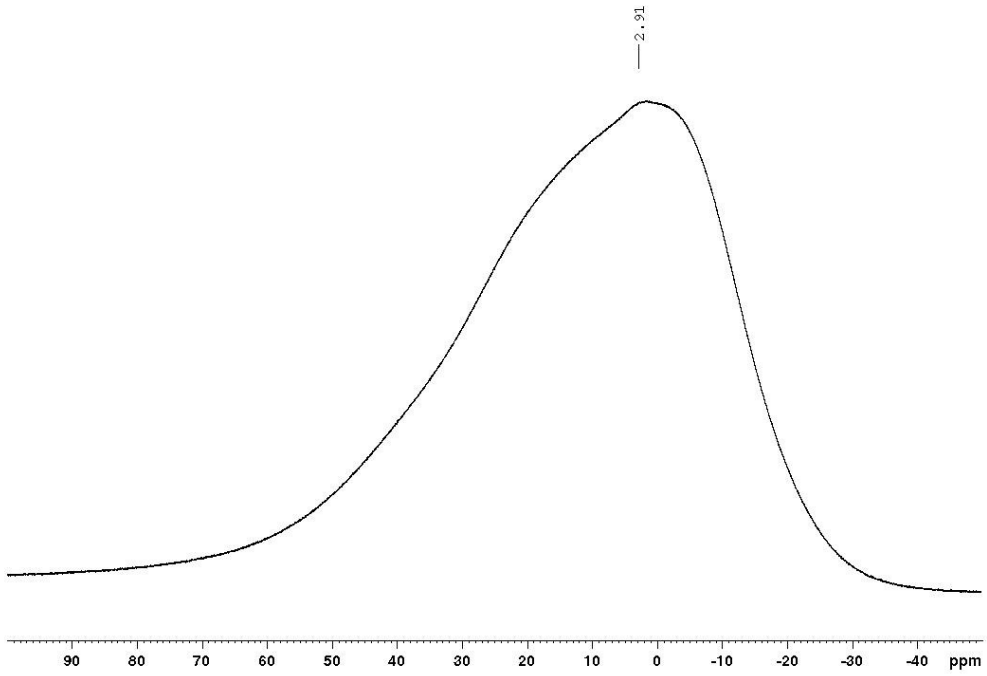

Figure 9.1-35. $^{11}B\{^{1}H\}$ NMR spectrum of **[TipPBBI]**$_4$ in $CDCl_3$ at 160 MHz.

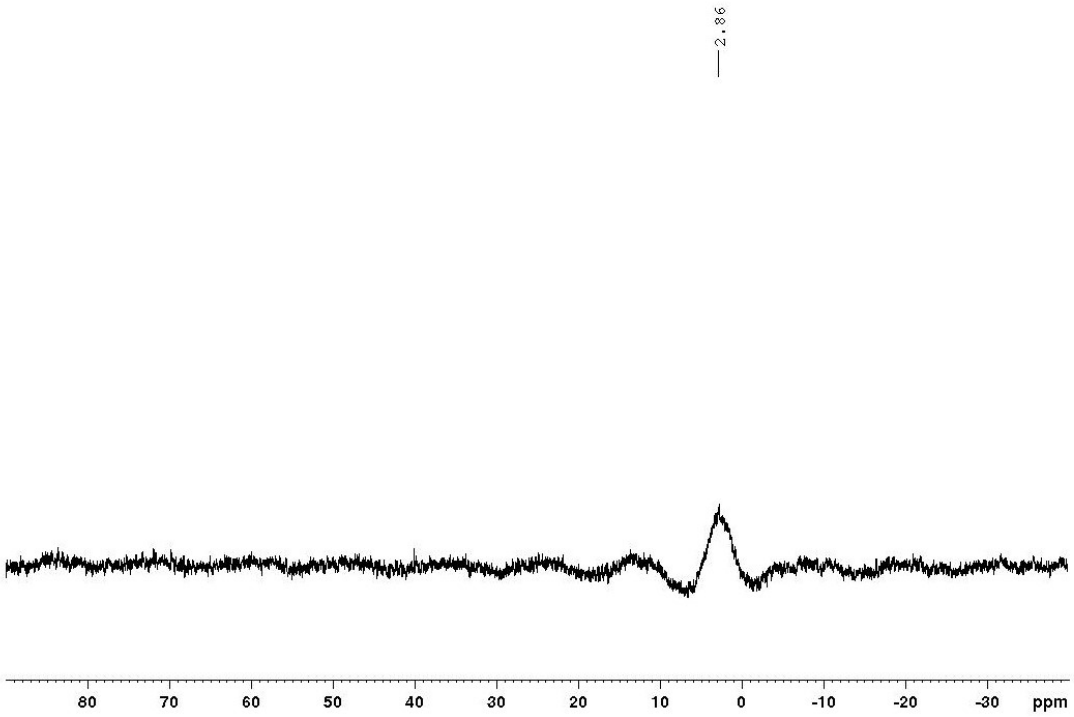

Figure 9.1-36. $^{11}B\{^{1}H\}$ NMR spectrum of **[TipPBBI]**$_4$ in $CDCl_3$ at 160 MHz with background removed by linear backwards prediction.

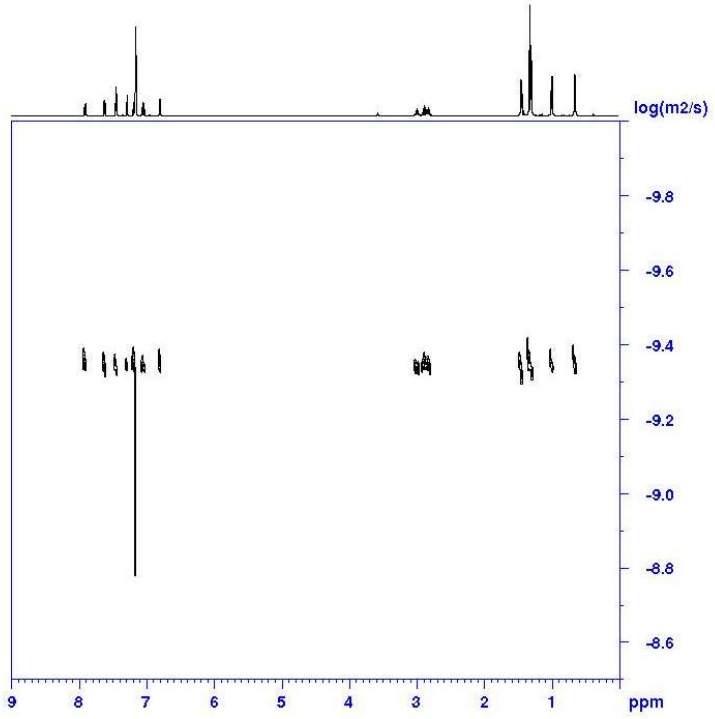

Figure 9.1-37. ^{1}H DOSY spectrum of **[TipPBBI]$_4$** in C_6D_6 at +25 °C.

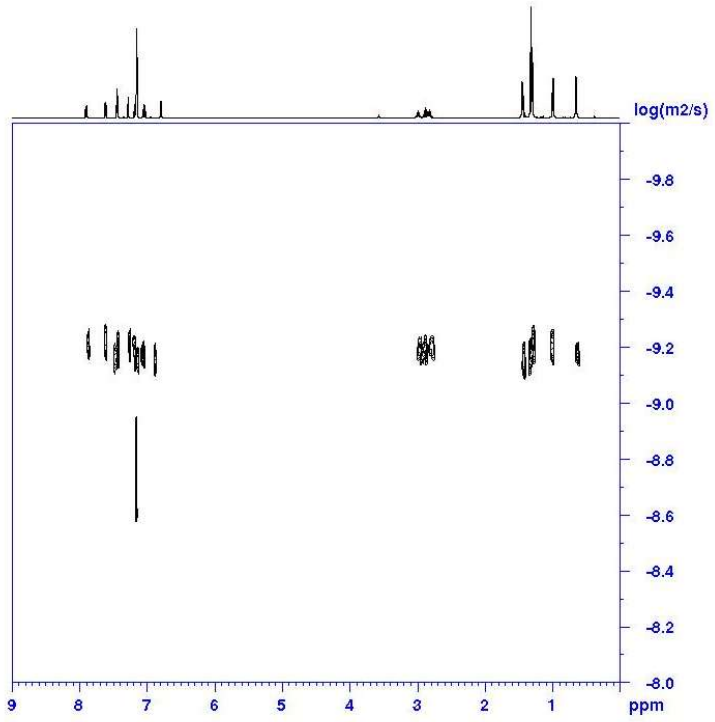

Figure 9.1-38. ^{1}H DOSY spectrum of **[TipPBBI]$_4$** in C_6D_6 at +50 °C.

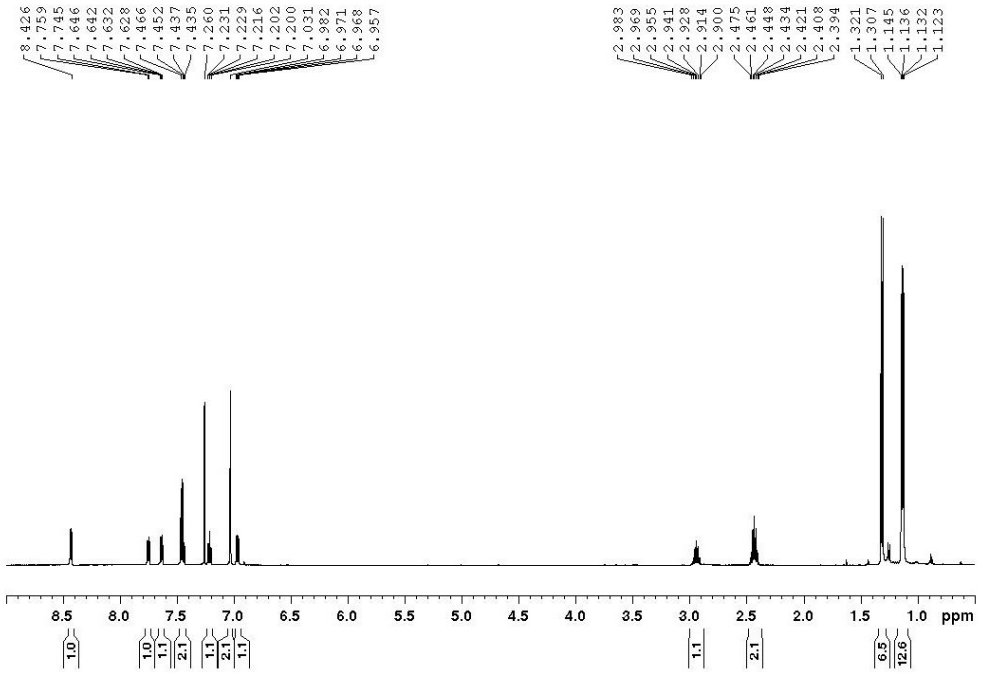

Figure 9.1-39. ^{1}H NMR spectrum of **TipPBB2** in $CDCl_3$ at 500 MHz.

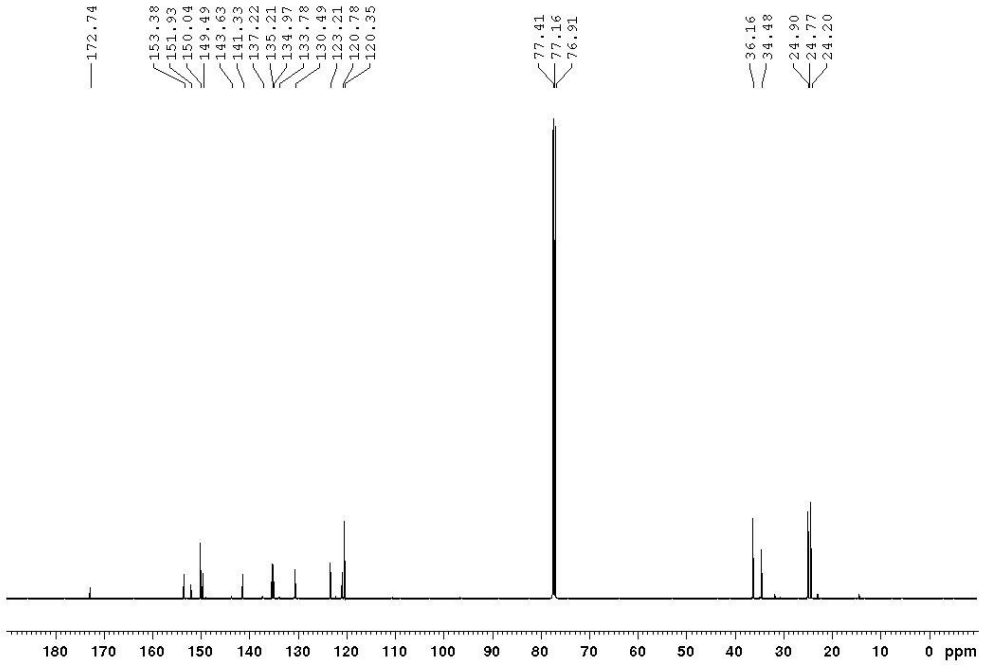

Figure 9.1-40. $^{13}C\{^{1}H\}$ NMR spectrum of **TipPBB2** in $CDCl_3$ at 125 MHz.

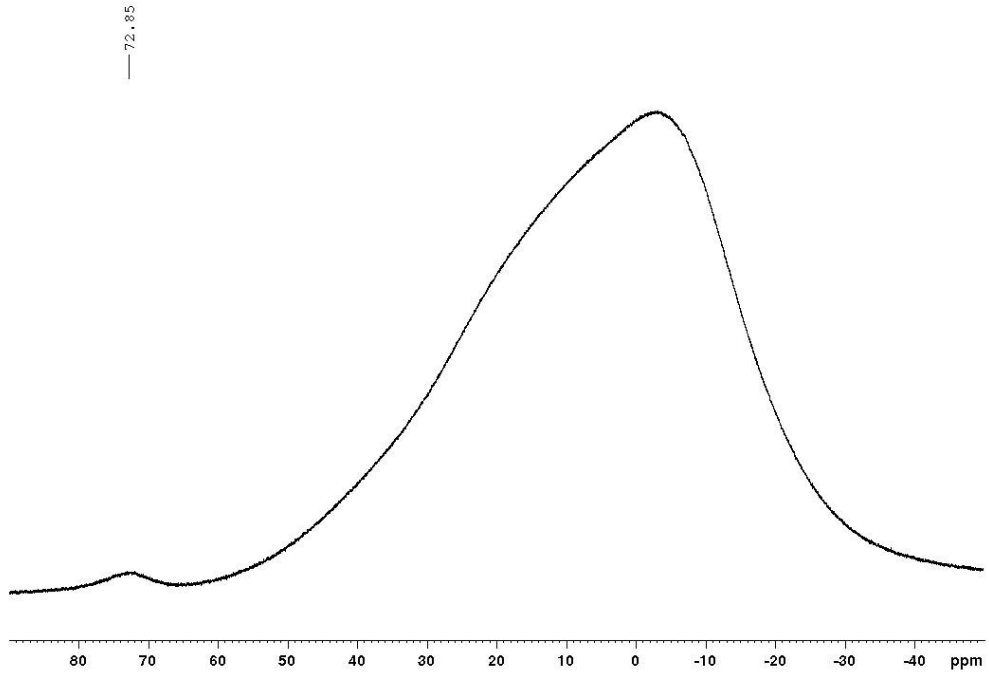

Figure 9.1-41. $^{11}B\{^1H\}$ NMR spectrum of **TipPBB2** in $CDCl_3$ at 160MHz.

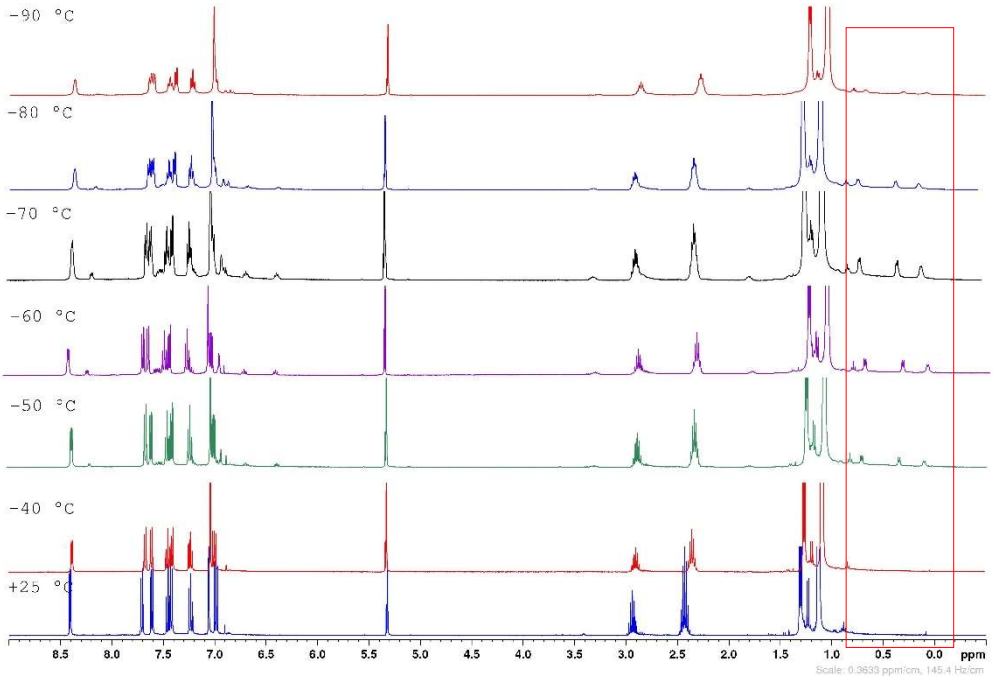

Figure 9.1-42. Low temperature ^1H NMR spectra of **TipPBB2** in CD_2Cl_2 at 400 MHz.

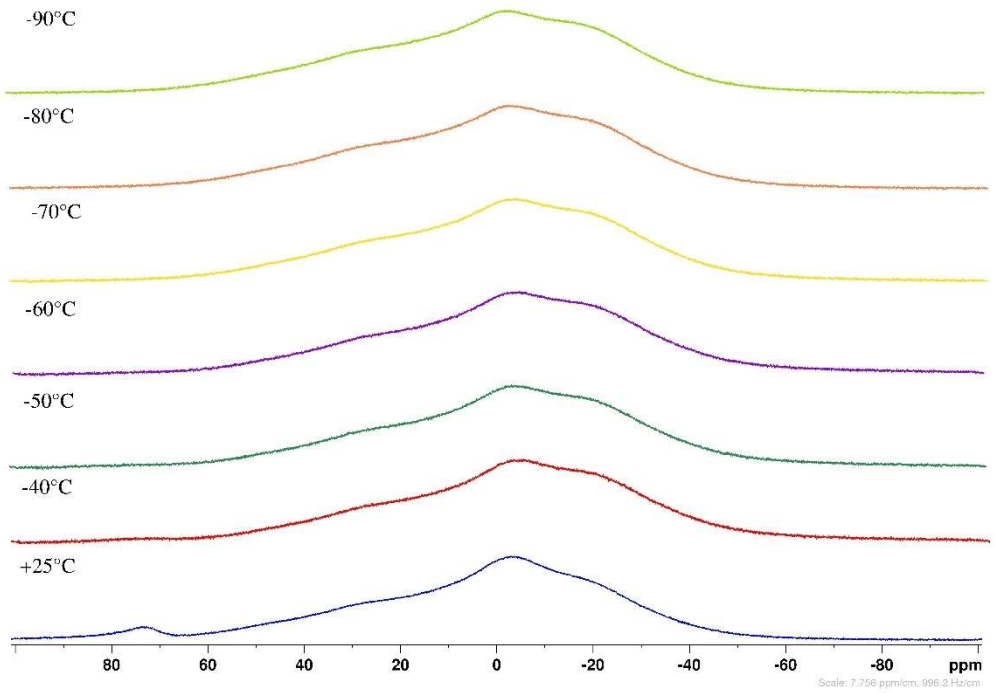

Figure 9.1-43. Low temperature $^{11}B\{^{1}H\}$ NMR spectra of **TipPBB2** in CD_2Cl_2 at 128MHz.

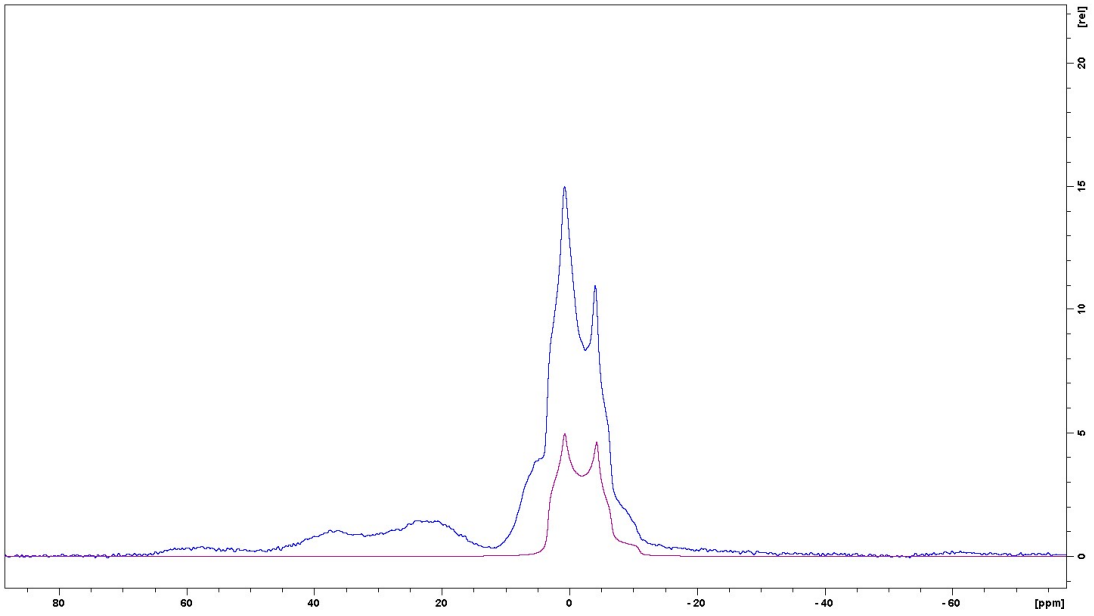

Figure 9.1-44. ^{11}B-SS NMR spectrum (128.3 MHz, 298 K) of **TipPBB2** (top) and simulated spectrum (bottom).

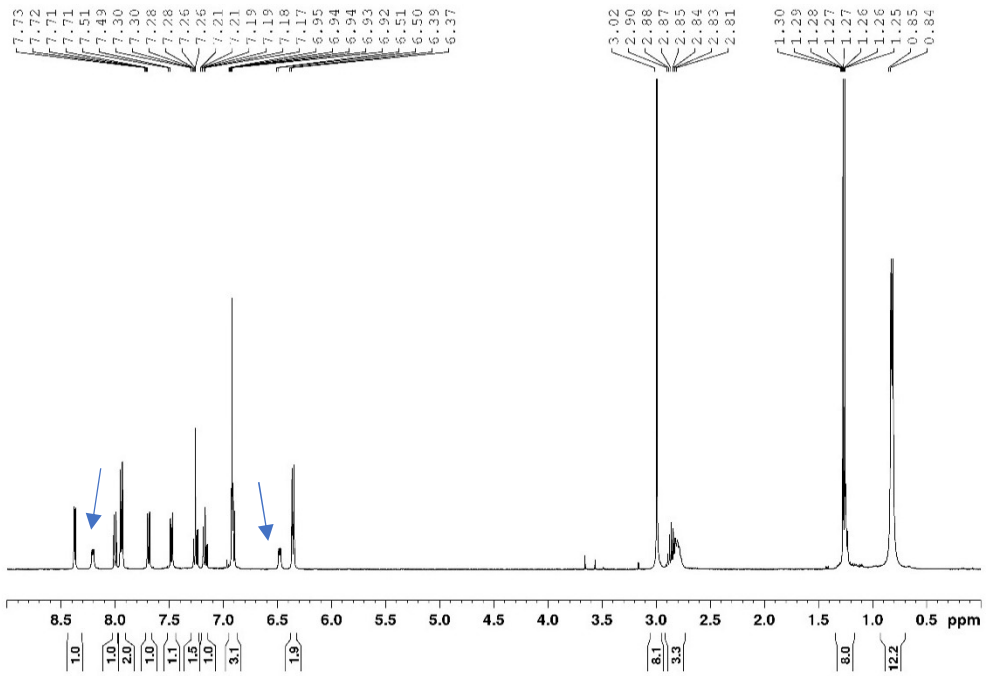

Figure 9.1-45. ^{1}H NMR spectrum of **TipPBB2** + DMAP in $CDCl_3$ at 400 MHz. The peaks marked with arrows are excess of DMAP.

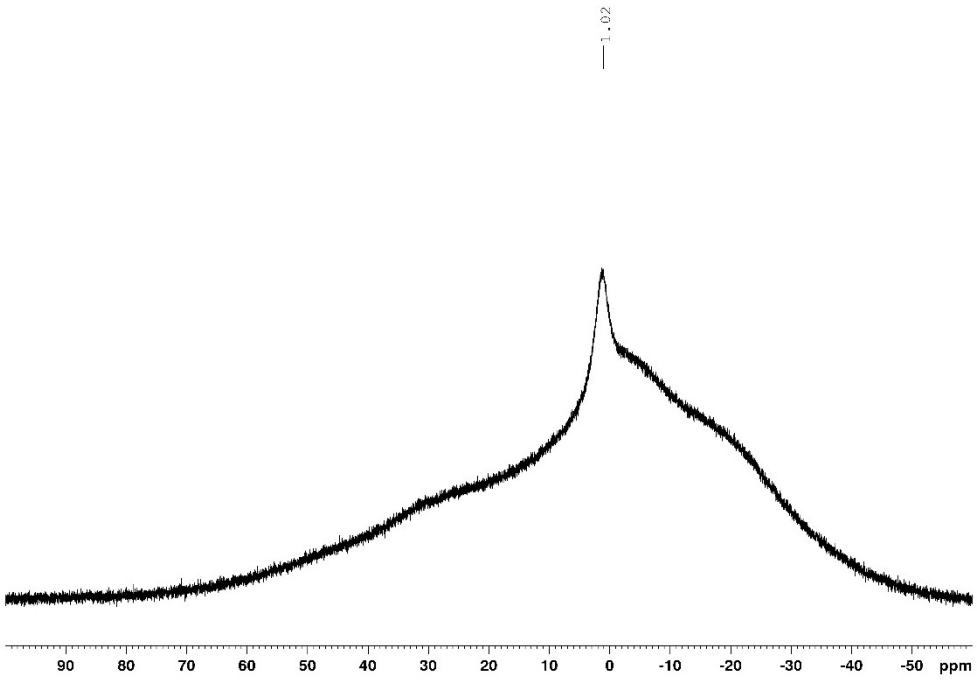

Figure 9.1-46. $^{11}B\{^{1}H\}$ NMR spectrum of **TipPBB2** + DMAP in $CDCl_3$ at 400 MHz.

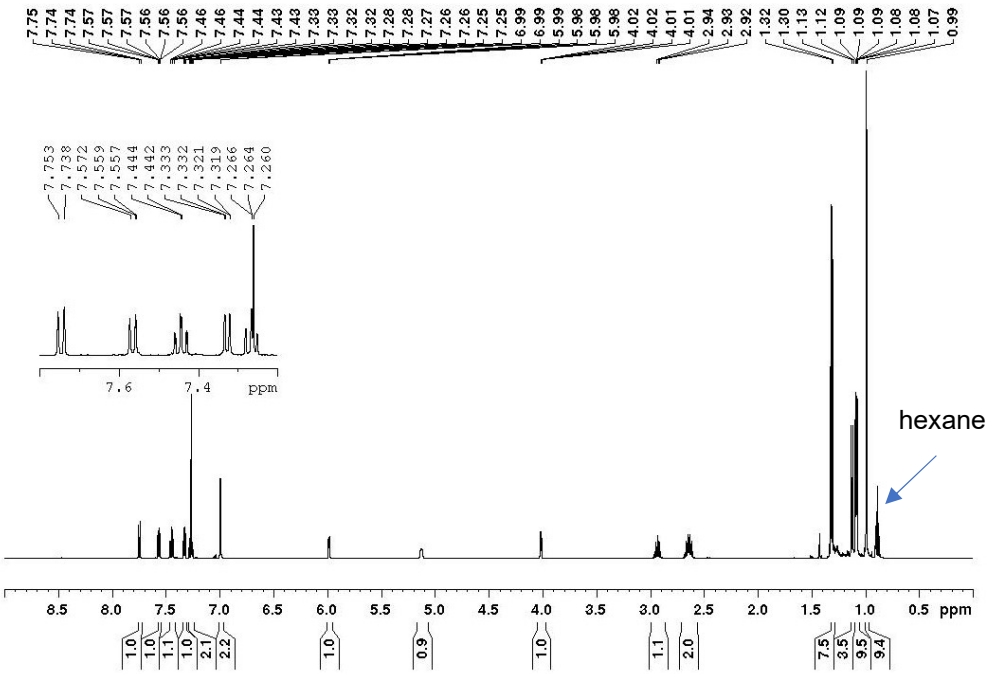

Figure 9.1-47. ^{1}H NMR spectrum of compound **10** in $CDCl_3$ at 500 MHz.

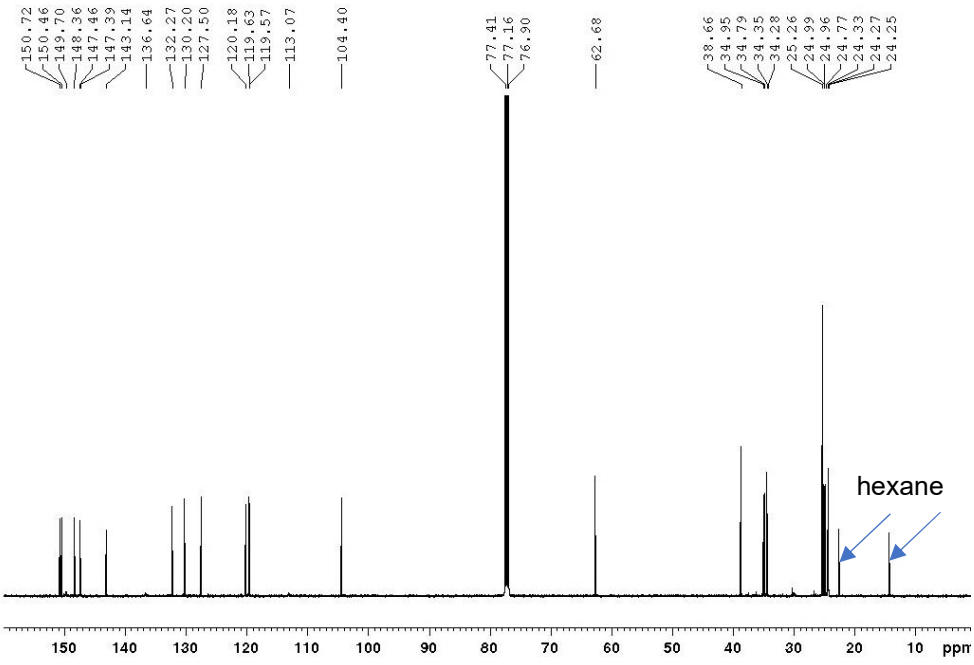

Figure 9.1-48. $^{13}C\{^{1}H\}$ NMR spectrum of compound **10** in $CDCl_3$ at 125 MHz.

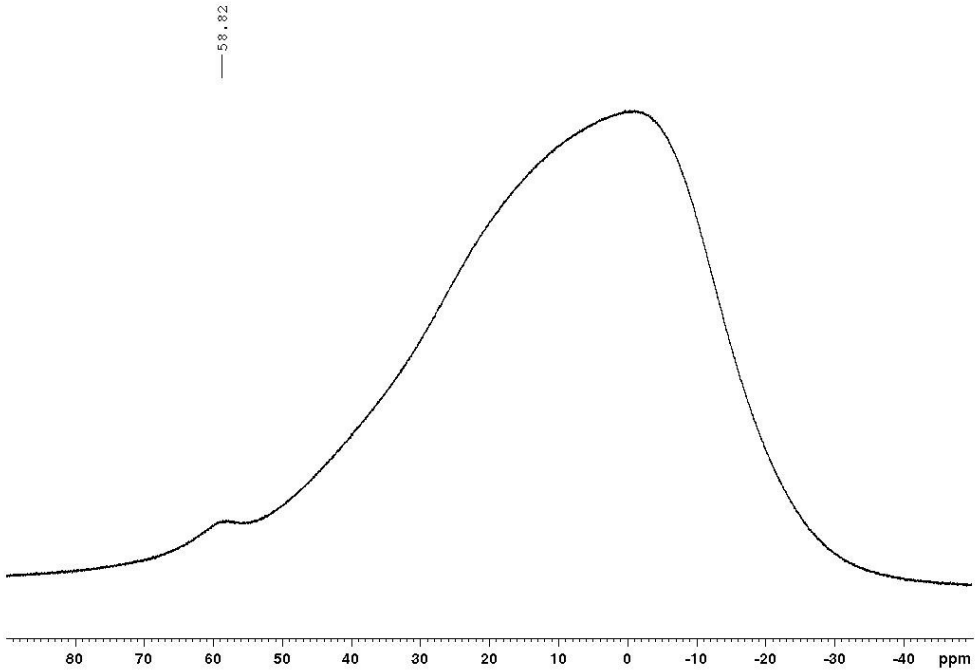

Figure 9.1-49. $^{11}B\{^{1}H\}$ NMR spectrum of compound **10** in $CDCl_3$ at 160 MHz.

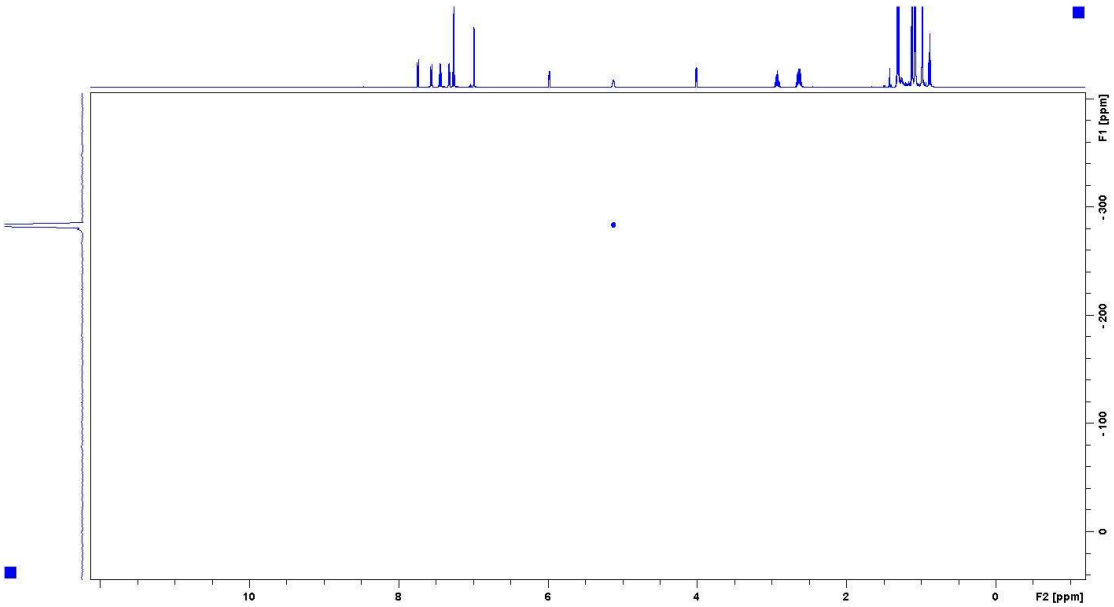

Figure 9.1-50. ^{1}H-^{15}N heteronuclear correlation NMR spectrum of compound **10** in $CDCl_3$.

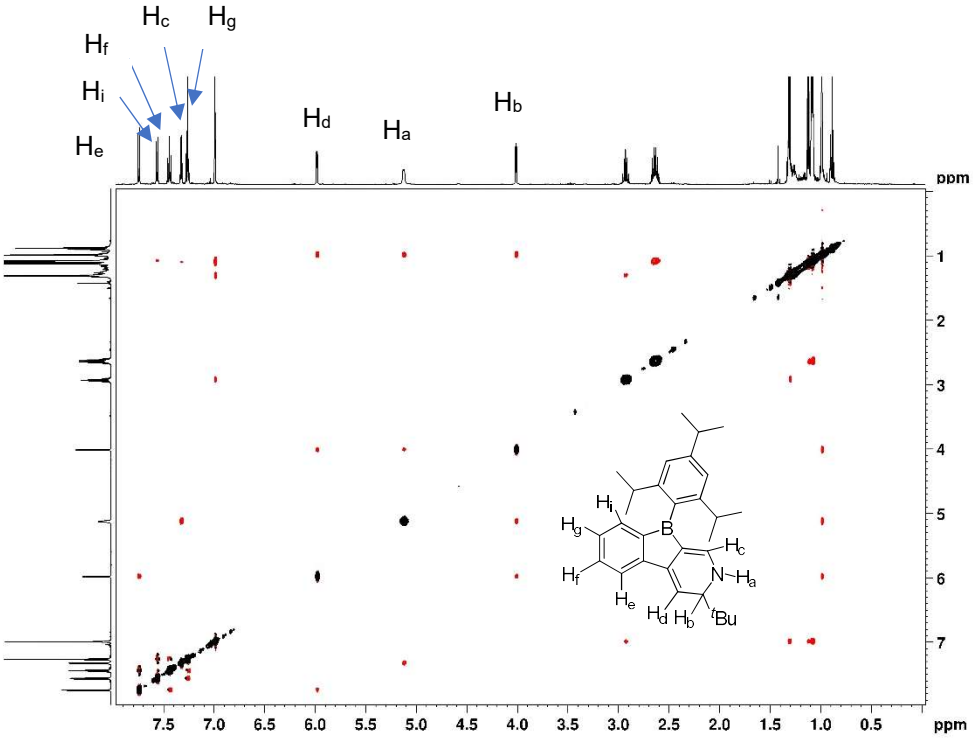

Figure 9.1-51. ^{1}H-^{1}H NOESY NMR spectrum of compound **10** in $CDCl_3$ at 500 MHz.

From ^{1}H-^{15}N heteronuclear correlation, we can assign the chemical shift of proton H_a (5.17-5.06 ppm). H_a is coupled to both H_b and H_c, but H_c only couples with H_a. Thus, H_c can be assigned (7.34-7.31 ppm). After H_c was assigned, H_b (4.01 ppm) was also assigned. H_b also couples with H_d, thus H_d was assigned with a chemical shift of 6.00-5.96 ppm. Since H_d has an NOE effect with H_e, H_e can be assigned and the other three protons (H_f, H_g and H_i) were assigned in the same way through coupling.

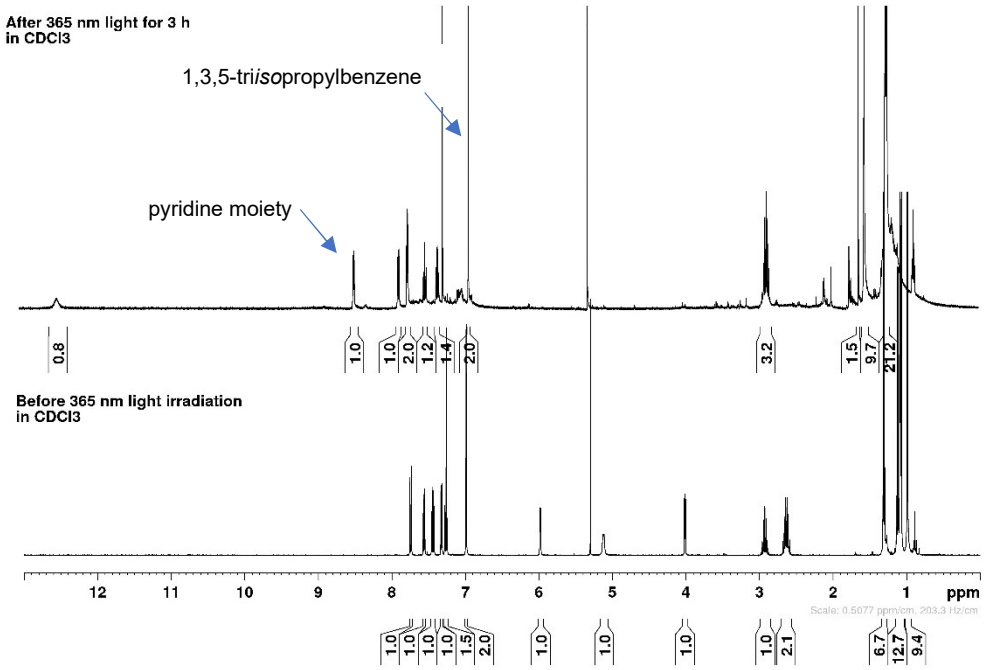

Figure 9.1-52. ^{1}H NMR spectra of compound **10** in $CDCl_3$ before (bottom) and after 365 nm light (top) at 400 MHz.

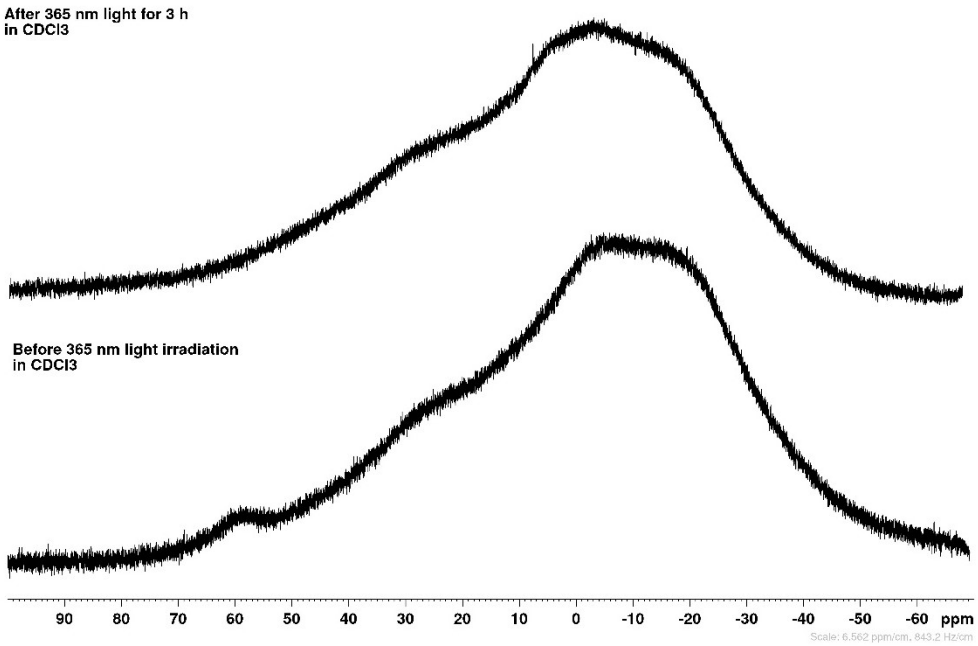

Figure 9.1-53. $^{11}B\{^{1}H\}$ NMR spectra of compound **10** in $CDCl_3$ before (bottom) and after 365 nm light (top) at 128 MHz.

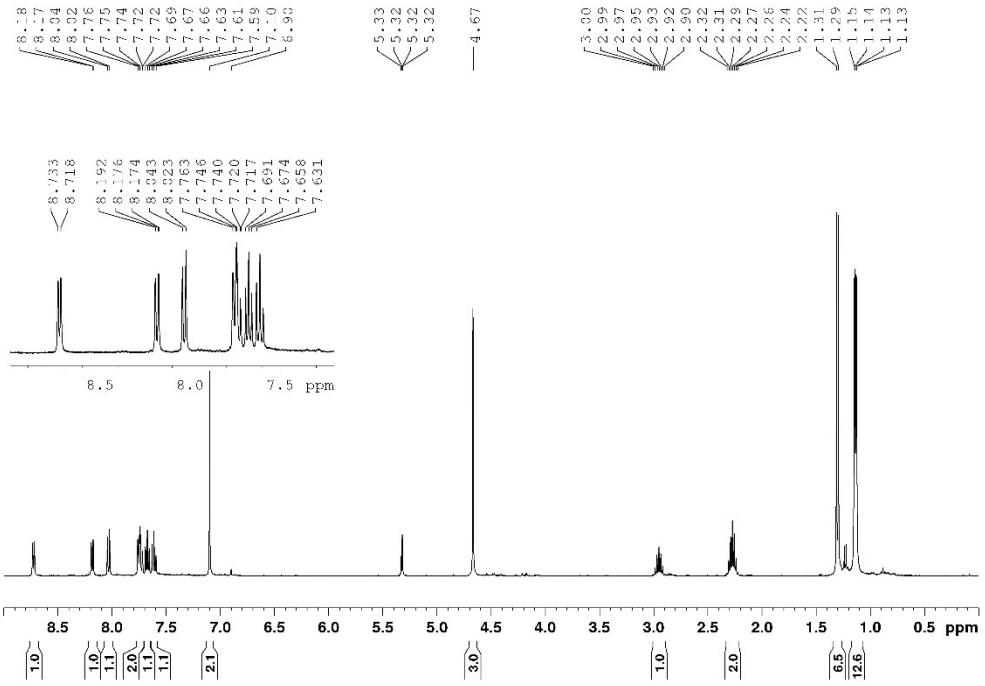

Figure 9.1-54. ^{1}H NMR spectrum of compound **11** in CD_2Cl_2 at 400 MHz.

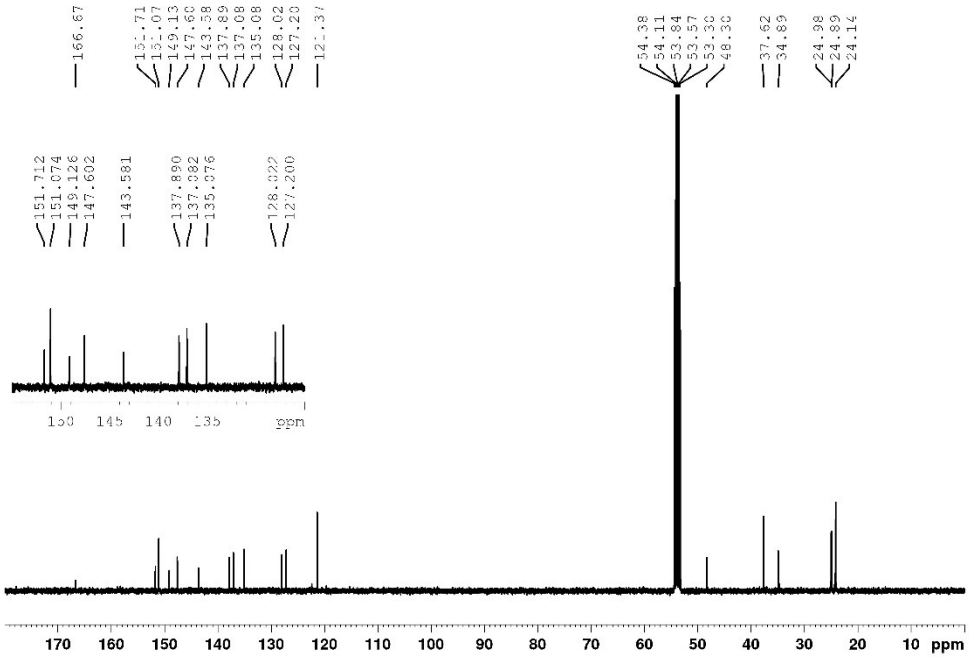

Figure 9.1-55. $^{13}C\{^{1}H\}$ NMR spectrum of compound **11** in CD_2Cl_2 at 100 MHz.

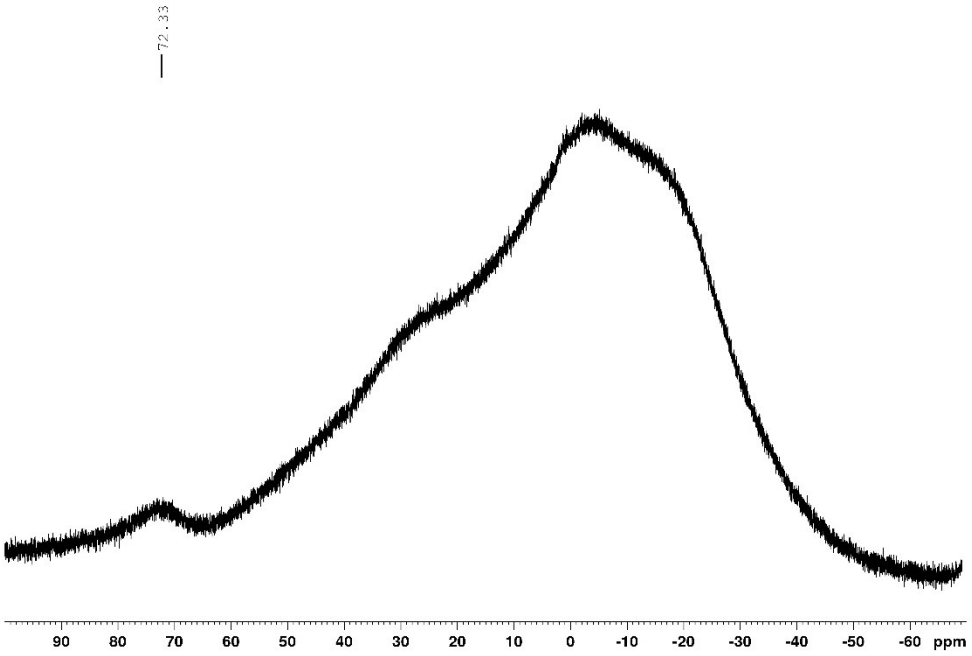

Figure 9.1-56. $^{11}B\{^{1}H\}$ NMR spectrum of compound **11** in CD_2Cl_2 at 128 MHz.

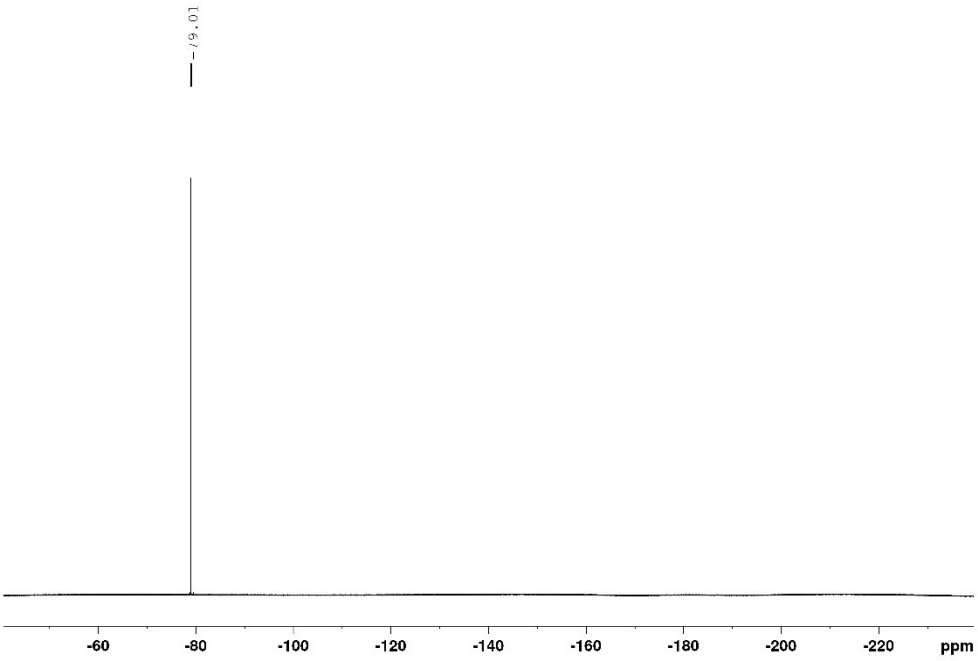

Figure 9.1-57. $^{19}F\{^{1}H\}$ NMR spectrum of compound **11** in CD_2Cl_2 at 376 MHz.

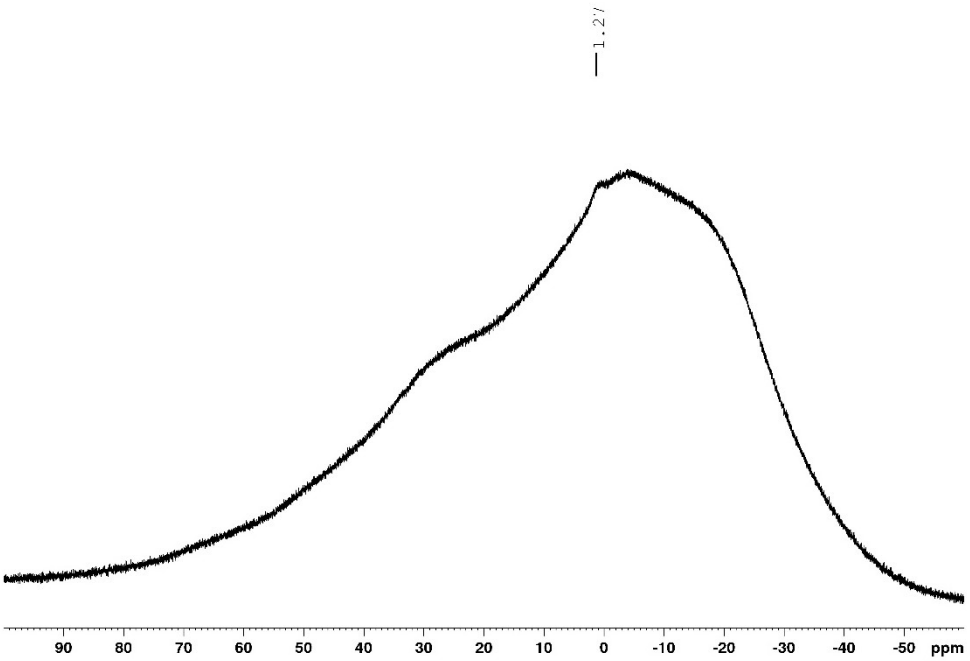

Figure 9.1-58. $^{11}B\{^{1}H\}$ NMR spectrum of compound **11** in d_8-THF at 128 MHz.

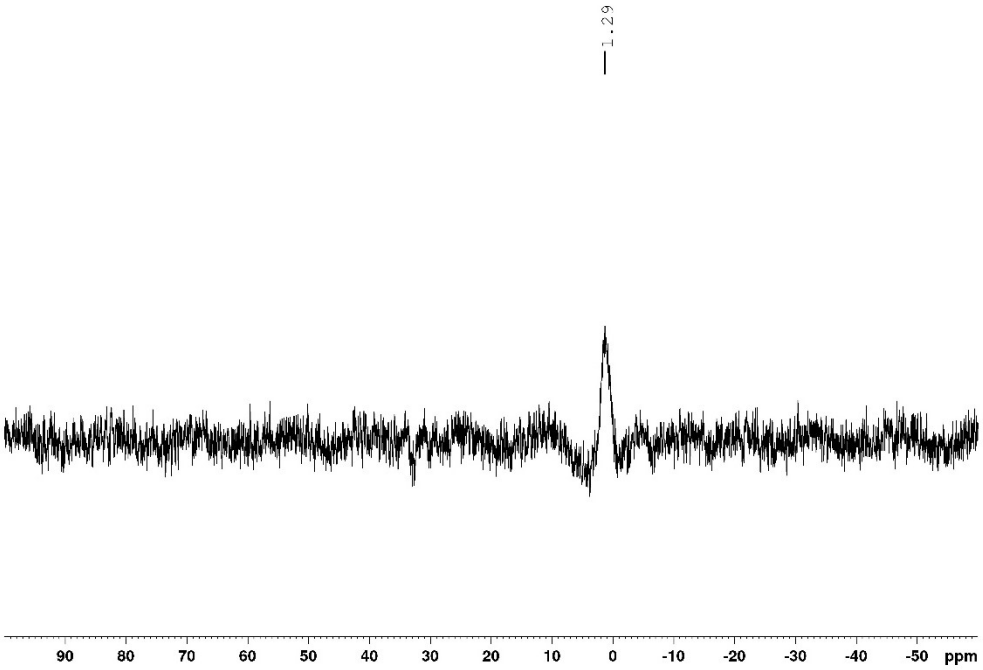

Figure 9.1-59. $^{11}B\{^{1}H\}$ NMR spectrum of compound **11** in d_8-THF at 128 MHz with background removed by linear backwards prediction.

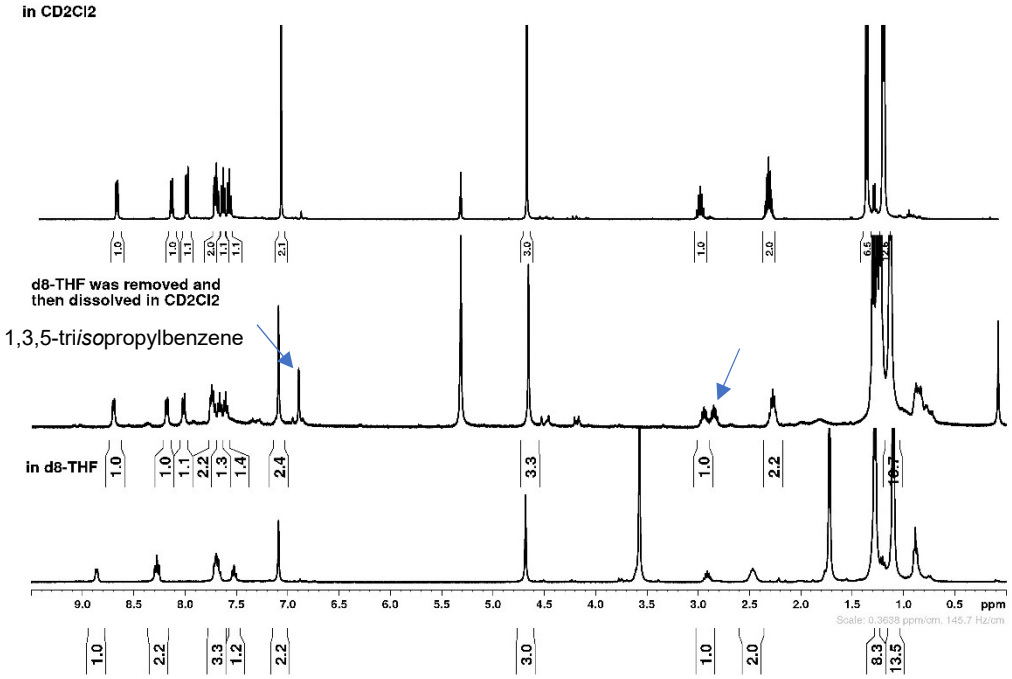

Figure 9.1-60. ^{1}H NMR spectra of compound **11** in d_8-THF (bottom), after d_8-THF was removed and the solid was re-dissolved in CD_2Cl_2 (middle) and in CD_2Cl_2 (top) at 400 MHz. The 1,3,5-tri*iso*propylbenene (marked with arrows) in the middle spectrum formed from decomposition.

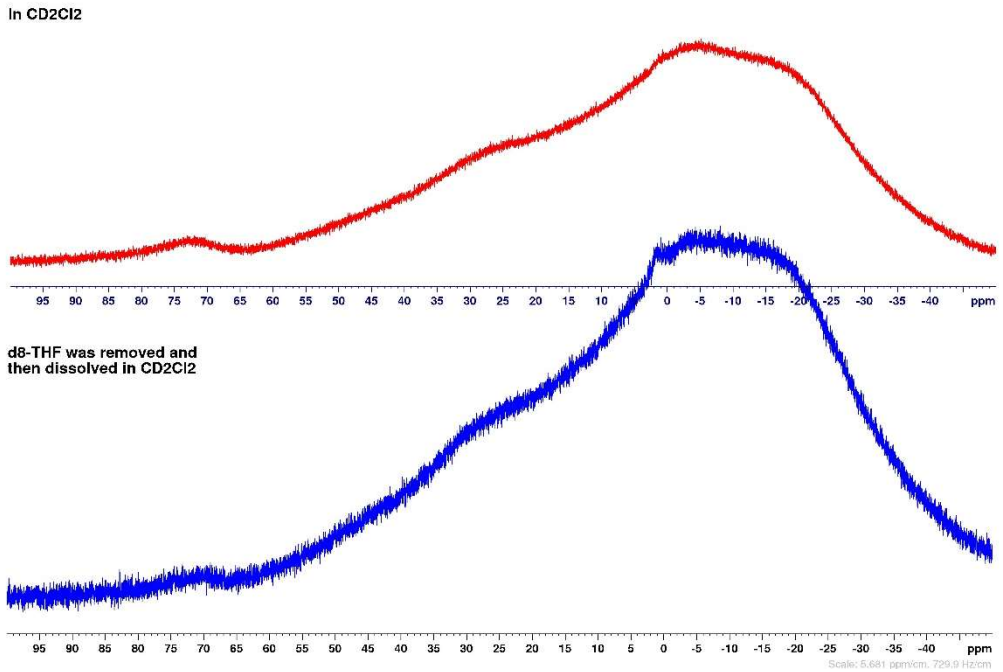

Figure 9.1-61. ^{11}B{^{1}H} NMR spectra of compound **11** in CD_2Cl_2 (top) and after the d_8-THF was removed and then the solid was re-dissolved in CD_2Cl_2 (bottom) at 128 MHz.

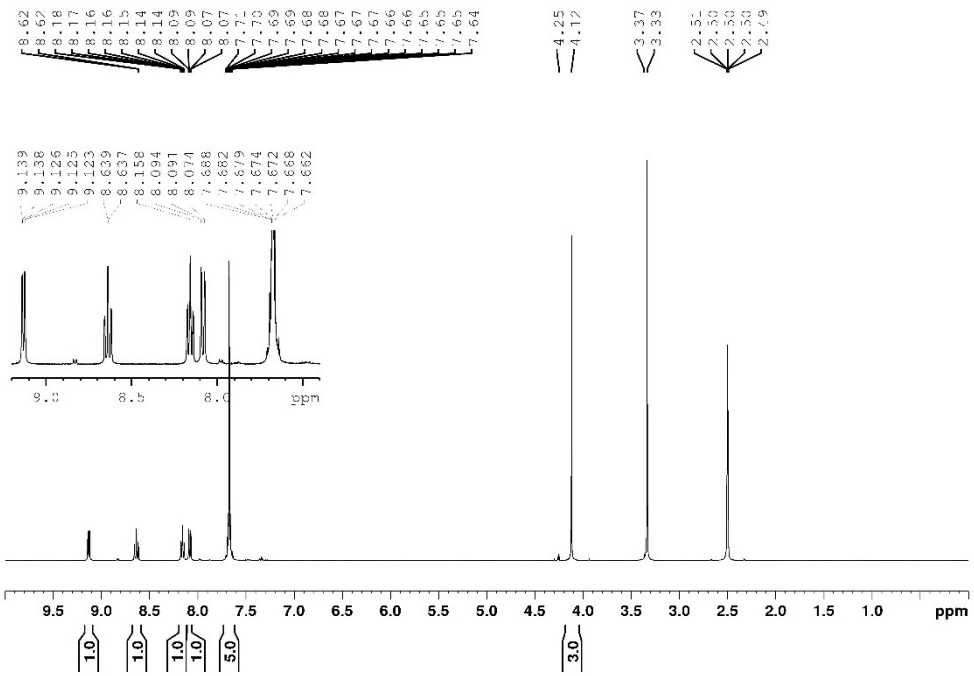

Figure 9.1-62. ^{1}H NMR spectrum of compound **12** in d_6-DMSO at 400 MHz.

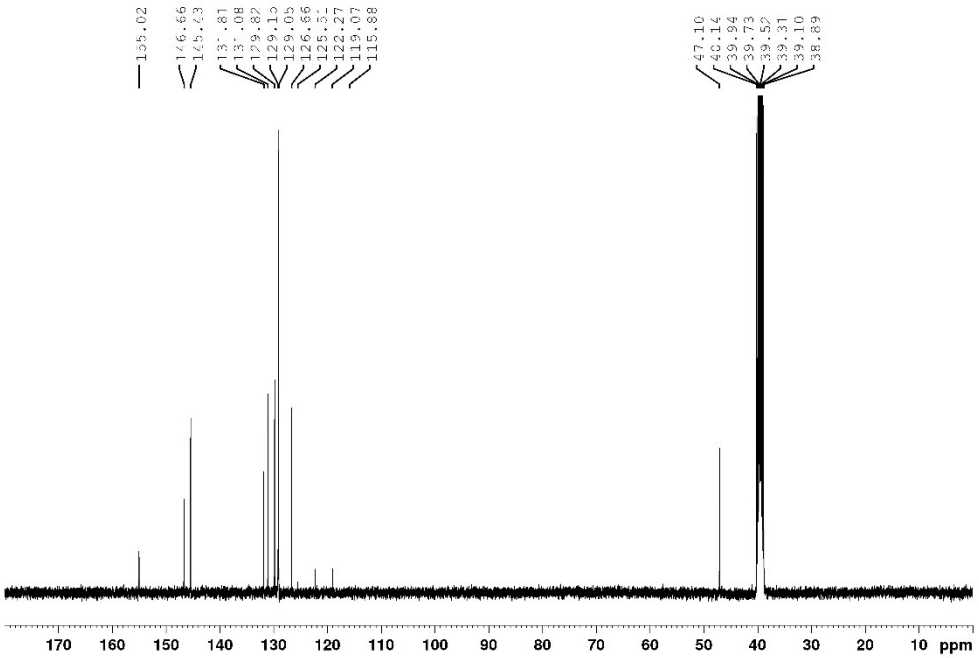

Figure 9.1-63. ^{13}C{^{1}H} NMR spectrum of compound **12** in d_6-DMSO at 100 MHz.

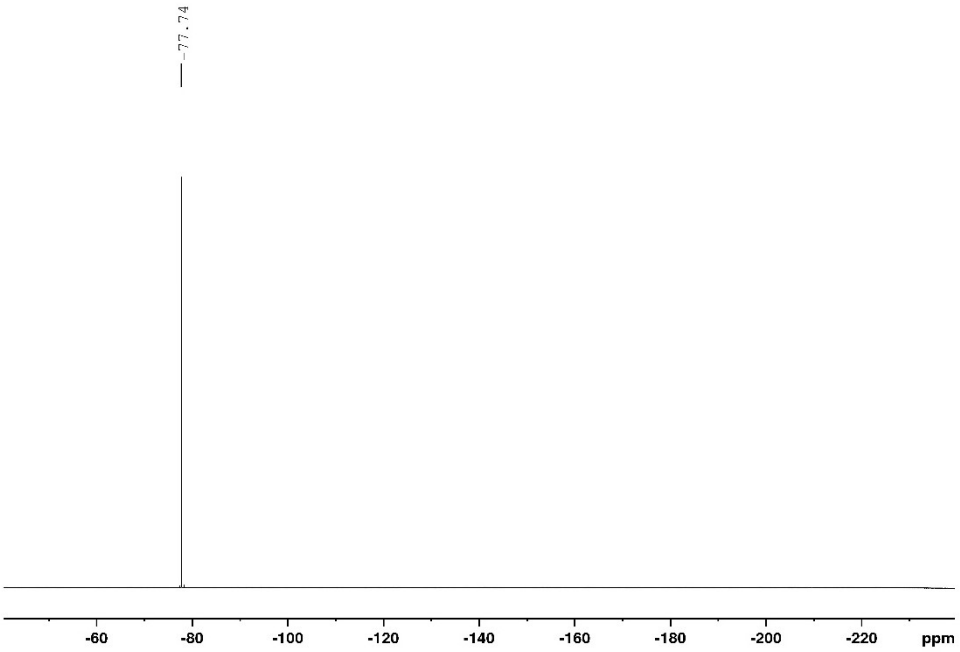

Figure 9.1-64. $^{19}F\{^{1}H\}$ NMR spectrum of compound **12** in d_6-DMSO at 376 MHz.

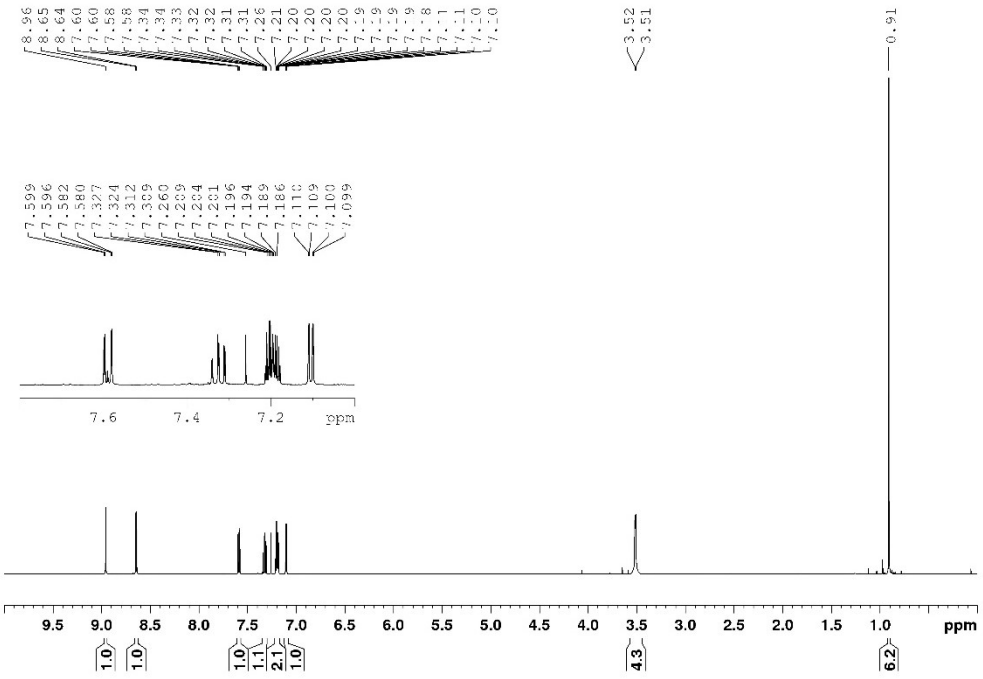

Figure 9.1-65. ^{1}H NMR spectrum of compound **14** in $CDCl_3$ at 500 MHz.

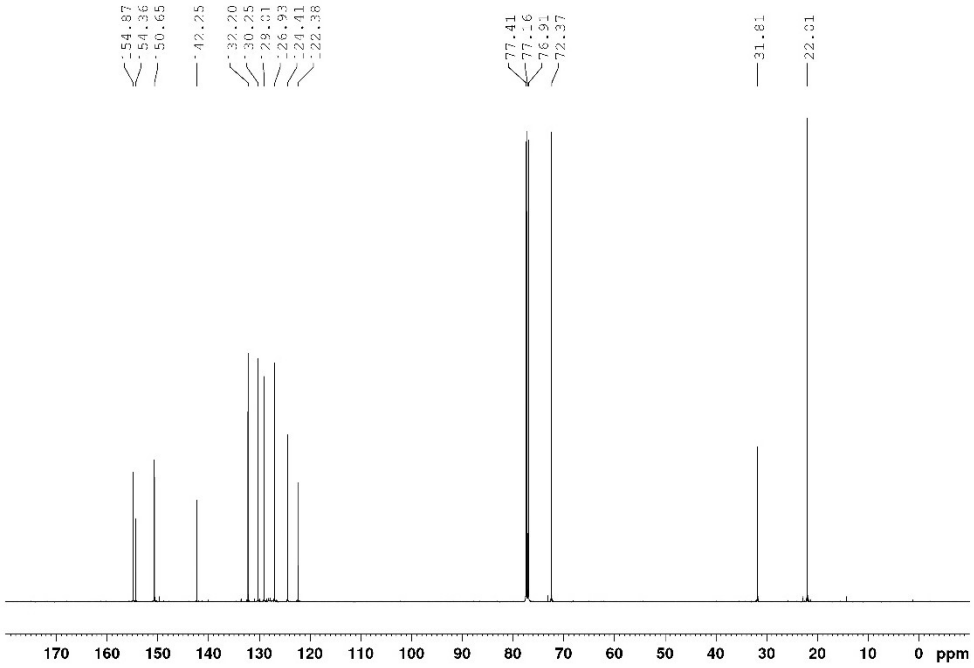

Figure 9.1-66. $^{13}C\{^{1}H\}$ NMR spectrum of compound **14** in $CDCl_3$ at 125 MHz.

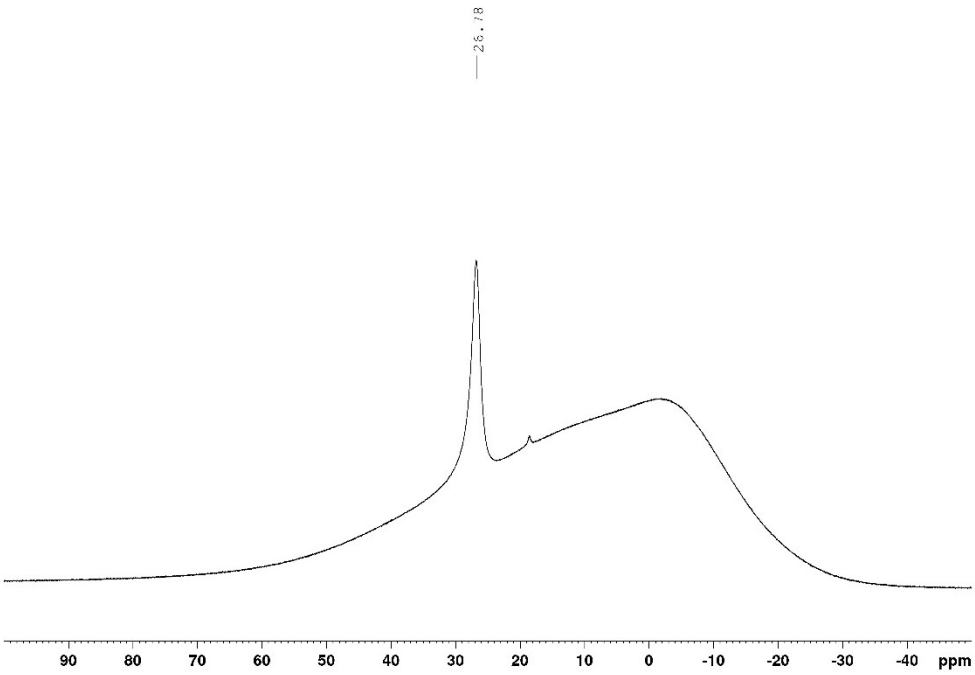

Figure 9.1-67. $^{11}B\{^{1}H\}$ NMR spectrum of compound **14** in $CDCl_3$ at 128 MHz.

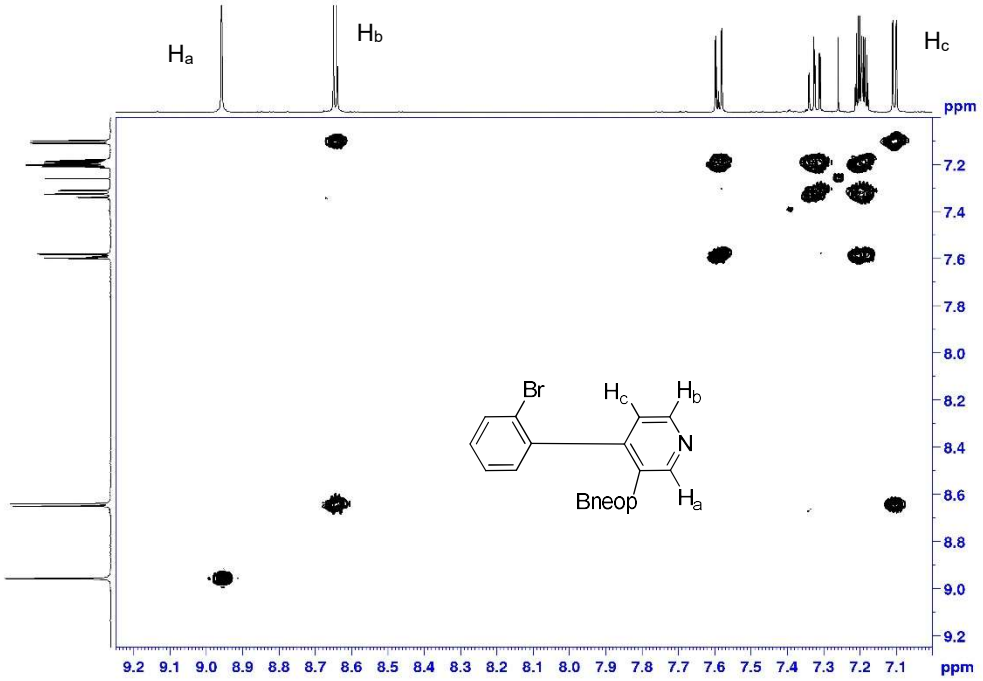

Figure 9.1-68. ^{1}H-^{1}H COSY spectrum of compound **14** in $CDCl_3$ at 500 MHz.

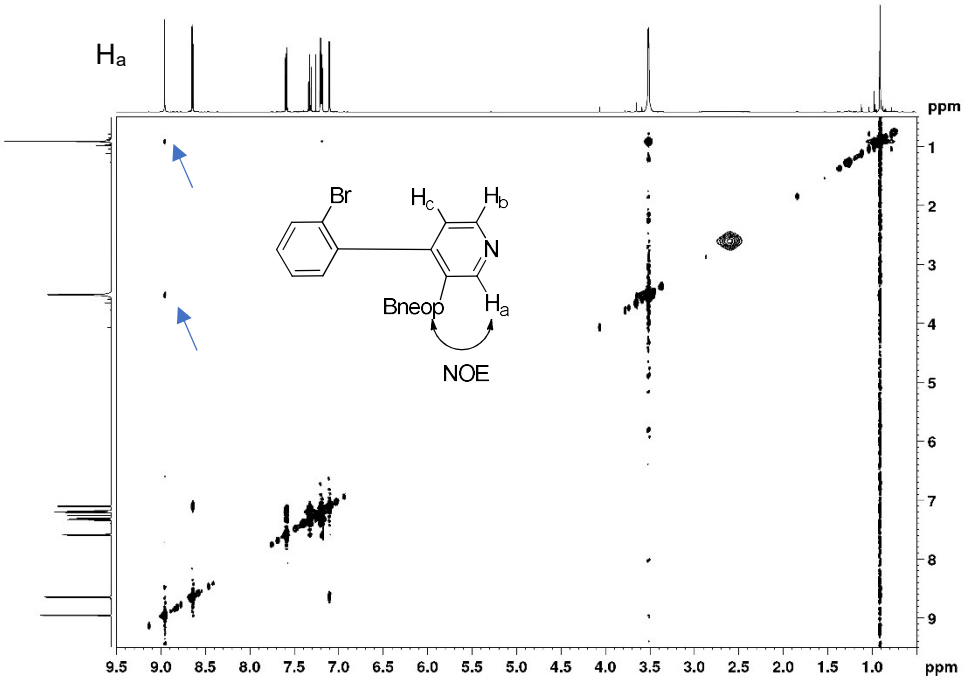

Figure 9.1-69. ^{1}H-^{1}H NOESY spectrum of compound **14** in $CDCl_3$ at 500 MHz.

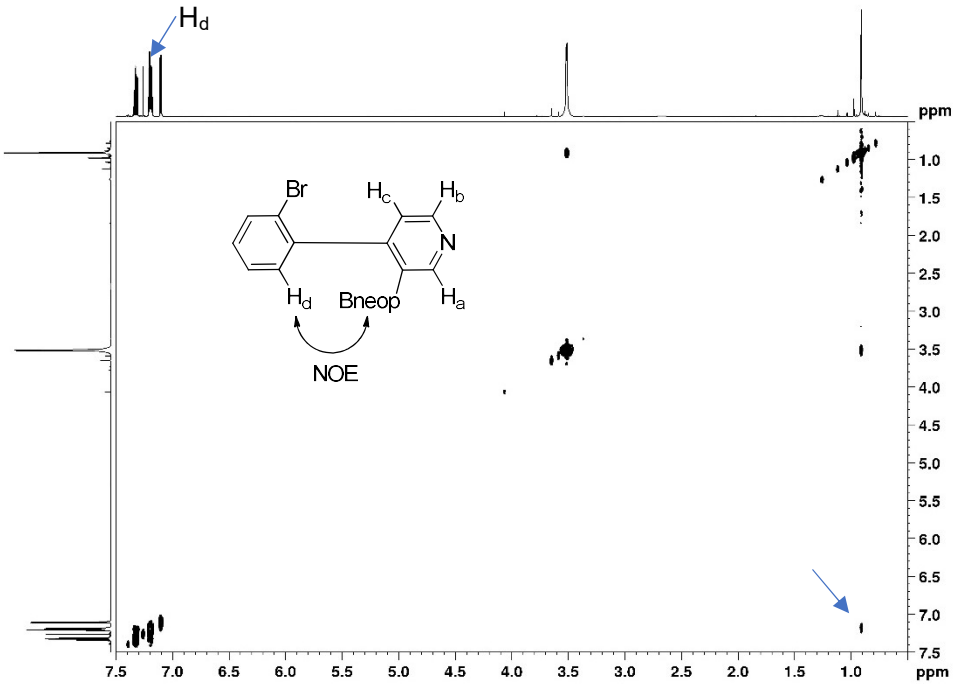

Figure 9.1-70. ^{1}H-^{1}H NOESY spectrum of compound **14** in $CDCl_3$ at 500 MHz.

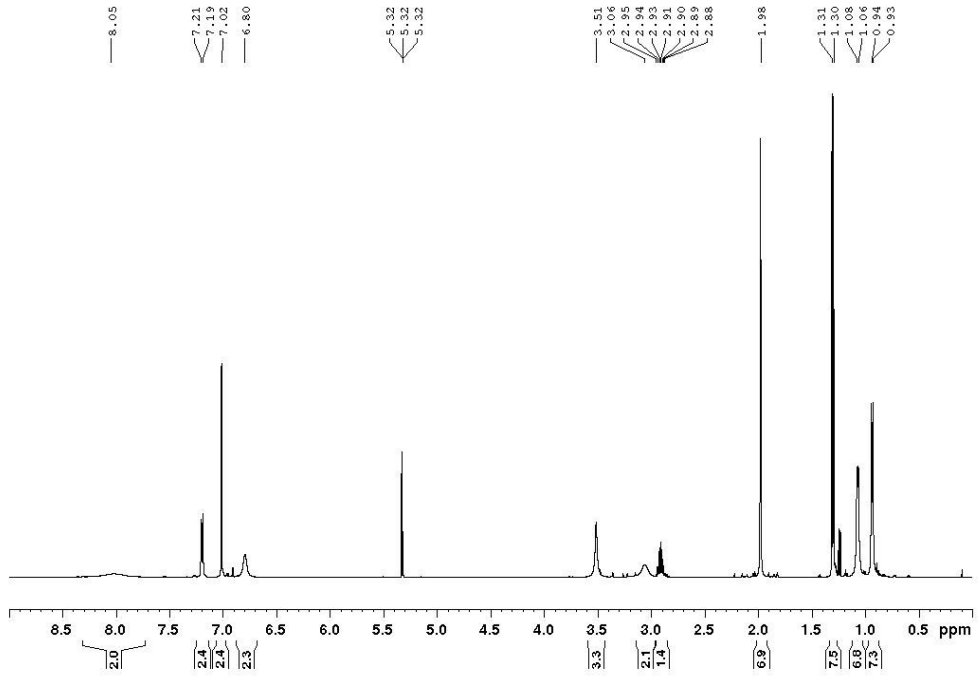

Figure 9.1-71. ^{1}H NMR spectrum of **[16]**$_2$ in CD_2Cl_2 at 500 MHz.

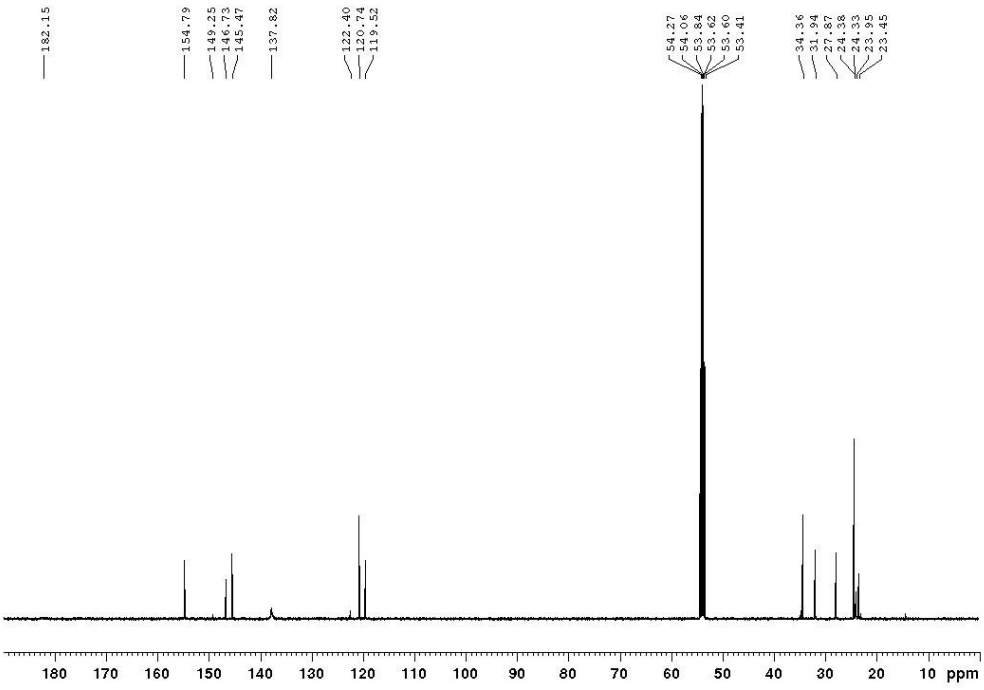

Figure 9.1-72. $^{13}C\{^{1}H\}$ NMR spectrum of **[16]**$_2$ in CD_2Cl_2 at 125 MHz.

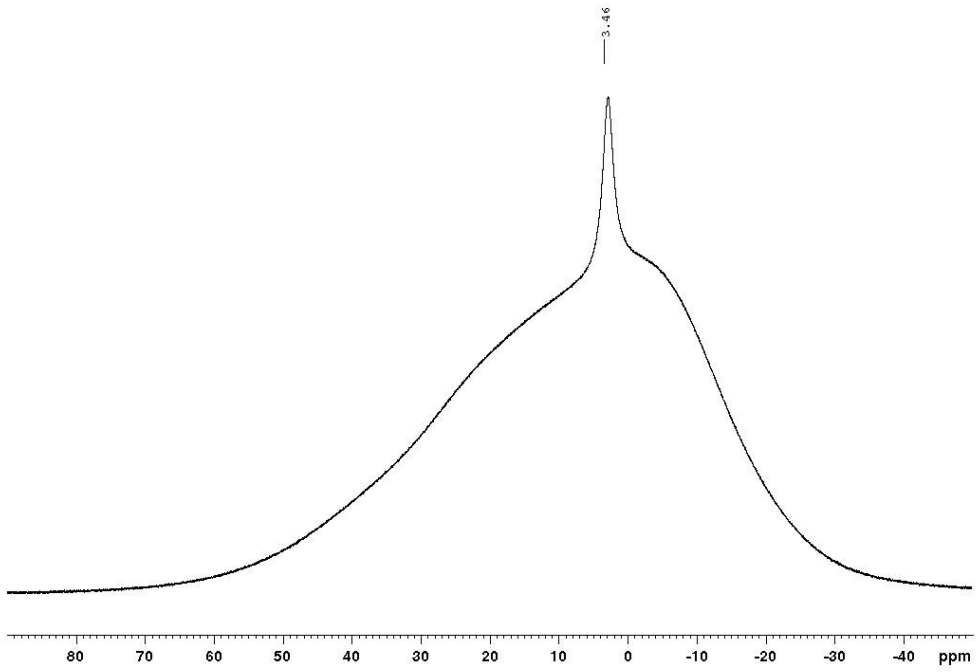

Figure 9.1-73. $^{11}B\{^{1}H\}$ NMR spectrum of **[16]**$_2$ in CD_2Cl_2 at 160 MHz.

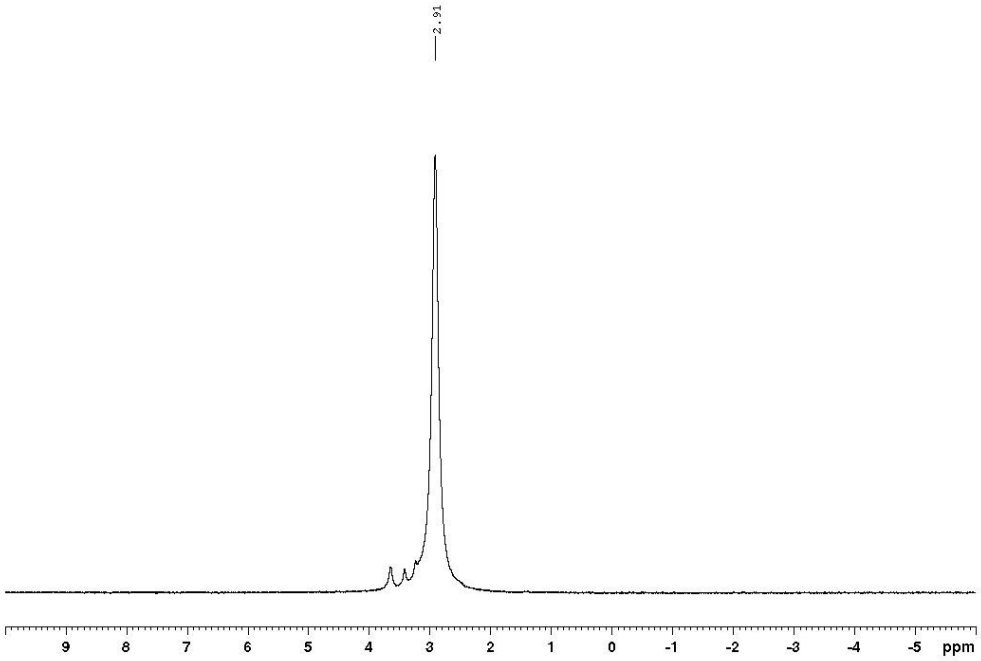

Figure 9.1-74. $^{7}Li\{^{1}H\}$ NMR spectrum of **[16]**$_2$ in CD_2Cl_2 at 194 MHz.

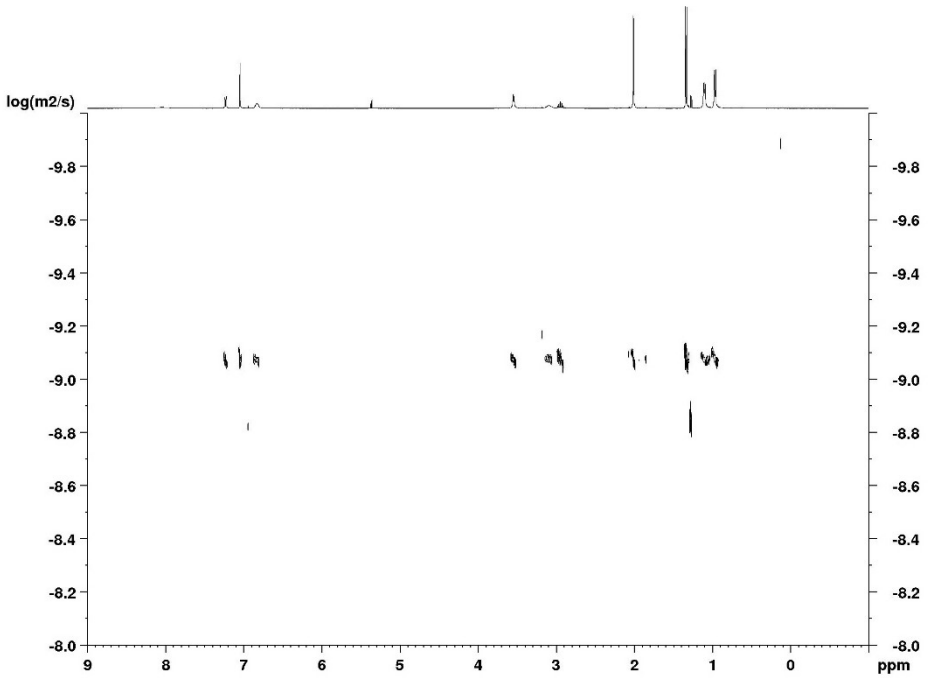

Figure 9.1-75. ^{1}H DOSY spectrum of **[16]**$_2$ in CD_2Cl_2 at +25 °C.

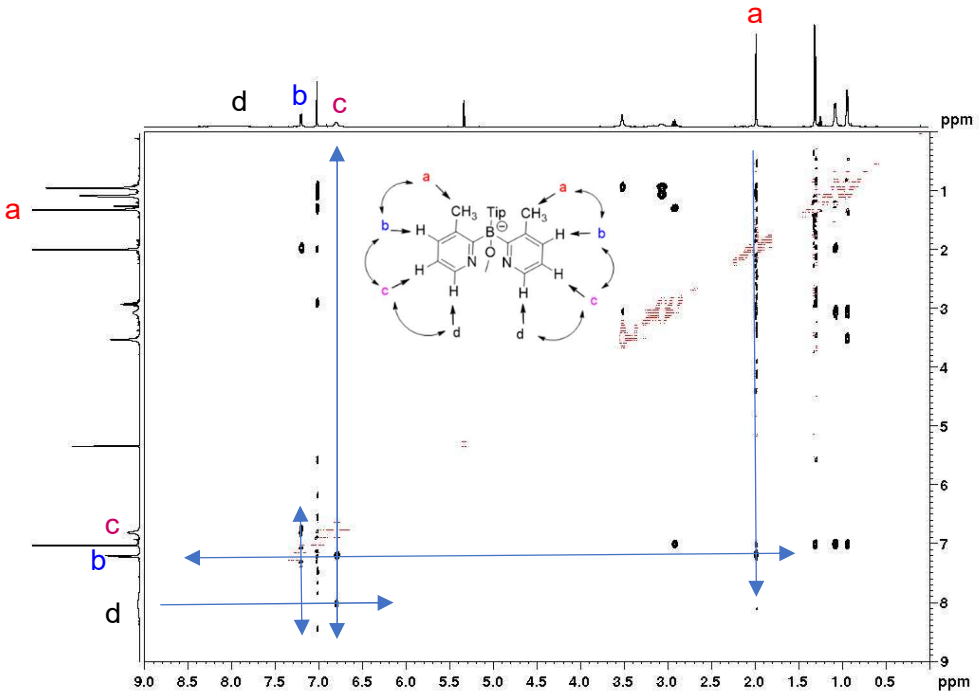

Figure 9.1-76. NOESY spectrum of **[16]**$_2$ in CD_2Cl_2 at 500 MHz.

9.2 Cartesian coordinates

Compound **1**

DFT B3LYP/6-31G+g(d), gas phase, S_0

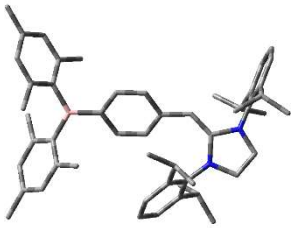

Point group: C_1

Total energy: –1,351,783.31 kcal mol^{-1}

Dipole moment: 6.27 D

Imaginary frequencies: 0

C	0.050985	-0.324350	0.593913
C	-0.642388	0.740063	0.030199
C	0.155349	1.795258	-0.548415
C	1.538391	1.754998	-0.492200
C	2.236139	0.658033	0.068328
C	1.435630	-0.371032	0.613455
B	3.777163	0.591909	0.101154
C	4.487624	-0.809203	0.270948
C	4.622051	1.919056	-0.030251
C	-2.076619	0.854773	-0.130979
C	-3.082273	-0.085368	-0.194350
N	-3.091109	-1.468329	-0.376597
C	-4.415858	-1.930093	-0.439100
C	-5.235814	-0.868922	-0.305723
N	-4.437402	0.267360	-0.177596
C	5.425647	-1.034492	1.310271
C	6.038995	-2.283729	1.448012
C	5.777432	-3.335310	0.564592
C	4.871582	-3.103498	-0.472209
C	4.218093	-1.874316	-0.623706
C	4.411506	3.005256	0.854519
C	5.191479	4.163750	0.744590
C	6.169781	4.304811	-0.240573
C	6.372915	3.232574	-1.115323
C	5.632928	2.050901	-1.017313
C	3.252052	-1.731816	-1.782320
C	3.380983	2.962777	1.966452
C	5.933108	0.936099	-1.996975
C	6.972411	5.576816	-0.372342
C	5.783722	0.051804	2.302520
C	6.439936	-4.680695	0.740028
C	-4.902550	1.558998	0.220385
C	-1.978734	-2.362264	-0.501940
C	-1.194043	-2.328412	-1.668927
C	-0.142511	-3.245164	-1.768806
C	0.123245	-4.152457	-0.745148
C	-0.662753	-4.158509	0.404500
C	-1.725834	-3.260293	0.553445
C	-5.345557	2.476025	-0.752568
C	-5.766639	3.735776	-0.302909
C	-5.741352	4.072626	1.048679
C	-5.297697	3.145689	1.989025
C	-4.872083	1.872543	1.595515
C	-5.452177	2.191025	-2.249188
C	-4.254024	1.481521	-2.902783
C	-6.764767	1.453870	-2.581625
C	-4.394198	0.873701	2.640114
C	-3.095329	1.346687	3.316836
C	-5.490870	0.579138	3.678628
C	-1.494405	-1.356955	-2.799562
C	-0.226637	-0.784720	-3.451315
C	-2.412867	-2.021992	-3.841439
C	-2.536723	-3.248629	1.843194
C	-3.352658	-4.544176	2.000928
C	-1.648656	-3.009700	3.077922
H	-0.507414	-1.114903	1.072863
H	-0.342935	2.640658	-1.019067
H	2.110125	2.580720	-0.910048
H	1.922909	-1.222907	1.082504
H	-2.447256	1.871206	-0.223687
H	-4.623352	-2.977305	-0.584980
H	-6.310993	-0.801806	-0.283992
H	6.748163	-2.437159	2.260275
H	4.669705	-3.899609	-1.187854
H	5.030289	4.976178	1.451951
H	7.136071	3.315506	-1.887972
H	2.218227	-1.882202	-1.457585

H	3.290872	-0.741174	-2.243422
H	3.471484	-2.474677	-2.558017
H	3.238595	1.957867	2.371344
H	3.680113	3.621755	2.789362
H	2.397481	3.295533	1.614078
H	6.691279	1.251175	-2.721662
H	6.300350	0.039574	-1.487307
H	5.041844	0.638098	-2.560888
H	6.954786	6.158300	0.555837
H	8.018856	5.366300	-0.622368
H	6.570814	6.216973	-1.169737
H	4.897140	0.452997	2.806319
H	6.455717	-0.335886	3.075449
H	6.278780	0.896569	1.812748
H	7.479158	-4.575456	1.072532
H	5.917331	-5.283853	1.495168
H	6.438303	-5.251914	-0.194812
H	0.483216	-3.244941	-2.654673
H	0.953447	-4.847279	-0.839305
H	-0.436420	-4.857717	1.204470
H	-6.113345	4.463809	-1.032327
H	-6.064822	5.059779	1.368165
H	-5.280140	3.414021	3.041473
H	-5.522152	3.180922	-2.718847
H	-4.318895	1.597471	-3.991216
H	-3.299207	1.900926	-2.572352
H	-4.244046	0.410912	-2.686975
H	-6.897713	1.389011	-3.668422
H	-7.631985	1.973879	-2.159612
H	-6.751732	0.432237	-2.188614
H	-4.170970	-0.068517	2.133461
H	-2.743515	0.590506	4.029133
H	-2.308263	1.510658	2.575018
H	-3.253045	2.281107	3.869088
H	-5.150235	-0.193740	4.377908
H	-6.409185	0.224737	3.196507
H	-5.741605	1.470765	4.265127
H	-2.034135	-0.507974	-2.377776
H	0.434047	-0.339739	-2.701605
H	0.336838	-1.546430	-4.003176
H	-0.503422	-0.002037	-4.167164
H	-1.919687	-2.886764	-4.302341
H	-2.668942	-1.310404	-4.635810
H	-3.345688	-2.369217	-3.382441
H	-3.244011	-2.416258	1.791818
H	-3.971535	-4.500893	2.905103
H	-4.013682	-4.708066	1.142518
H	-2.693989	-5.416843	2.084053
H	-2.268539	-2.954390	3.980826
H	-1.089315	-2.072435	2.993372
H	-0.925844	-3.821257	3.219496

Compound **2**

DFT B3LYP/6-31G+g(d), gas phase, S_0

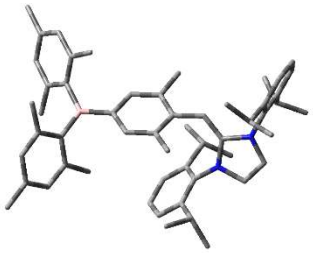

Point group: C_1

Total energy: –1,401,133.24 kcal mol^{-1}

Dipole moment: 5.53 D

Imaginary frequencies: 0

N	4.34982436	0.13364729	0.29038500
B	3.79408131	-0.52368772	0.30893240
C	4.56769392	0.81173258	0.63982432
C	4.31718922	1.99920896	-0.08912226
N	-2.85102593	1.52603811	-0.55837504
C	5.03183306	3.16901758	0.20105332
H	4.83966012	4.06348762	-0.39009831
C	5.98259302	3.21941715	1.22050187
C	6.22485385	2.04637125	1.94324996
H	6.96662684	2.05857779	2.74073589
C	5.55208436	0.85418899	1.66246898
C	4.58426887	-1.85320208	-0.00966550
C	5.53340228	-1.89776744	-1.06399697
C	6.22174584	-3.08103149	-1.34220048
H	6.93713151	-3.09570279	-2.16346699
C	5.10884819	-4.18995730	0.46188219
H	4.95426616	-5.07541175	1.07723952
C	6.02666052	-4.24309497	-0.58702791
C	4.38063133	-3.02806922	0.75180249
C	3.41263496	-3.08853797	1.91792704
H	3.79162198	-3.76240120	2.69500468
H	2.43227940	-3.46548610	1.60137999
H	3.23500540	-2.11169612	2.37262353
C	6.78039498	-5.51116472	-0.90912101
H	6.39945784	-5.97613742	-1.82836102
H	6.68646443	-6.24665495	-0.10302884
H	7.84783158	-5.31392575	-1.06557855
C	5.81586181	-0.68304905	-1.92275599
H	6.51769319	-0.93088888	-2.72604065
H	6.24522882	0.13455712	-1.33474407
H	4.90388381	-0.29315491	-2.38956693
C	3.30526201	2.06399930	-1.21364112
H	3.58023381	2.84643967	-1.93016964
H	2.30363137	2.29674371	-0.83953775
H	3.21488141	1.12197363	-1.76007218
C	2.24609009	-0.54513047	0.30963133
C	5.89676327	-0.36827292	2.48701655
H	6.34542647	-1.15498235	1.87214548
H	5.01169859	-0.80413587	2.96331556
H	6.60562641	-0.11055772	3.28094141
C	6.72205038	4.49524537	1.54454078
H	7.80002524	4.31914046	1.64388701
H	6.37592279	4.92374954	2.49469440
H	6.57282816	5.25134555	0.76630330
C	1.52026906	-1.59756439	-0.28564496
H	2.07037851	-2.39195990	-0.78566621
C	0.13133922	-1.66429278	-0.25594929
C	-0.60768728	-0.62336201	0.37137057
C	0.10221860	0.40198866	1.05230592
C	1.49201888	0.43576689	0.98494321
H	2.02070330	1.22568496	1.51484452
C	-0.57853416	-2.85463037	-0.85270575
H	0.12431201	-3.49766976	-1.39203804
H	-1.37274685	-2.55665569	-1.54373094
H	-1.05576020	-3.46530553	-0.07300508
C	-0.62969314	1.34990781	1.96735383
H	0.07706749	1.98992899	2.50416853
H	-1.21038197	0.78409635	2.70619989
H	-1.33959552	1.99171627	1.44468992
C	-2.06258331	-0.69191412	0.39717487
H	-2.50864808	-1.65603712	0.62438059
C	-2.97596308	0.28021987	0.07683288
C	-4.13404048	2.09217626	-0.71526107
H	-4.25885467	3.04588766	-1.19708137
C	-5.04045766	1.23918233	-0.20208237
H	-6.11391205	1.30576726	-0.12376513
C	-1.71857802	2.04311346	-1.28164657
C	-1.22529676	3.32267242	-0.94348328
C	-0.15218120	3.83293287	-1.68521056
H	0.24537766	4.81281311	-1.43938609
C	0.41892048	3.10483646	-2.72092083

H	1.26495650	3.50793370	-3.27017584
C	-0.10046127	1.85816320	-3.05841062
H	0.33991188	1.30964658	-3.88291550
C	-1.19230895	1.31409229	-2.37472143
C	-1.85414458	0.04202174	-2.88838674
H	-2.17155446	-0.54786866	-2.02670631
C	-3.11350981	0.39949624	-3.70414296
H	-2.84613322	1.00268649	-4.58042758
H	-3.83651121	0.96612853	-3.10952818
H	-3.60830813	-0.51348250	-4.05816358
C	-0.92431305	-0.85028895	-3.72147517
H	-0.67960875	-0.39953129	-4.69070436
H	-1.42217027	-1.80444538	-3.92761759
H	0.00878865	-1.06291967	-3.19047146
C	-1.84504713	4.20477961	0.13475201
H	-2.53046540	3.59342371	0.72920436
C	-0.79754708	4.80346492	1.09182853
H	-0.13152540	4.03735302	1.49444507
H	-1.29872121	5.30040797	1.93088696
H	-0.17945657	5.55587348	0.58925987
C	-2.66217622	5.34777389	-0.50273039
H	-2.00668756	6.01764635	-1.07158536
H	-3.16216476	5.94036091	0.27287720
H	-3.42627480	4.97733645	-1.19374638
C	-4.95015785	-1.03672231	0.84466063
C	-5.04453917	-1.15723478	2.24285391
C	-5.66309103	-2.30283276	2.75720664
H	-5.75788726	-2.42273413	3.83279606
C	-6.15675493	-3.29273037	1.90866873
H	-6.63717098	-4.17366628	2.32643699
C	-6.02698474	-3.16229756	0.52656533
H	-6.40292290	-3.94707767	-0.12381042
C	-5.41015187	-2.03733465	-0.03279162
C	-5.24659858	-1.90533346	-1.53856647
H	-4.60736727	-1.04042219	-1.72786770
C	-6.59823343	-1.63859665	-2.22400516
H	-6.45985491	-1.49960131	-3.30286359
H	-7.07437982	-0.73695689	-1.82275579
H	-7.28843593	-2.47787696	-2.07512802
C	-4.54709710	-3.12994949	-2.15054109
H	-4.35091706	-2.95805437	-3.21553879
H	-5.16297986	-4.03324322	-2.06897553
H	-3.59127383	-3.32582834	-1.65457727
C	-4.49484705	-0.08846919	3.17304464
H	-4.00600842	0.67008179	2.55579794
C	-3.42903638	-0.66593640	4.11995193
H	-2.62507627	-1.14608406	3.55283269
H	-3.85758878	-1.40873075	4.80355204
H	-2.98961058	0.13322152	4.72869644
C	-5.62415041	0.60370188	3.95636635
H	-5.21738764	1.40388667	4.58623544
H	-6.14823338	-0.10473073	4.60924347
H	-6.36357497	1.04453805	3.27791913

Compound **3**

DFT B3LYP/6-31G+g(d), gas phase, S_0

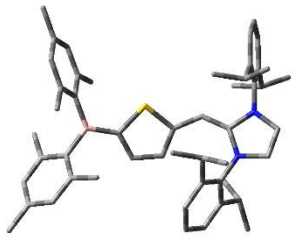

Point group: C_1

Total energy: –1,351,783.31 kcal mol^{-1}

Dipole moment: 7.03 D

Imaginary frequencies: 0

B	-3.555266	0.423918	-0.327586
N	3.194584	-1.713925	0.338193
S	-0.759121	1.116066	-0.126675
C	-2.098023	0.013028	-0.451540
N	4.218971	0.217354	0.086500
C	-1.566059	-1.217519	-0.832082
H	-2.209822	-2.051374	-1.095694
C	0.462928	-0.088707	-0.507650
C	-0.164486	-1.282204	-0.882092
H	0.374910	-2.160515	- 1.202308
C	1.834223	0.307854	-0.386567
H	2.013444	1.374817	-0.471849
C	4.542340	-1.886471	0.691619
H	4.904657	-2.847897	1.017695
C	2.970200	-0.393923	-0.033814
C	5.165830	-0.700038	0.540906
H	6.189599	-0.405487	0.707763
C	2.223416	-2.757476	0.470467
C	2.234747	-3.795894	-0.482235
C	1.281878	-4.810404	-0.340224
H	1.250921	-5.626247	-1.054229
C	0.354788	-4.779499	0.702401
H	-0.385399	-5.570603	0.789141
C	0.366519	-3.738102	1.626273
H	-0.370533	-3.722575	2.422001
C	1.304056	-2.702643	1.531970
C	1.339710	-1.573729	2.551856
H	1.756120	-0.692297	2.061032
C	2.274439	-1.937405	3.720757
H	2.331245	-1.107045	4.435323
H	3.289416	-2.151640	3.367929
H	1.906075	-2.822078	4.254481
C	-0.052305	-1.168958	3.054960
H	0.028612	-0.266977	3.671805
H	-0.513639	-1.947941	3.673592
H	-0.721155	-0.947095	2.219697
C	3.481744	-5.141395	-2.268373
H	4.279304	-5.060895	-3.015463
H	2.602615	-5.553597	-2.777531
H	3.801219	-5.859882	-1.504749
C	3.197743	-3.759307	-1.664624
H	4.154609	-3.363060	-1.307675
C	2.687503	-2.791943	-2.752648
H	3.402966	-2.746127	-3.582765
H	2.549242	-1.777550	-2.367820
H	1.725542	-3.134466	-3.152510
C	4.419727	1.629745	-0.006317
C	4.783553	2.181511	-1.247601
C	4.942648	3.570724	-1.317529
H	5.219559	4.032035	-2.260923
C	4.739671	4.371279	-0.194448
H	4.863160	5.448493	-0.269083
C	4.371853	3.798434	1.022459
H	4.207867	4.435473	1.886910
C	4.200284	2.414767	1.142260
C	3.760166	1.799412	2.462948
H	3.775390	0.711904	2.351598
C	4.726981	2.151439	3.606346
H	4.426961	1.636184	4.526349
H	4.730927	3.227762	3.814427
H	5.753335	1.852056	3.365073
C	2.315863	2.204029	2.810910
H	2.000906	1.716590	3.741400
H	1.619012	1.908681	2.020929
H	2.231302	3.287977	2.952953
C	4.953137	1.311293	-2.483257
H	4.949719	0.266981	-2.156091
C	3.763139	1.495039	-3.444168
H	3.870862	0.835699	-4.313937
H	3.707951	2.528812	-3.806843
H	2.817875	1.254600	-2.947658

C	6.290188	1.568691	-3.197429
H	6.414643	0.864851	-4.028663
H	7.137881	1.445122	-2.513642
H	6.339473	2.581526	-3.614080
C	-4.654465	-0.713977	-0.318822
C	-4.629072	-1.769520	0.623465
C	-5.623097	-2.758573	0.601519
H	-5.595420	-3.548800	1.350881
C	-6.647020	-2.756385	-0.344623
C	-6.668508	-1.713183	-1.277342
H	-7.460362	-1.685894	-2.024891
C	-5.708102	-0.699240	-1.271225
C	-5.812815	0.393682	-2.313382
H	-6.648246	0.200545	-2.994602
H	-4.901764	0.467176	-2.917708
H	-5.967874	1.374787	-1.852940
C	-7.701565	-3.836874	- 0.368143
H	-8.711756	-3.410935	-0.322064
H	-7.587228	-4.523569	0.477394
H	-7.643618	-4.429719	-1.290440
C	-3.573823	-1.877613	1.707303
H	-4.000656	-2.325028	2.612732
H	-3.147368	-0.909703	1.974982
H	-2.735355	-2.509196	1.389828
C	-3.932170	1.953894	-0.203426
C	-3.581420	2.885751	-1.206594
C	-3.920020	4.239668	-1.061318
H	-3.650355	4.936086	-1.854761
C	-4.593685	4.715209	0.061040
C	-4.942427	3.789438	1.053094
H	-5.470839	4.136119	1.940382
C	-4.633746	2.433879	0.935452
C	-5.036433	1.502696	2.058324
H	-5.577740	2.046601	2.839623
H	-4.161472	1.036644	2.527542
H	-5.676975	0.690375	1.700680
C	-4.936344	6.177676	0.215513
H	-4.381951	6.630080	1.048391
H	-6.004170	6.318434	0.424960
H	-4.693615	6.741768	-0.691349
C	-2.890135	2.488415	-2.495876
H	-1.921174	2.993490	-2.591483
H	-3.499342	2.780659	-3.361178
H	-2.703432	1.415796	-2.561637

Compound **4**

DFT B3LYP/6-31G+g(d), gas phase, S_0

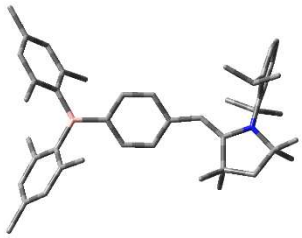

Point group: C_1

Total energy: –1,351,783.31 kcal mol^{-1}

Dipole moment: 4.82 D

Imaginary frequencies: 0

B	-3.784591	0.093293	-0.001429
N	4.414973	-0.683293	0.095992
C	-4.627530	-1.238168	-0.058436
C	-4.417703	-2.274693	0.884034
C	-5.194868	-3.438846	0.833399
H	-5.035975	-4.211489	1.584390
C	-6.168268	-3.634599	-0.147427
C	-6.369716	-2.611506	-1.079663
H	-7.128866	-2.738072	-1.850222
C	-5.633998	-1.423860	-1.041703
C	-3.392982	-2.168762	1.997290
H	-2.405355	-2.511789	1.667050
H	-3.691863	-2.787344	2.850917
H	-3.260348	-1.143905	2.353007
C	-5.936031	-0.362533	-2.078940
H	-6.671215	-0.728588	-2.803238
H	-5.040354	-0.068723	-2.637580
H	-6.334966	0.547417	-1.619154
C	-6.969154	-4.912648	-0.213611
H	-8.020533	-4.714562	-0.452893
H	-6.933217	-5.456329	0.736565
H	-6.580207	-5.582823	-0.992261
C	-4.489298	1.501652	0.068573
C	-4.198229	2.510003	-0.882849
C	-4.855651	3.744982	-0.821129
H	-4.637408	4.496528	-1.578567
C	-5.783593	4.038160	0.179562

C	-6.064731	3.042386	1.120553
H	-6.790688	3.245174	1.906649
C	-5.450346	1.787879	1.072339
C	-3.212135	2.299249	-2.015733
H	-3.199485	1.267789	-2.377466
H	-2.186966	2.530442	-1.703453
H	-3.457365	2.951115	-2.861570
C	-5.831615	0.763543	2.120614
H	-6.511610	1.201046	2.859061
H	-4.956590	0.385353	2.661122
H	-6.327266	-0.104307	1.673590
C	-6.450925	5.390122	0.257450
H	-7.502385	5.301472	0.554501
H	-6.411885	5.911082	-0.705307
H	-5.956947	6.032059	0.999555
C	-2.237775	0.014073	-0.011308
C	-1.430985	1.059204	0.490923
H	-1.911821	1.949891	0.889013
C	-0.047648	0.974497	0.502060
H	0.536856	1.795601	0.911669
C	0.639157	-0.159514	-0.003265
C	-0.166097	-1.183159	-0.551905
H	0.295100	-2.041155	-1.019617
C	-1.552607	-1.102871	-0.533179
H	-2.131348	-1.922442	-0.953654
C	2.092998	-0.116447	0.044161
H	2.464236	0.900698	0.138261
C	3.079257	-1.061866	0.050833
C	5.386916	-1.806988	0.173932
C	4.450053	-2.975775	0.530015
H	4.781571	-3.917505	0.081124
H	4.450918	-3.113230	1.617197
C	2.000680	-3.147226	1.077645
H	0.967606	-2.938064	0.798060
H	2.171386	-2.715478	2.069747
H	2.118461	-4.235493	1.153382
C	2.756271	-3.161407	-1.343276
H	1.775284	-2.880327	-1.729301
H	2.807073	-4.256744	-1.312595
H	3.499409	-2.809690	-2.063438
C	3.019224	-2.591388	0.068447
C	6.443304	-1.589514	1.265779
H	7.031720	-0.686464	1.074363
H	7.130361	-2.443058	1.278899
H	5.990544	-1.508137	2.255609
C	6.137258	-2.020252	-1.154134
H	5.465168	-2.227639	-1.988258
H	6.825040	-2.867764	-1.055907
H	6.729432	-1.134721	-1.403356
C	4.825519	0.684216	-0.015599
C	4.966976	1.272752	-1.294271
C	5.432256	2.590780	-1.373476
H	5.556851	3.054193	-2.348027
C	5.716209	3.325573	-0.225289
H	6.081541	4.346018	-0.307116
C	5.493051	2.761467	1.027787
H	5.664814	3.357456	1.919645
C	5.028395	1.446999	1.158072
C	4.534760	0.564439	-2.570209
H	4.288091	-0.466074	-2.312300
C	5.633719	0.540874	-3.645581
H	5.307912	-0.056936	-4.505238
H	6.566456	0.111749	-3.265907
H	5.856146	1.549225	-4.013477
C	3.249744	1.207225	-3.129444
H	3.424716	2.250149	-3.420160
H	2.445355	1.185860	-2.388940
H	2.909595	0.661396	-4.018135
C	4.667423	0.925299	2.542418
H	4.405374	-0.130223	2.441771
C	5.826573	1.048486	3.546345
H	6.052517	2.098273	3.766697
H	6.742975	0.583176	3.170673
H	5.559664	0.565567	4.494088
C	3.417639	1.647439	3.084062
H	3.600156	2.722801	3.197620
H	3.144501	1.245399	4.067395
H	2.562990	1.513069	2.415525

(BMe_3)TipPBBI(NMe_3)

DFT B3LYP/6-31+G(d), gas phase, S_0

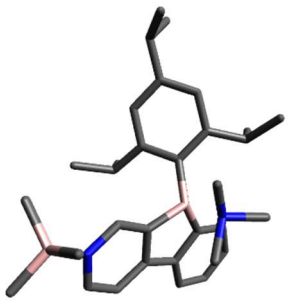

Point group: C_1

Total energy: –883,210.47 kcal mol^{-1}

Dipole moment: 7.97 D

Imaginary frequencies: 0

C	-0.24983000	3.63326100	-0.60960100
C	0.30680100	4.75151100	-1.25241300
C	1.62951100	4.72407100	-1.71177700
C	2.40564300	3.57254300	-1.53760200
C	1.84596700	2.46315500	-0.89348700
C	0.50509600	2.46937000	-0.40367800
C	2.48759200	1.16218500	-0.64032300
C	1.57433700	0.25840400	-0.02708000
B	0.15267600	1.01978600	0.24442700
C	3.79525500	0.75286800	-0.90860800
C	4.18827600	-0.52957900	-0.52227400
N	3.33913400	-1.39419800	0.08293600
C	2.04253100	-1.00768800	0.29521300
C	-1.21195500	0.18661400	-0.15279200
C	-2.51457900	0.36507100	0.42554200
C	-3.49070000	-0.64200900	0.33694800
C	-3.29009300	-1.81185300	-0.40209800
C	-2.12910800	-1.86744600	-1.17653200
C	-1.12627700	-0.88534200	-1.11161300
C	-3.00433800	1.71943400	0.95620600
C	-3.90435700	2.38709200	-0.11825000
C	-3.76456300	1.66229300	2.30167200
C	-0.11100200	-0.88807500	-2.26764200
C	0.51745200	-2.26023800	-2.58708600
C	-0.80475000	-0.31125600	-3.53179800
C	-4.32408200	-2.93229700	-0.44510600
C	-4.52212800	-3.57756900	0.94602400
C	-5.67542300	-2.45811700	-1.02849400
B	3.85882200	-2.88142600	0.69605400
C	5.41115400	-3.10848700	0.25991200
C	2.88388100	-4.03078500	0.06912500
C	3.70000200	-2.73055900	2.32017400
N	0.36010200	1.26970000	2.16755400
C	-0.33407400	2.48261900	2.73413200
C	1.82172000	1.46454300	2.51161200
C	-0.13309600	0.03706500	2.87541100
H	-1.28495800	3.68233300	-0.28826400
H	-0.29665500	5.64178700	-1.40313900
H	2.04939400	5.59109000	-2.21190200
H	3.42626800	3.54460300	-1.90895200
H	4.51662600	1.40488200	-1.38875400
H	5.19462700	-0.88652800	-0.67776500
H	1.41366800	-1.76497900	0.74130200
H	-4.44824100	-0.48658500	0.82521600
H	-2.01540300	-2.68901200	-1.87746700
H	-2.13974900	2.37231700	1.06763000
H	-4.21535200	3.38892900	0.20601000
H	-3.37182200	2.47901100	-1.07055200
H	-4.80620800	1.79042500	-0.29502800
H	-3.98225700	2.67523800	2.66324500
H	-3.20164400	1.13411300	3.08004000
H	-4.72483600	1.14707600	2.19216400
H	0.69984700	-0.20202900	-2.02766800
H	1.28445000	-2.14770700	-3.36292000
H	0.98909000	-2.71046000	-1.70963900
H	-0.22564400	-2.96956100	-2.97010500
H	-0.08794300	-0.24146400	-4.35975300
H	-1.20529000	0.68958300	-3.33714000
H	-1.63457100	-0.95294500	-3.85141100
H	-3.92993300	-3.70872000	-1.11667800
H	-5.22768400	-4.41529800	0.88744400
H	-3.57361400	-3.95501600	1.34366500
H	-4.92236300	-2.84976900	1.66269200
H	-6.37875300	-3.29646300	-1.10270300
H	-5.54418800	-2.02987600	-2.02832000
H	-6.13484900	-1.69224700	-0.39168200
H	6.11457100	-2.37176500	0.68233400
H	5.73105000	-4.08851600	0.64252700
H	5.56875200	-3.13820400	-0.83090200
H	1.81810000	-3.92212300	0.32852400

H	3.19479000	-5.0104050	0 0.46205800
H	2.95192400	-4.09251900	-1.02781800
H	4.04499400	-3.65511500	2.80651600
H	4.30723400	-1.90783800	2.73197000
H	2.65949000	-2.57392000	2.65234400
H	-1.40207000	2.31726300	2.79001400
H	0.03677500	2.67122100	3.74845400
H	-0.11880800	3.34517200	2.10353400
H	2.39288100	0.57060300	2.28304300
H	1.90721800	1.67673200	3.58341100
H	2.21308000	2.30814700	1.94238600
H	-0.02275300	0.15954700	3.95986700
H	-1.17723900	-0.13532600	2.62037900
H	0.45668300	-0.82078300	2.55365700

(BMe_3)TipPBB2(NMe_3)

DFT B3LYP/6-31+G(d), gas phase, S_0

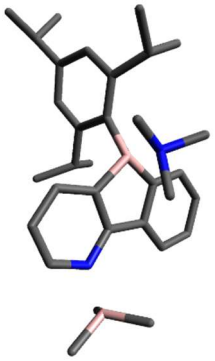

Point group: C_1

Total energy: –883,193.65 kcal mol^{-1}

Dipole moment: 8.27 D

Imaginary frequencies: 0

C	-0.62337100	1.59923100	2.39563400
C	-1.56224400	1.67590300	3.43492100
C	-2.84311300	1.14852500	3.24823400
C	-3.19763200	0.53238400	2.04065400
C	-2.26180100	0.44840100	0.9967570
C	-0.95386500	1.00426900	1.17409900
C	-2.33796500	-0.23514800	-0.33493500
C	-1.06228900	-0.16908400	-0.97916000
B	-0.05172500	0.79096000	-0.14690900
N	-3.39607100	-0.88360200	-0.9240730
C	-3.16046600	-1.54074300	-2.10163600
C	-1.92929800	-1.56546800	-2.73697900
C	-0.86269100	-0.85162000	-2.17444300
C	1.50073600	0.18112400	0.02065600
C	2.79518400	0.76702200	-0.22820600
C	3.96334100	-0.01978700	-0.23333100
C	3.96580500	-1.38400200	0.04660300
C	2.74236600	-1.93709600	0.41683400
C	1.54535100	-1.20430000	0.43688900
C	3.09773900	2.27397800	-0.34967800
C	3.61867200	2.81997300	1.00415600
C	4.07927700	2.65080500	-1.48707300
C	0.36097800	-1.98006300	1.04496100
C	0.07510200	-3.32955600	0.34642300
C	0.59011600	-2.19520300	2.56307800

C	5.23883100	-2.22317200	0.00364400
C	5.84627300	-2.27111400	-1.41734400
C	6.28683500	-1.74097200	1.03324700
N	-0.29535000	2.35582400	-1.05685200
C	0.01716800	3.55402300	-0.17820900
C	-1.74267700	2.57216100	-1.47584200
C	0.49412900	2.33558700	-2.34639900
B	-5.03696200	-0.90866400	-0.38355200
C	-5.08164100	-1.89855400	0.92740600
C	-5.98109800	-1.56595400	-1.54916000
C	-5.49627500	0.66060200	-0.23632300
H	0.37980200	1.98818400	2.55162100
H	-1.29319400	2.13199200	4.38317900
H	-3.57463500	1.20109700	4.04836200
H	-4.18721400	0.12309800	1.93707800
H	-4.00874200	-2.05157900	-2.52276800
H	-1.81787400	-2.12819800	-3.65676000
H	0.11317300	-0.84993000	-2.65110500
H	4.91089000	0.46534200	-0.44195000
H	2.72002300	-2.97981300	0.7200000
H	2.18236400	2.80768800	-0.56384300
H	3.79765500	3.90179600	0.94825800
H	2.90168700	2.62668400	1.8108490
H	4.56041400	2.33244100	1.27988400
H	4.11126300	3.74099700	-1.60679500
H	3.78142700	2.20951200	-2.44554900
H	5.10174700	2.32073500	-1.27785100
H	-0.54133500	-1.38554700	0.96185700
H	-0.83026900	-3.78333300	0.76751900
H	-0.08021600	-3.19734000	-0.72908000
H	0.89421600	-4.04500800	0.48336300
H	-0.27649400	-2.69885300	3.00893700
H	0.72934900	-1.23757300	3.07576800
H	1.47616900	-2.81346400	2.75020000
H	4.95662900	-3.25036700	0.2774050
H	6.72962700	-2.92104100	-1.43973900
H	5.11996900	-2.65321600	-2.14326300
H	6.15603600	-1.27144200	-1.74607100
H	7.16805400	-2.39408200	1.02315300
H	5.87102300	-1.73988100	2.04680100
H	6.62318900	-0.72179000	0.80646600
H	0.86564400	3.36638600	0.46854700
H	0.20793500	4.43130000	-0.80553900
H	-0.84726900	3.73983100	0.45756100
H	-2.03666800	1.82782300	-2.21104500
H	-1.82560100	3.57194300	-1.91604900
H	-2.39132800	2.49989800	-0.60541800
H	0.47254300	3.32722000	-2.81190700
H	1.51660200	2.02363900	-2.17663100
H	0.02144900	1.61506300	-3.01409500
H	-4.22073400	-1.85909000	1.60675300
H	-5.97793300	-1.69038800	1.53292600
H	-5.16257600	-2.94665400	0.60115800
H	-5.96618900	-1.03015100	-2.51217900
H	-7.01548300	-1.49961700	-1.17896100
H	-5.80416100	-2.63567600	-1.74715800
H	-6.49547700	0.69313500	0.22502500
H	-4.85975200	1.33244100	0.35129300
H	-5.60119200	1.11583800	-1.23429700

TipPBB2

DFT B3LYP/6-31G, gas phase, S_0

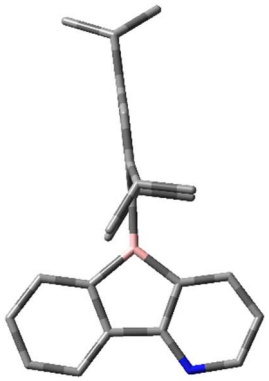

Point group: C_1

Total energy: –682,866.42 kcal mol^{-1}

Dipole moment: 1.49 D

Imaginary frequencies: 0

C	-1.75597300	-2.55849500	-0.11321600
C	-1.86223200	-1.16727000	-0.07157800
C	-3.17418100	-0.60956300	-0.11577500
H	-0.78494000	-3.04421200	-0.08296700
C	-1.76678300	1.30221400	0.01612400
C	-1.49812500	2.67201100	0.07522100
C	-2.56038600	3.59478800	0.05525300
C	-3.88495700	3.14749400	-0.02355600
C	-4.17786800	1.77248400	-0.08395600
C	-3.12045800	0.87068600	-0.06346600
H	-0.47280400	3.02621700	0.13640600
H	-2.35397500	4.65967200	0.10106700
H	-4.69584000	3.86944200	-0.03823900
H	-5.20079000	1.41670600	-0.14510700
B	-0.82836100	0.02651400	0.01833500
C	0.73953000	-0.00974700	0.09353800
C	1.53892200	0.04131400	-1.09283800
C	1.41834700	-0.04254300	1.35089300
C	2.93774700	0.11395000	-0.99185400
C	2.82168300	0.03225600	1.38876100
C	3.60536800	0.12294300	0.23687500
H	3.51558500	0.16280800	-1.91147600
H	3.31568500	0.01755000	2.35790300
C	0.74415400	-0.24785200	2.71937800
H	1.49543300	0.05880000	3.46087600
C	0.99821200	-0.06998300	-2.53004200
H	1.81568600	0.28273300	-3.17474000
C	0.46061000	-1.74936100	2.97884000
H	-0.30513800	-2.12923400	2.29434500
H	1.36766500	-2.34845500	2.84299000
H	0.09966100	-1.89884900	4.00414100
C	-0.51046400	0.59722500	3.01095000
H	-0.34869600	1.65660100	2.78946000
H	-1.38394100	0.26320000	2.44157400
H	-0.77255300	0.50549900	4.07219000
C	0.74475700	-1.54980000	-2.91475200
H	1.63665500	-2.15966200	-2.73392600
H	-0.08116800	-1.97195200	-2.33270600
H	0.48279200	-1.62935500	-3.97726200
C	-0.22517800	0.79725800	-2.88288100
H	-1.14832200	0.42877800	-2.42382900
H	-0.08856700	1.83873000	-2.57600700
H	-0.38396800	0.77813900	-3.96812600
C	-2.93316800	-3.32746700	-0.19550400
H	-2.89076800	-4.4105250	-0.22981000
C	-4.16842700	-2.67754100	-0.23293300
H	-5.09208900	-3.24376700	-0.29623600
N	-4.30725700	-1.32338500	-0.19412600
C	5.12572700	0.22017400	0.32615500
H	5.38764200	0.20324600	1.39418200
C	5.65222800	1.55044100	-0.26018000
C	5.82118000	-0.98877300	-0.34135200
H	5.43059500	1.62351100	-1.33181700
H	5.19091900	2.41051800	0.23752700
H	6.73959200	1.62346800	-0.13644100
H	5.47877400	-1.93236000	0.09764600
H	5.60889500	-1.02157500	-1.41685500
H	6.90897900	-0.92561200	-0.21618600

TipPBB1

DFT B3LYP/6-31G, gas phase, S_0

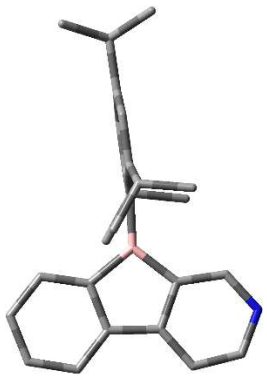

Point group: C_1

Total energy: –683,136.40 kcal mol^{-1}

Dipole moment: 2.83 D

Imaginary frequencies: 0

C	4.03262989	-2.79875575	-0.22492747
C	1.76049707	-2.52932920	-0.10530449
C	1.86880150	-1.14286707	-0.06837388
C	3.16994412	-0.57700028	-0.11491162
C	4.27386132	-1.41480300	-0.19455101
H	4.87059692	-3.49109534	-0.28707986
H	0.78526341	-3.01159892	-0.07225277
H	5.29235792	-1.03776586	-0.23293453
C	1.73841260	1.31382059	0.01298641
C	1.43856995	2.67142854	0.06924961
C	2.47526357	3.61713083	0.04750540
C	3.80643445	3.19871652	-0.03037620
C	4.12724495	1.83288439	-0.08792479
C	3.09327789	0.90381555	-0.06584963
H	0.40238949	2.99716807	0.12988156
H	2.24593183	4.67854550	0.09121342
H	4.60330299	3.93761977	-0.04667246
H	5.16666264	1.51950656	-0.14827086
B	0.82533332	0.02738312	0.01881239
C	-0.73392966	-0.01519463	0.09500247
C	-1.40272705	-0.04242653	1.34672512
C	-1.52482675	0.03435390	-1.08588485
C	-2.80142354	0.03851264	1.38914464
C	-2.91839045	0.11360673	-0.98767947
C	-3.58290069	0.13006564	0.23960470
H	-3.29481744	0.02565880	2.35988294
H	-3.49699716	0.15897954	-1.90800964
C	-0.96795956	-0.09851912	-2.50395419
H	-1.76212830	0.26343748	-3.17003186
C	-0.71149152	-0.25965129	2.69320081
H	-1.43566253	0.05959882	3.45412145
C	-0.73457206	-1.58217953	-2.85254668
H	0.06765493	-2.00646791	-2.24064349
H	-1.64055446	-2.17348645	-2.68055086
H	-0.44640555	-1.68980845	-3.90583575
C	0.28034485	0.73040585	-2.83077829
H	0.17213872	1.77537672	-2.52500860
H	1.18297542	0.33174464	-2.35588378
H	0.46243351	0.70458456	-3.91210307
C	-0.45050083	-1.76118463	2.92695581
H	-1.37096893	-2.34330868	2.80902878
H	0.28653265	-2.14546019	2.21479450
H	-0.06113425	-1.93173301	3.93856727
C	0.56601528	0.55058606	2.94560746
H	1.41579142	0.18391778	2.36014740
H	0.43201972	1.61211067	2.71676233
H	0.85399954	0.45872490	3.99999415
N	2.81889374	-3.36061937	-0.18255810
C	-5.09556048	0.23349282	0.32577514
H	-5.36057622	0.21950915	1.39195041
C	-5.78667191	-0.96865161	-0.34165658
H	-5.43969081	-1.91347990	0.09136098
H	-6.87456456	-0.90938525	-0.21424256
H	-5.57696733	-0.99667390	-1.41771434
C	-5.60741873	1.55923609	-0.26462127
H	-5.13471474	2.41781438	0.22537933
H	-5.38753849	1.62313846	-1.33714642
H	-6.69379840	1.64528699	-0.13936190

DipPBBI

DFT B3LYP/6-31G, gas phase, S_0

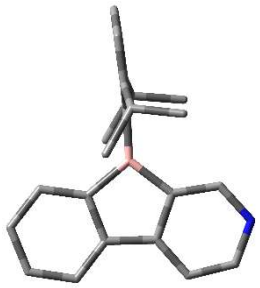

Point group: C_1

Total energy: –608,870.85 kcal mol^{-1}

Dipole moment: 3.14 D

Imaginary frequencies: 0

C	3.01845500	3.07678400	0.00007300
C	0.75124200	2.58608000	0.00000400
C	0.99496200	1.21306500	0.00000800
C	2.35449800	0.77652800	0.00003200
C	3.38000700	1.71715200	0.00006800
H	3.78418500	3.84642300	0.00009100
H	-0.26002200	2.98068500	-0.00002000
H	4.42750100	1.43380200	0.00007900
C	1.10274200	-1.25147500	-0.00013900
C	0.93998200	-2.63832200	-0.00026500
C	2.06875500	-3.47820800	-0.00028500
C	3.35538600	-2.92866300	-0.00018300
C	3.54118200	-1.53384200	-0.00006600
C	2.42026000	-0.70792900	-0.00004300
H	-0.05709600	-3.06965400	-0.00033700
H	1.94351900	-4.55644300	-0.00038000
H	4.22106200	-3.58379400	-0.00020600
H	4.54570700	-1.12095300	-0.00000400
B	0.06050700	-0.05918600	-0.00007100
C	-1.50614100	-0.16649300	0.00001500
C	-2.23695300	-0.24672600	-1.22812600
C	-2.23682800	-0.24681500	1.22825400
C	-3.62677500	-0.45866900	-1.19919600
C	-3.62664300	-0.45875600	1.19944500
C	-4.32325900	-0.57731700	0.00015200
H	-4.16458300	-0.52791700	-2.14084500
H	-4.16436900	-0.52804900	2.14113800
C	-1.64379100	-0.02387000	2.63102700
H	-2.38779100	-0.43532100	3.32783200
C	-1.64407100	-0.02367400	-2.63094800
H	-2.38807400	-0.43518900	-3.32771500
C	-1.53217600	1.48864700	2.95066800
H	-0.78664500	1.97304800	2.31154500
H	-2.49173300	1.99380500	2.79639800
H	-1.22883000	1.63755500	3.99447500
C	-0.31951000	-0.74275800	2.95116600
H	-0.35801500	-1.80496800	2.69075100
H	0.53559800	-0.29699700	2.43232300
H	-0.11225600	-0.66106600	4.02522900
C	-1.53268200	1.48890300	-2.95043200
H	-2.49229600	1.99392100	-2.79606200
H	-0.78719100	1.97331000	-2.31125400
H	-1.22938300	1.63798400	-3.99422700
C	-0.31970800	-0.74230700	-2.95125900
H	0.53535700	-0.29648600	-2.43239300
H	-0.35802500	-1.80456700	-2.69103400
H	-0.11251700	-0.66039100	-4.02531700
N	1.74349900	3.51880500	0.00003600
H	-5.39473800	-0.75244500	0.00021200

DipPBB2

DFT B3LYP/6-31G, gas phase, S_0

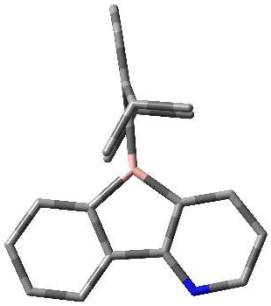

Point group: C_1

Total energy: –608,873.07 kcal mol^{-1}

Dipole moment: 1.16 D

Imaginary frequencies: 0

C	0.75090300	2.60022100	0.00011500
C	0.97767200	1.22282900	0.00003400
C	2.33445600	0.78283300	-0.00003400
H	-0.25950700	2.99871500	0.00017200
C	1.09690400	-1.24738900	-0.00007700
C	0.94777800	-2.63655800	-0.00014300
C	2.08727200	-3.46234400	-0.00022200
C	3.36934500	-2.89928100	-0.00023400
C	3.54211000	-1.50274400	-0.00017300
C	2.40938600	-0.69741100	-0.00010000
H	-0.04387200	-3.08055100	-0.00014000
H	1.97384600	-4.54205000	-0.00027200
H	4.24064300	-3.54716800	-0.00029100
H	4.53131300	-1.05761000	-0.00018400
B	0.05121200	-0.05865200	0.00001500
C	-1.51624300	-0.16281500	0.00003500
C	-2.24772500	-0.23830300	-1.22807200
C	-2.24767600	-0.23845100	1.22815600
C	-3.63921400	-0.43947300	-1.19920600
C	-3.63917000	-0.43962100	1.19931600
C	-4.33682100	-0.55234900	0.00006200
H	-4.17735800	-0.50609400	-2.14088600
H	-4.17727700	-0.50635900	2.14100800
C	-1.65246300	-0.02483000	2.63163900
H	-2.40330300	-0.42567300	3.32725700
C	-1.65256300	-0.02452300	-2.63154900
H	-2.40343700	-0.42526200	-3.32719200
C	-1.51941300	1.48536200	2.95404500
H	-0.76369400	1.95843200	2.31821500
H	-2.47108600	2.00493200	2.79769000
H	-1.21703500	1.62789900	3.99904800
C	-0.33928100	-0.76365500	2.95260900
H	-0.39269200	-1.82397800	2.68750100
H	0.52391000	-0.32999000	2.43738000
H	-0.13396200	-0.68952700	4.02759800
C	-1.51947400	1.48569800	-2.95377300
H	-2.47112100	2.00528100	-2.79730600
H	-0.76370500	1.95867900	-2.31793400
H	-1.21715000	1.62834300	-3.99877700
C	-0.33941300	-0.76334700	-2.95265400
H	0.52379700	-0.32979900	-2.43735900
H	-0.39286400	-1.82371500	-2.68772700
H	-0.13409800	-0.68903900	-4.02763100
H	-5.40956500	-0.71968600	0.00007000
C	1.85814800	3.47077300	0.00011900
H	1.72188900	4.54659300	0.00018000
C	3.14639500	2.93214200	0.00004600
H	4.01839200	3.57817900	0.00004400
N	3.40234400	1.59459200	-0.00002600

TipPBB3

DFT B3LYP/6-31G, gas phase, S_0

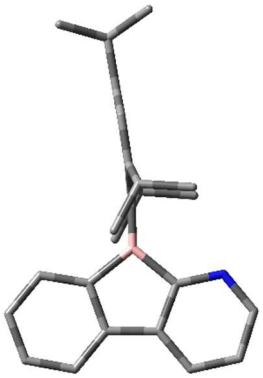

Point group: C_1

Total energy: –682,862.83 kcal mol^{-1}

Dipole moment: 2.87 D

Imaginary frequencies: 0

C	4.15292100	-2.71866500	-0.23830500
C	1.92793900	1.11460500	-0.07478100
C	3.22082000	-0.51667300	-0.11525400
C	4.35021700	-1.32846300	-0.19818200
H	4.99951300	-3.39400800	-0.30286500
H	5.35278700	-0.91280700	-0.23129700
C	1.72530300	1.33826900	0.02229700
C	1.39320900	2.69271500	0.08625600
C	2.40760300	3.66784600	0.07243200
C	3.75000100	3.28319700	-0.00523100
C	4.10672300	1.92302400	-0.07055300
C	3.09932900	0.96227300	-0.05669400
H	0.35107800	2.99353600	0.14667000
H	2.15018300	4.72117400	0.12208000
H	4.52782000	4.04068400	-0.01542600
H	5.15408100	1.64130000	-0.13051800
B	0.83279500	0.03296600	0.01847800
C	-0.72983400	-0.04129700	0.09166500
C	-1.40797300	-0.08180000	1.34711700
C	-1.52815500	0.00817800	-1.09333800
C	-2.80844900	0.02582200	1.38841300
C	-2.92435600	0.11357100	-0.99359800
C	-3.58950400	0.14639600	0.23676900
H	-3.30180200	0.00613700	2.35787000
H	-3.50139100	0.16138900	-1.91386800
C	-0.97920400	-0.18149200	-2.51604900
H	-1.77442400	0.16455100	-3.19187000
C	-0.72745900	-0.37044900	2.69403100
H	-1.45382600	-0.07598300	3.46507800
C	-0.76798200	-1.69119200	-2.80377500
H	-0.03523100	-2.12552300	-2.11491300
H	-1.70691600	-2.24209800	-2.68022900
H	-0.41415500	-1.84113900	-3.83192600
C	0.27885300	0.62563000	-2.88758200
H	0.17324000	1.68650800	-2.64001200
H	1.17965000	0.24830900	-2.39086500
H	0.46075800	0.54169000	-3.96611500
C	-0.49515100	-1.89611200	2.85209400
H	-1.44336100	-2.44011100	2.77908900
H	0.16758400	-2.27742400	2.06756500
H	-0.04607200	-2.11781200	3.82879600
C	0.56309600	0.41230800	3.00068800
H	1.41107800	0.07461000	2.39448300
H	0.43786600	1.48778800	2.84078400
H	0.84681300	0.25212800	4.04816500
C	2.85418400	-3.23581500	-0.19465200
H	2.68080300	-4.30606600	-0.22450400
N	1.74696400	-2.45299000	-0.11383000
C	-5.10660000	0.28461000	0.32767300
H	-5.36753400	0.27757500	1.39610000
C	-5.83565800	-0.90675400	-0.33558300
C	-5.59769000	1.62701100	-0.26169900
H	-5.62602700	-0.94797100	-1.41130400
H	-5.51712900	-1.85783900	0.10497800
H	-6.92128200	-0.81431900	-0.20864900
H	-5.11316300	2.47561300	0.23381800
H	-5.37398500	1.69125300	-1.33350600
H	-6.68277500	1.72975700	-0.13815200

DipPBB3

DFT B3LYP/6-31G, gas phase, S_0

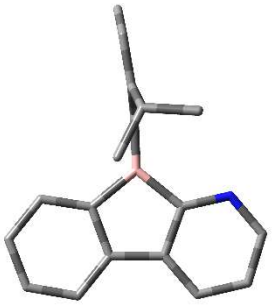

Point group: C_1

Total energy: –608,869.52 kcal mol^{-1}

Dipole moment: 3.13 D

Imaginary frequencies: 0

C	3.04602400	3.04985800	0.00003600
C	1.01832600	1.19577300	0.00002800
C	2.37256400	0.75219100	-0.00005600
C	3.40212100	1.69102500	-0.00005000
H	3.81013500	3.81997100	0.00004300
H	4.44678200	1.39494600	-0.00011000
C	1.09858300	-1.26616300	-0.00010100
C	0.92384600	-2.65122100	-0.00016000
C	2.04456200	-3.50217400	-0.00024600
C	3.33511800	-2.96327300	-0.00027400
C	3.53363100	-1.56961800	-0.00021600
C	2.42167000	-0.73208500	-0.00013100
H	-0.07771300	-3.07198000	-0.00014000
H	1.90957000	-4.57918900	-0.00029200
H	4.19551900	-3.62552100	-0.00034100
H	4.54269200	-1.16750800	-0.00023900
B	0.06200100	-0.07262900	-0.00000700
C	-1.50109000	-0.18316300	0.00004400
C	-2.22982200	-0.27541000	-1.22646700
C	-2.22973600	-0.27555500	1.22659600
C	-3.60806600	-0.55028600	-1.19988500
C	-3.60798300	-0.55042500	1.20007600
C	-4.29647300	-0.71009400	0.00011000
H	-4.14358100	-0.62992300	-2.14213200
H	-4.14343300	-0.63017300	2.14235100
C	-1.64319500	0.03728100	2.61185600
H	-2.36081600	-0.37037500	3.33827500
C	-1.64337200	0.03758800	-2.61172900
H	-2.36101900	-0.37002000	-3.33814800
C	-1.60036900	1.57216100	2.83291100
H	-0.95565100	2.05958400	2.09340300
H	-2.60258500	2.00390700	2.73545900
H	-1.22161300	1.80577700	3.83624400
C	-0.28297300	-0.60099000	2.95059000
H	-0.27291700	-1.67644300	2.74771200
H	0.54379400	-0.14235300	2.39692100
H	-0.06488500	-0.45083000	4.01510200
C	-1.60061300	1.57249200	-2.83263100
H	-2.60284000	2.00419100	-2.73508400
H	-0.95587600	2.05986500	-2.09310800
H	-1.22191700	1.80622300	-3.83596000
C	-0.28314300	-0.60059800	-2.95060000
H	0.54363500	-0.14199400	-2.39692000
H	-0.27303900	-1.67607300	-2.74784000
H	-0.06511400	-0.45031400	-4.01510700
H	-5.35832400	-0.93691100	0.00013400
C	1.69520800	3.41234800	0.00011200
H	1.39969700	4.45590800	0.00017900
N	0.68437100	2.50491500	0.00010800

TipPBB4

DFT B3LYP/6-31G, gas phase, S_0

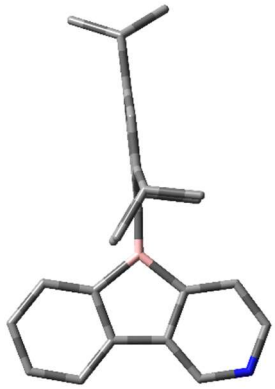

Point group: C_1

Total energy: –682,862.76 kcal mol^{-1}

Dipole moment: 2.72 D

Imaginary frequencies: 0

C	-1.75312800	-2.54565800	-0.11416900
C	-1.87740100	-1.15705600	-0.07279300
C	-3.18904000	-0.60019400	-0.11694600
C	-4.29210300	-1.44428500	-0.19890100
H	-0.78029100	-3.02637200	-0.08375100
H	-5.30991900	-1.06848800	-0.23509300
C	-1.76751700	1.31018300	0.01714600
C	-1.48448200	2.67690700	0.07785100
C	-2.53333600	3.61360500	0.05946700
C	-3.86081700	3.17879600	-0.01956900
C	-4.16816900	1.80679000	-0.08157300
C	-3.12603400	0.88335400	-0.06305600
H	-0.45434300	3.01681500	0.13921800
H	-2.31539000	4.67587500	0.10652600
H	-4.66584600	3.90719300	-0.03335700
H	-5.20394800	1.48669900	-0.14250200
B	-0.83309700	0.03830900	0.01856400
C	0.73337600	-0.00469100	0.09351300
C	1.53269700	0.04622600	-1.09294600
C	1.41200100	-0.03949600	1.35090600
C	2.93129800	0.12068800	-0.99174900
C	2.81513900	0.03718900	1.38892300
C	3.59869700	0.13044900	0.23713700
H	3.50912900	0.16984400	-1.91133300
H	3.30899800	0.02140000	2.35809800
C	0.73882400	-0.25311600	2.71844300
H	1.48060700	0.07322300	3.46110900
C	0.99297300	-0.07124600	-2.52987800
H	1.80187600	0.30029700	-3.17481200
C	0.48857700	-1.76030400	2.98056200
H	-0.26484600	-2.15941700	2.29316600
H	1.40955000	-2.33885400	2.85017000
H	0.12641600	-1.91571900	4.00449200
C	-0.53629200	0.56218600	3.00362300
H	-0.39952800	1.62523100	2.78332900
H	-1.39927300	0.20588700	2.43103300
H	-0.80151900	0.46360500	4.06341700
C	0.77016400	-1.55585000	-2.91598400
H	1.67515700	-2.14683600	-2.73811500
H	-0.04482300	-1.99643800	-2.33198400
H	0.50715200	-1.63983500	-3.97783600
C	-0.24965900	0.76871800	-2.87974200
H	-1.16347500	0.37896500	-2.41876000
H	-0.13593600	1.81341700	-2.57481100
H	-0.41133800	0.74437800	-3.96440400
C	-2.92184300	-3.32695900	-0.19712000
H	-2.86662900	-4.41015100	-0.23138800
N	-4.16062000	-2.79716900	-0.23873500
C	5.11884500	0.23019300	0.32658100
H	5.38070100	0.21301600	1.39458700
C	5.64296200	1.56176400	-0.25893700
C	5.81625400	-0.97718700	-0.34169700
H	5.42153000	1.63502500	-1.33060200
H	5.18015500	2.42080400	0.23919200
H	6.73013000	1.63654300	-0.13489000
H	5.47533600	-1.92165200	0.09650700
H	5.60440900	-1.00954900	-1.41729200
H	6.90386700	-0.91230400	-0.21615200

DipPBB4

DFT B3LYP/6-31G, gas phase, S_0

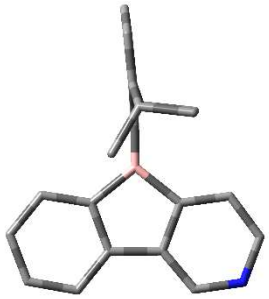

Point group: C_1

Total energy: –608,869.38 kcal mol^{-1}

Dipole moment: 2.48 D

Imaginary frequencies: 0

C	0.73583200	2.58957600	0.00007500
C	0.98801600	1.21777200	0.00000500
C	2.34681700	0.78615600	-0.00006800
C	3.36830600	1.73089200	-0.00006900
H	-0.27814400	2.97726700	0.00013400
H	4.41747900	1.45222700	-0.00013100
C	1.10620600	-1.25089100	-0.00009900
C	0.95006600	-2.63919000	-0.00015800
C	2.08198600	-3.47383700	-0.00024800
C	3.36500500	-2.91585500	-0.00027700
C	3.54481400	-1.51998000	-0.00022100
C	2.42094500	-0.69786600	-0.00013300
H	-0.04526700	-3.07485700	-0.00014300
H	1.96273600	-4.55266000	-0.00029400
H	4.23460800	-3.56591500	-0.00034200
H	4.54768900	-1.10377500	-0.00024500
B	0.05834700	-0.07136200	-0.00000400
C	-1.50778000	-0.17704600	0.00005700
C	-2.23882200	-0.25515700	-1.22813600
C	-2.23871200	-0.25530000	1.22830300
C	-3.62891900	-0.46518100	-1.19921200
C	-3.62881300	-0.46532000	1.19947900
C	-4.32550800	-0.58319100	0.00015800
H	-4.16674600	-0.53409900	-2.14087700
H	-4.16655400	-0.53435400	2.14118400
C	-1.64607500	-0.03142500	2.63111400
H	-2.38419400	-0.45372700	3.32764500
C	-1.64630700	-0.03111400	-2.63097000
H	-2.38447400	-0.45336000	-3.32748500
C	-1.55196000	1.48158200	2.95505300
H	-0.81183700	1.97541300	2.31648800
H	-2.51753000	1.97596600	2.80292300
H	-1.24934900	1.63105100	3.99895800
C	-0.31243800	-0.73393500	2.94732700
H	-0.33718800	-1.79583600	2.68464400
H	0.53659200	-0.27615900	2.42866000
H	-0.10443800	-0.65174500	4.02116400
C	-1.55225200	1.48192600	-2.95475400
H	-2.51781900	1.97627200	-2.80247900
H	-0.81207900	1.97571000	-2.31621200
H	-1.24974600	1.63151000	-3.99867300
C	-0.31268000	-0.73355900	-2.94737400
H	0.53638300	-0.27582400	-2.42872800
H	-0.33738300	-1.79549300	-2.68481100
H	-0.10477400	-0.65123800	-4.02121900
H	-5.39707800	-0.75766700	0.00019400
C	1.82863200	3.47784400	0.00007100
H	1.67361500	4.55183300	0.00012700
N	3.11222900	3.06640900	0.00000000

^{F}XylPBB1

DFT B3LYP/6-31G, gas phase, S_0

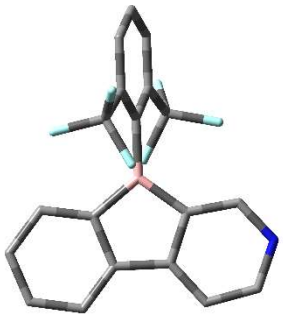

Point group: C_1

Total energy: –883,786.76 kcal mol^{-1}

Dipole moment: 3.51 D

Imaginary frequencies: 0

C	3.29642000	-2.18270700	-2.11069600
C	1.01380100	-1.89824600	-1.81032400
C	1.21576400	-0.90354000	-0.85654600
C	2.55783300	-0.54875200	-0.52651900
C	3.61349000	-1.19540700	-1.15863200
H	4.08734300	-2.71229400	-2.63275100
H	0.01827900	-2.22149300	-2.09500200
H	4.65080700	-0.96229600	-0.94232300
C	1.23248200	0.89262000	0.83907900
C	1.01938400	1.89105400	1.79163400
C	2.11828800	2.51740300	2.40764600
C	3.42204200	2.14405600	2.06826100
C	3.65835700	1.14124800	1.10855200
C	2.56975100	0.52423700	0.50226300
H	0.01128900	2.19665000	2.05268100
H	1.95468400	3.29442500	3.14727100
H	4.26410300	2.63264900	2.54858200
H	4.67675000	0.86339800	0.85442600
B	0.26274100	-0.00139600	-0.00470700
C	-1.31819900	0.00262100	0.00344200
C	-2.06758200	-1.03430600	0.60788900
C	-2.07115500	1.04098900	-0.59361300
C	-3.46796400	-1.03645700	0.61752100
C	-3.47183300	1.04488900	-0.59152300
C	-4.17342700	0.00466200	0.01578000
H	-3.99699200	-1.84860000	1.10142000
H	-4.00394200	1.85696300	-1.07220500
N	2.03767700	-2.53758500	-2.44014500
C	-1.37531200	2.21399700	-1.20370300
F	-2.13327700	2.82780100	-2.19447800
F	-0.15578800	1.85911700	-1.78748000
F	-1.08314000	3.20921800	-0.26652100
C	-1.36688700	-2.20818500	1.21150100
F	-2.12021300	-2.82526300	2.20407000
F	-0.14663000	-1.84979000	1.79370400
F	-1.07365000	-3.19832900	0.27190600
H	-5.25699700	0.00484600	0.01956500

[^{F}XylPBBI]$_4$

DFT B3LYP/6-31G, gas phase, S_0

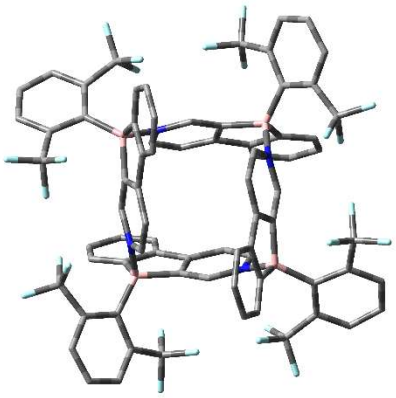

Point group: C_2

Total energy: –3, 535,213.90 kcal mol^{-1}

Dipole moment: 0.00 D

Imaginary frequencies: 0

C	2.82239900	-0.72083500	0.08056100
H	3.15814500	-0.95082400	-0.91889400
C	2.60437700	0.97827900	1.69289500
H	2.75833800	2.01950500	1.93826200
C	-2.82239400	0.72088600	0.08060300
H	-3.15816300	0.95092700	-0.91883300
C	2.28067400	-1.67336000	0.93267200
N	2.96078200	0.59584000	0.43481600
C	-2.28069400	1.67338600	0.93275600
N	-0.59578600	2.96075600	-0.43478400
C	0.72090600	2.82245200	-0.08057200
H	0.95091500	3.15817000	0.91888800
N	-2.96071800	-0.59581000	0.43479000
C	1.67345300	2.28077400	-0.93270300
N	0.59576000	-2.96073400	-0.43491500
C	2.32836400	1.24206400	-2.97708500
C	1.86864400	-1.24115300	2.22058400
C	-1.86865200	1.24113500	2.22064500
C	-0.09210400	2.06291900	-2.60789600
H	-0.45594900	1.77723300	-3.58739800
C	-1.14354700	3.50685800	2.18413300
C	-2.60428000	-0.97829900	1.69284600
H	-2.75817000	-2.01954600	1.93816200
C	1.24195700	-2.32830300	2.97703700
C	4.61378800	0.16005100	-4.12202400
H	5.51097800	-0.25331900	-4.57321100
C	-0.72093900	-2.82244300	-0.08071100
H	-0.95094200	-3.15816500	0.91874800
C	1.14345300	-3.50684800	2.18396600
C	-1.67346500	-2.28074800	-0.93283500
C	-1.24123700	-1.86867300	-2.22072400
C	1.24121800	1.86869000	-2.22058100
C	-0.97824700	2.60429100	-1.69284800
H	-2.01949500	2.75815300	-1.93817500
C	3.50695400	1.14363300	-2.18406900
C	-3.50692200	-1.14345200	-2.18410800
C	4.64990200	0.60293300	-2.78946900
H	5.57549600	0.51947800	-2.23514100
C	2.06297100	0.09213900	2.60794100
H	1.77734300	0.45597500	3.58746200
C	-0.25445800	3.43822400	4.87869100
H	0.08372700	3.42585600	5.91006900
C	0.97821300	-2.60430600	-1.69298400
H	2.01945900	-2.75817400	-1.93832000
C	-2.06291100	-0.09218400	2.60793200
H	-1.77726900	-0.45605600	3.58743600
C	0.60262700	-4.64978500	2.78926700
H	0.51912300	-5.57533400	2.23486800
C	-1.24202600	2.32827600	2.97715500
C	2.84909300	-4.38497200	0.15162000
C	0.09207000	-2.06294500	-2.60805000
H	0.45592300	-1.77728000	-3.58755400
C	-2.32837300	-1.24196200	-2.97717300
C	0.15970300	-4.61370700	4.12181000
H	-0.25375600	-5.51088700	4.57293600
C	4.38526400	2.84902300	-0.15166000
C	0.80276300	-2.28586300	4.30626100
H	0.90496600	-1.38016800	4.89796300
C	-0.60281200	4.64979500	2.78952400
H	-0.51933700	5.57538000	2.23518800
C	2.28588500	0.80291900	-4.30632200
H	1.38015400	0.90508700	-4.89797500
C	-2.84915500	4.38495400	0.15164000
C	-0.80289600	2.28579700	4.30639700
H	-0.90509700	1.38007400	4.89805700
C	2.48741800	-5.49003300	-0.68441200
C	5.49046400	2.48705000	0.68408600
C	3.43832300	0.25451100	-4.87862000

H	3.42595500	-0.08369200	-5.90999200
C	4.24147400	-4.35860700	0.47903300
C	6.17249800	4.79242600	1.04342900
C	-5.49015700	-2.48725300	0.68432500
C	-0.15994600	4.61367800	4.12208500
H	0.25344700	5.51085800	4.57327000
C	-4.24158100	4.35851500	0.47889100
C	0.25424300	-3.43829100	4.87847400
H	-0.08398700	-3.42595700	5.90983800
C	4.35906100	4.24148300	-0.47885200
C	-4.38509500	-2.84903700	-0.15167700
C	-2.28591500	-0.80275100	-4.30639000
H	-1.38021900	-0.90496400	-4.89808800
C	-4.64984900	-0.60261200	-2.78942000
H	-5.57540500	-0.51910800	-2.23503800
C	-2.48746000	5.49002100	-0.68438500
C	6.33507600	3.43633900	1.28679800
H	7.13901200	3.09723700	1.92735600
C	3.43690900	-6.33428600	-1.28726500
H	3.09802600	-7.13815900	-1.92802200
C	-4.35875200	-4.24146300	-0.47892200
C	5.20925900	5.18365600	0.12273900
H	5.12059000	6.22618800	-0.15263800
B	3.23812000	1.77136400	-0.69508900
C	-5.18398900	5.20826500	-0.12297200
H	-6.22648600	5.11945800	0.15250400
B	1.77127500	-3.23801300	0.69506100
B	-3.23809900	-1.77129300	-0.69519900
C	-5.20858900	-5.18380600	0.12293000
H	-5.11984500	-6.22631200	-0.15253100
B	-1.77131100	3.23804200	0.69517900
C	-3.43833000	-0.25421200	-4.87860800
H	-3.42598000	0.08402900	-5.90996900
C	-6.33441800	-3.43667500	1.28727900
H	-7.13827600	-3.09771800	1.92801700
C	-4.61375300	-0.15967200	-4.12195700
H	-5.51092100	0.25380500	-4.57308900
C	-6.17160900	-4.79275000	1.04391400
C	5.18390100	-5.20841900	-0.12273500
H	6.22637800	-5.11965600	0.15282300
C	-3.43695000	6.33420500	-1.28735200
H	-3.09805700	7.13808000	-1.92810000
C	4.79295600	-6.17144700	-1.04376200
C	-4.79300900	6.17129700	-1.04397900
H	5.52431900	-6.81271700	-1.52129700
H	-6.81289100	-5.52405300	1.52152300
H	6.81408600	5.52361200	1.52080600
H	-5.52436400	6.81251300	-1.52159900
C	4.84687700	-3.43191500	1.49776800
F	6.03604400	-3.95514700	2.02112400
F	5.20126400	-2.18772600	0.97514900
F	4.03773400	-3.20022600	2.60114600
C	5.89895300	1.07161300	0.98995800
F	7.27705500	0.97835800	1.21504400
F	5.31421700	0.54201800	2.14427400
F	5.64107900	0.18181500	-0.04726500
C	3.43202500	4.84725300	-1.49706600
F	3.95510600	6.03647700	-2.02039500
F	3.19980900	4.03839000	-2.60059000
F	2.18809700	5.20161700	-0.97387200
C	1.07207200	-5.89873900	-0.99032600
F	0.97905500	-7.27688800	-1.21521700
F	0.18219100	-5.64078800	0.04681200
F	0.54250200	-5.31422400	-2.14476400
C	-5.89886300	-1.07188700	0.99018100
F	-7.27697000	-0.97891000	1.21532500
F	-5.31416200	-0.54218200	2.14446400
F	-5.64115300	-0.18206200	-0.04706800
C	-3.43205900	-4.84701000	-1.49756500
F	-3.95541500	-6.03612200	-2.02092600
F	-3.20017200	-4.03793700	-2.60094700
F	-2.18796100	-5.20155600	-0.97483400
C	-4.84705000	3.43182300	1.49757800
F	-6.03613700	3.95518200	2.02099400
F	-5.20161600	2.18771900	0.97489200
F	-4.03791300	3.19997500	2.60093300
C	-1.07212800	5.89884200	-0.99021400
F	-0.97918400	7.27702400	-1.21494200
F	-0.18225800	5.64082300	0.04691300
F	-0.54248000	5.31449400	-2.14470300

Compound **10**

DFT B3LYP/6-31+G(d, p), gas phase, S_0

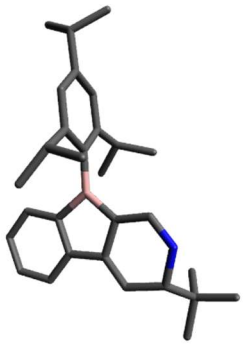

Point group: C_1

Total energy: –782,512.77 kcal mol^{-1}

Dipole moment: 3.97 D

Imaginary frequencies: 0

C	-0.43602100	4.35114800	-1.08834800
C	-1.83330300	4.38879800	-0.96051100
C	-2.53808700	3.26204900	-0.52988600
C	-1.83164000	2.09436700	-0.22514900
C	-0.41607000	2.03940800	-0.34722400
C	0.26716200	3.18323400	-0.78316300
C	-2.35762100	0.79261800	0.23563700
C	-1.21461500	-0.12276600	0.42401800
C	-3.62830600	0.42431100	0.48811100
C	-3.99645900	-0.97717500	0.92874800
N	-2.77353800	-1.75745700	1.20292900
C	-1.50747900	-1.35949600	0.92978200
C	-4.95440700	-1.73716300	-0.07098900
C	-6.26038700	-0.92973000	-0.21470100
C	-5.30497800	-3.12163700	0.51401200
C	-4.29077300	-1.90856900	-1.44769400
H	0.09628800	5.23625800	-1.42634000
H	-2.37135900	5.30211700	-1.19990300
H	-3.62057300	3.30211300	-0.43639400
H	1.34982000	3.16191900	-0.88381300
H	-4.44936400	1.12769300	0.38952200
H	-4.56047600	-0.91299600	1.87543400
H	-2.90040700	-2.66245300	1.62911200
H	-0.73716100	-2.09236200	1.15839600
H	-6.09519900	0.02976100	-0.71336000
H	-6.98509500	-1.49010200	-0.81532500
H	-6.72100200	-0.73315700	0.76157800
H	-4.43401700	-3.78542000	0.56075700
H	-6.04741600	-3.62284500	-0.11632700
H	-5.73159800	-3.03650600	1.52167400
H	-4.96296000	-2.43973900	-2.13110100
H	-4.04826200	-0.93954600	-1.89471600
H	-3.36327500	-2.48581600	-1.37413200
B	0.08728400	0.60041700	0.07364500
C	1.58728100	0.09277800	0.11420200
C	2.39928000	0.26883700	1.27306300
C	2.19235900	-0.51431500	-1.02846600
C	3.75035400	-0.11533200	1.24517300
C	3.54707300	-0.87696900	-0.99634500
C	4.35488300	-0.68195700	0.12501700
H	4.35228700	0.03803100	2.13938100
H	3.97802100	-1.32800300	-1.88768100
C	1.46338000	-0.88704500	-2.33076100
H	2.26372000	-1.13234100	-3.04031700
C	0.62489300	-2.17369700	-2.17315500
H	1.22855200	-2.98827200	-1.75856200
H	-0.23014800	-2.00899000	-1.51162200
H	0.23888600	-2.49778600	-3.14744400
C	0.63937700	0.22341500	-3.00429600
H	-0.28746900	0.44443900	-2.46960600
H	1.20850000	1.15454900	-3.08586400
H	0.36122600	-0.09386400	-4.01650400
C	5.82844200	-1.06672500	0.13763700
H	6.21474000	-0.81251100	1.13402100
C	6.03412100	-2.58111200	-0.06255100
H	5.68552300	-2.90198800	-1.05086500
H	7.09625400	-2.84104700	0.01631100
H	5.48435200	-3.15775100	0.68866900
C	6.64444800	-0.26027300	-0.89177100
H	6.52997400	0.81668500	-0.73086300
H	7.71040700	-0.50609200	-0.81910300
H	6.32028700	-0.48101800	-1.91522800
C	1.91815700	0.79891500	2.63500900
H	2.83814400	0.98461500	3.20354400
C	1.13739900	-0.27127400	3.42776000
H	0.17018100	-0.47988600	2.96205800
H	1.70137200	-1.20848400	3.48591300
H	0.94825400	0.07630500	4.45078700
C	1.15730500	2.13549200	2.63095900

H	1.67881300	2.89486200	2.04037600
H	0.14339400	2.04260700	2.23475100
H	1.07052100	2.50631500	3.65934000

Compound **11**

DFT B3LYP/6-31+G(d, p), gas phase, S_0

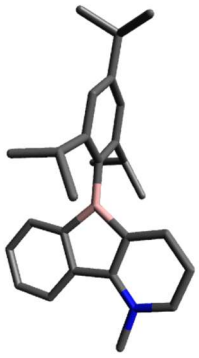

Point group: C_1

Total energy: –707,987.61 kcal mol^{-1}

Dipole moment: 12.43 D

Imaginary frequencies: 0

C	2.47565800	3.52052500	-0.20781100
C	3.77866900	3.02497000	-0.24028000
C	4.03069500	1.64533700	-0.18858900
C	2.95118100	0.75969200	-0.10309700
C	1.61305900	1.25924400	-0.06965700
C	1.39239900	2.63332100	-0.12234200
C	2.90065600	-0.72234400	-0.03341600
C	1.56738700	-1.19392700	0.04405400
N	3.93194200	-1.61091400	-0.03580400
C	3.67761000	-2.95766800	0.03690000
C	2.39819200	-3.45385300	0.11347100
C	1.31744400	-2.55293600	0.11722800
C	5.34628400	-1.18589500	-0.11453200
H	2.30279900	4.59133800	-0.24878300
H	4.61682400	3.71143400	-0.30654500
H	5.06067900	1.31949900	-0.21718700
H	0.37689000	3.01720700	-0.09695500
H	4.54893500	-3.59956600	0.02990200
H	2.25159900	-4.52637700	0.16907700
H	0.29604800	-2.91769600	0.17690400
H	5.97796000	-2.07201300	-0.10060500
H	5.51631400	-0.64120300	-1.04427000
H	5.59133600	-0.55961700	0.74438600
B	0.58886100	0.07054100	0.02711400
C	-0.97085100	0.04099500	0.09382700

C	-1.65302300	0.05193700	1.34676300
C	-1.75723400	-0.06011600	-1.09549100
C	-3.04764900	-0.09235700	1.37640300
C	-3.14688500	-0.20114500	-0.99787700
C	-3.82113800	-0.23309100	0.22499800
H	-3.54665300	-0.09287100	2.34321500
H	-3.71747200	-0.28647600	-1.91931800
C	-1.21643100	0.06630200	-2.52619800
H	-1.98048900	-0.38795400	-3.16812300
C	-1.10979100	1.54711100	-2.95171800
H	-2.05714100	2.07084000	-2.79461300
H	-0.33655300	2.07160700	-2.38077400
H	-0.85084200	1.62375100	-4.01361600
C	0.08782100	-0.67960900	-2.83559600
H	0.95763000	-0.22028400	-2.34862400
H	0.03782100	-1.73323600	-2.54457400
H	0.29142600	-0.63790200	-3.91109200
C	-0.99872900	0.30451700	2.71152300
H	-1.70469900	-0.09111500	3.45133100
C	-0.86937400	1.81745100	2.99377200
H	-0.14947800	2.28914900	2.31681800
H	-1.83047400	2.32459800	2.86906100
H	-0.52527500	1.98858700	4.01985300
C	0.33212400	-0.41025300	2.97802700
H	0.26586100	-1.48603900	2.78931900
H	1.15528500	0.00240200	2.38062100
H	0.62368700	-0.27056700	4.02462600
C	-5.33100700	-0.40625500	0.30849400
H	-5.59503100	-0.38499500	1.37376600
C	-6.08181600	0.75218500	-0.37730700
H	-7.16234600	0.63964900	-0.23987100
H	-5.78572000	1.72103400	0.03765100
H	-5.88595300	0.77317100	-1.45527700
C	-5.78249100	-1.76895800	-0.25322200
H	-5.56926100	-1.84881700	-1.32518200
H	-5.27644100	-2.59717000	0.25357400
H	-6.86171000	-1.89775600	-0.11960200